UNIVERSITÀ
DEGLI STUDI
DI PADOVA

Department of Agronomy, Food, Natural resources, Animals and Environment

---

PhD School in Crop Science

XXVIII Cycle

Soil carbon management for future challenges in agriculture: the role of crop residues and biochar

Head of the school: Ch.mo Prof. Antonio Berti

Supervisor: Ch.mo Prof. Francesco Morari

PhD student: Chiara Pituello

Padova, 1 Febbraio 2016

Declaration

I hereby declare that this submission is my own work and that, to the best of my knowledge and belief, it contains no material previously published or written by another person nor material which to a substantial extent has been accepted for the award of any other degree or diploma of the university or other institute of higher learning, except where due acknowledgment has been made in the text.

Chiara Pituello, February 1st 2016

A copy of the thesis will be available at *http://paduaresearch.cab.unipd.it/*

Dichiarazione

Con la presente affermo che questa tesi è frutto del mio lavoro e che, per quanto io ne sia a conoscenza, non contiene materiale precedentemente pubblicato o scritto da un'altra persona né materiale che è stato utilizzato per l'ottenimento di qualunque altro titolo o diploma dell'università o altro istituto di apprendimento, a eccezione del caso in cui ciò venga riconosciuto nel testo.

Chiara Pituello, 1 Febbraio 2016

Una copia della tesi sarà disponibile presso *http://paduaresearch.cab.unipd.it/*

Table of contents

Riassunto

La perdita di sostanza organica da parte dei suoli è ampiamente riconosciuta come una minaccia a livello globale. Per questo motivo, lo studio riguardante le pratiche di gestione del suolo che si focalizzano sul carbonio rappresenta una necessità molto urgente per la comunità scientifica. La pratica di restituire a fine stagione i residui colturali al suolo al fine di reintegrare le perdite di carbonio organico è stata recentemente messa a repentaglio a causa del loro alternativo uso per la produzione di biocombustibili (specialmente biogas). Nell'area del Nord-Est italiano la diffusione degli impianti per la produzione di biogas ha generato due principali effetti negativi: in primo luogo ha privato i suoli di un'importante fonte di carbonio organico, utilizzando biomassa che altrimenti sarebbe stata lasciata in campo; secondariamente ha fatto sì che ci sia la necessità di smaltire in modo sicuro una grande quantità di digestati. L'utilizzo di questi ultimi come ammendanti ha tuttavia degli svantaggi (ad es. aumento della produzione di gas serra, lisciviazione dell'azoto e scarso contributo al carbonio stabile del suolo, diffusione di batteri patogeni). Una via alternativa di smaltimento-valorizzazione potrebbe consistere nel loro utilizzo per la produzione di biochar. Tuttavia, per dare una robusta valutazione sul valore ambientale di questa proposta alternativa, è necessario comparare gli effetti sul suolo dei residui colturali e del biochar. Per questo motivo, gli obiettivi di questa tesi sono quelli di valutare gli effetti di queste due forme molto diverse di input carboniosi su: i) la produttività delle colture; ii) le dinamiche del carbonio organico del suolo; e iii) alcuni parametri di fertilità fisica del suolo. Questi studi sono stati fatti utilizzando suoli con tessiture molto differenti: un argilloso, un franco-limoso ed un sabbioso. Inoltre, per quanto riguarda i residui colturali, è stato utilizzato un corpus di dati proveniente da una prova di campo di lungo periodo (43 anni), mentre nel caso del biochar i suoi effetti sono stati studiati dopo due anni di applicazione in campo. I risultati hanno dimostrato che il biochar ha influenzato positivamente le rese delle colture, nonché il contenuto di carbonio e la stabilità degli aggregati dei suoli. Tutti gli effetti si sono verificati già dopo un anno dall'applicazione, ma con diverse intensità per i diversi suoli. Infatti, la fertilità è stata influenzata in modo maggiore nel medio-limoso, mentre gli effetti sulla produttività si

sono verificati prevalentemente nel suolo sabbioso. Al contrario, l'influenza dei residui colturali nel breve periodo è stata meno pronunciata, infatti i risultati hanno mostrato che i contenuti di carbonio organico dei suoli sono stati modificati solo nel lungo periodo (43 anni), con effetti quantitativamente maggiori nel suolo argilloso e alti incrementi relativi nel sabbioso. Inoltre questi cambiamenti non sono rimasti circoscritti allo strato più superficiale del suolo, ma si sono verificati anche a profondità maggiori, specialmente nel caso del franco-limoso e del sabbioso. I sopra descritti effetti sul carbonio organico non sono stati accompagnati da cambiamenti rilevanti nella distribuzione dei pori (dalla nano- fino alla macro-porosità), anche se è stato osservato un aumento della porosità totale. In aggiunta, anche se poco influenzata a livello quantitativo, l'architettura dei pori ha mostrato un ri-arrangiamento verso una struttura più allungata ed irregolare. In aggiunta, l'influenza dei residui sulla produttività delle colture è stata generalmente bassa, con incrementi modesti di biomassa nei suoli più fertili, ed un effetto ampiamente compensabile dalla fertilizzazione azotata. In conclusione, l'utilizzo del biochar si configura come una pratica raccomandabile per incrementare la fertilità dei suoli nelle condizioni pedo-climatiche specifiche del Nord-Est italiano, con risultati immediatamente visibili. Tuttavia i suoi effetti nel lungo periodo rimangono per ora sconosciuti, ed il loro studio è di fondamentale importanza per prevenire possibili conseguenze negative sull'ambiente ed elaborare linee guida riguardanti la sua applicazione e gestione. L'utilizzo dei residui colturali al contrario si configura come una pratica, seppur utile, applicabile solo con una prospettiva di lungo periodo.

Summary

Soil loss of organic carbon is a widely recognised global threat. In this view, the study on management practices which precisely focus on soil C is a pressing need for the research community. The incorporation of crop residues at the end of the growing season to reintegrate organic matter losses has been currently jeopardised by their alternative use for bioenergy (mostly biogas production). In north-eastern Italy the fast spread of biogas production has generated two major drawbacks: firstly it has deprived soils from an important source of organic carbon utilizing plant parts which would otherwise be left in the field; secondly, it has produced huge quantities of digestates which need to be safely disposed. The return of digestates to soils as amendants has some disadvantages (*i.e.* increased GHGs emissions, nitrogen leaching and scarce contribution to stable soil organic matter, spread of pathogenic bacteria). An alternative disposal-valorisation route would be to use them as feedstocks for biochar production. However, to soundly evaluate the environmental value of this alternative pathway, information about the effects on soil properties of the head-of-the-chain product (crop residues) and of the final material (biochar) need to be comparatively evaluated. For these reasons, the objectives of this thesis are to clarify the effects of these two very different forms of carbon (crop residues as a source of mostly labile C, and biochar as a source of mostly stabile C) on: (i) crop productivity, (ii) soil organic carbon dynamics and (iii) selected indicators of soil physical fertility. These parameters have been studied considering soils with contrasting textures: clay, sandy-loam and sandy. For crop residues, a corpus of data deriving from a long-term (43 years) field rotation was used. Biochar effects were analysed after two years of field application. The results showed that biochar application had positive effects on crop yields and aggregate porosity and stability indexes. Furthermore, it resulted useful in increasing the carbon content of the soils. All the effects were clearly visible after one year of application and on all the soils considered, even if with different intensities. Indeed, soil properties were affected in a more pronounced way in sandy-loam, while crop yield was especially boosted in sandy soil. On the contrary, residue effects in the short-term were slighter, indeed our results showed that soil

organic carbon was significantly affected only by the long-term (43 years) incorporation of crop residues with effects quantitatively more evident in clay soil and high relative increments in sandy soil. The effects were not limited to the upper soil layer, but extended to lower depths especially for sandy and sandy-loam soil. The residue-induced effects on soil organic carbon were not accompanied by a relevant change in soil pore size distribution from nano to macro scale, even though residues induced an increase in total porosity. In addition, even if only slightly influenced in quantitative terms, the pore network showed a rearrangement towards a more elongated and irregular structure. On the contrary, residue influence on crop yields was relatively low, with modest increments of biomass in the most fertile soils, and their effect could be compensated by N fertilization. In conclusion, the use of biochar emerges as a recommendable practice to increase soil fertility in the climatic conditions of North-Eastern Italy, while its long-term effects remain a knowledge gap that needs to be investigated to prevent possible side-effects and elaborate effective application and management guidelines. Conversely crop residue effects, although present, design this practice as effective only with a long-term perspective.

Chapter I

General introduction

The importance of soil carbon management

Soils are one of the greatest stocks of carbon (C) on earth, containing an estimated quantity ranging from 684 to 724 Pg in the surface horizon (0-30 cm depth) (Batjes, 1966). This is equal to almost twice the amount of C present in the atmosphere as carbon dioxide (CO_2) and three times that contained in the above ground vegetation (Powlson et al., 2011a). These numbers highlight the fundamental role of soils within the global CO_2 cycle, and thus their potential to either worsen or mitigate climate change. For example, a change of just 10% in the soil organic carbon (SOC) content will be equivalent to the anthropogenic CO_2 emissions of 30 years (Kirschbaum, 2000). Globally, annual losses of SOC due to agricultural activities are estimated in 78 Gt/yr (Smith et al., 2005). More specifically, in the last fifty years SOC in North-Eastern Italy decreased at rates ranging from 0.02 to 0.58 t ha^{-1}/year as a consequence of the intensification and simplification of cropping systems. Some other important numbers related to global soil carbon are listed in Table 1. The depletion of SOC stock, along with increasing CO_2 emissions in atmosphere, negatively influences soil fertility by degrading soil structure (Oades et al., 1984), it reduces the ability of soils to retain nutrients and increases erosion risks (Creamer et al., 2010)(Figure 1), finally jeopardizing the ability of soil to provide essential ecosystem services.

Table 1. *Global soil carbon parameters (adapted from Banwart et al., 2015).*

Amount of carbon in the top 1 m of Earth's soil (2/3 as organic matter)[a]	2200 Gt
Fraction of antecedent soil and vegetation carbon characteristically lost from agricultural land since 19th century [b]	60%
Fraction of global land area degraded in past 25 years due to soil carbon loss[c]	25%
Rate of soil loss due to conventional agriculture tillage[d]	~ 1 mm $year^{-1}$
Rate of soil formation[d]	~ 0.01 mm $year^{-1}$
* Global mean land denudation rate[e]	0.06 mm $year^{-1}$
Soil greenhouse gas contributions to anthropogenic emissions, in CO_2 equivalents[f]	25%

**Rate of land lowering due to chemical and physical weathering losses.* [a] Batjes, 1966*;* [b]Houghton (1995)*;* [c]Bai et al., (2008)*;* [e]Montgomery, (2007)*;* [f] Wilkinson & McElroy (2009)*;* [g]*2004 data not including CH4, IPCC (2007).*

In order to prevent soil degradation, every agricultural practice able to increase or at least maintain the levels of soil organic carbon should be highly endorsed (Lal, 2011). There are diverse ways to preserve SOC stocks, grouped in the Recommended Management Practices (RMPs): reduced or zero tillage, application of biosolids (e.g. manure and compost), cover and deep-rooting crops, conversion to grassland and woodland, improved rotations, fertilization, drip, furrow or sub- irrigation and integrated pest management (Lal, 2004). Biochar and crop residue incorporation have been included in the RMPs (Creamer et al., 2010; Lal, 2011), however, several doubts still remain on the actual effects of these two radically different forms of carbon on soil quality (Lal, 2005) and crop productivity.

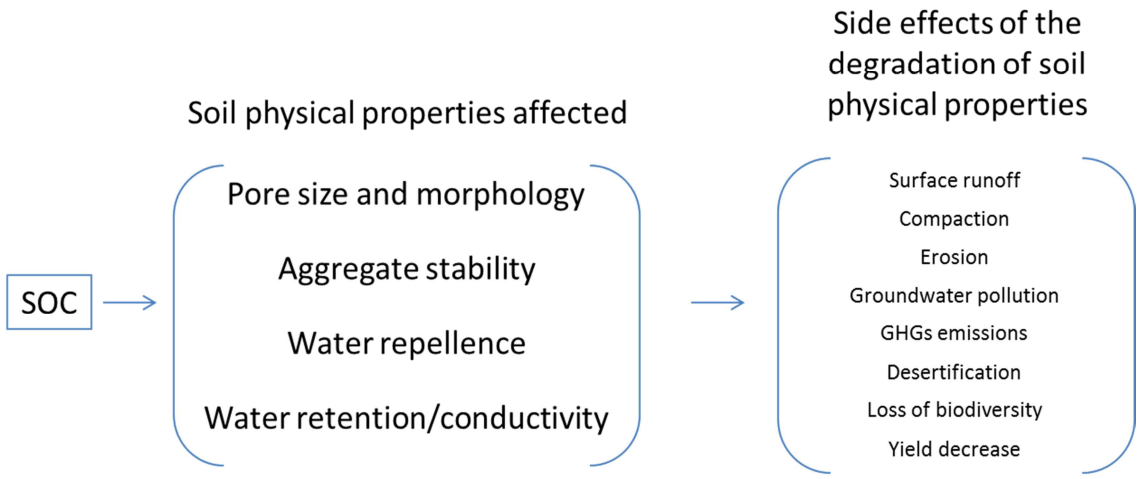

Figure 1. *Schematic representation of the link between soil organic carbon, soil physical properties and detrimental side effects associated with a degradation in those specific soil functions.*

Crop residues

Long term effects of residue incorporation on SOC stocks have been studied by many authors with contrasting findings. Powlson et al. (2011), reviewing the data from 23 long-term experiments with a wide range of climatic and pedologic conditions (from temperate regions of Europe and North America to subtropical sites in Australia) found a trend of residue-induced increase in soil organic carbon in all sites, but it resulted significant only in five and it was in the majority of cases lower than 10%. This reflects that the magnitude of SOC variations strongly depends on factors such as climate and soil type

(Powlson et al., 2011b). A recent meta-analysis considering 176 peer-reviewed articles published from 1900 to 2012, revealed that straw return significantly increases SOC of 12.4% ± 0.4% on average (Liu et al., 2014). Furthermore Raffa et al. (2015) reviewing a large database of studies concluded that the removal of residues caused a loss in SOC of 12% and 18% in temperate and tropical climates, respectively. They evidenced though a large variability in the dataset used. More specifically, a recent study by Monforti et al. (2015) highlights that 50% residue removal would have no effect on soil carbon stocks only in some European regions (e.g. northern France, central Germany, Po valley, central Spain and most of the UK), whereas their complete removal will result in a decrease in SOC in almost all European countries. Clearly, variations in SOC contents induced by residues can produce a cascade of effects on other soil (i.e. physical properties) and crop indicators (i.e. productivity and nitrogen use efficiency). In fact, Powlson et al. (2011b) underlined that even minor changes in residue-induced carbon stock can trigger notable variations in soil physical properties such as aggregate stability, water infiltration and plough draft. This apparent inconsistency between minimal SOC variations and significant effects on some primary physical properties is due to the effect of a small fraction of SOC usually called “active C” (i.e. the fraction that can be oxidized by very dilute potassium dichromate, about 10% of total C) which increases - or decreases - faster than total soil C when residues are incorporated - or removed (Powlson et al., 2011b). The residue-mediated effect on the soil physical properties was also observed by other authors. For instance, maize residue incorporation or removal induced changes in soil bulk density and total porosity (Lal, 2009) as well as in soil water content and resistance to penetration (Fuentes et al., 2009). Thus, the variation in soil physical properties could be both a direct estimate of soil fertility, and an indirect signal of changes in the more labile and difficult to analyse part of soil C pool. Crop residue management influences crop productivity in particular in tropical climates, while less evident effects are detected in temperate climates (Raffa et al., 2015); however a sound generalisation has to be taken carefully, since in tropical climates the variation in seasonal rainfall (and consequently the ability of soils to retain water) represents the major drive in yield fluctuations, explaining the variability in the results between studies. On the contrary, in temperate

climates, it appears that different crops are affected in diverse ways, with maize being sensible to crop residue incorporation while winter wheat does not (Raffa et al., 2015). Likewise studies on the use of crop residues to increase nitrogen use efficiency (NUE) in different climates and soil types have led to inconclusive results. Malhi et al. (2011) studying two long-term (26 years) rotations in a Black Chernozem and in a Orthic Gray Luvisol in Canada, found in the first type of soil an increase (+ 5.2 Kg N ha^{-1}) in N uptake by seed and straw. On the contrary in the Luvisol, the uptake increment was registered only for a limited portion of the experiment duration. Accordingly, three years of straw incorporation in a Haplic Luvisol produced no significant improvements in NUE of winter wheat (Brennan et al., 2014). In a recent meta-analysis summarizing studies on rice cultivations in China, Huang et al. (2013) found that the incorporation of rice residues allowed a 29.4% reduction of inorganic N inputs without significant decreases in yield. These apparently contrasting results could be partly explained by the numerous and complicated factors that affect the residue-derived N cycle in field conditions, such as soil pH, salinity and texture, temperature and moisture conditions, freezing and thawing cycles, wetting and drying cycles, along with macro and microorganisms (Kumar and Goh, 1999).

Biochar

Among the different components of soil organic carbon (e.g. plant-derived, microbial-derived etc..), fire-derived (also called pyrogenic) organic matter decomposition pathways are currently the more unexplored and mysterious (Knicker, 2011; Schmidt et al., 2011). Fire-derived organic matter is a component ubiquitously found in most soils, but its functions on soil dynamics are still debated. Studies on anthropogenic soils containing high levels of pyrogenic organic carbon (*Terra Preta*) reveal that these soils hold an higher fertility due to a remarkable content of organic matter, if compared to the surrounding Oxisols (Glaser et al., 2001). The comparison between mean residence times of bulk soil organic matter and of its singular components, highlights that fire-derived organic matter (coupled with protection mechanisms and interactions between different components of SOC) could play a

fundamental role in this process, by consistently increasing the recalcitrance of organic matter. Indeed, while crop residue mean residence time is in the order of decades, that of pyrogenic organic matter is expected to be between hundreds to thousands of years (Lehmann et al., 2006). In recent years, a form of industrially produced pyrogenic organic matter (i.e. biochar) has gathered much interest as a tool to improve soil carbon sequestration along with enhancing soil fertility. Recently it has been included in the list of amendants approved for soil application in Italy (Gazzetta Ufficiale del 12-08-2015, Serie Generale n. 186). Pyrolysis (the thermal treatment of biomass at low levels of oxygen) is nowadays used especially in gasification plants to produce renewable fuels such as syngas and bio-oil. The resulting solid by-product of the process is a carbonaceous material called biochar. The reasons of the interest in biochar are its highly aromatic structure and specific surface characteristics which, along with its high porosity, provide it with the attributes of a double phase material: one stable and recalcitrant core of aromatic carbon along with a charged and porous surface that can interact with other soil components and nutrients. These two phases could explain its long-lasting stability in soils coupled with its ability to increase nutrient bioavailability, and thus to increase crop productivity (Shackley et al., 2010). A recent review reveals that biochar increases crop yield of 10% on average, with the largest effects in coarse and medium texture soils with acidic pH (Jeffery et al., 2011). Positive effects of biochar on yield and total biomass production are confirmed by Biederman and Harpole (2013). Most of the published research focuses on biochar effects on soil chemical parameters and microbiology (Farrell et al., 2013; Quilliam et al., 2013; Jaafar et al., 2014) though abundant evidences suggest also a biochar-mediated alteration of the soil structure (bulk density, aggregation and water holding capacity) (Lei and Zhang, 2013; Peake et al., 2014) but the effects appear not ubiquitously spread and vary as a function of soil and biochar characteristics (Hardie et al., 2013; Jeffery et al., 2015; Ojeda et al., 2015). Nevertheless data on biochar effects on soil physics, especially on soil aggregation are still scarce (Mukherjee and Lal, 2013). The need to have new insights on biochar effects on soil physics appear fundamental also considering that the responses are soil and site-specific and may vary between pot and field conditions. Even though there are no doubts that pyrolysis process would be a net C sequestration, the life cycle assessment

considering the biomass type, and the energy balance of the entire process has to be considered (Powlson, et al., 2011a). Certainly, not all biomass sources possess the same "sustainability". Indeed, a key point in biochar potential use as soil amendment is the fact that pyrolysis process is *per se* a promising alternative method for treating biomasses of difficult disposal, such as digestate from biogas production plants and sewage sludge from aerobic wastewater treatment, with benefits at different levels. As a matter of fact, the logistics of waste storage, transport and spreading are improved by reducing the volumes and water content; greenhouse gas emissions are mitigated during the storage (Rehl and Muller, 2011), and sanitation costs are consistently abated. Regarding the latter, pasteurization is a practice recommended by the European Union Regulation (EC 1774/2002) to reduce microbial contamination. Despite being more effective after digestion, its benefits can be neutralized by the digestate vulnerability to recontamination because bacterial spores are not destroyed during aerobic/anaerobic treatments (Schnürer et al., 2009). Thus, processing biomass through pyrolysis plants and the subsequent use of biochar as a soil amendment can give an additional value to those biomasses whose disposal routes (such as farmland application) may be subject to strict legislative constraints. Nevertheless, biochars produced from biowastes can contain toxic compounds and high concentrations of heavy metals, whose bioavailability assessment is vital before their use becomes a common practice (Jeffery et al., 2015).

Project objectives

Soil loss of organic carbon is a widely recognised global threat. In this view, management practices which precisely focus on soil C and research on the dynamics involving it as a continuum of substances at different decomposition stages (Lehmann and Kleber, 2015) are pressing needs for the research community. The incorporation of crop residues at the end of the growing season to reintegrate organic matter losses has been currently jeopardised by their alternative use for bioenergy (mostly biogas production). In north-eastern Italy the fast spread of biogas production has generated two major drawbacks: firstly it has deprived soils from an important source of organic carbon utilizing plant parts

which would otherwise be left in the field; secondly, it has produced huge quantities of digestates which need to be safely disposed. The return of digestates to soils as amendants has some disadvantages such as increased GHGs emissions, nitrogen leaching and scarce contribution to stable soil organic matter. In addition, they can contain significant amounts of pathogenic bacteria, which can pose serious risks once entered in the food chain. An alternative disposal-valorisation route would be to use them as feedstocks for biochar production. This would indeed meet the aim of sanitising the biomass while reducing its volume and costs of transport (the same logic could be applied to every form of organic waste for which difficulties exist in the disposal process). However, to soundly evaluate the environmental value of this alternative pathway, information about the effects on soil properties of the head-of-the-chain product (crop residues) and of the final material (biochar) need to be comparatively evaluated. Furthermore, if considering a more globally-oriented vision, due to the challenges that soils are expected to face in the near future, the full comprehension of the dynamics that involve organic carbon (from the more labile to the more recalcitrant fraction) is urgently needed. This may help provide and strengthen the view of soil as a critical non-renewable resource which offers a range of ecosystem services essential to sustain life on the planet. For these reasons, the objectives of this thesis are to clarify the effects of two very different forms of carbon (crop residues as a source of mostly labile C, and biochar as a source of mostly stabile C) on: (i) crop productivity, (ii) soil organic carbon dynamics and (iii) selected indicators of soil physical fertility. These parameters have been studied considering soils with contrasting textures: clay, sandy-loam and sandy. This because among the different factors influencing C storage, soil texture (i.e. clay + silt fraction) is known to play a major role (Hassink, 1997; Schjønning et al., 2012; Stewart et al., 2007), as it determines the maximum achievable level of C that can be stored in a specific type of soil. For crop residues, a corpus of data deriving from a long-term (43 years) field rotation was used. Biochar effects were analysed after two years of field application.

Dissertation outline

The thesis consists of a preliminary part in which biochars produced at different temperatures and from several feedstocks (mainly biowastes) have been chemically and physically analyzed in order to evaluate the effect of pyrolysis temperature and heating rate on biochar structure, porosity and surface chemistry. This part will be described in the first chapter of the thesis: **Characterization of chemical-physical, structural and morphological properties of biochars from biowastes produced at different temperatures.**

The second part of the project consists in the characterization of the effects of forty-three years of crop residue incorporation on soil physical properties (i.e. pore morphology from the nano to the macroscale, soil hydraulic conductivity and water retention curves), organic carbon dynamics and crop productivity. The methodologies and results will be described in the second chapter of the thesis: **Long-term crop residue and effects on crop productivity and soil properties.**

The final part of the project consists in the evaluation of the comparative effects of crop residues and biochar on crop productivity, soil organic carbon dynamics and aggregate stability. For this purpose, the experimental design of the long-term field test has been changed introducing the application of waste wood biochar at two doses. The results of the first two years of experimentation are exposed in the last chapter: **Comparative effects of crop residues and biochar on maize (*Zea mais* L.) productivity, soil organic carbon and aggregate structure in three contrasting soils.**

References

Bai, Z. G., Dent, D. L., Olsson, L., Schaepman, M. E. (2008). Proxy global assessment of land degradation. *Soil Use and Management*, *24*(3), 223–234. doi: 10.1111/j.1475-2743.2008.00169.

Banwart, S. A., Black H., Cai Z., Gicheru P. T., Joosten H., Victoria, R. L., Milne E., Noellemeyer, E., Pascual, U. (2015). The Global Challenge for Soil Carbon. In S. A. Banwart, E. Noellemeyer, E. Milne (Eds.), *Soil Carbon: Science, management and policy for multiple benefits.* (SCOPE seri., pp. 1–9).

Batjes, N. H. (1966). Total carbon and nitrogen in the soils of the world. *European Journal of Soil Science*, *47*(June), 151–163. doi: 10.1111/j.1365-2389.1996.tb01386.x

Biederman, L. A., Harpole, W. S. (2013). Biochar and its effects on plant productivity and nutrient cycling: a meta-analysis. *GCB Bioenergy*, *5*(2), 202–214. doi:10.1111/gcbb.12037

Brennan, J., Hackett, R., McCabe, T., Grant, J., Fortune, R. A., Forristal, P. D. (2014). The effect of tillage system and residue management on grain yield and nitrogen use efficiency in winter wheat in a cool Atlantic climate. *European Journal of Agronomy*, *54*, 61–69. doi:10.1016/j.eja.2013.11.009

Creamer, R. E., Brennan, F., Fenton, O., Healy, M. G., Lalor, S. T. J., Lanigan, G. J., Regan ,J.T.,Griffiths, B. S. (2010). Implications of the proposed Soil Framework Directive on agricultural systems in Atlantic Europe - a review. *Soil Use and Management*, *26*(3), 198–211. doi:10.1111/j.1475-2743.2010.00288.x

Farrell, M., Kuhn, T. K., Macdonald, L. M., Maddern, T. M., Murphy, D. V., Hall, P. A., Singh, B. P., Baumann, K., Krull, E. S., Baldock, J. A. (2013). Microbial utilisation of biochar-derived carbon. *Science of the Total Environment*, *465*, 288–297. doi:10.1016/j.scitotenv.2013.03.090

Fuentes, M., Govaerts, B., De Léon, F., Hidalgo, F., Dendooven, L., Sayre, K.D., Etchevers, J., (2009). Fourteeh years of applying zero and conventional tillage, crop rotation and residue management systems and its effect on physical and chemical soil quality. *European Journal of Agronomy, 30*, 228-237. doi: 10.1016/j.eja.2008.10.005

Gazzetta Ufficiale della Repubblica Italiana, Serie Generale n.186 del 12-08-2015. Modifica degli allegati 2,6 e 7 del Decreto Legislativo 29 Aprile 2010, n.75.

Glaser, B., Haumaier, L., Guggenberger, G., Zech, W. (2001). The “Terra Preta” phenomenon: a model for sustainable agriculture in the humid tropics. *Naturwissenschaften*, *88*(1), 37–41. doi:10.1007/s001140000193

Hardie, M., Clothier, B., Bound, S., Oliver, G., Close, D. (2013). Does biochar influence soil physical properties and soil water availability? *Plant and Soil*, *376*(1-2), 347–361. doi:10.1007/s11104-013-1980-x

Hassink, J. (1997). The capacity of soils to preserve organic C and N by their association with clay and silt particles. 77–87. doi: 10.1023/A:1004213929699

Houghton, R. A. (1995). *Changes in the storage of terrestrial carbon since 1850*. In: Soils and Global Change. Lal R., Kimble J., Levine E., Stewart B.A. (Eds.). Lewis Publishers, CRC Press. London.

Huang, S., Zeng, Y., Wu, J., Shi, Q., Pan, X. (2013). Effect of crop residue retention on rice yield in China: A meta-analysis. *Field Crops Research*, *154*, 188–194. doi:10.1016/j.fcr.2013.08.013

Jaafar, N. M., Clode, P. L., Abbott, L. K., (2014). Microscopy observations of habitable space in biochar for colonization by fungal hyphae fromsoil. *Journal of Integrative Agruculture, 13(3),* 483-490. doi: 10.1016/S2095-3119(13)60703-0

Jeffery, S., Bezemer, T. M., Cornelissen, G., Kuyper, T. W., Lehmann, J., Mommer, L., Sohi, S.P.,van De Voorde, T. F.J., Wardle, D.A., van Groenigen, J. W. (2015). The way forward in biochar research: targeting trade-offs between the potential wins. *GCB Bioenergy*, *7*(1), 1–13. doi:10.1111/gcbb.12132

Jeffery, S., Verheijen, F. G., van der Velde, M., Bastos, C. (2011). A quantitative review of the effects of biochar application to soils on crop productivity using meta-analysis. *Agriculture, Ecosystems & Environment*, *144*(1), 175–187. doi:10.1016/j.agee.2011.08.015

Kirschbaum, M. U. F. (2000). Will changes in soil organic carbon act as a positive or negative feedback on global warming? *Biogeochemistry*, *48*(Batjes 1996), 21–51. doi: 10.1023/A:1006238902976

Knicker, H. (2011). Pyrogenic organic matter in soil: Its origin and occurrence, its chemistry and survival in soil environments. *Quaternary International*, *243*(2), 251–263. doi:10.1016/j.quaint.2011.02.037

Kumar, K., Goh, K. M. (1999). Crop residues and management practices: effects on soil quality, soil nitrogen dynamics, crop and nitrogen recovery. *Advances in Agronomy*, *68*, 197–319. doi:10.1016/S0065-2113(08)60846-9

Lal, R. (2004). Soil carbon sequestration to mitigate climate change. *Geoderma*, *123*(1-2), 1–22. doi:10.1016/j.geoderma.2004.01.032

Lal, R. (2005). World crop residues production and implications of its use as a biofuel. *Environment International*, *31*(4), 575–84. doi:10.1016/j.envint.2004.09.005

Lal, R. (2009). Soil quality impacts of residue removal for bioethanol production. *Soil and Tillage Research*, *102*(2), 233–241. doi:10.1016/j.still.2008.07.003

Lal, R. (2011). Sequestering carbon in soils of agro-ecosystems. *Food Policy*, *36*, S33–S39. doi:10.1016/j.foodpol.2010.12.001

Lehmann, J., Gaunt, J., Rondon, M. (2006). Bio-char Sequestration in Terrestrial Ecosystems – A Review. *Mitigation and Adaptation Strategies for Global Change*, *11*(2), 395–419. doi:10.1007/s11027-005-9006-5

Lehmann, J., Kleber, M. (2015). The contentious nature of soil organic matter. *Nature*, *528*, 0–8. doi:10.1038/nature16069

Lei, O., Zhang, R. (2013). Effects of biochars derived from different feedstocks and pyrolysis temperatures on soil physical and hydraulic properties. *Journal of Soils and Sediments*, *13*(9), 1561–1572. doi:10.1007/s11368-013-0738-7

Liu, C., Lu, M., Cui, J., Li, B., Fang, C. (2014). Effects of straw carbon input on carbon dynamics in agricultural soils: a meta-analysis. *Global Change Biology*, *20*(5), 1366–81. doi:10.1111/gcb.12517

Malhi, S. S., Nyborg, M., Solberg, E. D., Dyck, M. F., Puurveen, D. (2011). Improving crop yield and N uptake with long-term straw retention in two contrasting soil types. *Field Crops Research*, *124*(3), 378–391. doi:10.1016/j.fcr.2011.07.009

Monforti, F., Lugato, E., Motola, V., Bodis, K., Scarlat, N., Dallemand, J.-F. (2015). Optimal energy use of agricultural crop residues preserving soil organic carbon stocks in Europe. *Renewable and Sustainable Energy Reviews, 44*, 519-529. doi:10.1016/j.rser.2014.12.033

Montgomery, D. R. (2007). Soil erosion and agricultural sustainability. *Proceedings of the National Academy of Sciences*, *104*(33), 13268–13272. doi:10.1073/pnas.0611508104

Mukherjee, A., Lal, R. (2013). Biochar Impacts on Soil Physical Properties and Greenhouse Gas Emissions. *Agronomy*, *3*(2), 313–339. doi:10.3390/agronomy3020313

Oades, J. M., Osmond, G., Fungalhyphae, E., Iron, G., Periodate, M., Rhizosphere, P., Slaking, R. (1984). Soil organic matter and structural stability : mechanisms and implications for management Microaggregates Swelling and dispersion, *337*, 319–337. doi: 10.1007/BF02205590

Ojeda, G., Mattana, S., Àvila, A., Alcañiz, J. M., Volkmann, M., Bachmann, J. (2015). Are soil–water functions affected by biochar application? *Geoderma*, *249-250*, 1–11. doi:10.1016/j.geoderma.2015.02.014

Peake, L. R., Reid, B. J., Tang, X. (2014). Quantifying the influence of biochar on the physical and hydrological properties of dissimilar soils. *Geoderma*, *235-236*, 182–190. doi:10.1016/j.geoderma.2014.07.002

Powlson, D. S., Whitmore, P., Goulding, K. W. T. (2011a). Soil carbon sequestration to mitigate climate change: a critical re-examination to identify the true and the false. *European Journal of Soil Science*, *62*(1), 42–55. doi:10.1111/j.1365-2389.2010.01342.x

Powlson, D. S., Glendining, M. J., Coleman, K., Whitmore, A. P. (2011b). Implications for Soil Properties of Removing Cereal Straw: Results from Long-Term Studies. *Agronomy Journal*, *103*(1), 279. doi:10.2134/agronj2010.0146s

Quilliam, R. S., Glanville, H. C., Wade, S. C., Jones, D. L. (2013). Life in the "charosphere" - Does biochar in agricultural soil provide a significant habitat for microorganisms? *Soil Biology and Biochemistry*, *65*, 287–293. doi:10.1016/j.soilbio.2013.06.004

Raffa, W., D., Bogdanski, Tittonell, P. (2015). How does crop residue removal affect soil organic carbon and yield? A hierarchical analysis of management and environmental factors. *Biomass and Bioenergy*, *81*, 345–355. doi:10.1016/j.biombioe.2015.07.022

Rehl, T., and Muller, J., (2011) Life cycle assessment of biogas digestate processing technologies. *Resources Conservation & Recycling 56*, 92–104 doi: 10.1016/j.resconrec.2011.08.007.

Schjønning, P., de Jonge, L. W., Munkholm, L. J., Moldrup, P., Christensen, B. T., Olesen, J. E. (2012). Clay Dispersibility and Soil Friability—Testing the Soil Clay-to-Carbon Saturation Concept. *Vadose Zone Journal*, *11*(1). doi:10.2136/vzj2011.0067

Schmidt, M. W. I., Torn, M. S., Abiven, S., Dittmar, T., Guggenberger, G., Janssens, I., Kleber, M., Kögel-

Knaber, I., Lehmann, J., Manning, D.A.C., Nannipieri, P., Rasse, D.P., Weiner, S., Trumbore, S. E. (2011). Persistence of soil organic matter as an ecosystem property. *Nature*, *478*(7367), 49–56. doi:10.1038/nature10386

Schnürer A. (2009) Microbiological Handbook for Biogas Plants. Malmo: *Swedish Waste Management* U2009:03.

Shackley, S., and Sohi, S. (2010). An Assessment of the Benefits and Issues Associated with the Application of Biochar to Soil. Edinburgh: UK Biochar Research Centre

Smith, P., Andren, O., Karlsson, T., Perala, P., Regina, K., Rounsevell, M., Wesemael, B. (2005). Carbon sequestration potential in European croplands has been overestimated. *Global Change Biology*, *11*(12), 2153–2163. doi:10.1111/j.1365-2486.2005.01052.x

Stewart, C. E., Paustian, K., Conant, R. T., Plante, A. F., Six, J. (2007). Soil carbon saturation: concept, evidence and evaluation. *Biogeochemistry*, *86*(1), 19–31. doi:10.1007/s10533-007-9140-0

Wilkinson, B., McElroy, B. (2009). The impact of humans on continental erosion and sedimentation. In *American Geophysical Union Fall Meeting Abstracts* (Vol. 1, p. 1).

Chapter II

Characterization of chemical-physical, structural and morphological properties of biochars from biowastes produced at different temperatures.

Background and objectives

In recent years, biochar has gained interest as a tool to improve soil quality and promote soil carbon sequestration (Biederman and Harpole 2013; Jeffery et al. 2013; Schmidt et al. 2011). The highly aromatic structure of biochar and its specific surface characteristics, along with its high porosity, have been considered as the main reason for its long-lasting stability in soils and its ability to increase nutrient bioavailability, thus increasing crop productivity under specific pedo-climatic conditions (Jeffery et al. 2011; Shackley and Sohi 2010). Biochar characteristics change widely according to pyrolysis conditions and feedstock type (e.g. bioenergy crops, crop residues and by-products, industrial organic by-products) (Spokas et al. 2011); therefore, a wide diversity of its composition and property is expected (Gaskin et al. 2008; Ro et al. 2010). Chars produced by wood with high lignin contents have higher carbon (C) amount than those obtained from herbaceous feedstocks (Zabaniotou et al. 2008; Jeffery et al. 2013), but they are depleted in N (Cao and Harris 2010). Conversely, livestock manures are more enriched in nitrogen, phosphorus and micronutrients, and as a consequence, their pyrolysis produces biochars with higher nutrient content (Cantrell et al. 2012). Biochar made from biowaste, such as digestate from biogas production plants and sewage sludge from anaerobic wastewater treatment, maximizes the waste disposal with benefits at different levels (Jeffery et al. 2011). Thus, processing biowastes through pyrolysis plants and the subsequent use of biochar as a soil amendment can give an additional value to those biomasses whose disposal routes (such as farmland application) may be subject to strict legislative constraints. Robust information is still lacking on the potentialities of biochar production from biomasses of difficult disposal, also given that the heterogeneous nature of the feedstocks adds uncertainties to the results. For an agronomic benefit from biochar, it is important to understand how the physical and chemical properties are influenced by feedstock type and the pyrolysis conditions used in its production (Lehmann and Joseph 2009; Spokas et al. 2011). Moreover, hazardous materials may behave differently during pyrolysis, resulting in their elimination, enrichment or transformation in the final product. There is currently no consensus in the scientific community

regarding standardized analytical procedures for biochar characterization. Extensive analyses contribute to a better understanding of thermochemical transformations that take place during pyrolysis, providing support to the consumers on the use of a specific biochar for each particular agro-ecosystem. For this reason, there is a urgent need for simple analytical methods to obtain a " fingerprint " of each biochar. Fourier transform infrared (FT-IR) spectroscopy is a commonly applied technique to distinguish the main functional groups of organic matter such as carbohydrates, lignin, cellulose, lipids and proteins. In recent years, FT-IR spectroscopy has become a powerful technique for the characterization of biochar (Cantrell et al. 2012). However, this technique may not provide structural information on char produced at high pyrolysis temperature because the carbon formation produces weak signals in the FT-IR spectral range. Hyperspectral imagery is an emerging technique that combines conventional imaging and spectroscopy to obtain both spatial and spectral information from each pixel (Badireddy et al. 2012; Elmasry et al. 2012). It measures reflectance in a spectral range from the visible to the short-wave infrared region, and it has been recently found to be suitable and powerful for inspecting the quality and safety of food and agricultural products (Zhang et al. 2012). Currently, there are no applications of this technique to biochars. The aims of this paper were to characterize the chemical – physical, structural and morphological properties of biochars produced from biowastes, to investigate the effect of pyrolysis temperature on these properties, and to evaluate the potential contribution of hyperspectral imaging in improving biochar characterization.

Methodology

Feedstocks

Five feedstocks were collected from plants and experimental farms located in Veneto Region, Northeast Italy: (i) sewage sludge digestate (SS) from an anaerobic digestion plant treating urban wastewater; (ii) municipal organic waste digestate (MW) from a biogas plant that treats the organic fraction of municipal waste; (iii) cattle manure and silage digestate (CD) from a biogas plant that uses cattle manure mixed with silage maize (30 % c.a.); (iv) dry poultry litter (PL) from Italpollina® Italpollina SpA, Verona; and (v) vineyard pruning residues (PR) from the University farm. Their reuse for agronomic purposes is regulated by EU Directives (e.g. Nitrate Directive 91/EEC No. 676 1991) and Italian laws (Dlgs. 27/03/2000 2000; DM 7/4/2006 C 2006; Dlgs. 152/2006 2006) that set limitations for their disposal. Feedstocks were dried overnight at 65 °C until the initial moisture (ranging from 40 to 90 %) dropped to less than 7 % (except for dry poultry litter, moisture content 12 %) and then ground to a particle size of less than 2 mm.

Biochar production

The samples were pyrolyzed in lid-covered porcelain crucibles (Haldenwanger 79MF) in a muffle furnace, preheated at 100 °C, to a highest heating temperature of 250, 350, 450 and 550 °C with a heating rate between 16 and 19 °C/min and a residence time of 1 h. The crucibles were then moved with the lids on and left to cool at room temperature to prevent any loss in homogeneity due to accidental combustion. The biochar produced was weighted and stored in air-tight Falcon vials prior to further analysis. Ground and sieved biochar samples (500 μm) were used for chemical analysis.

Chemical analysis

Elemental analyses were carried out on biochars sieved at 500 µm. The total C, N and S contents were determined by combustion with an Elementar varioMACRO apparatus (Elementar Americas Inc., Mt. Laurel, NJ) and the metal concentration by using inductively coupled plasma – optical emission spectroscopy (ICP – OES) (Spectro Arcos,Ametek, Kleve, Germany). All samples were digested with 5 ml concentrated HNO_3 (67 % w/w, Suprapur Merck) and 3 ml $HClO_4$ (65 % w/w, Suprapur Merck).

The pH and electrical conductivity (EC) of biochar samples sieved at 2 mm were measured in a suspension (1:20 w/v) in deionized water by shaking at 70 rpm for 1 h. Ash was measured as the weight loss after heating for 8 h at 550 °C (Wiedner et al. 2013). All measurements were performed in triplicate.

Spectral and morphological analyses

Fourier transform infrared spectroscopy

Infrared spectral acquisition was performed on all feedstock and biochar samples by using a Nicolet 5700 FT-IR equipped with a diamond attenuated total reflectance (ATR) accessory and a DTGS detector (Nicolet, Madison, USA). The total number of scans averaged for each spectrum was 100 with a 4-cm^{-1} resolution. The background spectrum was acquired in air. Baseline correction and smoothing of spectra were obtained with Grams/386 spectral software (Galactic Industries,Salem, NH).

Hyperspectral imagery with enhanced dark-field microscopy

Ground biochar samples (500 µm) were visualized, in air and at room temperature, via their light scattering using an enhanced dark-field illumination system (CytoViva, Auburn,AL) attached to an Olympus microscope. The system consisted of a CytoViva 150 dark-field condenser in place of the microscope ’s original condenser, attached via a fibre optic light guide to a Solarc 24-W metal halide light source (Welch Allyn, Skaneateles Falls, NY). Improved optical performances are obtained by pre-aligned Koehler and the main feature of Critical illumination. A ×100 oil objective with an iris (Olympus

UPlanAPO fluorite, N.A. 1.35 – 0.55) was integral to the system. Spectral data within each pixel of the scanned field of view were captured with a CytoViva spectro-photometer and integrated CCD camera. The visible near-infrared spectrophotometer operates in the range 400 – 1000 nm. Spectral data were analysed by using the CytoViva Hyperspectral analysis software program (ENVI 4.4 and ITT Visual Information Solutions). Image processing and analysis involved the building of spectral libraries (spectral endmembers). The spectral endmembers were obtained by the selection of a region of interest on the scanned sample. Finally, Spectral Angle Mapper (SAM) was used to measure the similarity between the image pixels and endmember pixels.

Scanning electron microscopy

Dry samples of feedstocks and their pyrolysis products at 350 and 550 °C were mounted on aluminium stubs with silver glue and coated with gold-palladium film using an ion sputtering unit Balzer MED 010 (Balzers Union, Ltd, Balzers, Liechtenstein). The samples were observed under a Philips SEM 515 scanning electron microscope (Philips, Eindhoven, The Netherlands) at 7 Kv, and the pictures taken with a Nikon 5400 Coolpix digital camera (Nikon, Chiyoda-ku, Tokyo,Japan).

Physical analysis

Physical characterization was done on the 2 mm fraction. Specific density was determined using a helium pycnometer (Micro Ultrapyc 1200e, Quantachrome) (Lowell et al. 2004). Specific surface area was determined using N_2 and CO_2 sorption data obtained with a Sorptomatic 1990 after degassing of the sample at 105 °C overnight. External surface area (pores > 1.5 nm) was obtained from the linear part of the N_2 isotherm (at 77 K) using the Brunauer – Emmett – Teller theory (between pressure p/p_0 0.05 and 0.25). Internal surface area (including pores < 1.5 nm) was obtained using the Dubinin – Raduskevich method from the CO_2 adsorption isotherm. Mesopores (diameter between 2.6 and 50 nm) from N_2 isotherms were obtained using Horwath and Kawazoe's method (Horvath and Kawazoe 1983);

micropores from N_2 (0.8 – 2.6 nm) and CO_2 (0.5 – 0.8 nm) sorption data were obtained using the B.J.H. method (Barrett et al. 1951).

Statistics

CoStat 6.4 (CoHort Software, Monterey, CA, USA) was used to perform a two-way ANOVA using production temperature and feedstock type as a main factors. The normal distribution of data was verified using the Brown – Forsythe test. The Tukey ' s honestly significant difference test was applied to compare the differences between group means.

Results and discussion

Biochar chemical properties

The temperature effect on pH value of PL was particularly relevant (Table 1), as it varied from 6.9 (250 °C) up to 10.2 (550 °C). On the contrary, temperature did not influence the urban waste (SS and MW) pH, which remained neutral in the range of tested temperatures. Our results are not comparable with those described by Hossain et al. (2011) and Mendez et al. (2013) who found a substantial alkalization of biochar yielded from sewage sludge at temperatures over 500 °C. In general, EC showed a U-shaped response with higher values at low and high temperatures, with the exception of PR whose EC decreased with rising temperature. As observed by many authors (Shinogi and Kanri 2003; Cantrell et al. 2012; Hossain et al. 2011), ash content increased with temperature and was higher in the feedstocks with low C content. Char with a high ash percentage might be less suitable for soil amendment with respect to char from low-ash feedstocks because high levels of heavy metals can cause soil pollution (Brewer et al. 2009). Pyrolysis temperature significantly ($p<0.05$) influenced the nutrient content (Table 1). Total N content in the biochars increased with pyrolysis at 350 °C (Table 1). This may be related to the formation of recalcitrant N occurring in hetero-cyclic structures (Knicker 2007). In general, N concentrations decreased as the temperature increased to 550 °C to values lower than those of the initial feedstocks (data not shown). Nitrogen losses at 550° C might be due to cracking of nitrile-N and heterocyclic-N compounds from the dehydrogenation and polymerization of amine-N during pyrolysis (Tian et al.2013). On the contrary, CD and PR exhibited an increase in N concentration. Sulphur content decreased in MW (from 1 to 0.6 %) while an opposite trend was observed in PR. No significant variation for the other biochars was detected. Generally, phosphorus and K contents increased with pyrolysis temperature in all biochars. The increase in P content at 550 °C in CD, PL and PR biochars (over 100 %) was particularly relevant if compared to the P values of the initial feedstocks.

Table 1. *Biochar chemical properties*

Biochar	$pH_{1:20}$	EC	Ash	C	N	S	K	P
		µs cm^{-1}	%		$\%_{db}$ [a]		g Kg^{-1} [a]	
CD								
250	7.9 d	1156bc	8.6 op	52.2 e	1.9 i	0.3 fghi	10.3 fgh	4.5 k
350	8.6 c	691f	14.5 n	60.7 d	2.6 fg	0.3 fghi	17.1 de	7.3 j
450	10.3 a	1070cd	16.6 m	63.2 cd	2.2 hi	0.3 fghi	20.4 cd	7.7 ij
550	10.3 a	1695a	18.6 l	65.9 bc	2.2 hi	0.5 efghi	23.2 c	11.3 h
MW								
250	7.2 efg	1207 b	37.6 h	33.7 gh	4.1 c	1.0 a	5.6 hij	17.8 e
350	7.6 de	275kl	44.2 g	34.8 g	4.0 c	0.9 ab	6.5 hij	20.5 d
450	7.4 ef	362jk	55.1 e	29.4 hi	3.0 e	0.8 abc	8.0 ghij	24.7 b
550	7.1 efg	814e	61.1 c	26.2 ij	2.7 ef	0.6 bcde	8.7 ghij	26.1 a
PL								
250	6.9 fg	402 j	14.0 n	43.7 f	4.1 c	0.4 efghi	22.3 c	8.7 i
350	8.0 d	353jk	25.1 k	51.2 e	5.6 a	0.5 efghi	37.7 b	14.4 g
450	9.9 ab	432 hIj	28.8 j	51.2 e	4.5 b	0.4 efghi	43.2 a	16.4 f
550	10.2 a	419 Ij	32.6 i	51.1 e	3.7 d	0.5 defgh	48.0 a	19.4 d
PR								
250	6.0 h	961 d	3.5 q	48.7 e	0.9 k	0.2 i	4.6 j	1.0 m
350	6.8 g	590 fg	7.4 p	65.9 bc	1.3 j	0.2 hi	9.7 fghi	2.0 lm
450	9.0 c	517 ghi	7.9 p	69.3 b	1.3 j	0.3 efghi	11.7 fg	2.4 l
550	9.7 b	540 gh	9.8 o	75.1 a	1.3 j	0.4 efghi	14.2 ef	3.0 l
SS								
250	6.9 fg	691 f	48.6 f	28.3 i	3.8 cd	0.8 abcd	4.2 j	17.3 ef
350	7.3 efg	92 n	58.1 d	27.5 i	3.6 d	0.6 bcdef	4.4 j	19.6 d
450	7.2 efg	130 mn	67.0 b	22.5 jk	2.8 ef	0.6 cdefg	4.9 ij	21.9 c
550	7.1 fg	210 lm	73.2 a	20.1 k	2.3 gh	0.6 bcdef	4.2 j	23.6 b

Values reported as means (n=3). Different letters within columns indicate significant differences (p<0.05). [a] *Values calculated on a dry basis.*

The use of biochars may be an alternative to mineral fertilization, P being an important element for plant growth. At this phase, it is not possible to determine whether these nutrients are bioavailable. The pyrolysis is a complex process that may influence in diverse ways the availability of elements of soil fertility (Yin Chan and Xu 2009). Heavy metals were retained in the biochars during pyrolysis (Table 2); this is consistent with the fact that some heavy metals volatilize only at high temperatures (> 600 °C) (Kristler et al. 1987). As a result, some heavy metals such as Cu, Pb and Zn in SS, Cu and Zn in MW and Zn in PL exceeded the Italian guidelines for amendants (Dlgs. 27/03/2000 2000) (Table 2). Some authors

reported that these elements are stabilized in biochar (Kristler et al. 1987; Cao and Pawloski 2012), however the long-term soil applications of biochar should be carefully monitored in order to avoid their potential accumulation.

Table 2. *Heavy metals concentration in biochars*

	As	Cd	Cr	Cu	Ni	Pb	Zn
				ppm_{db} [a]			
CD							
250	dl*	dl	6.55 ± 0.1	18.85 ± 1.07	3.72 ± 0.13	15.23 ± 2.86	70.77 ± 1.54
350	dl	dl	7.72 ± 0.3	32.42 ± 2.95	4.36 ± 0.12	6.50 ± 2.25	115.28 ± 3.32
450	dl	dl	7.70 ± 0.03	40.81 ± 6.54	4.75 ± 0.25	3.69 ± 0.27	129.44 ± 3.8
550	dl	0.16 ± 0.08[b]	10.21 ± 1.10	38.89 ± 11.3	5.45 ± 0.21	8.78 ± 1.18	171.49 ± 0.34
MW							
250	4.14 ± 0.56	0.46 ± 0.01	45.01 ± 0.55	170.37 ± 3.23	53.76 ± 0.82	21.51 ± 0.28	407.72 ± ù8.29
350	3.71 ± 036	0.68 ± 0.02	48.81 ± 0.35	203.35 ± 2.01	61.71 ± 0.79	23.91 ± 0.51	480.1 ± 5.6
450	4.56 ± 0.21	0.96 ± 0.11	59.44 ± 0.66	253.61 ± 2.59	76.3 ± 0.73	28.31 ± 0.75	601.63 ± 10.05
550	6.77 ± 0.21	1.13 ± 0.04	64.17 ± 0.19	268.93 ± 0.66	83.42 ± 0.89	30.71 ± 0.45	690.48 ± 4.73
PL							
250	dl	dl	7.67 ± 0.16	62.02 ± 0.39	4.96 ± 0.07	1.28 ± 0.09	315.41 ± 1.55
350	dl	0.16 ± 0.08	11.28 ± 0.13	106.14 ± 0.36	7.86 ± 0.16	1.75 ± 0.18	546.06 ± 3.21
450	dl	0.16 ± 0.08	12.23 ± 0.16	123.241.18	8.53 ± 0.11	1.52 ± 0.1	627.13 ± 1.8
550	dl	0.23 ± 0.01	16.19 ± 0.2	137.56 ± 1.18	10.66 ± 0.16	dl*	772.01 ± 7.41
PR							
250	dl	dl	5.04 ± 0.28	29.82 ± 4.66	2.07 ± 0.04	3.31 ± 0.15	54.1 ± 1.17
350	dl	dl	5.43 ± 0.38	49.32 ± 1.29	2.83 ± 0.15	5.12 ± 0.46	94.74 ± 0.55
450	dl	dl	5.46 ± 0.28	68.53 ± 2.81	2.72 ± 0.25	8.13 ± 1.34	123.67 ± 2.57
550	dl	dl	6.55 ± 0.01	63.63 ± 0.44	2.96 ± 0.08	8.89 ± 1.24	137.48 ± 2.20
SS							
250	13.82 ± 0.28	0.78 ± 0.07	379.71 ± 3.02	337.55 ± 2.48	38.21 ± 0.31	98.78 ± 0.71	819.91 ± 5.01
350	13.39 ± 0.25	1.02 ± 0.03	461.08 ± 2.34	404.61 ± 2.53	47.33 ± 0.42	118.27 ± 0.94	966.521 ± 1.97
450	12.94 ± 0.50	0.98 ± 0.01	516.72 ± 7.08	470.55 ± 4.24	51.45 ± 0.79	141.28 ± 4.92	1090.81 ± 8.18
550	24.28 ± 0.16	1.72 ± 0.01	579.29 ± 2.63	513.86 ± 1.77	56.46 ± 0.35	148.6 ± 0.72	1276.55 ± 3.37

*[a] Values calculated on a dry basis. [b]Values reported as means (n=3) followed by standard error. *Values below detection limit.*

Spectral and morphological properties of biochar

FT-IR characterization

Pyrolysis temperature had an unequivocal effect on chemical properties as supported by other researches (Antal and Grønli 2003). In particular in this experiment, SS and MW showed structural

modifications as the pyrolysis temperature increased from 350 to 550 °C (Figure 1a and b). No considerable structural modification was observed for biochars pyrolyzed at 250 °C. Comparing the biochars heated at 350 °C with initial feedstocks (SS and MW), the formation of a new broad peak could be observed at around 1,596 cm^{-1}, while the peaks around 1520 and 1250 cm^{-1} disappeared. This phenomenon may be due to a deamination and decarboxylation process and the formation of amorphous C in both biochars (SS and MW) (Zhai et al. 2012). The biochars produced at 450 and 550 °C did not differ from one another in the investigated spectral region, being characterized by two broad bands (1596 and 1430 cm^{-1}) assigned to amorphous C formation. It can be inferred that the pyrolysis temperature of 350 °C represents a first step of interest in biochar yield because most decomposition reactions of macromolecules (proteins, carbohydrates) are involved and there is only a slight transformation at higher temperatures. FT-IR spectra of PL and CD biochars heated at 250 °C resulted as being strongly influenced by the temperature (Fig. 1c, d). In fact, both biochars showed a structural modification ascribable to the deamination reaction. The presence of amides associated with PL and CD biochars was supported by the high N content (Table 1). The pyrolysis of PL and CD at 350 °C produced a strong structural transformation and by 450 °C, most of the CD spectral features had been lost and the spectrum had begun to resemble graphite-like carbon. For PL, the peaks attributable to C=C (centred at 1577 cm^{-1}) and C=N functional groups (1495, 1371 and1,320 cm^{-1}) (Xiu et al. 2010) were very intense. These changes might be due to the formation of pyridines which has been commonly observed during manure pyrolysis (Das et al.2009). At 550 °C, the functional groups present in unpyrolyzed PL were not recognizable in char. The PR biochar exhibited a considerable spectral profile change as the pyrolysis temperature increased from 350 to 550 °C (Fig. 1e). In particular, at 350 °C, the biochar lost C=O (1730 and 1237 cm^{-1}) and CH (1370 cm^{-1}) groups, and the lack of the band at 1511 cm^{-1}, assigned to aromatic skeletal vibration of lignin, was probably ascribable to condensation reactions. However, the observed changes would mainly involve hemicellulose and cellulose thermal decomposition that terminates at 400 °C, while lignin decomposes slowly over a much wider temperature range of 180 – 900 °C (Yang et al. 2007). At higher temperatures (450 and 550 °C), the biochar completely lost all the PR features and

the spectra were dominated by typical bands of amorphous C (1579 and 1411 cm^{-1}). In general, all biochar pyrolyzed from 450 to 550 °C became amorphous C.

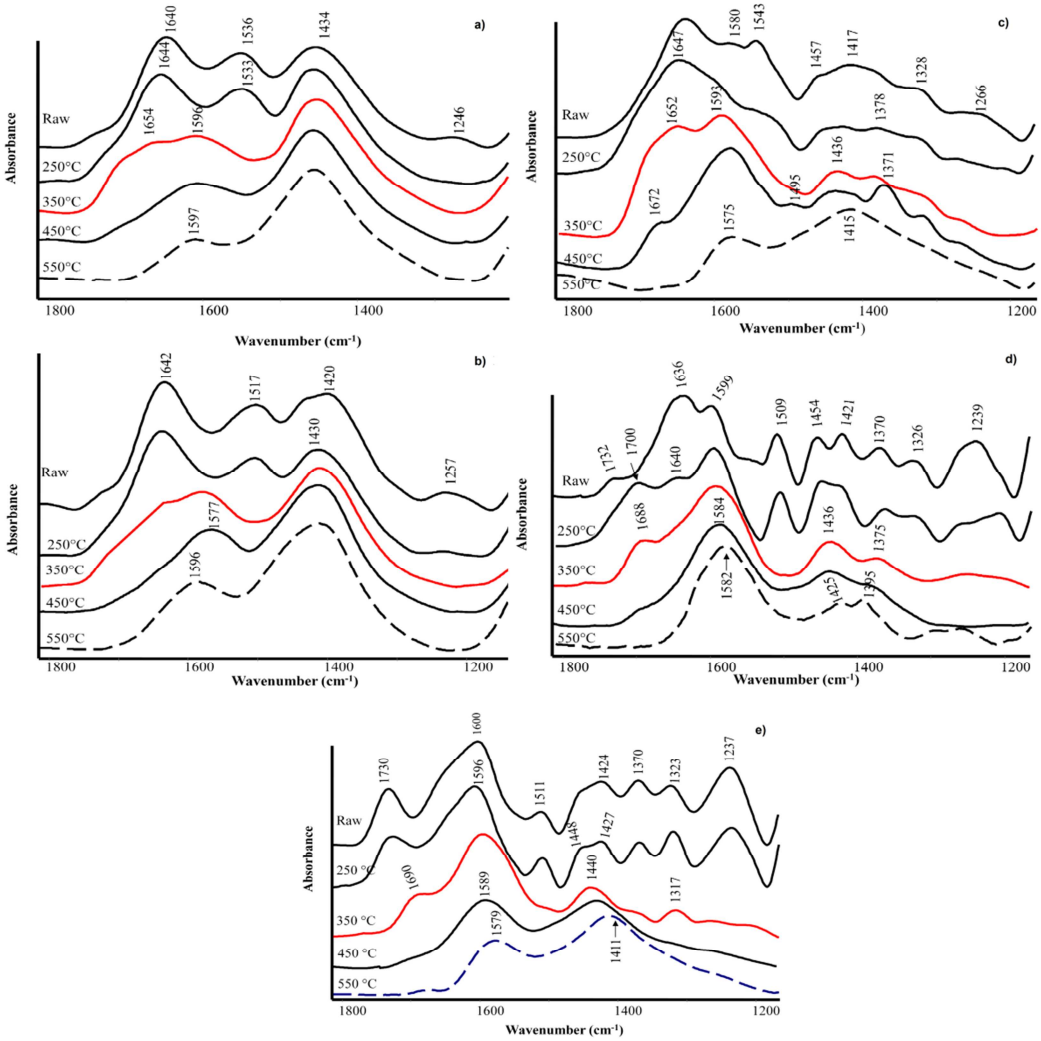

Figure 1. *FT-IR spectra of a) SS, b) MW, c) PL, d) CD and e)PR of raw feedstock and biochars*

Hyperspectral analysis

Hyperspectral analysis showed that the most affected samples were those yielded at 550 °C. The biochars showed a different physical structure depending on the initial composition of the feedstocks. The bright spots in the EDFM image of CD (Fig. 2a), reflecting light more efficiently, indicated the formation of semicrystalline aggregates in this char, whereas amorphous structures prevailed in the other biochars as also supported by FT-IR analysis. Among the seven spectra originated from light scattering of the five samples and identified as characteristic, two (endmembers 1 and 3) give rise to the

main contribution to the total scattering of CD (~80 %) (Fig. 2g), as shown from their spatial distribution on the sample (Fig. 2d).

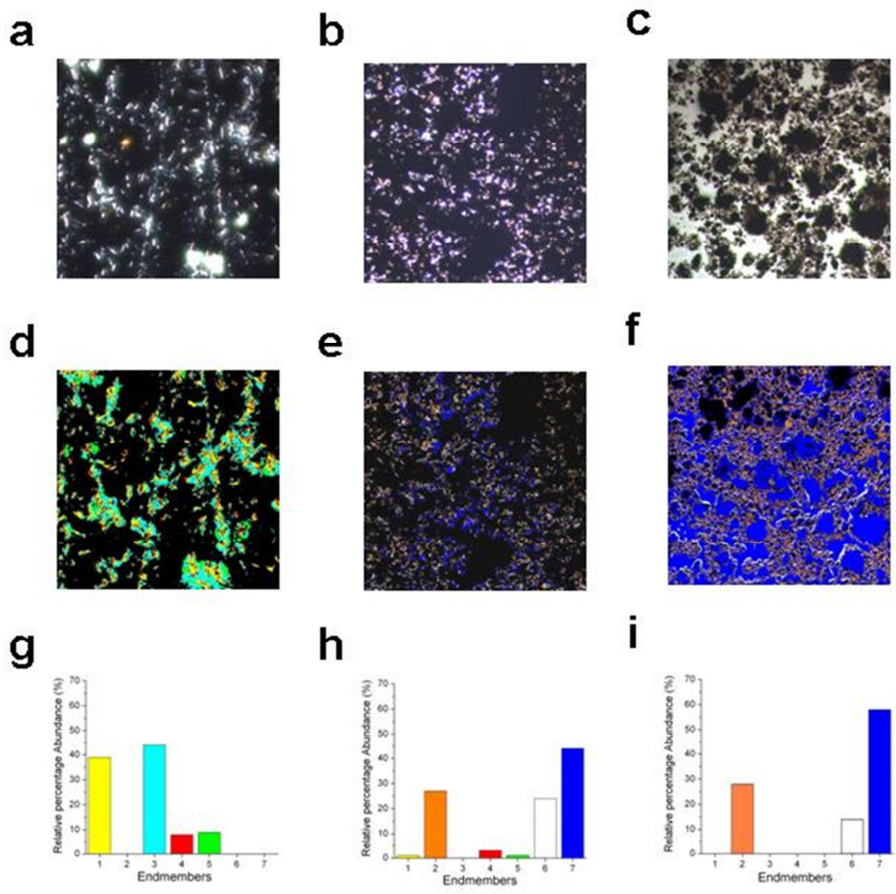

Figure 2. *Spectral mapping of biochars produced at 550 °C placed on glass slides. a – c EDFM images; d – f spectral mapping (coloured areas indicate the matching with the spectral profiles). a), d) Cattle manure mixed with silage digestate (CD); b), e) pruning residues (PR); and c), f) municipal organic waste digestate (MW). Seven main spectra (endmembers) were found and marked with a number from 1 to 7. g – i. Relative percentage abundance of the seven spectral profiles, revealed by the SAM analysis of the hyperspectral images.*

These two spectra may be due to the presence of anaerobic digestion products and can be considered the most representative for this char. On the contrary, other two spectral profiles (endmembers 2 and 7) are characteristic of both PR and MW (~70 and 90 %, respectively) (Fig. 2h, i). This similarity of spectral patterns between the two samples might be attributed to the abundance of hemicelluloses and lignin in the raw feedstocks. The contribution of all seven endmembers was also

found for SS and PL, as shown by the maps displaying the relative distribution of the main spectra by colours (Figure 3).

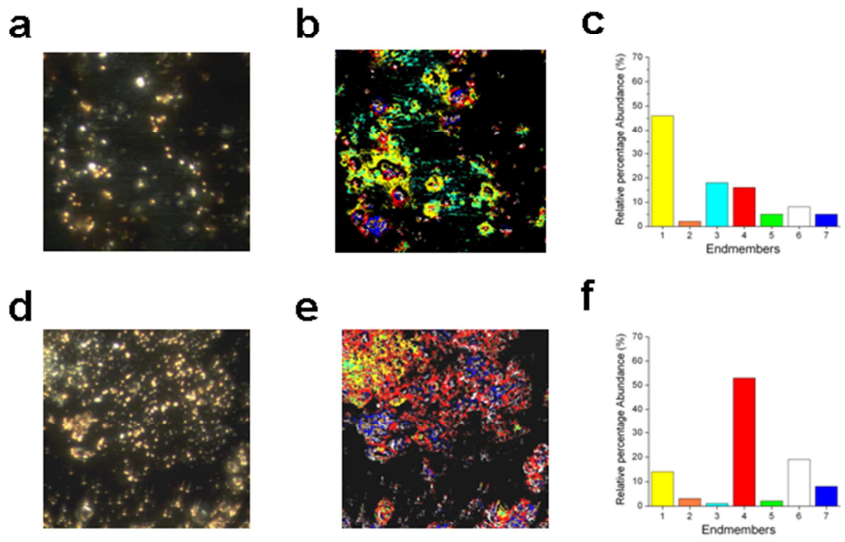

Figure 3. *Spectral mapping of biochar yields at 550 °C deposited onto glass substrate. a), d) EDFM images; b), e): Spectral mapping (coloured areas indicate the matching with the spectral profiles). a) and b): SS. d) and e): PL. Seven main spectra (Endmembers) were found and marked with a number from 1 to 7. c) and f) Relative percentage abundance of the seven spectral profiles, revealed by the SAM analysis of the hyperspectral images.*

Scanning electron microscopy

Scanning electron microscopy (SEM) images of biochars produced at 350 and 550 °C are shown in Fig. 4. CD biochar at 350 °C (Fig. 4a) displayed longitudinal fibrous structures probably arising from the cellulosic structure of maize that can be grouped into fibrous, prismatic and spherical. At 550 °C (Fig. 4b), most of the morphology had changed, as revealed by the irregular surface. Similarly, the image of PR biochar at 350 °C (Fig. 4g) retained the fibrous structures of woody plants mainly composed of individual particles of lignin with polygonal shape and multiple conchoidal fracture surfaces. At 550 °C (Fig. 4h), the fibrous structures were destroyed. The surface texture had become coarse, and the cross-section image showed that the internal texture of the fibre bundles had become sparse. Other regions

showed signs of plastic deformation. MW biochar at 350 °C exhibited a partially smooth surface with irregular porosity (Fig. 4c).

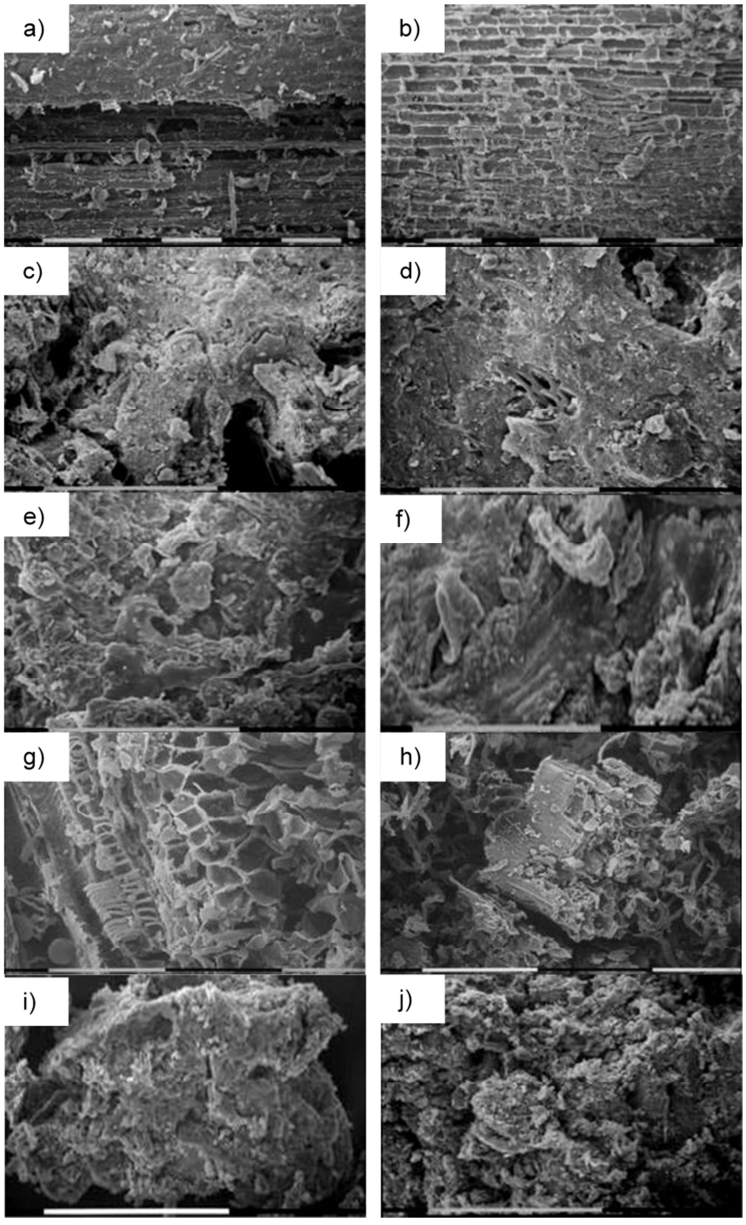

***Figure 4**. Scanning electron micrographs (SEM) of biochars: cattle manure and silage digestate (CD biochar) at 350 °C (a) and 550 °C (b); organic fraction of municipal solid waste digestate (MW biochar) at 350 °C (c) and 550 °C (d); poultry litter (PL biochar) at 350 °C (e) and 550 °C (f); vineyard pruning residues (PR biochar) at 350 °C (g) and 550 °C (h); and sewage sludge digestate (SS biochar) at 350 °C (i) and 550 °C (j). Bars 0.1mm.*

Residues of individual particles of lignin with polygonal shape and multiple conchoidal fracture surfaces were displayed. The biochar morphology had become more complex at 550 °C, reflecting the

heterogeneity of the parent biomass and the depolymerization reaction that takes place during pyrolysis (Fig. 4d). The images of biochars yielded from CD, PR and MW showed clearly visible plant structure residues; this shows that lignin degradation takes place at the highest pyrolysis temperatures (> 550 °C). In addition, the morphological modifications were not supported by functional group changes observed in the FT-IR spectra that were instead dominated by typical bands of amorphous C (1579 and 1411 cm^{-1}). PL biochar at 350 °C (Fig. 4e) exhibited a complex morphology due to the presence of particle aggregations of mineral compounds from chicken manure, such as K and P (Table 1). PL at 550 °C clearly revealed a more compact surface enriched with mineral components (Fig. 4f). The interactions among components of the mixture might affect pyrolysis behaviour of the various constituents and increase the heterogeneity of biochar. SS biochar at 350 °C (Fig. 4i) showed structures resembling nanotube bundles with different particle dispersal of inorganic components as also supported by high metal content (Table 2). At 550 °C, the surface had become rougher and visible pores were limited to some particles (Fig. 4j).

Physical properties

Production temperature had different effects on the surface area (SA) according to the measurement methods (i.e. N_2 and CO_2) (Tab. 3). In general the relationship between SA and temperature was positive as already observed by several other authors (Downie et al., 2009; Keiluweit et al., 2010). However, SA_{N2} showed a non-linear response with sharp increases at 550 °C, while SA_{CO2} increased almost linearly with a higher ratio in C-rich feedstocks. At 550 °C, SA_{N2} was highest in MW (77.72 m^2g^{-1}) and CD (58.60 m^2g^{-1}) and lowest in PL (3.61 m^2g^{-1}). At 250 °C, SA_{N2} showed a narrow range, from 0.5 m^2g^{-1} (PL and PR) to 1.4 m^2g^{-1} (CD). CO_2 surface area was found to be 1.1 to 200 times higher than N_2 surface area, indicating CO_2 ability to penetrate smaller pores (Lowell et al., 2004), but at extremely different levels for different chars. At 550 °C, SA_{CO2} was > 230 m^2g^{-1} for CD and PR (254.3 and 234.1 m^2g^{-1}) and < 84 m^2g^{-1} for chars from urban wastes (SS and MW). Regarding SA_{CO2}, differences between feedstocks at 250 °C were more remarkable than for SA_{N2}, indicating a more complex variability in the pore matrix architecture at

nanoscale (<2.7 nm). The largest CO_2 surface area was found in samples that exhibited the highest C content, as the strong correlation between the two variables ($r = 0.84$; $p<0.05$) suggests. This was maybe due to the conversion from amorphous C to graphene-like forms (Keiluweit et al., 2010), which creates voids in the structure, increasing the microporosity (Ammonette and Joseph, 2009).

Table 3. *Biochar surface area (N_2 and CO_2), total pore volume and average mesopore radius.*

Biochar	SA_{N2}	Meso+MicroPV[a] 0.8-50 nm	SA_{CO2}	MicroPV[b] 0.5-0.8 nm	Specific density
	m^2g^{-1}	cm^3g^{-1}	m^2g^{-1}	cm^3g^{-1}	$g\ cm^{-3}$
CD					
250	1.4	0.003	70.2	0.011	1.3
350	2.2	0.008	128.3	0.025	1.3
450	2.9	0.014	185.9	0.038	1.4
550	58.6	0.065	254.1	0.055	1.5
MW					
250	0.7	0.006	47.9	0.007	1.5
350	5.6	0.045	40.5	0.007	1.7
450	27.3	0.123	62.8	0.011	1.9
550	77.7	0.144	83.6	0.017	2.0
PL					
250	0.5	0.002	36.9	0.004	1.4
350	0.9	0.006	88.9	0.015	1.5
450	2.4	0.020	110.0	0.021	1.5
550	3.6	0.006	151.7	0.032	1.6
PR					
250	0.5	0.002	73.1	0.009	1.1
350	1.3	0.004	118.4	0.022	1.2
450	1.1	0.004	235.5	0.046	1.3
550	19.2	0.043	254.3	0.052	1.4
SS					
250	0.8	0.005	25.7	0.004	1.7
350	2.0	0.012	23.1	0.004	1.9
450	7.2	0.023	36.4	0.007	2.1
550	12.7	0.038	60.0	0.011	2.3

[a]Sum of micropore volume (0.8-2.7 nm) and mesopore volume (2.7-50 nm) calculated from N_2 adsorption data. [b] Micropore volume (0.5-0.8 nm) calculated from CO_2 adsorption data.

The presence of semi-crystalline aggregates was confirmed by previous FTIR and hyperspectral analyses for CD while it was less evident for PR. Pore volumes calculated from N_2 isotherms increased for

all feedstocks according to the rising temperature. The effect was particularly apparent in the transition from 450 °C to 550 °C in biomass-based chars, with 4-fold increments for CD and 9-fold for PR. It is worth noting that both micro and mesopores contributed to the increase of porosity, as highlighted by pore size distributions (Fig. 5a and d). At 550 °C, CD and PR showed a sharp increase in the range 0.5 - 2 nm and 17.3 - 19.3 nm, with the highest peaks in PR corresponding to pore diameter 4.8 - 5.40, 14.0 - 15.6 and 32.7 - 36.4 nm. This suggests an ex-novo formation of pores due to the voids left by physical-chemical degradation of biomass components, as confirmed by both FTIR analysis and SEM images (Fig. 4a, b, d, and e). The other feedstocks showed a similar behaviour, but the structural changes were more gradually distributed over all production temperatures (Fig. 5b, c and e). Pore size distributions obtained from CO_2 isotherms showed a gradual increase in pore volumes (0.5 - 0.8 nm) caused by production temperature for CD, PL and PR (Fig. 6a, c and d). This is confirmed by micropore volume, which was linearly correlated with temperature for all these feedstocks ($r = 0.99; 0.98; 0.95$ $p<0.05$). Urban waste based biochars were shown to be less prone to thermal degradation below 450 °C, with the highest increases in pore volumes at 450 and 550 °C (Fig. 6b and e). Micropores in the range 0.5-0.8 nm resulted as the more relevant component of total porosity in biomass-based chars, being up to 5 times the 0.8-50 nm porosity. On the contrary, the latter was predominant in chars from urban waste (SS and MW) with a shift towards large-pore diameters (mesopores) at 550 °C. Production temperature positively influenced specific density, with the higher values found for MW and SS (2.0 and 2.3 g cm^{-3}, respectively). These values are relatively high if compared to the density of solid graphite (2.25 g cm^{-3}), but they could be explained by a high ash content of chars, as indicated by the high correlation coefficient ($r=0.99$ for MW and $r=0.99$ for SS, $p<0.01$) between this variable and specific density. SEM images (Fig. 4) confirmed the presence of inorganic compounds on SS surface. Anyway, even in the other feedstocks, specific density increased according to the increase of temperature, most likely because of the conversion of low-density disordered carbon to high-density turbostratic carbon (Byrne, 1996; Kercher and Nagle, 2002).

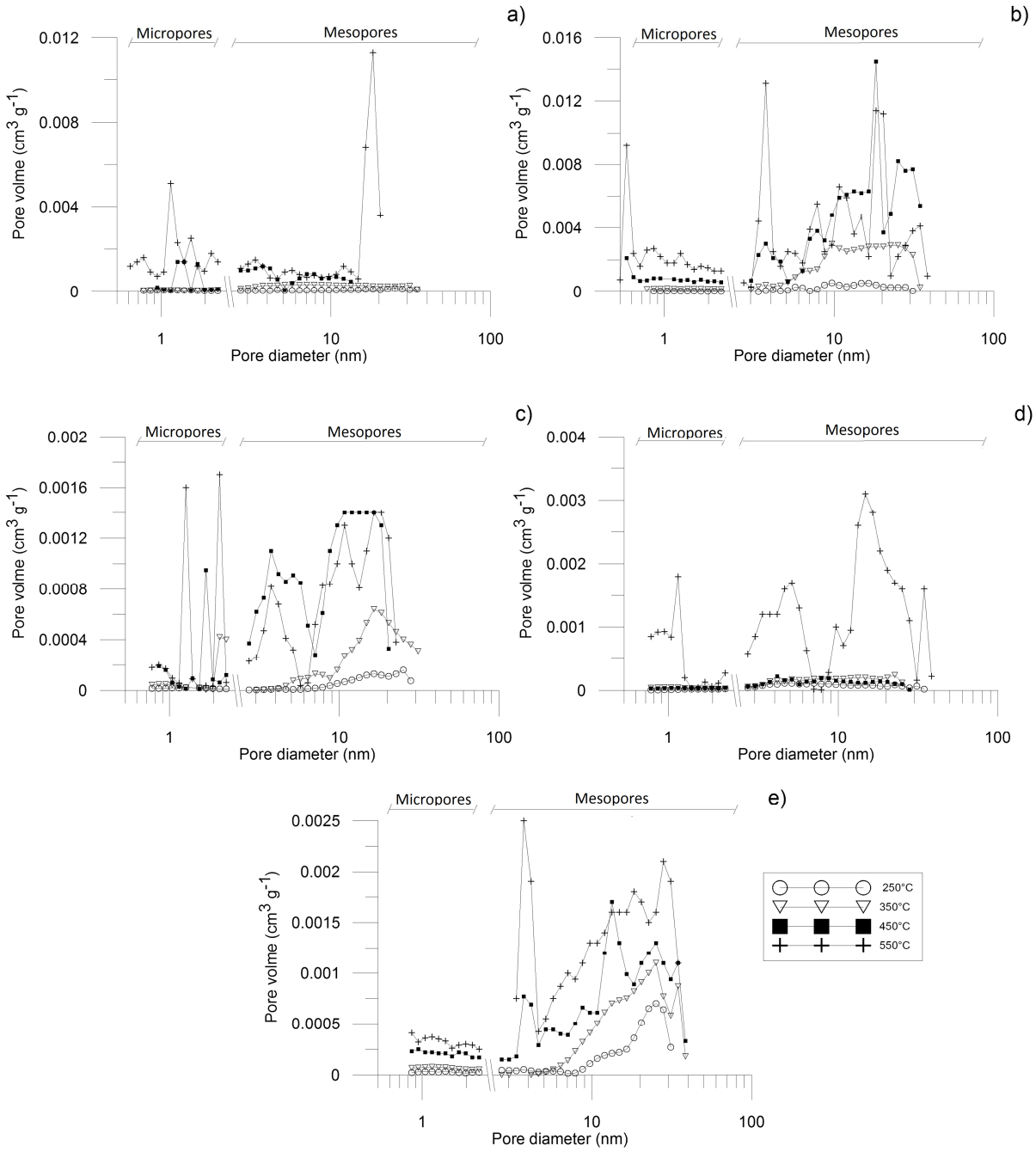

***Figure 5**. Pore size distribution of biochars obtained from N_2 isotherms (Micropores 0.8-2.6nm; Mesopores 2.6-50nm). a) Cattle manure digestate (CD); b) Municipal waste digestate (MW); c) Poultry litter (PL); d) Pruning residues (PR); e) Sewage Sludge (SS).*

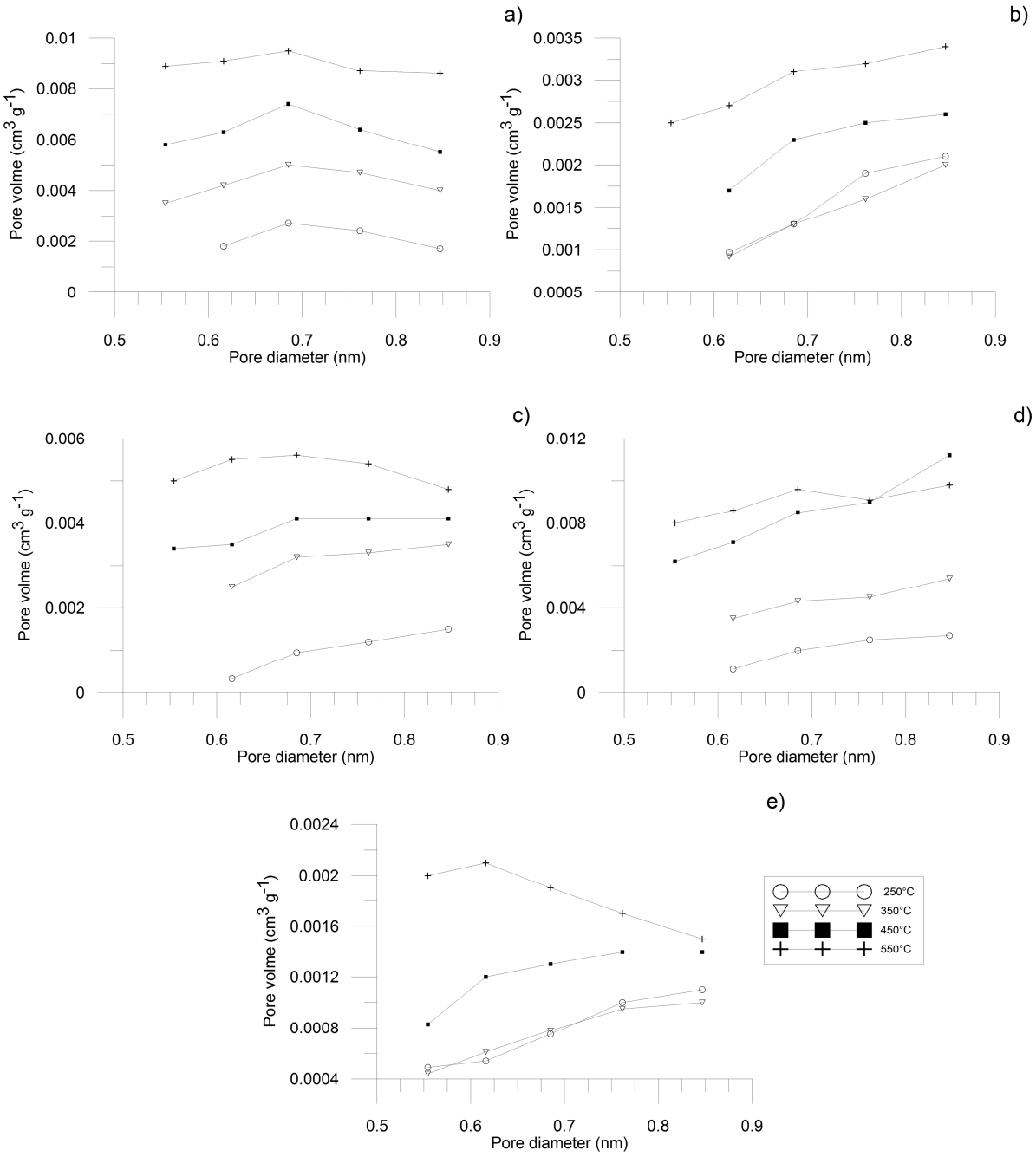

***Figure 6**. Pore size distributions of biochars obtained from CO_2 isotherms (Micropores 0.5-0.8nm). a) Cattle manure digestate (CD); b) Municipal waste digestate (MW); c) Poultry litter (PL); d) Pruning residues (PR); e) Sewage Sludge (SS).*

Conclusions

Biochars derived from different feedstocks (SS, MW, CD, PL and PR) have contrasting physical and chemical properties depending on temperature. Pyrolysis of these feedstocks generates biochars with predominately aromatic carbon structures rich in inorganic minerals, as shown by FT-IR and SEM. These techniques have provided the structural and morphological information needed to reliably track changes in char structure. Some partially pyrolyzed biomass (in poultry litter and cattle manure digestate) may still be recognizable at low temperature (350 °C), while most char morphology changes as the pyrolysis intensifies (550 °C). The presence of N-containing compound like pyridine is only found in poultry litter biochar. Biochars showed a wide variability in surface area and pore size distribution that increased by the temperature. Each one has displayed a distinctive hyperspectral image related to its chemical composition and inherent physical structure, scattering electromagnetic energy in distinctive patterns at specific wavelengths. This technique can thus be used to make a direct assessment of different components simultaneously, but also to locate their spatial distribution. Thus, the results demonstrate that biochars exhibited specific physical – chemical properties according to feedstock and temperature, and therefore it is not possible to identify an " ideal " biochar able to improve both soil nutrient content and structure. Moreover, the long-term soil applications of biochar should be carefully monitored in order to avoid the potential accumulation of heavy metals. Finally, the application of different spectroscopic, morphological and physical techniques presented in this paper can be used in studies for rapid screening of feedstocks and their pyrolysis products.

References

Ábrego, J., Arauzo, J., Sánchez, J. L., Ponzalo, A., Cordero, T., Rodríguez-Mirasol, J. (2009). Structural changes of sewage sludge char during fixed bed pyrolysis. *Ind Eng Chem Res 48*: 3211-3221 doi: 10.1021/ie801366t

Amonette, J., Joseph, S. (2009). Characteristics of biochar: Micro chemical properties. In J. Lehmann and S. Joseph (eds.) Biochar for environmental management: Science and technology. Earthscan, London. pp. 33-52

Antal, M. J., Grønli, M. (2003). The art, science and technology of charcoal production. *Ind Eng Chem Res 42*: 1619-1640 doi: 10.1021/ie0207919.

Badireddy, A. R., Wiesner, M. R., Liu, J. (2012). Detection, characterization, and abundance of engineered nanoparticles in complex waters by hyperspectral imagery with enhanced dark field microscopy *Environ Sci Technol 46*: 10081-10088 doi: 10.1021/es204140s.

Barrett, E. P., Joyner, L. G., Halenda, P. P. (1951). The determination of pore volume and area distributions in porous substances. I. Computations from nitrogen isotherms. *J Am Chem Soc 73*: 373-380 doi: 10.1021/ja01145a126.

Biederman, L. A., Harpole, W. S. (2013). Biochar and its effects on plant productivity and nutrient cycling: A meta-analysis. *GCB Bioenergy 5*:202-214 doi:10.1111/gcbb.12037.

Brewer, C. E., Schmidt-Rohr, K., Satrio, J. A., Brown, R. C. (2009). Characterization of biochar from fast pyrolysis and gasification systems. *Environ Prog Sustain Energy 28*:386-396 doi: 10.1002/ep.10378.

Byrne, C. (1996). Polymer, Ceramic, and Carbon Composites Derived from Wood, PhD thesis. The Johns Hopkins University, US

Cantrell, K. B., Hunt, P. G., Uchimiya, M., Novak, J. M., Ro, K. S. (2012). Impact of pyrolysis temperature and manure source on physicochemical characteristics of biochar. *Bioresour Technol 107*:419-428 doi:org/10.1016/j.biortech.2011.11.084.

Cao, X., Harris, W. (2010). Properties of dairy-manure-derived biochar pertinent to its potential use in remediation. *Bioresour Technol 101*: 5222-5228 doi.org/10.1016/j.biortech.2010.02.052.

Cao, Y. Pawloski, A. (2012). Sewage sludge-to-energy approaches based on anaerobic digestion and pyrolysis: Brief overview and energy efficiency assessment. *Renew Sust Energ Rev 16*:1657-1665 doi.org/10.1016/j.rser.2011.12.014

Das, D. D., Schnitzer, M. I., Monreal, C. M, Mayer, P. (2009). Chemical composition of acid–base fractions separated from bio-oil derived by fast pyrolysis of chicken manure. *Bioresour Technol 100*: 6524–6532 doi:org/10.1016/j.biortech.2009.06.104.

Dlgs. 152/2006 (2006). Norme in materia ambientale. Gazzetta Ufficialen.88, 11 Aprile 2006

Dlgs. 27/03/2000 (2000). Disposizioni tecniche per l ' aggiornamento degli allegati alla legge n. 748 del 1984, in materia di fertilizzanti. Gazzetta Ufficiale n. 149, 28 Giugno 2000

DM 7/4/2006 C (2006). Criteri e norme tecniche generali per la disciplina regionale dell ' utlizzazione agronomica degli effluenti di allevamento, di cui all ' articolo 38 del decreto legislativo 11 Maggio 1999, n.152. Gazzetta Ufficiale n.109. 12 Maggio 2006

Downie, A., Crosky, A., Munroe, P. (2009). Physical properties of biochar. In J. Lehmann and S. Joseph (eds.) Biochar for environmental management: Science and technology. Earthscan, London. pp. 13-29

EEC No. 676 (1991). Council directive 91/676/EEC of 12 December 1991 concerning the protection of waters against pollution causedby nitrates from agricultural sources

Elmasry, G., Kamruzzaman, M., Sun, D. W., Allen, P. (2012). Principles and applications of hyperspectral imaging in quality evaluation of agro-food products: A review. *Crit Rev Food Sci Nutr* 52:999-1023 doi: 10.1080/10408398.2010.543495

Gaskin, J. W., Steiner, C., Harris, K., Das, K. C., Bibens, B. (2008). Effect of low-temperature pyrolysis conditions on biochar for agricultural use. Trans ASABE 51:2061-2069

Horvath, G. Kawazoe, K. (1983). Method for the calculation of effective pore size distribution of molecular sieve carbon. *J Chem Eng Jpn* 16:470- 475

Hossain, M. K., Strezov, V., Yin Chan, K., Ziolkowski, A., Nelson, P. F. (2011). Influence of pyrolysis temperature on production and nutrient properties of wastewater sludge biochar. *J Environ Manage 92:* 223-228 doi: org/10.1016/j.jenvman.2010.09.008.

Jeffery, S., Verheijen, F. G. A., van der Velde, M., Bastos, A. C. (2011). A quantitative review of the effects of biochar application to soils on crop productivity using meta-analysis. Agric Ecosyst Environ 144:175 – 187

Jeffery, S., Bezemer, T. M., Cornelissen, G., Kuypert, T. W., Lehmann, J., Mommer, L., Sohi, S. P., Van De Voordet, F., Wardle, D. A., Van Groenigen, J. W. (2013). The way forward in biochar research: targeting trade-offs between the potential wins. GCB Bioenergy 11 – 13, doi: 10.1111/gcbb.12132

Keiluweit, M., Nico, P. S., Johnson, M. G., Kleber, M. (2010). Dynamic molecular structure of plant biomass-derived black carbon (biochar). *Environ Sci Technol 44*:1247-1253 doi: 10.1021/es9031419.

Kercher, A. K., Nagle, D. C. (2002). Evaluation of carbonized medium-density fiberboard for electrical applications. *Carbon 40*: 1321–1330 doi: 10.1016/S0008-6223(01)00299-8

Knicker 2007

Kristler, R. C., Widmer, F., Brunner, P. H. (1987). Behavior of chromium, nickel, copper, zinc, cadmium, mercury, and lead during the pyrolysis of sewage sludge. *Environ Sci Technol 21*:704–708 doi: 10.1021/es00161a012.

Lehmann, J. Joseph, S. (2009). Biochar for environmental management: science and technology. Earthscan, London.

Lowell, S., Shields, J. E., Thomas, M. A., Thommes, M. (2004). Characterization of porous solids and powders: surface area, pore size and density. Springer-Kluwer Academic Publishers, Dordrecht. pp 152-156.

Mendez, A., Gómez, A., Paz-Ferreiro, J., Gascó, G. (2013). Effects of sewage sludge biochar on plant metal availability after application to a Mediterranean soil. *Chemosphere 89* (2012) 1354–1359 doi: 10.1016/j.chemosphere.2012.05.092

Ro, K. S., Cantrell, K. B., Hunt, P. G. (2010). High-temperature pyrolysis of blended animal manures for producing renewable energy and value-added biochar. *Ind Eng Chem Res 49*: 10125–10131 doi: 10.1021/ie101155m.

Shackley, S., Sohi, S. (2010). An Assessment of the Benefits and Issues Associated with the Application of Biochar to Soil. Edinburgh: UK Biochar Research Centre

Schmidt, M. W. I., Torn, S., Abiven, S., Dittmar, T., Guggenberger, G., Janssens, A. I., Kleber, M., Kogel-Knabner, I., Lehmann, J. D. A., Manning, C., Nannipieri, P., Rasse, D. P., Weiner, S., Trumbore, S. E. (2011). Persistence of soil organic matter as an ecosystem property. *Nature 478*: 49-56 doi:10.1038/nature10386.

Shinogi, Y., Kanri, Y. (2003). Pyrolysis of plant, animal and human waste: physical and chemical characterization of the pyrolytic products. *Bioresour Technol 90*: 241-247 doi: 10.1016/S0960-8524.

Spokas, K. A., Cantrell, K. B., Novak, J. M., Archer, D. A., Ippolito, J. A., Collins, H.P., Boateng, A. A., Lima, I. M., Lamb, M. C., McAloon, A. J., Lentz, R. D., Nichols, K. A. (2011). Biochar: A synthesis of its agronomic impact beyond carbon sequestration. *J Environ Qual 41*:973-989. doi: 10.2134/jeq2011.0069

Tian, Y., Zhang, J., Zuo, W., Chen, L., Cui, Y., Tan, T. (2013). Nitrogen conversion in relation to NH3 and HCN during microwave pyrolysis of sewage sludge. Environ Sci Technol 47:3498 – 3505

Verheijen, F., Jeffery, S., Bastos, A. C., van der Velde, M., Diafas, I. (2010). Biochar application to soils. A Critical Scientific Review of Effects on Soil Properties, Processes and Functions. Luxemburg: European Commission Joint Research Centre. Institute for Environment and Sustainability.

Wiedner, K., Rumpel, C., Steiner, C., Pozzi, A., Maas, R., Glaser, B. (2013). Chemical evaluation of chars produced by thermochemical conversion (gasification, pyrolysis and hydrothermal carbonization) of agro-industrial biomass on a commercial scale. *Biomass and Bioenergy 59*:264 doi: org/10.1016/j.biombioe.2013.08.026.

Xiu, S., Shahbazi, A., Wang, L., Wallace, C. W. (2010). Supercritical ethanol liquefaction of swine manure for bio-oils production. *Am J Eng Appl Sci 3*: 494-500 doi: 10.1016/j.jaap.2010.02.011

Yang, H. P., Yan, R., Chen, H. P., Lee, D. H., Zheng, C. G. (2007). Characteristics of hemicellulose, cellulose and lignin pyrolysis. *Fuel 86*: 1781-1788 doi: 10.1016/j.fuel.2006.12.013.

Yin Chan, K., Xu, Z. (2009). Biochar: nutrient properties and their enhancement. In In J. Lehmann and S. Joseph (eds.) Biochar for environmental management: Science and technology. Earthscan, London. pp. 67-81

Zabaniotou, A., Stavropoulos, G., Skoulou, V. (2008). Activated carbon from olive kernels in a two stage process: Industrial improvement. *Biores Technol 99*:320-326 doi: 10.1016/j.biortech.2006.12.020

Zhai, Y., Peng, W., Zeng, G., Fu, Z., Lan, Y., Chen, H., Wang, C., Fan, X. (2012). Pyrolysis characteristics and kinetics of sewage sludge for different sizes and heating rates. *J Therm Anal Calorim 107*:1015-1022 doi:10.1007/s10973-011-1644-0

Zhang, R., Ying, Y., Rao, X., Li, J. (2012). Quality and safety assessment of food and agricultural products by hyperspectral fluorescence imaging. J Sci Food Agric 92:2397 – 2409

Chapter III

Long-term crop residue effects on crop productivity and soil properties

Background and objectives

The use of crop residues for bioenergy production has gathered a lot of interest in recent years. It has been estimated that this practice, by substituting the use of fossil fuels, is more effective in mitigating climate change than residues use for carbon sequestration in soil (Powlson et al., 2011a; Cherubini and Ulgiati, 2010). However, these evaluations need to consider residue possible effects on other soil properties (such as structure and water dynamics) and on crop yield (Lal, 2005), which are still poorly understood. Yields are reported to generally increase by >10% as a consequence of residue incorporation, and this seems to be mainly due to an increase in nitrogen use efficiency and in water retention. However these mechanisms are deeply influenced by meteorological conditions and are expected to achieve different intensities in soils with contrasting characteristics. Thus, in these regards the effectiveness of residue use is still a matter of debate. In addition, organic carbon accumulation as a result of residue inputs risks to be widely underestimated in short term studies, since the peak in their mineralisation is expected to be between 1 to 3 months after their incorporation (Abiven et al., 2009). Accordingly, longer periods are required for the effects to be measurable. Given this complexity, long-term field experiments appear to be the more suitable tools to investigate these dynamics and develop effective management practices (Richter et al., 2007). Organic inputs have demonstrated to interact with soil pore architecture at different scales (Dal Ferro et al., 2013). Nonetheless, most research regarding the long-term effects of organic input on the soil pore network focused on intra-aggregate structure (e.g. Wuest, 2007; Paul et al., 2013; Zhang et al., 2014; Villamil et al., 2015), without considering inter-aggregate porosity (i.e. macropores). Macropores play a pivotal role in several soil processes, e.g. water and biogeochemical cycles (Jarvis, 2007) and gas exchange with the atmosphere (Deurer et al., 2009). Moreover they are an efficient indicator of soil structure dynamics, as they are extremely sensitive to different types of stresses (Sumner, 1999). As already highlighted by previous papers (e.g., Dal Ferro et al., 2014; Cnudde et al., 2009), the combined use of mercury intrusion porosimetry (MIP) and X-ray computed microtomography (µCT) is a promising way to analyse the

complexity of the soil pore network at a scale ranging from 0.01 µm up to several mm. MIP can detect pores < 100 µm, which are important for water retention mechanisms as well as for the physical protection of organic matter (Lützow et al., 2006). µCT is particularly useful for identifying the 2D and 3D macropores and cracks morphology (e.g. pore orientation, fractal dimension, shape and connectivity) that are mainly involved in water infiltration and gas exchanges. However, these two methods do not cover the nanoporosity below 0.01 µm which plays a major role in the physical-chemical interaction between soil matrix and solutes (Lal and Shukla, 2004). In this context, gas adsorption methods are valuable analytical tools to fully characterise crop-residue induced changes in soil porosity at the nanometre scale. At present, few studies have tested the effects of residue incorporation on soil hydraulic properties. Generally they are assumed to increase water retention due to the reduction in bulk density and the consequent increase in soil porosity (Lal, 2009). Residues are also supposed to increase soil aggregation and aggregate stability (Blanco-canqui & Lal, 2009; Hammerbeck et al., 2012), properties which further improve soil hydrological functions. These studies however describe residue influence on soil hydraulic functions only by means of indirect indicators, as a consequence the direct measurement of water retention curves and water conductivity in absence and in presence of residue inputs represents a still unexplored topic which would surely give new insights on their behaviour. This part of the project thus aims at answering the following questions: i) Is long-term incorporation of crop residues effective in increasing yield and nitrogen use efficiency of different crops?; ii) Are residues useful in maintaining and/or increasing the carbon stocks of contrasting soils? and iii) Does the possible increase in soil organic carbon caused by residue incorporation influence other important soil properties such as pore architecture and hydrology?

Methodology

Long-term field experiment and plant sampling

The long-term experiment is located on the Experimental Farm of the University of Padova (45°21' N; 11°50' E, 6 m a.s.l.). The climate is sub-humid with an annual mean rainfall of 825 mm. The rainfall shows inter-annual variability, with peaks in June and October (100 and 90 mm). The lowest values are registered in winter (50 - 60 mm). The temperature reaches minimum values in January (averaging 2.3 °C) and maximum between July and August (average 22.4 °C). Reference evapotranspiration (ET_0) is 945 mm, with maximum values in July (5 mm d^{-1}). ET_0 exceeds rainfall from April to September. During the experimental period (1970-2013) mean annual rainfall followed an oscillatory pattern, without a clear long-time tendency. The years 1972 and 1996 were the most rainy, with 1019 and 1014 mm, respectively. On the opposite, the most dry year (617 mm) was 1983. A clear increase (+2.1°c) in average maximum temperatures is evident in the last 10 years of experimentation, with peaks in years 1997, 2000 and 2001. The coldest year was 1980 with an average maximum temperature of 15.1°C. The experiment started in 1970 and is constituted by 108 4 m^2 lysimeters, 80 cm deep, with three types of soil: sandy-loam (SNDL), sandy (SND) and clay (CL). The main physical and chemical characteristics of the soils at the beginning of the experiment are listed in Table 1. The sandy-loam soil is classified according to FAO-UNESCO as a Fluvi-Calcaric Cambisol and contains prevalently dolomite (35%) and quartz (28%), with considerable amounts of feldspar (15%) and mica (13%). The other two soils were brought from two locations in the Veneto region: the clay soil from the south-western plain, and the sandy soil from the central coastal area. The clay soil, classified as a Gleyi-Vertic Chernozem (FAO-UNESCO, 2008), has higher montmorillonite (16%) than the other soils, and a considerable presence of mica (19%) and dolomite (15%). The sandy soil (Calcaric Arenosol, FAO-UNESCO, 2008) contains predominantly quartz and feldspar and a significant amount of dolomite (16%). The original soil profiles were reconstructed in the lysimeters. The experimental design is a randomized block with three replicates.

***Table 1**. Main physical and chemical properties of the soils at the beginning of the experiment (1970).*

	Clay	Sandy-loam	Sandy
Sand (2-0.05 mm) %	40.6	57.1	98.8
Silt (0.05-0.002 mm) %	18	23.7	0
Clay (<0.002 mm) %	41.4	19.2	1.2
pH (H_2O)	7.7	7.8	8.4
SOC % [a]	1.06	0.62	0.05
Total $CaCO_3$ %	6.2	30.8	22.9
P_2O_5 labile (g Kg^{-1})	5.29	1.24	1.19
P_2O_5 ass. (mg Kg^{-1}) [b]	59	23	19
K_2O exc. (mg Kg^{-1}) [c]	1.1	4.6	1.9
N tot (g Kg^{-1})	1.7	0.9	0.1

[a]Rotini method; [b] Ferrari method; [c] Exchangeable K_2O with 25% $NaNO_3$ pre-treatment.

Until 1987, the trial involved a biennial maize-wheat rotation, subjected to three nitrogen application rates combined with four types of crop residue management (residues removal, incorporation of the wheat straw, incorporation of the corn stalks and incorporation of both wheat straw and corn stalks).

***Table 2.** Description of the experimental treatments in the long-term field experiment*

Period	Crop rotation	Residue management types	Fertilization doses (Kg N ha^{-1})
1970-1987	Biennal Maize-Wheat rotation	Residue removal Incorporation of corn stalks Incorporation of wheat straw Incorporation of stalks+straw	0, 100, 200 for maize 0, 80, 160 for wheat
1987-2013	Free Maize-Wheat rotation including sugarbeet, potato and tomato	Residue removal Residue incorporation	0, 50, 10, 200, 300, 400

From 1987 to 2013 a less rigid crop succession based on the quadrennial rotation of wheat, maize, tomato, and sugar beet was adopted. The residue management was simplified, testing only incorporation and removal, and the rates of nitrogen application were increased to six (0, 50, 100, 200, 300, 400 kg N ha^{-1}) in a factorial combination with the residue management types. The experimental treatments are exposed in Table 2. On average, the yearly amount of incorporated residues in non - fertilized plots and in plots receiving 400 kg N ha^{-1} , was 4.69 and 9.09 t dry matter ha^{-1} in clay soil, 4.00

and 7.86 t dry matter ha^{-1} in sandy-loam, and 1.73 and 5.73 in sandy soil. Residues were incorporated after harvest by manually ploughing in the 0-20 cm soil layer. At the end of the growing season, the fresh and dry weights of yield and aerial biomass produced in the entire plot were measured.

Modelling of crop yield data

The long-term trends of biomass production with and without residue incorporation were compared through a Sign test within each of the three soils considered.

The relationships between $N_{applied}$ and yield were studied with a hyperbolic model:

$$Yield = Y_0 + \frac{a \cdot N_{applied}}{1 + \frac{a \cdot N_{applied}}{b}} \quad (1)$$

where Y_0 is the yield without N distribution, a is the initial slope and b is the asymptote of the hyperbola. The asymptotic maximum yield (Y_M) is then equal to Y_0+b.

The effects of residue incorporation can be mainly due to nutritional effects (i.e. rapid mineralization of residues and interception of this amount of nutrients by crop roots) and/or to an improvement of soil characteristics (e.g. increased SOC with possible effects on structure, porosity, and water retention). In the first case it is expected that the potential crop yield is unaffected passing from RR to RI. The effect of residues should then correspond to an increase of N availability, graphically equivalent to a shift towards right of the origin of the graph relating N applied to yield (Fig. 1). If the effect of residues is solely due to their nutrient content an increase of 'Y_0' is then expected and a decrease of both 'a' and 'b', with the maximum yield 'Y_M' remaining constant. On the other hand, if the effect of residues is mediated by changes in overall soil fertility, not directly related to the nutrient effect, Y_M should increase, while the behaviour of the other parameters is not directly predictable.

To directly express the maximum yield as a function parameter, eq. (1) was rewritten as:

$$Yield = (Y_M - b) + \frac{a \cdot N_{applied}}{1 + \frac{a \cdot N_{applied}}{b}} \quad (2)$$

Curves were at first fitted for each 'crop x year' combination separately for each soil and with or without residue incorporation (complex model – modC). Two possible simplifications of this model were then considered: Y_M unaffected by residue incorporation, the other parameters being allowed to change from RR to RI (simplified model 1 – modS1); Same Y_M, a and b parameters independently of residue management (simplified model 2 – modS2)

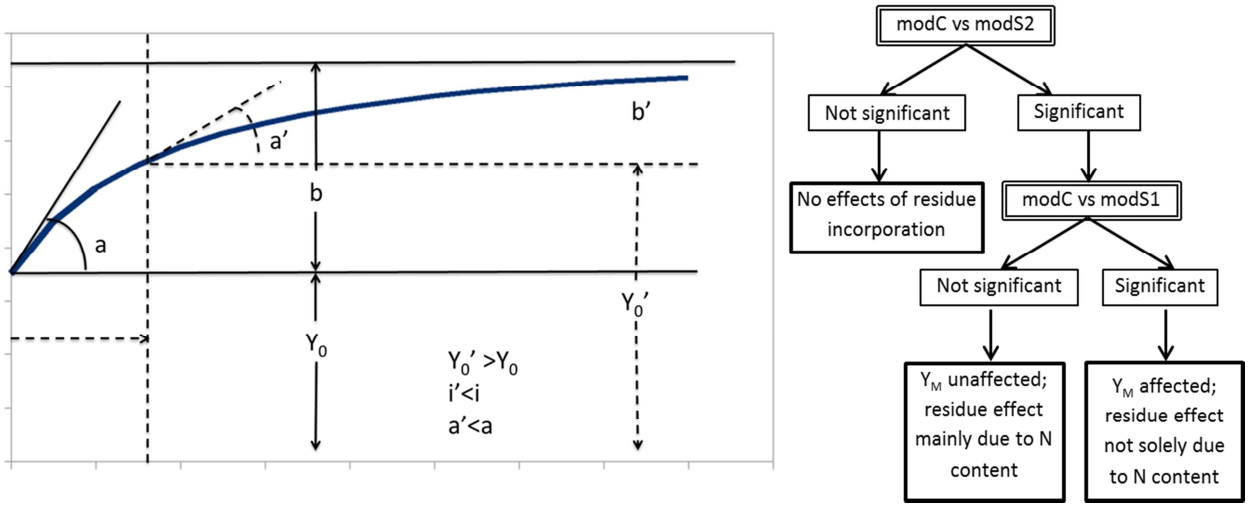

Figure 1. *Scheme of the hyperbolic model used to describe the relationship between Yield and $N_{applied}$ and decision tree for the comparison of crop yield models. 'Y_0' is the yield without N distribution and 'a' and 'b' are the initial slope and asymptote of the hyperbola. The asymptotic maximum yield (Y_M) is equal to Y_0+b. Y_0', a' and b' are the yield without N distribution, the initial slope and asymptote of the hyperbola in the case of a purely nutritional effect.*

The complex model (modC) considered corresponds to the independent fit of each data set (crop x year x soil x residue management combinations). The two simplified models are intended to test the constancy of Y_M (modS1) or the absence of effects of residue incorporation (modS2). Depending on the significance of the comparison between models, it is then possible to determine if residue incorporation affects crop yield and, in this case, if the effect is mainly due to the nutritional input or also depends on the modification of other soil parameters, leading to an increase in the potential yield (Fig. 1).

The reduction of model complexity (i.e. presence of common parameters within a soil for RR and RI) was tested with a partial F test comparing the complex (all the parameter specific) and simplified (some parameter common) models.

To estimate the amounts of N recovered from mineral fertilisation and from residues, the observed N recoveries were fitted with the following equation:

$$N_{rec} = N_0 + \frac{N_{min} \cdot k_{min} \cdot a}{1 + \frac{N_{min} \cdot k_{min} \cdot a}{b}} + \frac{N_{res} \cdot k_{res} \cdot a}{1 + \frac{N_{res} \cdot k_{res} \cdot a}{b}} \quad (3)$$

where N_0 is the amount of N recovered from natural availability for a specific soil-crop combination, N_{min} and N_{res} are the amount of N of mineral fertilisation and of incorporated residues, k_{min} and k_{res} are constants related to nitrogen availability for mineral fertilisers and residues and a and b are regression parameters.

The Nitrogen use efficiency (NUE) for both mineral and organic forms can then be obtained dividing the amount recovered from a specific source by the amount distributed;

$$NUE_{min} = \frac{N_{min} \cdot k_{min} \cdot a}{1 + \frac{N_{min} \cdot k_{min} \cdot a}{b}} \cdot \frac{1}{N_{min}} = \frac{k_{min} \cdot a}{1 + \frac{N_{min} \cdot k_{min} \cdot a}{b}} \quad (4)$$

and:

$$NUE_{res} = \frac{N_{res} \cdot k_{res} \cdot a}{1 + \frac{N_{res} \cdot k_{res} \cdot a}{b}} \cdot \frac{1}{N_{res}} = \frac{k_{res} \cdot a}{1 + \frac{N_{res} \cdot k_{res} \cdot a}{b}} \quad (5)$$

The relative efficiency of N from residues can be obtained as the ratio of the constants related to nitrogen availability for mineral fertilisers and residues:

$$Relative\ efficiency = \frac{k_{res}}{k_{min}} \quad (6)$$

Soil sampling

Disturbed samples were taken in July 2013 from three different points in the plot and bulked to obtain a sample of about 1 kg. Samples were air-dried. During the drying operation the bulk soil was broken along natural fissures into small pieces by gentle hand manipulation. Once dried, a fraction of the sample was ground and sieved at 0.5 mm for organic carbon, total Kjeldhal nitrogen and gas

adsorption analyses. The remainder was sieved at 2 mm for texture and mercury intrusion porosimetry analyses.

In order to measure bulk density and perform X-ray microtomography and hydraulic analysis, undisturbed soil cores (6.1 cm height and 7.2 cm diameter) were taken at the same time from the 7-14 cm layer using a manual hydraulic core sampler (Eijkelkamp, The Netherlands). Samples were then stored at 5 °C. Before X-ray microtomography analyses, each core was reduced in size to 2.5 cm height by 2 cm diameter. Due to the long analysis time the samples analysed were reduced to the treatments receiving the lowest and the highest nitrogen fertilisation (0 and 400 Kg N ha^{-1}, referred to as NO FERT and FERT treatments, respectively). On the contrary, soil organic carbon (SOC) and total Kjeldhal nitrogen (TKN) were measured in all 108 plots and at three different depths: 0-20 cm; 20-50 cm and 50-70 cm.

Soil analysis

Soil organic carbon and total Kjeldhal nitrogen

Total organic carbon (OC) was determined using an elemental analyser (Elementar vario MACRO) after treatment with 10% HCl (ISO 10694). Total Kjeldhal nitrogen was obtained via Kjeldhal digestion (ISO 11261).

Particle size distribution

Soil texture was determined by laser diffractometry using a Malvern Mastersizer 2000 (Malvern Instruments, Malvern, England). Before analysis, samples were soaked for 24h in a 5% (v/v) sodium hexametaphosphate solution to enhance the dispersion of clay particles (Dane and Topp, 2002).

Pore-size distribution, total porosity and pore morpholgy

Soil pore size distribution was analysed from nanometre to millimetre scale by applying different techniques: gas adsorption (N_2) in the range 0.25-50 nm; mercury intrusion porosimetry (MIP) from 0.01

µm to 100 µm; X-ray microtomography (µCT) in the range 25-2500 µm. Total porosities obtained from both MIP (TPV_{MIP}) and µCT ($TPV_{\mu CT}$) were calculated as the sum of the volumetric pore size classes that were measured by the respective methods. By contrast, total porosity from gas adsorption was not calculated because the different methods used to obtain the pore size distributions were not comparable.

Gas adsorption

The Brunauer-Emmett-Teller (BET) surface area was determined using the linear part of the N_2 isotherm (between pressure p/p_0 0.05 and 0.35) obtained with a Sorptomatic 1990 at a temperature of -195.15 °C, after degassing the sample at 105 °C overnight. Pore size distribution (PSD_{N2}), including pores between 0.25 and 50 nm, was calculated with B.J.H. method (Barrett et al., 1951) in the range 2-50 nm and Horvath and Kawazoe method (Horvath and Kawazoe, 1983) in the range 0.25-2 nm.

Mercury intrusion porosimetry (MIP)

Accessible porosity and pore size distribution within the diameter range of 0.0074-100 µm were measured with a Thermo Finnigan (Waltman, USA) Pascal 140 (3.8-100 µm) and a Pascal 240 (0.0074-15 µm). The pore radius was calculated using the Young-Laplace equation:

$$R = \frac{2\gamma cos\theta}{P} \quad (7)$$

where γ is the surface tension of pure mercury, θ is the contact angle (140°) between mercury and the sample and P is the pressure.

X-ray microtomography

All samples were equilibrated to a matric potential of -3 kPa and then scanned using a Skyscan 1172 X-ray microtomography system (Skyscan, Belgium). Source was set at 100 kV and 100 µA and samples were scanned using a 0.3° angular incremental step, with a 180° rotation. Images were collected using a 16 bit camera (2048 × 1024 pixel) with an exposure time of 2400 ms. Cone beam effect was reduced with a 0.5 mm Al filter. The distance between the source, sample and camera was adjusted to obtain a

final image resolution of 13.62 µm. In order to avoid pixel misclassification that might occur during scanning (Hsieh, 2009), 2D projections were resized using NRecon® software (v 1.6.9.8, Skyscan, Belgium) by means of a 2 × 2 mean filter obtaining a final pixel size of 27.25 µm. Lastly, projections were elaborated using NRecon® to obtain a stack of at least 600 slices in 8-bit depth.

Image processing and analysis

Single slices were filtered to reduce noise and the thresholding was done using Otsu's method (Otsu, 1979). After binarization, black and white objects <5 pixels were removed due to difficulties in their attribution to either porosity or soil matrix (Vogel et al., 2010). Selected volumes of interest (on average 3 cm^3) in the obtained stack of binary images were analysed using CTan® software (v. 1.13.11.0, Skyscan, Belgium). Total porosity was defined as the number of pore voxels divided by the number of total voxels. Pore size distribution was obtained as an average of the local thickness for each voxel representing pores (Ulrich et al., 1999). Local thickness for a point in solid is defined by Hildebrand and Rüegsegger (1997) as the diameter of a sphere that encloses the point and is entirely bounded within the solid surfaces. Degree of anisotropy (DA), i.e. an indicator of the 3D global symmetry of the structure that varies between 0 (total isotropic) and 1 (total anisotropic), was calculated according to the mean intercept length (MIL) method (Harrigan and Mann, 1984). Fractal dimension (FD) was inferred using the Kolmogorov or "box counting" method, and connectivity was obtained following the Euler-Poincaré equation divided by the volume analysed to provide a more comparable measure of "connectivity density" (CD):

$$CD = \frac{(\beta_0 - \beta_1 + \beta_2)}{VOI} \quad (8)$$

where $\beta_0$is the number of pores, β_1 is the connectivity, β_2 is the number of enclosed cavities and VOI is the volume analysed ($pixel^3$). 2D pore shape (S) was analysed for each slice using the freeware software ImageJ (Vs. 1.47v, National Institute of Health, http://rsb.info.nih.gov/ij) and calculated according to Pagliai et al. (2004):

$$S = \frac{P^2}{4\pi A} \quad (9)$$

where A is the pore area and P is the pore diameter. Pores were classified as regular (S < 2), irregular (2 < S < 5), and elongated (S > 5).

Saturated hydraulic conductivity

Saturated hydraulic conductivity (Ks) was measured with a laboratory permeameter (Eijkelkamp, The Netherlands) by using the constant head (Ks > 1 cm d^{-1}), or falling head method (with Ks between 0.001 and 100 cm d^{-1}) depending on the soil characteristics (Reynolds et al., 2002). The equation used for the constant head method is:

$$Ks = \frac{V \times L}{A \times t \times h} \quad (10)$$

Where V (cm^3) is the water volume inside the burette; L (cm) is the height of the water column; A (cm^2) is the area of the sample; t (d) is the time between two measurements; and h (cm) is the hydraulic head. For the falling head method the equation is the following:

$$Ks = \left[\frac{a \times L}{A \times (t_2 - t_1)}\right] \times \ln\left(\frac{h_1}{h_2}\right) + \frac{(x - a \times L)}{a \times \sqrt{(h_1 - h_2)}} \quad (11)$$

Where a (cm^2) is the area of sample holder; L (cm) is height of the water column; A (cm^2) is the area of the sample; (t_2-t_1) (d) is the analysis time; h_1-h_2 (cm) is the water level difference between inside and outside the sample holder at time respectively of t_1 (start of experiment) and t_2 (end of experiment); x is an evaporative index (0.0864 cm d^{-1}).

Soil water characteristic curve and unsaturated hydraulic conductivity

Water retention curve between 0 and - 800 cm was obtained with a ku-pF apparatus DT 04-01 (UGT, 2005), on previously pre-saturated soil cores. Two tensiometers were carefully inserted in the soil at depths of 1.5 and 4.5 cm from the surface, respectively, in order to measure the matric potential with a time interval of 10 minutes. The device automatically measured the sample weight by an electronic

balance in correspondence with the measurement of hydraulic tension. Each point of the water-retention curve was then calculated on the basis of the soil water content at time t and the mean tension in the sample at that time (Schindler et al., 2010).

Numerical inversion

Observed matric potential data were analyzed using Hydrus 1D (Šimůnek et al., 2008) in the "parameter estimation" mode. Hydrus 1D solves numerically the following Richards equation:

$$\frac{\partial \theta}{\partial t} = \frac{\partial}{\partial z}\left(K\frac{\partial h}{\partial z} + K\right) \tag{12}$$

In which θ is the water volumetric content; h is the potential; z is a spatial coordinate, t is the time, and K is the hydraulic conductivity. The numerical inversion is a method to estimate parameters that are deduced from the observed data, and it is based on the minimization of an objective function, which expresses the difference between the observed values and the prediction of the estimate. Initial estimates of the optimized system parameters are then iteratively improved during the minimization process until a desired degree of precision is obtained (Šimůnek et al., 2008). Minimization of the objective function Φ is achieved by using the Levenberg-Marquardt nonlinear minimization method. The objective function is defined as:

$$\Phi(b,q,p) = \sum_{j=l}^{m_q} v_j \sum_{i=l}^{n_{ql}} w_{i,j}\ \left[q_j^*(x,t_i) - \ q_j\ (x,t_i,b)\right]^2$$

$$+\sum_{j=l}^{m_p} \overline{v_j}\ \sum_{i=l}^{n_{pl}} \overline{w_{i,j}}\ \left[p_j^*(\theta_i) - \ p(\theta_i,b)\right]^2 + \ \sum_{j=l}^{n_b} \widehat{v_j}\ \ \left[b_j^* - b_j\ \right]^2 \tag{13}$$

Where the first term represents deviations between measured and calculated time-space variables; the second describes the differences between independently measured and predicted soil hydraulic properties and/or hydraulic conductivity. The last term constitutes a penalty function for deviations between prior knowledge of the soil hydraulic parameters and their final estimates. The description of each symbol meaning is given in Šimůnek et al., 2008.

The inversion was done considering a single porosity model as described by the van Genuchten-Mualem model (van Genuchten, 1980; and Mualem, 1976):

$$\theta(h) = \begin{cases} \theta_r + \frac{\theta_s - \theta_r}{\left[1 + |\alpha^h|^n\right]^{-m}}, & h < 0 \\ \theta_s, & h \geq 0 \end{cases} \quad (14)$$

$$K(h) = K_s S_e{}^l \left[1 - \left(1 - S_e{}^{\frac{l}{m}}\right)^m\right]^2 \quad (15)$$

Where h_s *is the* air-entry value [L]; θ_s is the saturated water content; θ_r is the residual water content; α, m, n are empirical parameters; S_e is the effective water content; K_s is the saturated hydraulic conductivity ; K_r is the relative hydraulic conductivity; K_k (h_k) is the unsaturated hydraulic conductivity at pressure head h_k.

Soil water content at low matric potential

The water content at low matric potentials (between - 1500 and - 20000 cm) was derived by means of a hygrometer Dewpoint Potentiameter WP4-C (Decagon, Decagon Devices Inc., Pullman WA) which uses the chilled-mirror dewpoint technique to measure the pressure of the water evaporated from a sample and in turn calculates the water potential. A sample of wet soil is firstly left to equilibrate in a plastic sample holder (1.4 cm height, 4 cm diameter) at constant temperature (20 °C) for about 24 hours. After equilibration, the sample is ready for measurement with the hygrometer WP4-C by introducing it in a sealed chamber that contains a mirror and a means of detecting condensation on it. After reaching an equilibrium, the water potential of the air in the chamber is the same as the water potential of the sample. The water potential is then calculated as follows:

$$\Psi = \frac{RT}{M} \times \ln \frac{p}{p_0} \quad (16)$$

Where p is the vapor pressure of the air; p_0 is the saturation vapour pressure at sample temperature, R is the gas constant (8.31 J/mol K), T is the Kelvin temperature of the sample, and M is the molecular mass of water. The vapour pressure of the air is measured using the chilled mirror, and p_0 is computed

from sample temperature. The water potential measured by the instrument is a sum of osmotic and matric head, thus it has to be corrected estimating the osmotic potential of the sample in function of its electric conductivity (EC):

$$\Psi_{os} = -0.036 \times EC \quad (17)$$

This is then used to calculate the osmotic component of the matric potential using the following equation:

$$\Psi = \Psi_{os}\left(\frac{\theta_s}{\theta}\right) \quad (18)$$

In correspondence of each measured matric potential, the sample is carefully weighed to determine its water content. As a result, at the end of measurements it is dried at 105 °C overnight. Plant available water (PAW) was finally calculated as the difference between the water content at -330 cm and that at -15000 cm.

Statistical analysis of soil data

A three-way ANOVA considering soil type, residue management and fertilisation level as main factors was used, applying the Duncan's post-hoc test to compare the differences between group means in SOC, TKN, pore architecture and soil hydrology analyses (CoStat 6.4 - CoHort Software, Monterey, CA, USA). Multiple stepwise regression analysis with backward selection was also applied in order to identify dependencies between hydraulic properties, SOC and texture; and between pore classes, SOC and texture. Furthermore, in order to facilitate statistical comparison between treatments pores were classified according to different size classes. Pores measured by MIP encompassed cryptopores (0.01-0.1 µm), ultramicropores (0.1-5 µm), micropores (5-30 µm), mesopores (30-75 µm) and macropores (75-100 µm) (Cameron and Buchan, 2006). Pore classes analysed by µCT mainly included mesopores and macropores that were classified as follows: 1) 25-76 µm; 2) 76-126 µm; 3) 126-480 µm; and 4) 480-2500

µm. Ultramicropores analysed by BET were split according to the methods used for their calculation (B.J.H and Horvath and Kawazoe), with pores between 2 and 50 nm divided in four size classes: 1) 2-10 nm; 2) 10-18 nm; 3) 18-26 nm and 4) 26-50 nm. A principal component analysis (PCA) on 19 selected variables was adopted to highlight the general interdependences between pore size distributions, morphological porosity parameters and texture indices of the samples. The variables were selected according to Kaiser's measure of sampling adequacy (MSA), which resulted as 0.74, indicating that the group of variables were appropriate for the analysis (Kaiser, 1974). Only rotated orthogonal components with eigenvalues >1 were extracted. Multiple regression and PCA analyses were performed using Statistica (StatSoft Inc., Tulsa, USA).

Results

Crop yield and nitrogen use efficiency

Average yields

Biomass production trends present a discontinuity passing from the maize-wheat rotation (until 1986) to the more complex open rotation adopted since 1987. In the first period yields were almost constant on average while modification of the crop sequence led to a progressive increase in yields, particularly evident in the sandy soil (Fig. 2). In all soils, residue incorporation caused an increase in yields in comparison with residue removal (sign test with $p<0.01$ for the three soils).

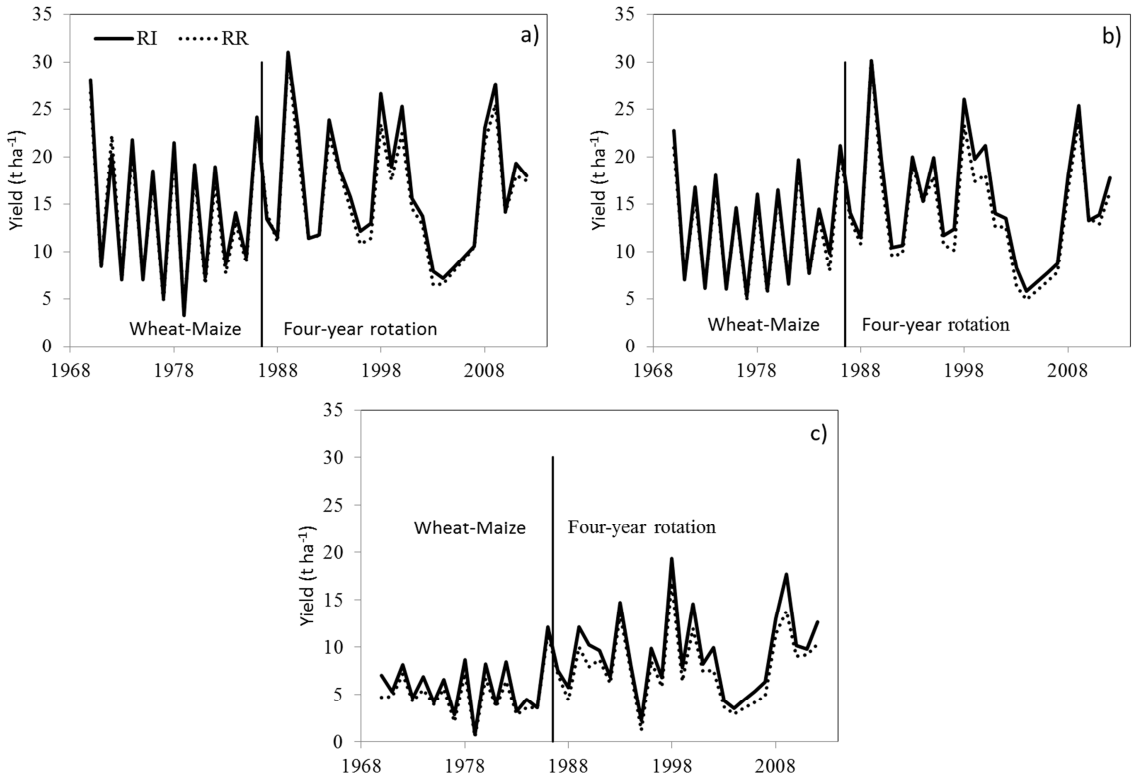

Figure 2. *Total aerial biomass trends over the 43 years, (average of the N fertilizations) of a) clay, b) sandy-loam and c) sandy soil.*

The effect of residue incorporation is however inversely proportional to soil fertility, with an average increase of biomass equal to 5.5, 7.4 and 18.1% respectively for clay, sandy-loam and sandy soils. This is mainly visible in sugarbeet, winter wheat and maize, for which the increases in yield were very pronounced in sandy soil (+27.6%, +19.51% and +21.65%, respectively), if compared with clay (+4.82%, +2.10% and +7.27%) and sandy-loam (+7.70%, +2.76% and +7.46%). On the contrary, in potato and tomato, the residue-induced increase in yield was less pronounced in clay soil (+8.45% and +5.81%, respectively), than in the other two (+14.08% and +10.76% in sandy-loam; +14.52% and 13.52% in sandy).

Yield response to N application with or without residue incorporation

The comparison of the complex model with modS2 (Tab. 3) indicates highly significant differences for maize ($p<0.001$) in all soil types, thus highlighting a residue-mediated effect on yield. The comparison of modS1 with the complex one was always not significant. With modS1 (Y_M constant with or without residue incorporation), '*a*' parameter with R shows a reduced variability and a tendency to be lower than NR (mean value 0.0544 with R against 0.0588 with NR). Along with the absence of significant differences between modC and modS1, this indicates that the increase in productivity for all soils could be caused mainly by a nutritional effect. Wheat seems to undergo a mainly nutritional effect only in clay and sandy-loam soil, while in sandy soil other indirect mechanisms (i.e. variation of soil physical traits) could be involved in the observed increase in yield, as the significant difference between the complex model and modS1 points out. In sugarbeet, significant differences are detected between the complex model and the modS2 in sandy-loam ($p=0.005$) and sandy soil ($p=0.018$), with the opposite in clay soil. Considering modS1, when Y_M is constant, the parameter '*a*' increases with residue incorporation, while parameter '*b*' remains constant (data not shown), thus suggesting that the mechanisms involved in the observed effect may be different from the purely nutritional one. In potato, residues caused significant increases in yield only in clay and sandy-loam soil (comparison between complex model and modS2 significant at $p=0.017$ and $p=0.006$, respectively). The absence of effect in sandy soil could be ascribable to the low yields observed.

Table 3. *Comparison between complex and simplified models for the relationship between crop yield and N supply.*

Crop	Model	Soil type	Residual SS	Total SS	d.f.	F	p
Sugarbeet	ModC	Clay	278.3	3243.9	90		
		Sandy-loam	262.3	2540.2	90		
		Sand	135.0	1156.1	90		
	ModS1	Clay	282.2	3243.9	93	0.430	0.732
		Sandy-loam	281.4	2540.2	93	2.190	0.095
		Sand	141.5	1156.1	93	1.452	0.233
	ModS2	Clay	296.2	3243.9	99	0.645	0.755
		Sandy-loam	337.9	2540.2	99	***2.886***	***0.005***
		Sand	167.3	1156.1	99	***2.393***	***0.018***
Wheat	ModC	Clay	29.3	931.2	246		
		Sandy-loam	32.7	879.0	246		
		Sand	37.1	920.6	246		
	ModS1	Clay	30.6	931.2	259	0.865	0.590
		Sandy-loam	34.3	879.0	259	0.882	0.572
		Sand	42.4	920.6	259	***2.713***	***0.001***
	ModS2	Clay	36.1	931.2	99	***1.461***	***0.046***
		Sandy-loam	41.9	879.0	99	***1.762***	***0.006***
		Sand	58.8	920.6	99	***3.695***	***0.000***
Maize	ModC	Clay	287.9	5151.9	306		
		Sandy-loam	273.5	5707.9	306		
		Sand	430.5	5623.1	306		
	ModS1	Clay	305.0	5151.9	321	1.213	0.260
		Sandy-loam	288.7	5707.9	321	1.137	0.322
		Sand	451.7	5623.1	321	1.003	0.451
	ModS2	Clay	415.2	5151.9	351	***3.007***	***0.000***
		Sandy-loam	366.3	5707.9	351	***2.309***	***0.000***
		Sand	645.3	5623.1	351	***3.391***	***0.000***
Potato	ModC	Clay	270.6	2803.0	90		
		Sandy-loam	385.3	1468.8	90		
		Sand	193.4	985.2	90		
	ModS1	Clay	280.1	2803.0	93	1.051	0.374
		Sandy-loam	389.5	1468.8	93	0.321	0.810
		Sand	207.2	985.2	93	2.130	0.102
	ModS2	Clay	336.1	2803.0	99	***2.419***	***0.017***
		Sandy-loam	492.3	1468.8	99	***2.777***	***0.006***
		Sand	223.5	985.2	99	1.555	0.141
Tomato	ModC	Clay	105.7	1172.2	60		
		Sandy-loam	74.0	852.9	60		
		Sand	87.1	537.3	60		
	ModS1	Clay	111.9	1172.2	62	1.784	0.177
		Sandy-loam	78.7	852.9	62	1.906	0.158
		Sand	88.8	537.3	62	0.598	0.553
	ModS2	Clay	117.1	1172.2	66	1.086	0.381
		Sandy-loam	100.9	852.9	66	***3.630***	***0.004***
		Sand	95.2	537.3	66	0.933	0.478

For clay and sandy-loam soils, the absence of significant differences between the complex model and modS1, along with the increase in parameter '*a*' suggests that residue effect on yield is caused by a mixture of direct nutritional effects and changes in soil physical properties. Residue effects on tomato

yield were observed only in sandy-loam soil (complex model vs modS2 significant at p=0.004). Considering the comparison of the complex model with modS1 (p>0.05), an increase in parameter '*a*' is observed, thus suggesting mechanisms other than the purely nutritional effect also being present in this crop. The relationships between crop yield and N distribution, calculated on the average yields for each N level (Fig. 3), show the general positive effect of residue incorporation on crop yield. While the differences between soil types are reduced for maize and wheat, the differences between the sandy and the two other soils are substantial in sugarbeet, potato and tomato. As observed above, the effects of residue incorporation in wheat seems to be negligible in the most fertile soils.

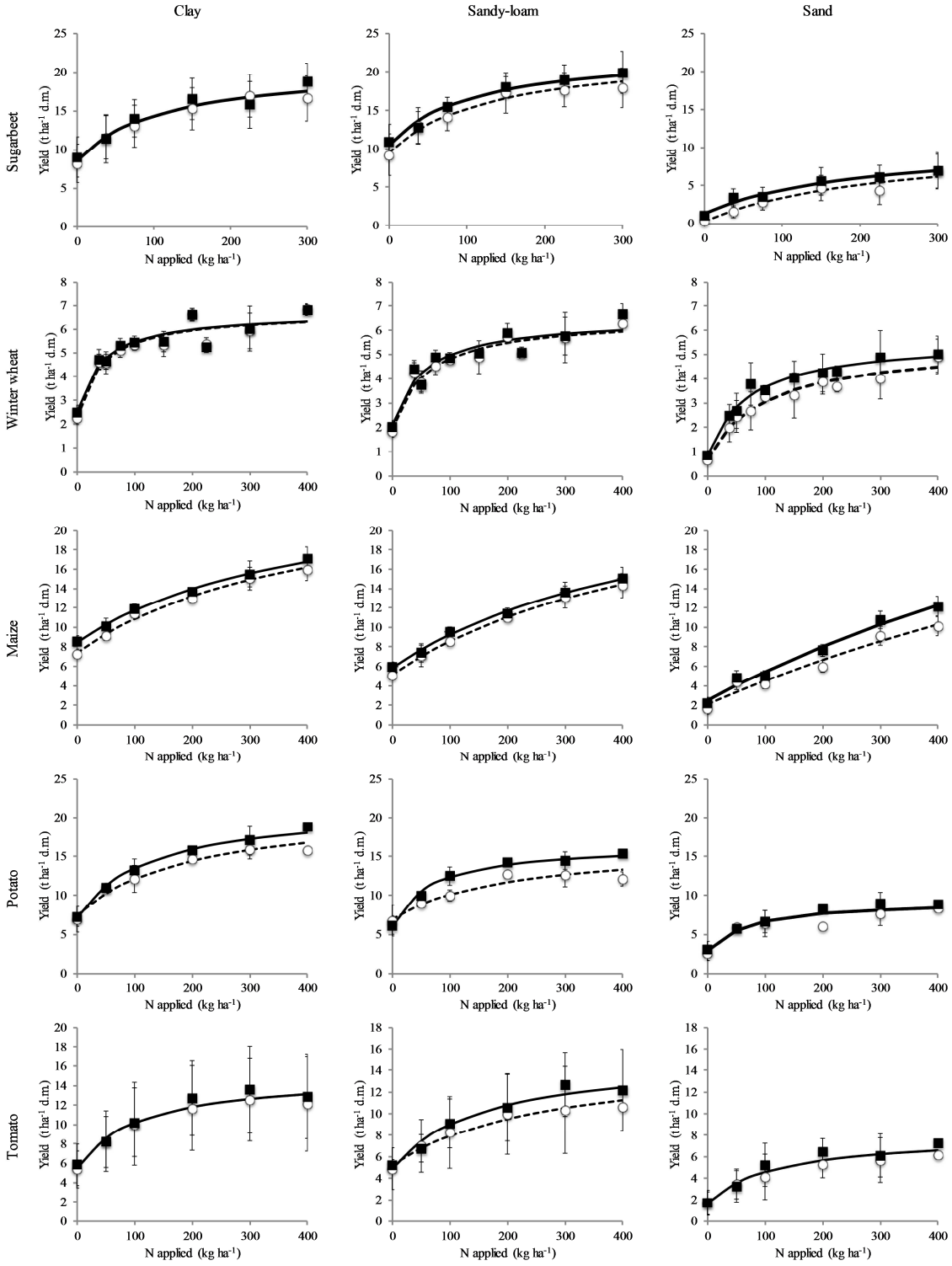

Figure 3. *Yield response curves to N with and without residue incorporation. Continuous lines represent R treatment, dashed lines NR treatment.*

Nitrogen recovery with and without residue incorporation

The model used for the estimation of the amounts of N recovered from mineral fertilisers and residues relies on some assumptions. First of all, the natural availability parameter N_0 is unique for all the treatments and is strongly related to the N adsorption in the unfertilised check with residue removal. The natural availability should be higher for high fertilisation treatments and with residue incorporation but the experimental layout did not allow to consider a unfertilised strip within each treatment. Assuming a constant N_0 would lead to an overestimation of NUE for fertilised treatment and this effect should be more evident at low fertilisation levels. Furthermore, the model doesn't consider explicitly the interaction between mineral and organic forms of N.

Table 4. *Parameters of the model describing N recovery with and without residue incorporation.*

Crop	Soil	N_0	k_{min}	k_{res}	a	b	Residual SS	Total SS	n
Sugarbeet	Clay	155.2	1.354	0.192	1.244	384.0	1431.60	74337.76	12
	Sandy-loam	174.1	1.666	0.267	0.992	315.9	637.04	58131.73	12
	Sandy	16.0	1.037	0.445	0.721	297.4	1247.96	28304.92	12
Wheat	Clay	67.4	2.605	0.017	0.941	124.6	1763.75	22216.94	20
	Sandy-loam	57.4	2.271	0.041	0.941	125.6	1653.40	22255.97	20
	Sandy	19.0	1.782	0.168	0.816	126.5	480.66	21409.61	20
Maize	Clay	182.7	0.927	0.247	0.968	295.6	725.98	44636.24	12
	Sandy-loam	140.1	0.917	0.207	0.950	358.6	335.56	51148.85	12
	Sandy	51.1	0.763	0.450	0.921	402.8	983.89	51864.32	12
Potato	Clay	127.4	1.658	0.438	0.935	283.2	926.98	61606.01	12
	Sandy-loam	109.7	2.084	0.618	0.841	188.8	1361.51	38835.75	12
	Sandy	48.3	2.059	0.400	0.764	131.9	958.38	20254.94	12
Tomato	Clay	160.3	2.222	0.300	1.021	284.3	1781.68	73400.61	12
	Sandy-loam	143.8	1.422	0.446	0.988	282.0	1682.85	58954.31	12
	Sandy	46.1	1.732	0.317	0.887	172.9	978.15	29662.03	12

The values obtained have then to be considered as a first approximation of the real values. Nevertheless, we assume that these values can be used to estimate the relative contribution of mineral and organic forms of N to plant uptake. The equation gave an excellent fit to observed data in all the combinations 'crop x soil' (Tab. 4), with natural N availability (N_0) and maximum N uptake (b) decreasing from clay to sandy soil and constants related to nitrogen availability of N inputs (k_{min} and k_{res}) always higher for the mineral inputs. For both the N forms, the model allows to estimate a specific NUE, as the ratio of N uptake and the N input for this form of N (mineral fertilisers or residues).

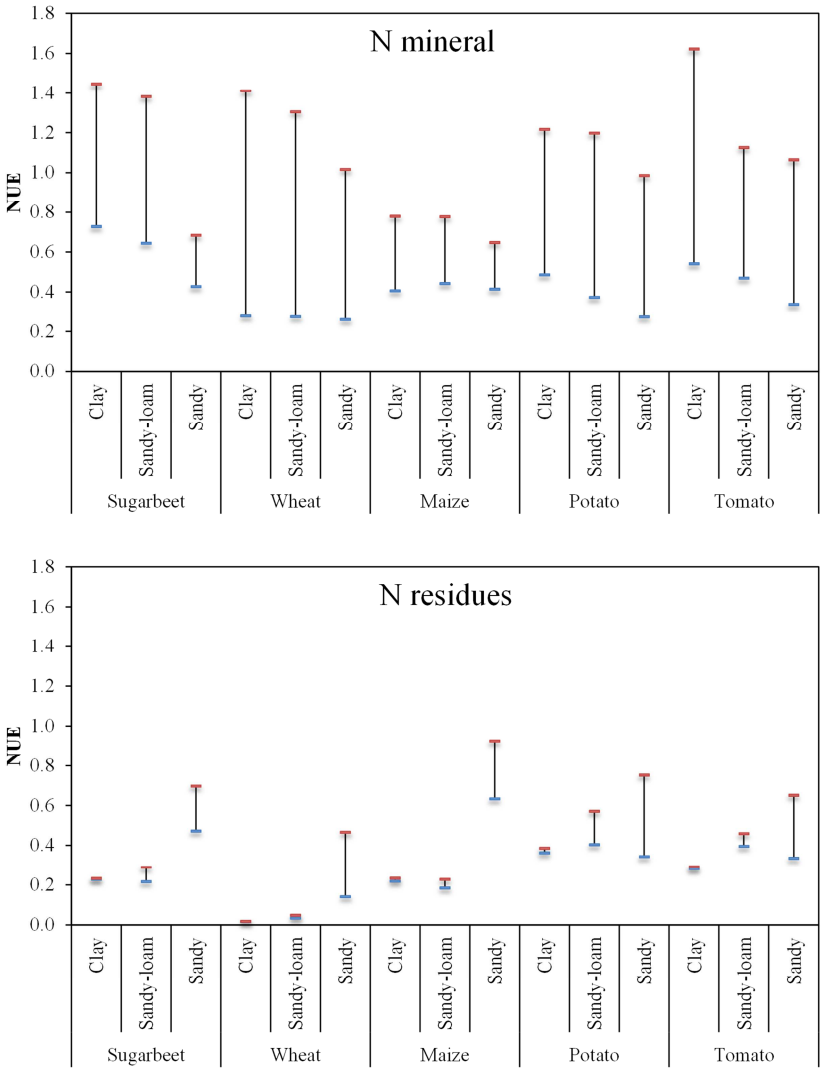

Figure 4. *Nitrogen use efficiencies from a) mineral and b) crop residues N sources*

The NUE for mineral sources (Figure 4) is highly variable, depending on soil type and crop. For the more fertile soils the amount of N recovered from soil is high and, for the lower mineral N inputs, uptake is higher than input, leading to NUE higher than 1. For all the crops, NUE for mineral sources is lower and less variable across fertilisations in the sandy soil. In this soil the strong limitation of crop potential yield reduces N adsorption and, in turn NUE. The efficiency of residue N follows an opposite trend (Figure 4), with lower values in clay and sandy-loam soils and higher in the sandy soil. Furthermore, crops show a very different behaviour: while in wheat the effect of residues seems always low, in sugarbeet and maize NUE for residues varies from ca. 0.2 for clay and sandy-loam soils, to quite high values (0.6-0.8) in the sandy soil. In the two solanaceous crops, recovery of residue N is still high in the sandy soil, as in the other summer crops, but is also appreciable in the clay and sandy loam soils.

***Table 5**. Relative efficiency (%) of residue nitrogen compared to mineral nitrogen*.

	Clay	Sandy-loam	Sandy
Sugarbeet	14.19	16.01	42.95
Wheat	0.66	1.80	9.42
Maize	26.69	22.57	58.98
Potato	26.43	29.65	19.44
Tomato	13.51	31.34	18.30

The relative efficiency of N input for residues (ratio between k_{res} and k_{min}) is very low in wheat, confirming that this crop is only marginally affected by residue incorporation (Table 5). In the spring-summer crops, residues have a higher relative efficiency, ranging from 15 to 30% of that of mineral inputs in clay and sandy-loam and higher (from 18 to 60%) in the sandy soil.

Soil parameters

Bulk density

In the superficial soil layer (0-20 cm) bulk density varied significantly between soils (Fig. 5), with sandy showing higher values (1.44 g cm^{-3}), followed by sandy-loam (1.21 g cm^{-3}) and clay soil (1.02 g cm^{-}

^{3}). These differences were maintained also in the other two soil layers (20-50 and 50-70 cm depth). Furthermore, bulk density grew passing from the superficial to the deeper soil layer of 0.30, 0.23 and 0.19 g cm^{-3} in clay, sandy-loam and sandy soil. Residues affected this parameter only to the first soil layer, where they reduced soil density of 0.05 g cm^{-3}, on average ($p < 0.01$). On the contrary, no significant effects of nitrogen fertilization were observed neither in the upper, nor in the deeper soil layers.

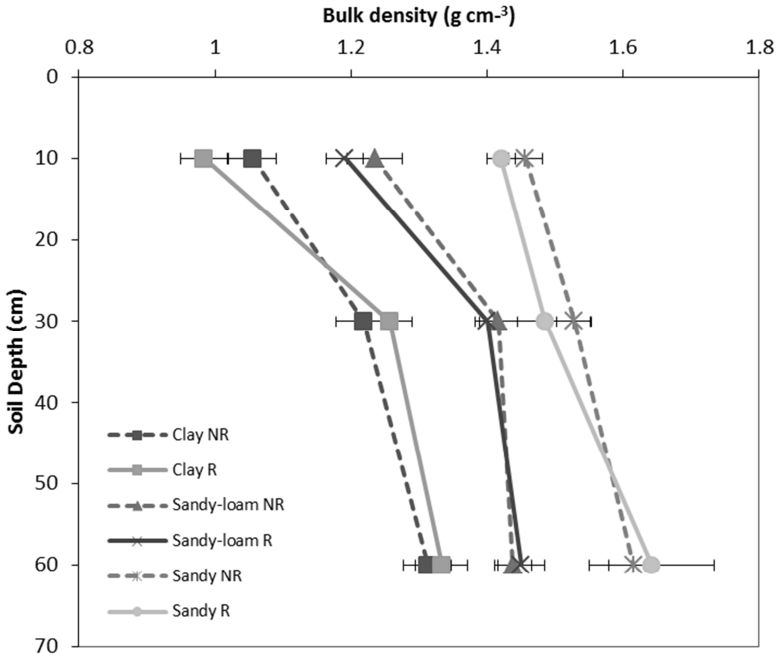

Figure 5. *Bulk densities of the three soils as a function of residue management in the three soil layers examined.*

Soil organic carbon and Kjeldhal nitrogen

Residue incorporation caused a significant rise in SOC and TKN stock in all the three soils, and this increase was extended to the entire profile (Figure 6a and b, Figure 8a and b). The effect was more relevant in the two upper soil layers (0-20 and 20-50 cm depth) and less pronounced in the lower one (50 - 70 cm depth).

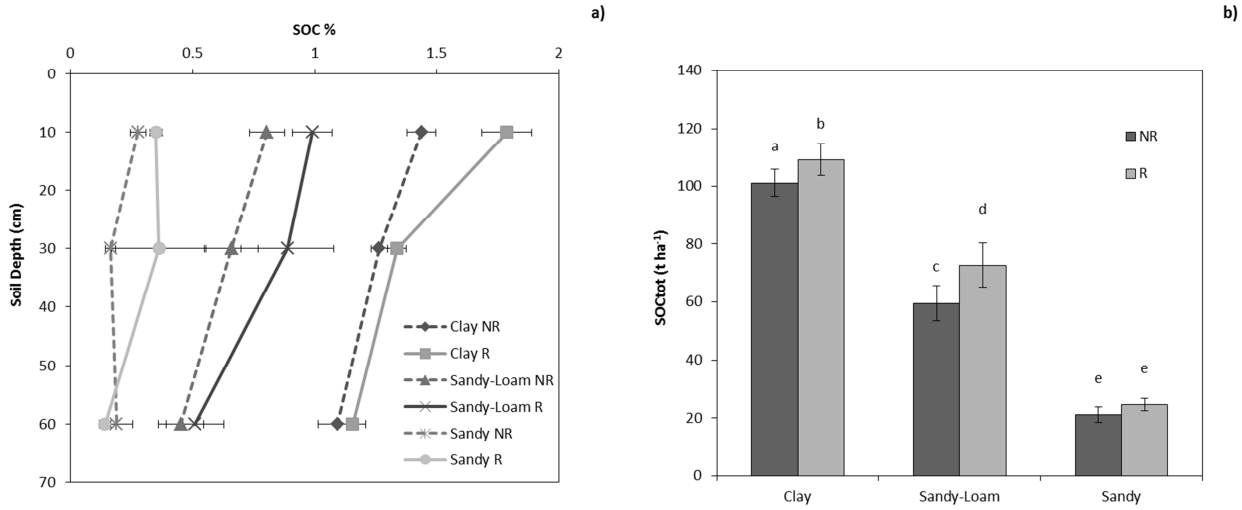

Figure 6. *a) Soil organic carbon concentrations at three depths with (R) and without residues(NR); b) carbon stock in the entire profile with and without residues.*

In particular, in the upper horizon (0-20 cm), SOC concentration increased on average from 0.84% in NR plots to 1.04% in R plots ($p<0.01$). However the magnitude of the effects was different in the three soils, with SOC variations from 1.43% to 1.79% in clay, from 0.80% to 0.90% in sandy-loam, and from 0.28% to 0.35% in sandy soil (NR vs R, Figure 6a). In the medium soil layer (20-50 cm) SOC varied from 0.86% in NR to 0.69% in R plots; on average. All the three soils were interested by residue-mediated changes in SOC, indeed it increased from 1.09% to 1.15% in clay, from 0.45% to 0.51% in sandy-loam, and from 0.19% to 0.14% in sandy (NR vs R). Residue effects extended also to the deeper soil layer, even if they did not result significant (on average the SOC concentration in NR plots was 0.60% and in R plots it was 0.58%)(Figure 6a). Due to the very different bulk densities of the three soils, the variations in SOC were also expressed as carbon stocks in tons per hectare. The stock of organic carbon in the entire profile (Fig. 6b) in NR and R treatments was 101 and 109 t ha^{-1} in clay, 60 and 73 t ha^{-1} in sandy-loam, and 21 and 25 t ha^{-1} in sandy soil. This resulted in residue-induced SOC increases of +8%, +12% and +19% in clay, sandy-loam and sandy soil.

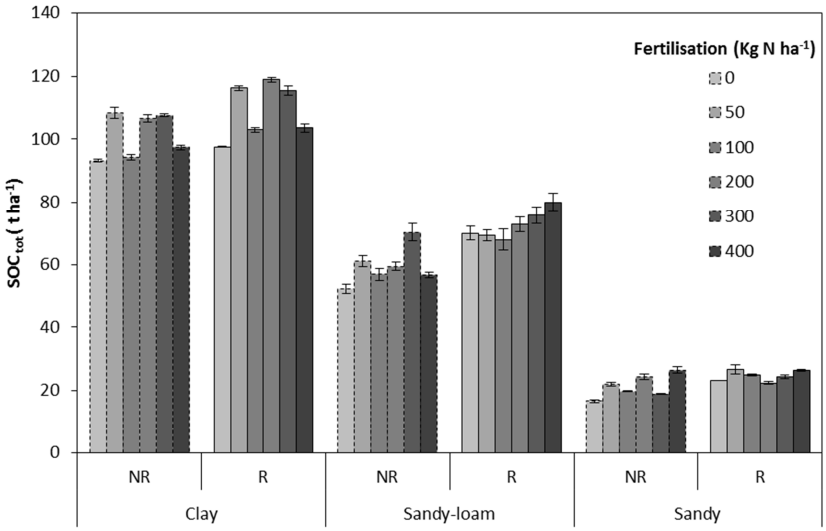

Figure 7. *SOC stocks in soils with different residue management types, as a function of inorganic fertilization.*

Organic carbon content changed also as a function of nitrogen fertilization, however the variations followed different trends if compared with those induced by residue incorporation (Figure 7) and were not proportional to the dose of fertilizer applied. Indeed, the highest fertilization rate increased SOC of 5.08 t ha^{-1} in clay soil and of 6.5 t ha^{-1} in sandy soil. The organic carbon content of sandy-loam soil was the most affected by inorganic fertilization and showed the highest increment (+7.1 t ha^{-1}).

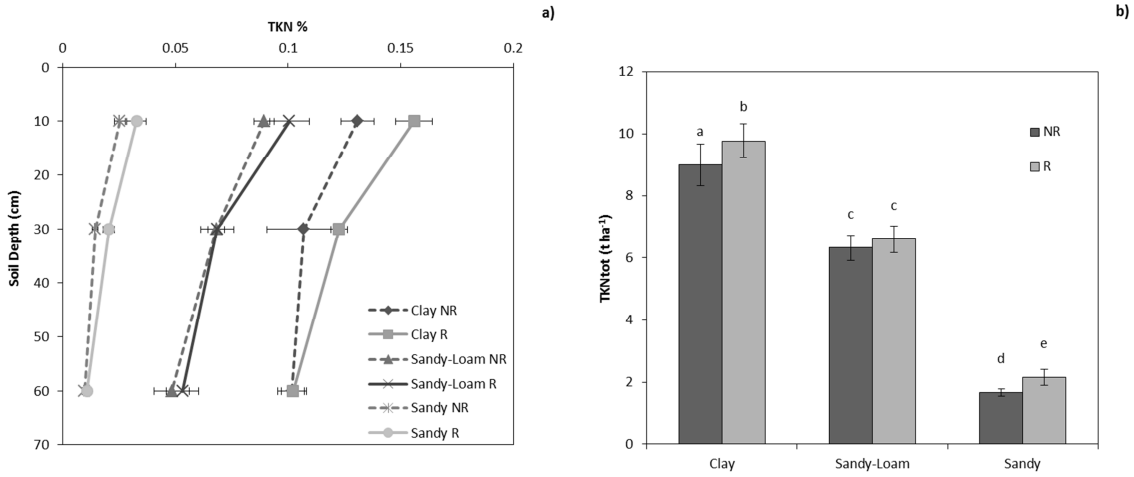

Figure 8. *a) total Kjeldhal nitrogen concentrations at three depths with (R) and without residues(NR); b) nitrogen stocks in the entire profile with and without residues.*

In the first 50 cm of soil, nitrogen content varied significantly according to soil type and nitrogen fertilization, with the maximum values detected in clay plots with the highest N dose (400 Kg N ha^{-1}). In the deeper soil layer (50-70 cm) only the differences between soil types were maintained ($p<0.05$) due to the fact that N fertilization did not result effective anymore. Residue management influenced nitrogen concentration in the superficial soil layer (Fig. 8a), with effects more evident in clay and sandy-loam soil (interaction residue management x soil type significant at $p<0.005$). Clay soil with residue removal exhibited a nitrogen content of 0.13%, while that of plots with residue incorporation was 0.15%. In sandy-loam plots residues caused a growth in nitrogen concentration from 0.09% to 0.10%. In sandy soil no differences were found, and plots either receiving or not residues showed a nitrogen concentration of 0.03%. The residue effect extended to the medium soil depth in clay and sandy soil. In the first, N concentration was 0.11% and 0.12% in NR and R treatments, while in the second it was 0.01% in NR and 0.02% in R treatments. On the contrary sandy-loam showed no influences of residue incorporation in this soil layer. These differences in nitrogen concentration caused by residue incorporation were not detected in the deepest soil layer (50-70 cm). Despite this, nitrogen stocks calculated as t ha^{-1} (Fig. 8b) resulted significantly influenced by residue incorporation in the entire soil layer analysed (0 - 70 cm) with an average enrichment in nitrogen stock of 9%. More precisely, clay soil exhibited the maximum absolute increase (+ 0.79 t ha^{-1}) followed by sandy soil (+ 0.48 t ha^{-1}), and sandy-loam (+ 0.27 t ha^{-1}). On the contrary the relative increments were more marked in sandy-loam soil (+ 28.57%), intermediate in clay (+ 8.78%), and minor in sandy (+ 4.26%). Nitrogen stock was influenced by fertilization in an evident way only in sandy soil and sandy-loam, while no clear trends were observed in clay soil (significant interaction soil type x fertilization). The three soils exhibited significantly diverse C/N ratios. The higher one was ascribed to sandy soil, which presented a ratio of 12, while lower ratios were observed in clay (C/N = 11) and sandy-loam soil (C/N = 10). Interestingly, C/N ratio was significantly increased by residues in sandy-loam soil (form 9.4 to 11.1), with opposite but not significant effects in the other two soils (form 11.4 to 11.2 in clay, and from 12.7 to 11.9 in sandy)(Figure 9).

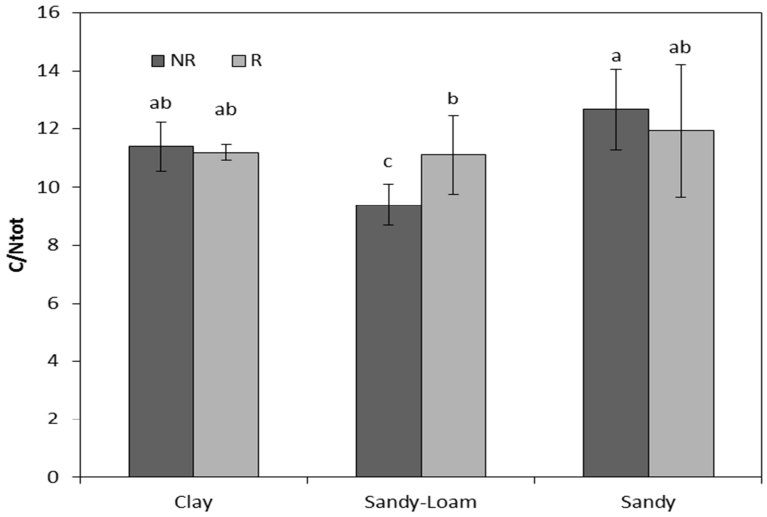

Figure 9. *C/N ratios in the three soils as a function of residue management.*

Pore architecture

Total pore volume (TPV_{core})

Total pore volume (TPV_{core}) varied between treatments, ranging from a minimum of 0.46 cm^3 cm^{-3}, observed in SNDL without residue incorporation and fertilisation, to a maximum of 0.66 cm^3 cm^{-3} in CL managed with residue incorporation and N fertilisation.

Table 6. *Total pore volumes and selected pore morphological parameters of the soils.*

	TPV_{core} cm^3 cm^{-3}	TPV_{MIP} cm^3 cm^{-3}	$TPV_{\mu CT}$ cm^3 cm^{-3}	DA	CD × 10^{-8} μm^{-3}	FD
Clay	0.63a	0.16	6.48b	0.60	0.79b	1.98b
Sandy-loam	0.47c	0.42	7.07b	0.56	0.45b	2.05b
Sandy	0.55b	0.33	16.17a	0.57	3.41a	2.30a
NR[a]	0.54b	0.31	9.42	0.57	1.38	2.10
R	0.56a	0.29	10.40	0.58	1.68	2.11
NO FERT[b]	0.54b	0.33	9.08	0.58	1.38	2.08
FERT	0.56a	0.27	10.73	0.57	1.68	2.13

Values are reported as means (n=12),Values reported as means (n=24), different letters indicate significant differences between treatments. [a] NR: Residue removal; R: residue burial. [b] NO FERT: no N fertilization; FERT; fertilization 400 kg N ha^{-1}. TPV_{MIP} total pore volume measured with mercury intrusion porosimetry; $TPV_{\mu CT}$: total pore volume measured with x-ray µCT; TPV_{PIC}: total pore volume measured with helium pycnometer; DA: degree of anisotropy; CD: connectivity; FD: fractal dimension.*

In fact, both nitrogen and residue inputs significantly increased TPV_{core} by 3.6% and 3.2% if compared to the NR and NO FERT treatments (Table 6). Moreover, multiple regression analysis showed a positive correlation between TPV_{core} and both sand ($\beta_2 = 1.86$) and clay ($\beta_3 = 2.32$) content (Table 7).

Pore size distribution

Pore size distribution, investigated with gas adsorption (PSD_{N2}) in the range 0.25-50 nm, was not affected by either residue management (Table 9) or fertilisation. However, a clear difference was observed between soils since almost all the pore classes were predominant in CL with respect to the others (Table 8). The smallest PSD_{N2} class (0.25-2 nm), estimated by the Horvath and Kawazoe method, occupied 0.019 $cm^3\ cm^{-3}$ in CL, 0.002 $cm^3\ cm^{-3}$ in SNDL and only 0.001 $cm^3\ cm^{-3}$ in SND. Similarly, the pores of 2-50 nm (B.J.H. method) increased from 0.006 $cm^3\ cm^{-3}$ in SND to 0.016 $cm^3\ cm^{-3}$ in SNDL and to 0.070 $cm^3\ cm^{-3}$ in CL. Pore frequency, expressed in relative terms (Table 8), highlighted that pores of 2-10 nm were very numerous in all soils, being 54.6%, 38.0% and 46.6% in CL, SNDL and SND, respectively. SOC affected PSD_{N2} over the whole range, apart from the pore size class 2-10 nm (Table 7). Indeed, SOC was negatively correlated with pores in the range 0.25-2 nm (β_1=-0.24, $p < 0.05$) and positively correlated with those > 10 nm ($p < 0.05$). An opposite effect was observed for the clay content, with positive dependencies with the smallest pores < 10 nm and negative with the largest (26-50 nm). Total porosity, estimated by mercury intrusion porosimetry (TPV_{MIP}), was significantly different between soils as it averaged 0.42 $cm^3\ cm^{-3}$ in SNDL, decreasing to 0.33 $cm^3\ cm^{-3}$ and 0.16 $cm^3\ cm^{-3}$ in SND and CL, respectively.

Table 7. *Correlation factors of selected variables following the multiple regression equation* $y = \alpha + \beta_1 OC(\%) + \beta_2 Sand(\%) + \beta_3 Clay(\%)$. *Correlation factors are significant at* $p<0.05$.

	Regression coefficients				
	Intercept	**OC**	**Sand**	**Clay**	**multiple R^2**
	α	β_1	β_2	β_3	
TPV_{core}[a]	14.85	-	1.86	2.32	0.80
TPV_{MIP}[b]	0.8422	-	-1.34	-1.95	0.73
$TPV_{\mu CT}$[c]	-4.23	-	1.32	0.60	0.62
PSD_{N2}[d](nm)					
0.25-2*	-0.0169	-0.24	0.61	1.77	0.92
2-10	-0.0422	-	0.62	1.54	0.96
10-18	-0.0022	0.96	-	-	0.93
18-26	-0.0006	0.96	-	-	0.92
26-50	-0.0004	2.13	-	-1.40	0.84
PSD_{MIP}[e](µm)					
0.01-0.1**	0.0014	-	-	0.97	0.95
0.1-5	0.60	-	-2.61	-2.52	0.90
5-30	0.4973	-	-2.13	-2.17	0.63
30-75	-0.0352	-0.56	1.27	1.0	0.90
75-100	-0.1335	-	1.83	0.99	0.95
$PSD_{\mu CT}$[f](µm)					
25-76**	-36.54	-	1.81	1.54	0.45
76-126	3.28	-	1.35	0.68	0.57
126-480	76.90	-	-1.48	-1.12	0.35
480-2500	56.37	-	-1.58	1.23	0.39
Pore shape					
Regular	82.67	-	-1.17	-1.32	0.23
Irregular	11.77	-	1.48	1.53	0.31
Elongated	4.40	0.38	-	-	0.15
DA[g]	0.5553	-	-	0.33	0.11
CD[h]	-0.0009	-	1.77	1.08	0.77
FD[i]	1.93	-	0.67	-	0.45

**Pore size range (nm). **Pore size range (µm). [a] Total pore volume analysed with helium pycnometer. [b] Total pore volume calculated with MIP; [c] Total pore volume calculated with µCT; [d] Pore size distribution obtained with gas adsorption; [e] Pore size distribution obtained with MIP; [f] Pore size distribution obtained with µCT; [g] Degree of anisotropy; [h] Connectivity density; [i]Fractal dimension.*

FERT was also a significant factor influencing TPV_{MIP} in all soil types, with a reduction of total pore volume in fertilised plots of 28% in CL, 19% in SNDL and 6% in SND. Pore size distribution, as revealed by MIP in the range 0.01-100 µm (PSD_{MIP}), changed significantly between soils (Table 8). Indeed, SNDL showed the highest pore volume between 0.1 and 30 µm (totally 0.35 $cm^3\ cm^{-3}$, i.e. 84% of TPV_{MIP}) while

SND in pore classes >30 µm (0.26 cm^3 cm^{-3}, i.e. 79% of TPV_{MIP}). In contrast, CL mainly had pores of a few micrometres, especially in the range 0.1-5 µm (0.04 cm^3 cm^{-3}, i.e. 27% of TPV_{MIP}). Residue incorporation (Tab. 9) affected PSD_{MIP} only in the pore class 30-75 µm ($p < 0.01$), being reduced in SNDL by 0.027 cm^3 cm^{-3}, followed by CL (0.016 cm^3 cm^{-3}) and SND (0.002 cm^3 cm^{-3}).

Table 8. *Pore size distributions of the three soils examined with the three different techniques.*

		Clay		Sandy-Loam		Sandy	
Pore size classes		cm^3 cm^{-3}	%	cm^3 cm^{-3}	%	cm^3 cm^{-3}	%
0.25-2		0.019±1E-03[a]	20.8±2.0	0.002±4E-04	11.5±2.1	0.001±1E-04	12.7±1.0
2-10		0.048±1E-03	54.6±1.7	0.007±6E-04	38.0±2.2	0.003±2E-04	46.6±1.1
10-18	nm	0.012±2E-03	13.9±1.4	0.004±3E-04	20.8±1.0	0.001±4E-05	18.8±1.1
18-26		0.006±7E-04	6.4±0.7	0.002±4E-04	12.3±2.3	0.001±1E-04	12.1±1.5
26-50		0.004±1E-03	4.4±1.3	0.003±7E-04	17.4±2.9	0.001±1E-04	9.7±2.4
0.01-0.1		0.038±2E-03	23.2±5.3	0.018±2E-03	4.3±0.7	0.006±1E-03	1.8±0.3
0.1-5		0.043±4E-03	26.6±3.3	0.188±7E-03	46.3±5.1	0.025±2E-03	7.7±0.7
5-30	µm	0.034±1E-02	20.7±3.5	0.165±4E-02	37.9±6.0	0.036±5E-03	10.9±0.9
30-75		0.032±1E-02	19.3±4.4	0.038±5E-03	9.1±1.1	0.154±2E-02	46.2±3.5
75-100		0.011±4E-03	6.5±2.0	0.009±1E-03	2.6±0.8	0.106±9E-03	32.8±3.9
25-76		0.019±3E-03	36.2±3.9	0.013±1E-03	21.4±3.4	0.075±7E-03	47.2±3.0
76-126		0.010±2E-03	17.7±0.8	0.012±2E-03	18.1±1.2	0.047±8E-03	28.6±1.2
126-480	µm	0.026±1E-02	34.9±5.0	0.030±9E-03	41.9±2.8	0.040±9E-03	24.0±2.4
480-2500		0.009±6E-03	11.1±1.6	0.017±1E-02	18.6±3.4	0.001±3E-04	0.2±0.1

Values are reported as means followed by standard errors.

Similar findings were observed as a result of N fertilisation input, which caused a reduction of the pore size class 30-75 µm in all three soils. Multiple regression analysis showed that both TPV_{MIP} and PSD_{MIP} were significantly affected by sand and clay. Negative correlations were observed with MIP total

porosity as well as with PSD classes 0.1-5 µm and 5-30 µm, while there were positive correlations with the largest pores (> 30 µm). Lastly, SOC and the pore size class 30-75 µm showed a negative relationship (β_1 = -0.56).

***Table 9**. Pore size distributions of the three soils as a function of residue management.*

	Clay		Sandy-loam		Sandy	
	NR	R	NR	R	NR	R
PSD_{N2}(nm)	cm^3cm^{-3}		cm^3cm^{-3}		cm^3cm^{-3}	
0.25-2	0.020±2E-05	0.018±2E-03	0.002±1E-04	0.003±2E-04	0.001±1E-04	0.001±9E-05
2-10	0.048±7E-04	0.048±1E-03	0.008±2E-04	0.007±1E-04	0.003±2E-04	0.003±2E-04
10-18	0.011±8E-04	0.014±2E-03	0.004±2E-04	0.004±2E-04	0.001±2E-05	0.001±1E-05
18-26	0.005±6E-04	0.007±2E-04	0.002±5E-04	0.003±1E-05	0.001±1E-04	0.001±1E-04
26-50	0.003±1E-03	0.005±6E-06	0.004±7E-04	0.003±6E-04	0.001±9E-05	0.001±2E-04
PSD_{MIP}(µm)						
0.01-0.1	0.039±7E-04	0.037±5E-04	0.018±5E-04	0.017±4E-04	0.0063E-04	0.0064E-04
0.1-5	0.044±2E-03	0.042±9E-04	0.183±2E-03	0.192±2E-03	0.025±4E-04	0.026±9E-04
5-30	0.041±4E-03	0.028±2E-03	0.150±1E-02	0.180±1E-02	0.037±7E-04	0.035±2E-03
30-75	0.040±3E-03	0.024±2E-03	0.039±2E-03	0.037±1E-03	0.168±4E-03	0.141±6E-03
75-100	0.014±1E-03	0.008±7E-04	0.009±2E-04	0.009±3E-04	0.110±3E-03	0.1032E-03
$PSD_{\mu CT}$(µm)						
25-76	0.021±2E-03	0.018±2E-03	0.077±5E-03	0.072±6E-03	0.014±3E-04	0.012±1E-03
76-126	0.012±2E-03	0.009±1E-03	0.044±6E-03	0.050±5E-03	0.014±9E-04	0.010±1E-03
126-480	0.031±9E-03	0.021±7E-03	0.035±7E-03	0.045±6E-03	0.029±4E-03	0.031±8E-03
480-2500	0.010±5E-03	0.008±3E-03	0.000±1E-04	0.001±3E-04	0.010±3E-03	0.023±1E-02

Values are expressed as means followed by standard errors.

Total pore volume in the size range revealed by µCT ($TPV_{\mu CT}$) was significantly higher in SND (0.16 cm^3 cm^{-3}) than in CL and SNDL (0.07cm^3 cm^{-3} in both soils) (Table 6). Furthermore, residue incorporation

caused a reduction of 0.016 cm^3 cm^{-3} in $TPV_{\mu CT}$ managed without mineral fertilisation, while an opposite effect (+0.035 cm^3 cm^{-3}) was found when R was associated with FERT treatment (interaction FERT × R significant at $p < 0.05$). The analysis of µCT pore size distribution (25-2500 µm diameter) revealed that sandy soils were mainly composed of pores in the range 25-480 µm (Table 8), with the largest pore class (480-2500 µm) being only 0.2% of µCT total porosity, while in clay and sandy-loam the largest pore class was more numerous (11% and 18%, respectively).

Pore morphology

There were significantly more regular pores ($S < 2$) in SNDL (41.37%) than in the other two soils (29.24% in SND and 23.88% in CL). However, irregular porosity ($2 < S < 5$) was the most numerous class in all soils (averaging 59.94%), although more predominant in clay and sandy (65.16 and 63.80%) than in sandy-loam (50.82%) ($p < 0.001$). Residues decreased the regular pores ($S > 5$) by 11.25% ($p < 0.05$), while significantly increasing the irregular and elongated ones (+6.78 % and +4.50%, respectively), as shown in Figure 10.

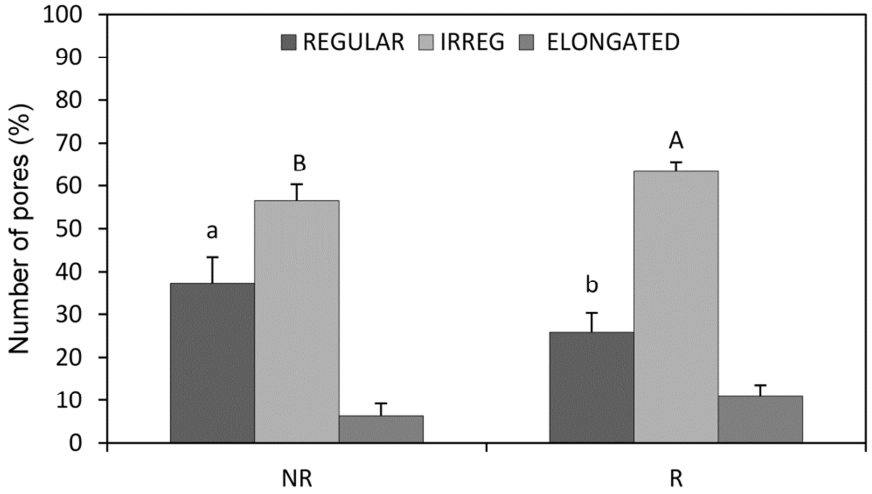

Figure 10. *Pore shape differences between plots with residue removal (NR) and residue incorporation (R).*

Structural differences between soil types were also observed in terms of 3D pore morphology (Fig. 12). The pore connectivity (CD), estimated by means of the Euler number algorithm, had the highest value (3.41 μm^{-3}) in the sandy soils, emphasizing a low number of redundant connections between pore

branches (Table 6). This effect was especially pronounced when residue incorporation was coupled with N fertilisation (4.94 μm^{-3}), underlining their negative effect on the soil macropore connections (interaction FERT ×R significant at $p<0.05$). By contrast, degree of anisotropy (0.58, on average) and fractal dimension (2.11, on average) were not able to identify any morphological difference in pore architecture, either between soils or between treatments. A general overview of the factors influencing the soil structure was provided by PCA (Table 10 and Figure 11).

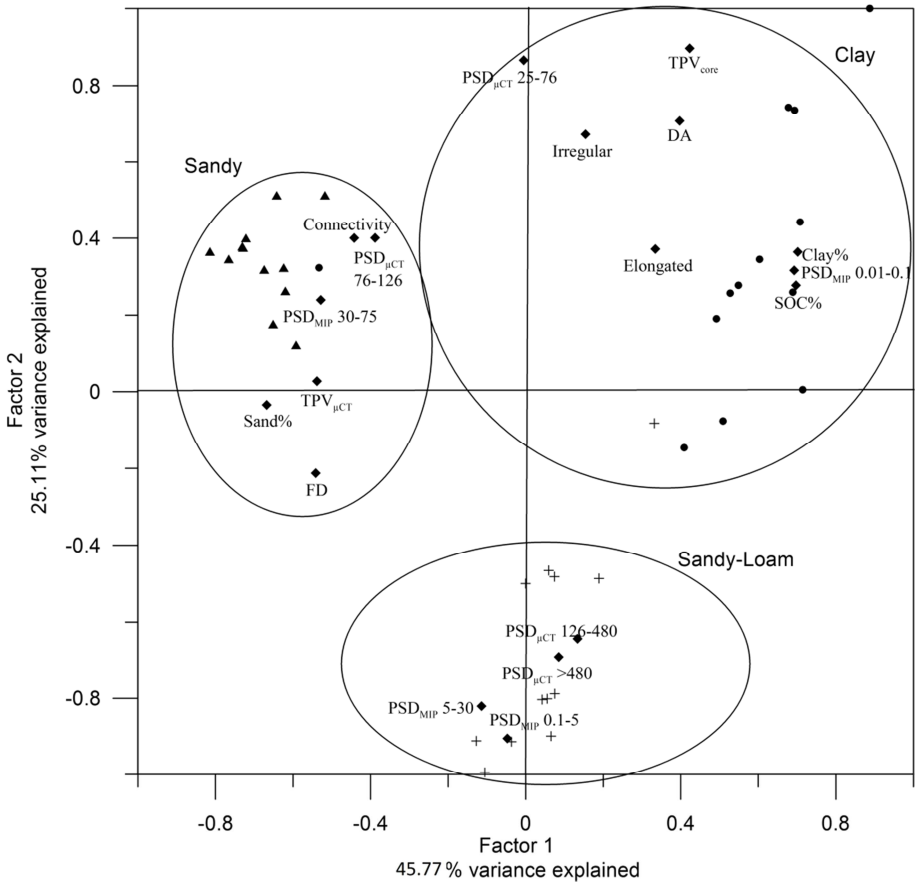

Figure 11. *Principal component analysis of selected variables. TPV_{core}, total pore volume analysed with helium pycnometer; DA, degree of anisotropy; Irregular, percentage of irregular pores; Elongated, percentage of elongated pores; SOC%, concentration of soil organic carbon; FD, fractal dimension; PSD_{MIP}, pore size distributions obtained with mercury intrusion porosimetry and $PSD_{\mu CT}$ pore size distributions obtained with micro tomography (each followed by pore size range). Symbols without labels represent the cases analysed (Triangles: sandy soil samples; points: clay soil samples; crosses: sandy-loam soil samples).*

Two principal components with eigenvalue > 1 were extracted, which accounted for 70.9% of the total variance. The first principal component explained 45.8% of the variance and was positively correlated with PSD_{MIP} class 0.01-0.1, clay and SOC content, while negatively with the largest PSD_{MIP}

classes (30-100 µm), $TPV_{\mu CT}$, the pore morphological parameters (CD and DA) and sand content. The second accounted for 25% of explained variance and was only correlated with TPV_{core} from helium pycnometry and pore size classes from MIP (0.1-30 µm) and µCT (25-76 µm).The distribution of variables on the xy-plane identified three clusters corresponding to the three soils (Figure 11). SND was associated to sand content and highly unconnected (high CD) pores in the range 30-126 µm, CL was identified by clay content and the cryptopores as detected by MIP (0.01-0.1 µm), while SNDL was associated to both micro- and macropores. PCs were not able to separate the single soil treatments on the planes (residues and/or fertilisation management).

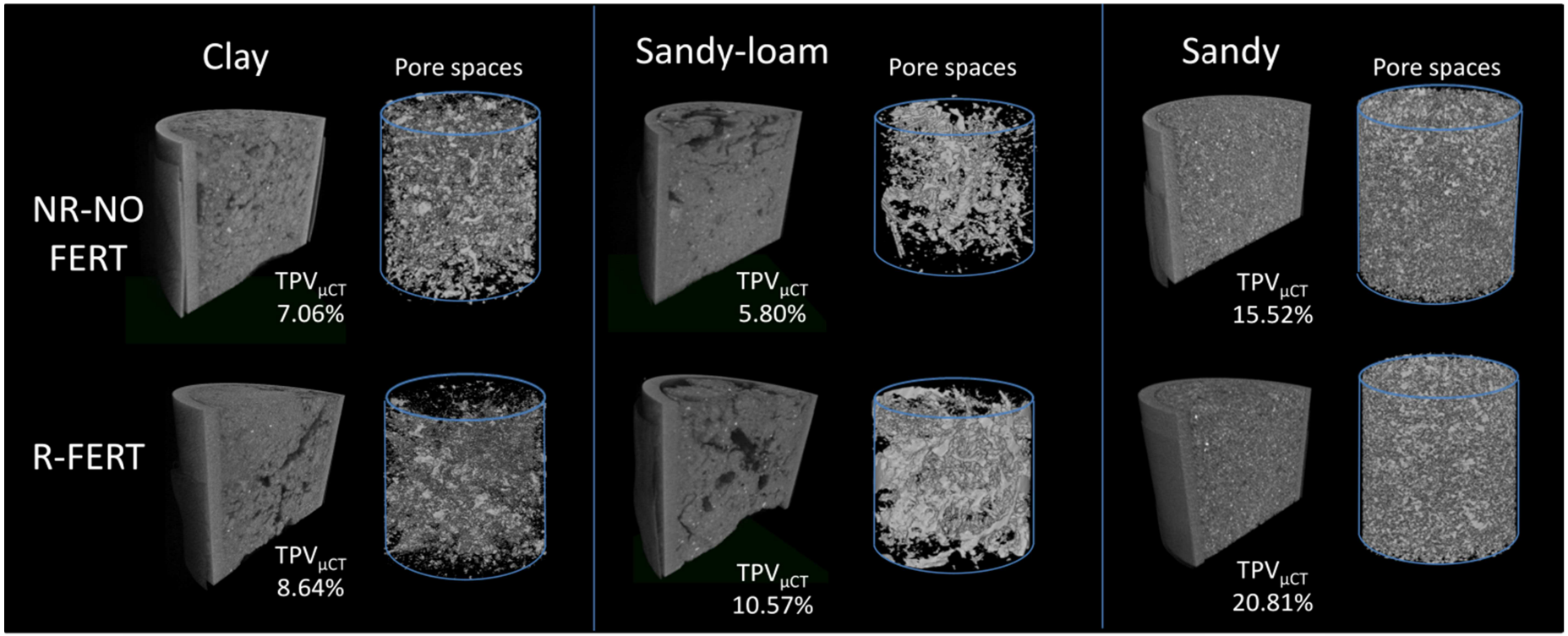

Figure 12. *3D reconstruction of selected soil cores and pore spaces of residue removal and no fertilization (NR-NOFERT) treatment and residue incorporation and 400 Kg N ha-1 fertilization (R-FERT) treatment with respective total pore volumes measured with micro tomography (TPVμCT).*

Soil hydraulic properties

Saturated hydraulic conductivity (Ks)

Measured Ks was higher in clay soil (41.9 md^{-1}) and lower in sandy-loam soil (1.1 md^{-1}), while sandy soils exhibited intermediate values of 8.8 md^{-1}. A significant interaction between soil type and fertilization level was detected (Figure 13). Indeed, fertilization caused a decrease of Ks in clay soil (from 57.3 md^{-1} to 26.4 md^{-1}), with the opposite taking place in sandy (from 5.4 md^{-1} to 12.3 md^{-1}) and in sandy-loam soil (from 0.7 to 1.5 md^{-1}). In addition, the effect of residue incorporation did not result substantial ($p>0.05$), with a decrement in conductivity in clay soil of 4.7 md^{-1}, and an increase from 7.8 md^{-1} (NR) to 9.8 md^{-1} (R) in sandy-loam and from 1.2 md^{-1} to 2.1 md^{-1} in sandy (NR vs R).

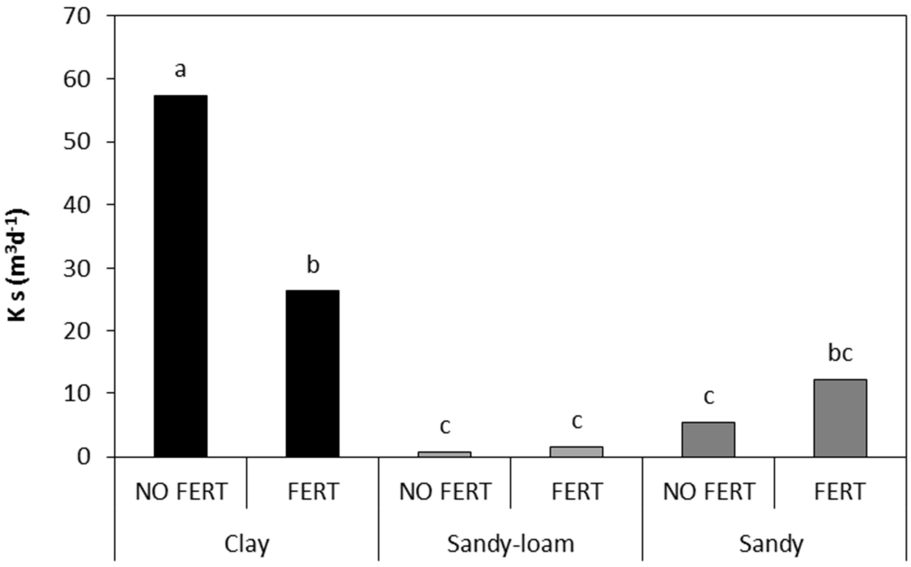

Figure 13. *Saturated hydraulic conductivity on the three soils in function of the N fertilisation.*

Soil water retention curve and unsaturated hydraulic conductivity

As expected, water retention curves were significantly different between the three soils (Table 10 and Figure 14a). Clay showed a higher residual water content (θr, 0.28 cm^3cm^{-3}), water content at saturation (θs, 0.60 cm^3cm^{-3}) and reciprocal of air entry potential (α, 0.12). Moreover, θr and α were significantly correlated with the clay content of the soils (Table 11). Sandy-loam soil presented the lower

values of θr and n, and intermediate values of θs and n. In addition, sandy-loam pores were the most tortuous, as revealed by a high tortuosity parameter (L) that was on average 1.13.

Table 10. *Van Genuchten parameters obtained by inversion.*

	θr	θs	α	n	Ks_{sim}	L
	cm^3cm^{-3}				$m\ d^{-1}$	
Clay	0.28a	0.60a	0.12a	1.35b	7.86b	-0.06b
Sandy-loam	0.03b	0.52b	0.04b	1.28b	2.50b	1.13a
Sandy	0.07b	0.42c	0.04b	2.85a	25.34a	0.01b
NO FERT	0.13	0.50b	0.06	1.84	13.88	0.52
FERT	0.12	0.53a	0.08	1.81	9.92	0.20
NR	0.13	0.51	0.07	1.80	12.50	0.02b
R	0.13	0.52	0.06	1.85	11.30	0.71a

Values expressed as means, different letters indicate significant differences($p<0.05$).

Sandy soil curves exhibited the highest slope (high 'n' parameter: 2.85) and this is underlined also by the positive correlation between this parameter and sandy content of soil (β=1.39). Additionally, in this soil the simulated Ks was significantly higher if compared with clay and sandy-loam (Table 10). Fertilization significantly increased the water content at saturation in the three soils, while it did not affect the other parameters (Table 10). The Van-Genuchten parameters of the water retention curves were differently influenced by residues in the three soils (Figure 14b, c and d), but the effects were statistically significant only in the regards of tortuosity parameter (L, Table 10). Indeed θr increased in clay soil (from 0.27 to 0.29 cm^3cm^{-3}, Figure 14), with an opposite effect in sandy and sandy-loam soil (0.01 cm^3cm^{-3} difference between the two treatments for both soils). The water content at saturation was improved by residues only in sandy soil (from 0.41 to 0.43 cm^3cm^{-3}) while it remained unaffected in the other two soils (Figure 14). The reciprocal of air-entry potential (α) showed opposite trends in sandy and sandy-loam soil, if compared with clay (it increased in the first two and diminished in the last one). There was a slight decrement in the curve slope of clay soil, while it increased in sandy-loam (0.05 and 0.001 difference, respectively). In sandy soil the effect was more pronounced, with a variation from 2.75

to 2.94 (Table 10). A residue-induced increase across all the soils was found for the tortuosity parameter, even if only in the NO FERT plots (interaction residues x fertilisation significant at $p<0.05$). Unsaturated hydraulic conductivity curves (Ku) of clay and sandy-loam soil showed small decrements in conductivity per unit of matric potential decrease, if compared to sandy soil (Figure 15a). On the contrary of what observed in the retention curves, for this parameter the residue effect was not clearly detectable (Figure 15b, c and d), with no evident differences between soils receiving residues (R) and the ones not receiving them (NR).

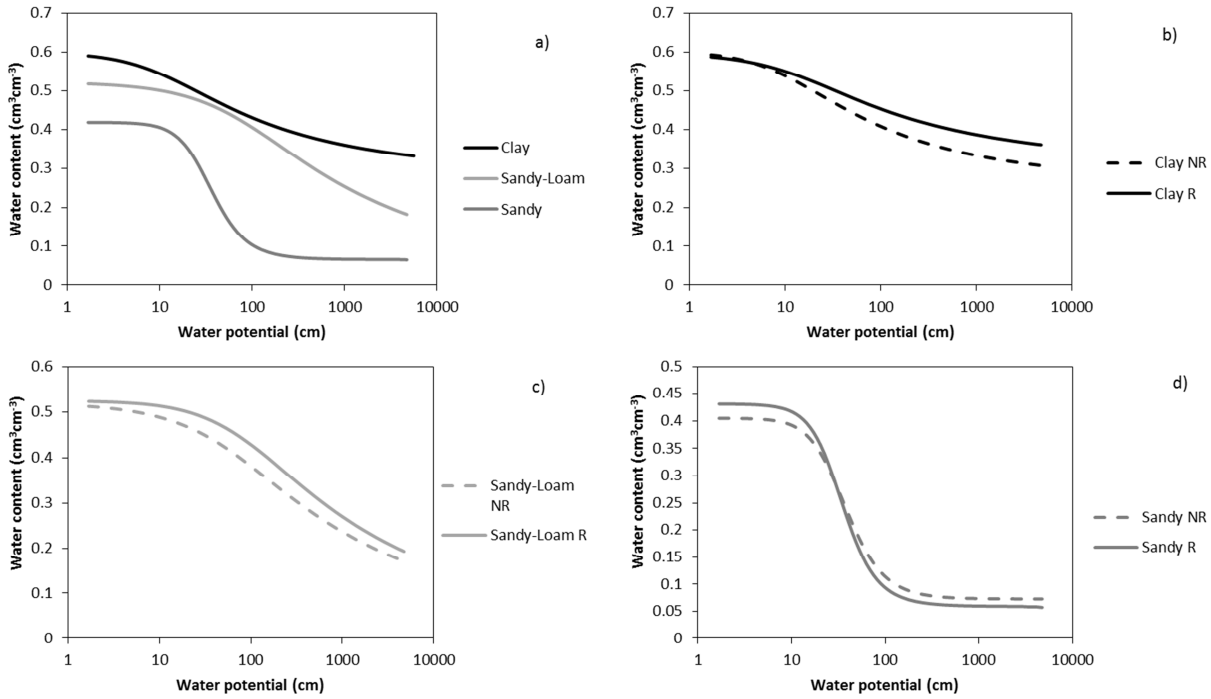

Figure 14. *Water retention curves interpolated with Hydrus. A) average curves for the three soils; b) average curves for clay soil with residue incorporation (R) or removal (NR); c) average curves for sandy-loam soil with residue incorporation (R) or removal (NR); d) average curves for sandy soil with residue incorporation (R) or removal (NR).*

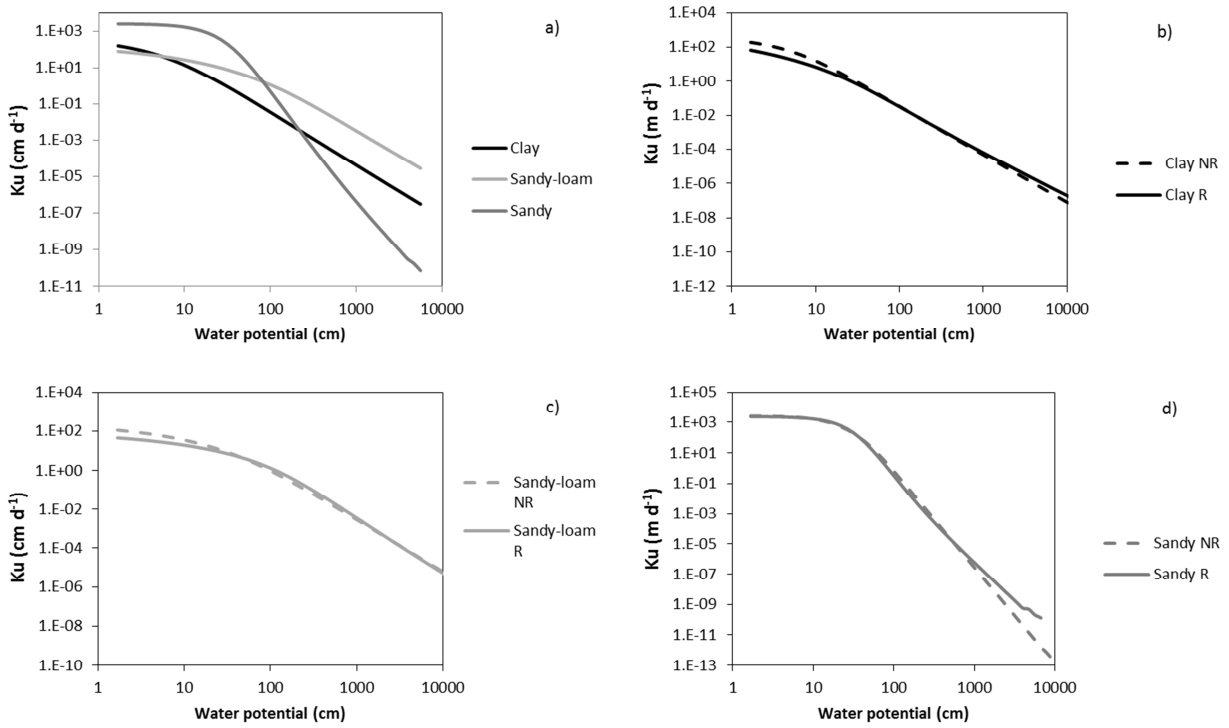

Figure 15. *Unsaturated hydraulic conductivity curves (Ku) obtained with Hydrus. A) average curves for the three soils; b) average curves for clay soil with residue incorporation (R) or removal (NR); c) average curves for sandy-loam soil with residue incorporation (R) or removal (NR); d) average curves for sandy soil with residue incorporation (R) or removal (NR).*

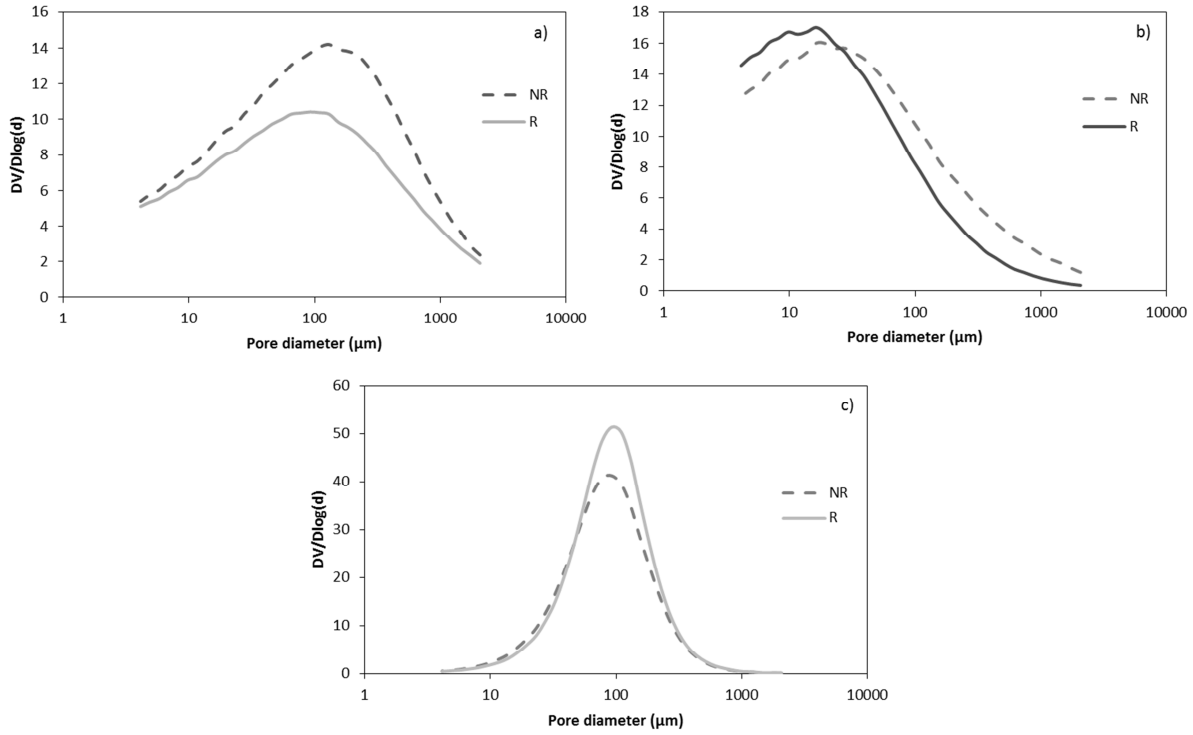

Figure 16*. Pore size distributions derived from water retention curves of a) clay, b) sandy-loam and c) sandy soil.*

Pore size distributions derived from water retention curves (Fig. 16) show for clay and sandy-loam soil a shift in the peak of the distribution towards left in soils subjected to residue incorporation, indicating a reduction in the dimension of the more frequent class of pores. On the contrary, the sandy curves do not display a visible shift in the more frequent class of pores, indicating slight effects of residues in these regards. The strong variations in hydraulic properties between the soils were noticed also if considering the water contents at -100 and -330 cm and their correlations with the texture parameters of soils (Table 11). For both water contents, clay exhibited the highest values (0.44 and 0.39 cm^3cm^{-3} at -100 and -330 cm of matric potential, respectively). Intermediate values of 0.40 and 0.33 cm^3cm^{-3} (at -100 and -330 cm) were observed in sandy-loam soil. Sandy soil showed very low water contents both at -100 cm (0.12 cm^3cm^{-3}) and at -330 cm (0.08 cm^3cm^{-3}). As a matter of fact, both were negatively correlated with sand content of samples (Table 11).

Table 11. *Multiple correlations between the variables analzed and soil content of organic carbon, sand and clay percentage.*

	Regression coefficients				
Variables	Intercept	% SOC	% Sand	% Clay	Multiple R^2
	α	β_1^*	β_2	β_3	
θr	-0.25	-	0.81	1.55	0.86
θs	0.6	-	-0.87	-	0.76
α	0.011	-	-	0.59	0.35
N	0.028	-	1.39	0.53	0.92
L	2.88	-	-0.82	-0.81	0.16
Water contents at:					
5000 cm	-0.001	-	-	0.94	0.88
15000 cm	0.001	-	-	0.95	0.90
330 cm	0.42	-	-0.97	-	0.94
100 cm	0.48	-	-0.97	-	0.94
PAW	0.42	-	-1.44	-0.71	0.78

**Standardised betas. Correlations are significant at p<0.05.*

The incorporation of crop residues significantly influenced both the water content at -100 cm (residue main effect significant) and at -330 cm (significant interaction soil x residues). More specifically, residues increased the water content at -100 cm (Figure 17a) on average of 0.02 cm^3cm^{-3}, with

predominant effects in clay and sandy-loam soil (from 0.42 to 0.46 cm^3cm^{-3} and from 0.38 to 0.41 cm^3cm^{-3} in NR and R treatments), and an opposite trend in sandy soil (decrease from 0.13 to 0.10 cm^3cm^{-3}). In addition, residues caused an increment of water content at -330 cm, on average (from 0.25 to 0.28 cm^3cm^{-3}). However, if the soils are considered separately (Figure 17b), the same behaviour found for the water contents at -100 cm is identified, with the increase in water content attributable only to clay and sandy-loam, and a slight decrease taking place in sandy soil (interaction soil x residues significant at p=0.058).

Water content at low matric potentials and plant available water (PAW)

The water contents at matric potentials of -5000 and -15000 cm were highly different between soils ($p<0.001$), with the clay soil showing the maximum values (0.21 and 0.18 cm^3cm^{-3} at -5000 and -15000 cm). This is consistent with the observed positive correlation between the water contents and clay percentage of soils (Table 11).

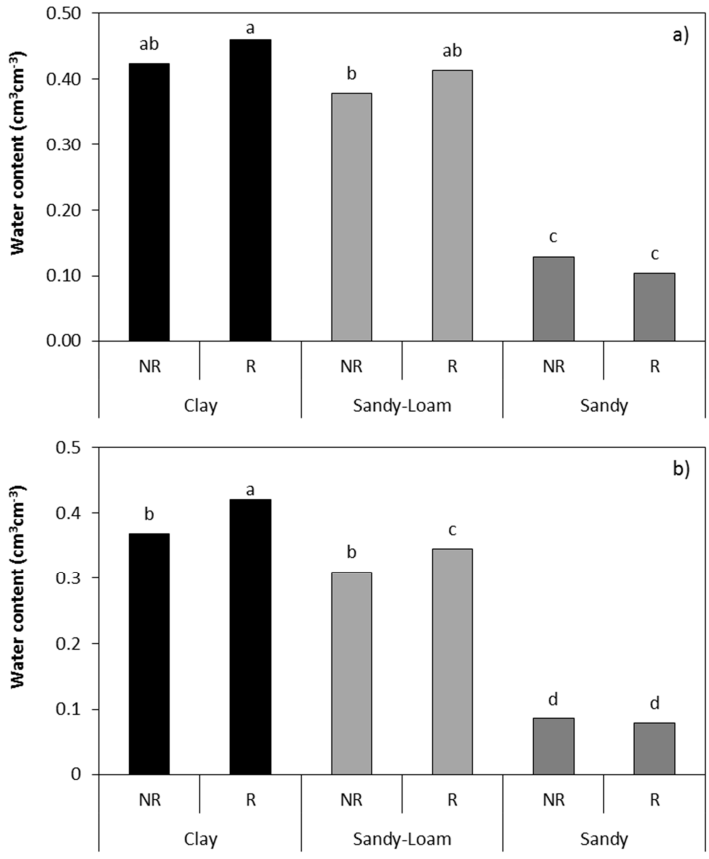

Figure 17. *Water contents at defined pressure heads as a function of the residue management type: a) pressure head of - 100 cm, and b) - 330cm.*

Sandy-loam presented intermediate water contents (0.11 and 0.08 cm^3cm^{-3}), and the lowest values were found in sandy soil (0.03 and 0.02 cm^3cm^{-3}).

Residues affected the water content at -5000 cm (Figure 18a), with effects varying with soil type and fertilization level (interaction soil x fertilization x residues significant at p=0.04). Indeed, in clay soil there was a residue – mediated reduction of water content of non-fertilized plots coupled with an increase in fertilized ones. In sandy the effect was specular, with a residue-induced increment in water content in NO FERT and a decrease in FERT plots. Lastly, in sandy-loam soil the water content of plots subjected to residue incorporation was greater for both the NON FERT and the FERT treatments.

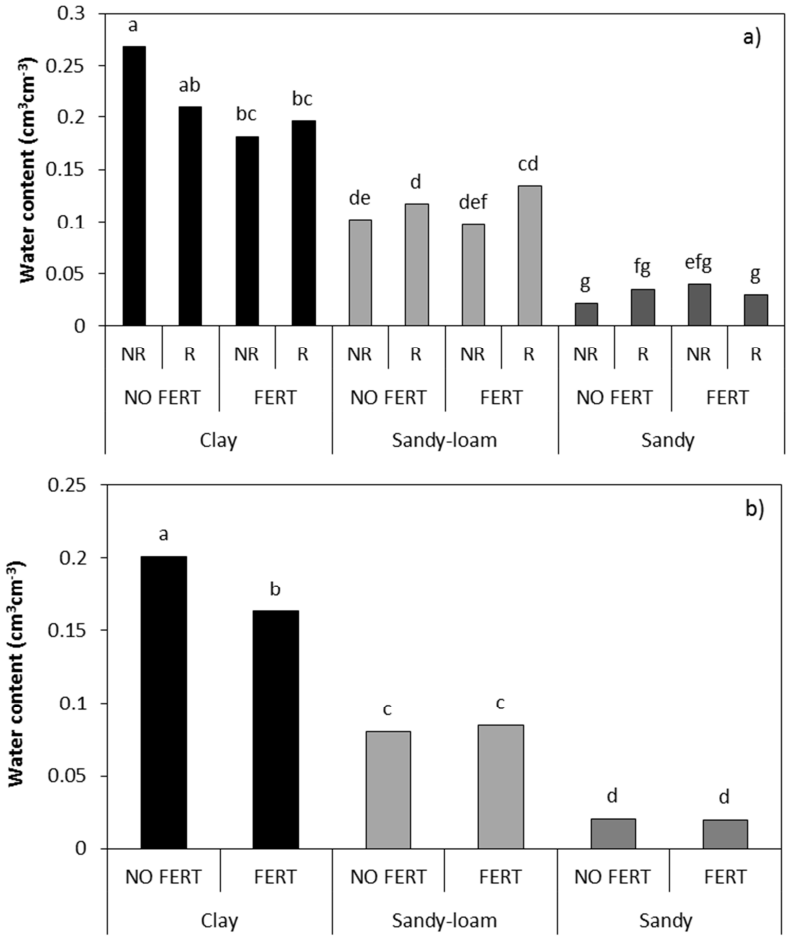

Figure 18. *Water content at a) -5000 cm and b)-15000 cm, as a function of soil type, fertilization and residue management.*

Regarding the water contents at -15000 cm, a significant interaction between the soil type and the fertilization level was found (Fig. 18b), indeed the positive effects on water content caused by FERT treatment were clearly visible in sandy-loam (increment of 0.01 cm^3cm^{-3}) while only slightly present in sandy soils (increase of 0.0006 cm^3cm^{-3}), and became negative in clay (decrement of 0.04 cm^3cm^{-3}).

Plant available water (PAW) of sandy-loam (0.24 cm^3cm^{-3}) was higher if compared with clay soil (0.21 cm^3cm^{-3}) and sandy soil, which showed the lowermost values of 0.08 cm^3cm^{-3}. Furthermore, PAW was significantly increased by residue incorporation in clay and sandy-loam soil (increase of 0.07 and 0.03 cm^3cm^{-3}, respectively (Figure 19). The opposite (but not significant) effect was found in sandy soil, with water contents of 0.07 cm^3cm^{-3} and 0.06 cm^3cm^{-3} for NR and with R treatments, respectively.

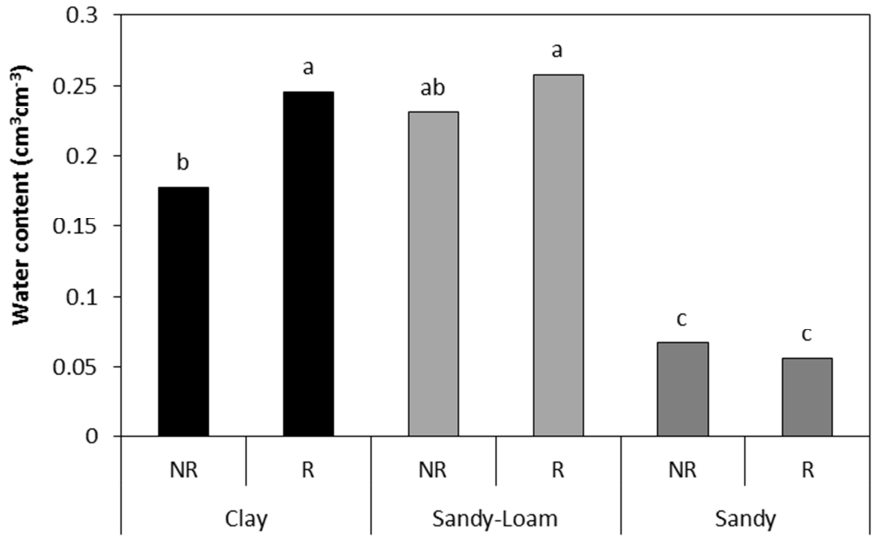

Figure 19. *Plant available water (PAW) as a function of residue removal (NR) and incorporation (R).*

Discussion

Crop yield and nitrogen use efficiency

The long-term incorporation of crop residues caused a slight but almost ubiquitous increase in yield, however the mechanisms behind this increase differ for the different crops and types of soil, as the coupled analysis of yield response curves and nitrogen use efficiency highlights. The crop- and soil-specific response to residue use is confirmed by the apparently contrasting results found in the literature (e.g. Brennan et al., 2014; Malhi et al., 2011). In sugarbeet and cereals, the efficiency of residue incorporation appears more pronounced in soils with the lowest fertility, thus this practice is surely advisable in these soils in order to increase their fertility. The absence of evident effects on sugarbeet yield in clay may be due to the fact that in these soils the crop finds an intrinsic high nutrient content that is sufficient to reach maximum production levels and so nutrient input by residue decomposition is not very effective in increasing crop yield. Indeed, it is well recognised that sugarbeet gives its best growth performances in rich loamy soils (Fageria, 2012). In the sandy soil, the productivity enhancement attained seems to be caused by other mechanisms along with the purely nutritional effect, especially at low fertilization levels, where the increase in yield is coupled with an increase in nitrogen use efficiency. Consequently, residue use for this crop appears more useful in medium to low fertility soils and at low fertilization levels. In accordance with the results found by Petersen et al. (2013) and Brennan et al. (2014), winter wheat appears to be slightly influenced by residue incorporation. In our study this may be attributed to the fact that the period of maximum N uptake is earlier than in other crops and takes place when the mineralization of residues is still slow due to low soil temperature. Accordingly residue effect is likely to be marginal both on crop yield and on nitrogen use efficiency especially in highly fertile soils. On the other hand, in sandy soil their use is likely to favour crop yield, even if the effect is lower than the one observed in summer crops.

In maize the effects of residues on yields are modest in clay and sandy-loam soils. Instead, the more pronounced increase in yields in sandy soil can be related to a relatively high uptake of N from residues. Potato and tomato are not affected by residue incorporation in sandy soil while strong effects are evident in the sandy-loam. The sandy-loam soil has a relatively high silt and carbonates content, leading to a tendency to form a surface crust. Residue incorporation can lead to an improvement of soil characteristics and particularly to surface permeability, with positive effects for both solanaceous crops.

Soil parameters

Soil bulk density, organic carbon and total Kjeldhal nitrogen

The removal of residues is indicated by some studies as a cause of increased soil susceptibility to compaction (Verhulst et al., 2011) mediated by the increase in bulk density (Lal, 2009). Our results suggest that these conclusions can be extended to a range of soils with contrasting textural characteristics, but the effects are mainly concentrated in the upper soil layer (0-20 cm). The absence of significant impacts of nitrogen fertilization may further indicate that root-derived organic matter is less important than residual aboveground plant biomass in the reduction of bulk density. Powlson et al. (2011a), reviewing 25 experiments on residue incorporation or removal, found that the C increase was relatively low (< 10%) in the majority of cases and significant only in six, although they observed a high variability in C content (0% to 37.5%) as a result of soil type, straw input and experiment length. In our case this was true only for clay soil which showed the lowest increase in SOC and TKN content between R and NR treatments (+8% for SOC and +9% for TKN) as a result of the major role of fine particles (both clay and silt) on the physical protection of organic matter. It is of particular interest that sandy soil exhibited a low quantitative C and N increase (+4 t ha^{-1} and +0.48 t ha^{-1}, respectively) although the highest in relative terms (+19% and +29%) as a consequence of residue incorporation, indicating that some stabilization mechanisms may act in the long term independently of the scarce ability of this soil to protect SOC from degradation. Lugato et al. (2009), in a similar long-term experiment, observed that when larger porosity dominates (e.g. sandy soils), mechanisms of physical protection are less relevant

and the protection of SOC is mainly due to the selective preservation of more recalcitrant or less decomposable materials. These soils, being also more water conductive, can be prone to a selective transport of particulate or dissolved organic materials in the lowest soil layers where the activity of soil microorganisms is limited and thus the mineralization is slowed. This is confirmed by the fact that in our results the increase in carbon concentration as a result of residue incorporation was extended until 50 cm of depth in sandy and sandy-loam soils. A general C accumulation was also observed as a result of high N input. According to Lemke et al., (2010), the application of fertilizers induced an increase in the amount of residues (on average, the fertilized plots of our study produced 4 t ha^{-1} $year^{-1}$ more residues than unfertilized ones) and most likely of root debris and exudates as a result of nutrient stimuli to plant growth. The absence of significant effects on the C/N ratio of clay and sandy soil indicates that nitrogen deficiencies caused by the addition of residues (which have an high C/N ratio) if occurred, were quickly neutralized and did not result in a long-lasting N immobilisation. Only in sandy-loam soil, residue incorporation increased the C/N ratio in a stabile way. Anyway, this change may not have caused a significant nitrogen immobilization by microorganisms, or if it took place, its magnitude may have not been sufficient to cause detrimental effects on plant growth, as yields resulted improved by residue incorporation (cfr. Chapter *Crop yield and nitrogen use efficiency* in the Results section).

Pore architecture

The comparison of the clay, sandy-loam and sandy soils showed substantial differences in terms of soil structure, while the effect of residue incorporation was only partially detectable. In fact, the highly contrasting soil texture was crucial to distinguish the pore network characteristics, as also emphasized by the clusters in the PCA analysis, probably masking the subtle structure changes induced by residues. In particular, the clay soil dominated the pore size classes < 0.1 µm as their volume, detected with N_2 adsorption and partly with MIP, was always higher than in sandy-loam and sandy soils. Conversely pores > 30 µm, as detected by MIP and µCT, were particularly numerous in the sandy soils although negligible when > 480 µm with µCT imaging. Indeed, the sandy soil was unable to form stable aggregates due to the absence of clay-OC complexes (Lugato et al., 2010), while the soils dominated by fine particles (both

clay and sandy-loam soils) showed pores greater than 480 µm, symptom of existing cracks and inter-aggregate pores (Hillel, 1998). Nevertheless, total pore volume measured with the core method gave higher values as affected by both residue incorporation (+3.6%) and high fertilisation rate (+3.2%), while total pore volumes measured with mercury intrusion porosimetry and microtomography did not show differences between treatments. In fact, both MIP (0.01-100 µm) and µCT (25-2500 µm) porosities were only partial measures of the total pore volume within the samples, while the core method included all the pores. Similar results were observed by Blanco-Canqui and Lal (2008), showing that an increase in maize stover removal produced a decrease in soil water content at saturation and consequently in soil porosity. However, the full evaluation of pore size distribution from nanometres to millimetres highlighted the effect of crop residue incorporation, and consequently of organic carbon accumulation, on the soil structure. Indeed nanopores, estimated by means of N_2 adsorption, were significantly correlated with SOC as they interacted with it in two ways. Firstly, the pores in the range 0.25-2 nm were negatively correlated with OC content, emphasizing its effect on pore filling or blockage, as also reported by Zaffar and Lu (2015), who found a SOC pore occlusion effect for pores < 2 nm. Secondly, the positive correlation between 10-50 nm pore size class and C content was likely due to an OC-mediated stimulus to clay particle aggregation (Mayer et al., 2004). The effect of OC content on the soil structure also extended to the micrometre scale. Indeed a reduction of mesopores (30-75 µm) was estimated by means of MIP in correspondence to the increase in OC values, as reported by other authors (Lugato et al., 2009). Lugato et al. (2009) also found a positive correlation between MIP pore size class 0.01–0.1 µm and SOC which, on the contrary, was not observed in our MIP results. Although µCT analysis did not reveal significant differences between treatments in terms of pore size distribution, it still allowed the effect of crop residues on the pore structure to be identified. Indeed, their incorporation led to morphological changes in the pore structure, decreasing regular pores and increasing irregular and elongated ones, as already observed by other authors. In particular Pagliai et al. (2004), studying the effects of different organic carbon inputs on pore morphology, found a significantly high percentage of elongated pores in amended treatments. Furthermore Papadopoulos et al., (2009) suggested that the

pores of aggregates fertilised with organic input were mainly cracked and elongated. Although their findings were obtained as a consequence of manure instead of crop residue inputs, a similar effect between treatments can be hypothesized as both had high straw content.

Soil hydraulic properties

In relation to saturated hydraulic conductivity, soil texture played a major role while crop residue effect appeared limited. The high difference between soils may be justified with the fact that in our clay soil the presence of macropores and cracks produced a preferential flow, making it more conductive if compared to the other two soils (for which the macro- component of pore architecture was not so pronounced). Besides the relatively slight effect of residues, it is still possible to get important information from the analysis of soil conductivity in response to their management. In particular, the opposite behaviour of clay if compared with the other two soils could be explained by the fact that the accretion of residue organic carbon exerted a more pronounced water retention, thus lowering the hydraulic conductivity of this soil. In the other two (especially in sandy-loam), the residue-derived organic matter could have triggered soil aggregation and thus porosity, finally explaining the increase in water conductivity. The effects on water retention curves appear prevalently texture-dependent, as the significant correlations between the majority of them and the sand and clay content of soils reveal. Regarding clay soil, the increase in residual water content and tortuosity of pore system suggests that residue effect may have been prevalently guided by an increase in organic matter which is not quickly mineralized due to the physical protection of clay particles. Additionally, the reduction in curve slope indicates a slight extension in the range of pore sizes, which may be caused by the increase in organic matter. Finally the observed reduction in alpha parameter (i.e. increase of air-entry potential) may indicate that pore system is less prone to drainage. On the contrary in the other two soils the coupled decrease in residual water content with air-entry potential, suggests that water flow was incremented by the presence of residues and this may be due to an organic matter mediated intensification in soil aggregation and consequently in porosity. This is further confirmed by the observed increase in the slope of water retention curve, which indicates that the size distribution of pores is very narrow and

thus they are more prone to be quickly emptied from water. Residues increased the water contents at -100 cm and -330 cm and the PAW in the in clay and sandy-loam soil alike, while the absence of differences found in water content at saturation suggests that the range of pore sizes affected in the two soils was that of micropores (diameter between 8 and 30 µm) and possibly part of ultra-micropores (5 - 0.5 µm). However these conclusions are confirmed by the data on pore size distribution only for sandy-loam soils, which reveals a slight increase in porosity induced by residue incorporation (Cfr. paragraph *Pore architecture* in the section *Results* $p<0.05$). The same trends were observed by Blanco-Canqui and Lal (2008) on a clay loam and two silt loam soils. In contrast of what evidenced by studies of Zeleke et al. (2004) who found a residue-induced increase only in pores >10 µm in a sandy-loam, our results show that in this soil the increase in pore volume was extended to the smallest pores (i.e. cryptopores <0.5 µm) as the increase in water contents at -5000 cm reveals, while no effects in this range of pores were detected in the other two soils. The same trend can be seen also for water contents at -15000 cm, even if not in a significant way. Sandy soil displayed an opposite behaviour (decrease in water contents at -100, -330 and PAW coupled with an increase in water content at saturation) revealing that residues acted by increasing aggregation only in the larger macropore area (>100 µm), with a reduction in the area of all other pores. The pore-size distribution data confirms this hypothesis, even if the results are not significant.

Conclusions

Incorporation of residues seems to have different effects on productivity, depending on crop and soil type. For potato and tomato and, to a lesser extent, for sugarbeet, residues can improve crop productivity, while the effects on cereals (especially on winter wheat) seem to be lower. Regarding soil type, residues are proportionally more effective in sandy and sandy-loam soils, both through a direct nutritional effect and, possibly, an improvement of soil characteristics. Anyway the residue effect is relatively low, with modest increments of biomass in the most fertile soils, and their effect can be compensated by N fertilization. Soil organic carbon was significantly affected by the long-term incorporation of crop residues with effects quantitatively more evident in clay soil and high relative increments in sandy soil. The effects were not limited to the upper soil layer, but extended to lower depths especially for sandy and sandy-loam soil. The highest nitrogen fertilization induced increases in soil carbon comparable with those induced by residues, however the effects appeared not proportional to the application rate of fertilizer. The results suggest that in the pedo-climatic conditions of north-eastern Italy this practice could be suitable for maintaining the soil carbon content, especially in coarse-textured soils. The residue-induced effects on soil organic carbon were not accompanied by a relevant change in soil pore size distribution from nano to macro scale, even if they induced an increase in total porosity. Most likely, the intrinsic highly contrasting pore characteristics of the soils could have partly masked subtle changes caused by residues. Even if only slightly influenced in quantitative terms, the pore network showed a rearrangement towards a more elongated and irregular structure as revealed by microtomography. Regarding soil hydrology, residue effect appears texture-dependent, as the very different behaviours of the three soils suggest. In clay soil the analysis of retention curve and water contents at -330 and -100 cm suggest that residue effect is concentrated in a restricted range of porosity (i.e. mainly micropores and ultra-micropores). In sandy-loam soil residue-induced increase in porosity extended to a quite large range of pores (i.e. micropores, ultramicropores and cryptopores). In sandy soil there appears to be an increase in the presence especially of macropores, however in this soil the

effects are less evident than in the other two. It is to underline that these effects are only partially confirmed by the analysis of pore size distributions, which do not show clear influences of residues.

In conclusion, residue incorporation to soil appear surely an advisable practice to sustain yields and maintain the contents of soil organic carbon, and these effects take place in all the soils examined, even if with clearly different intensities. The increments in SOC increase soil porosity and pore shape and improve the available water content of the soils with the most fine texture, but do not have clear effects on sandy soil.

References

Abiven, S., Menasseri, S., Chenu, C. (2009). The effects of organic inputs over time on soil aggregate stability – A literature analysis. *Soil Biology and Biochemistry*, *41*(1), 1–12. doi:10.1016/j.soilbio.2008.09.015

Barrett, E., Joyner, L., Halenda, P. (1951). The determination of pore volume and area distributions in porous substances. I. Computations from nitrogen isotherms. *Journal of the American …*, *1896*(1948). Retrieved from http://pubs.acs.org/doi/abs/10.1021/ja01145a126

Blanco-Canqui, H., Lal, R. (2008). Corn stover removal impacts on micro-scale soil physical properties. *Geoderma*, *145*(3-4), 335–346. doi:10.1016/j.geoderma.2008.03.016

Blanco-canqui, H., Lal, R. (2009). Corn Stover Removal for Expanded Uses Reduces Soil Fertility and Structural Stability. *Soil Science Society of America Journal*, *73*(2). doi:10.2136/sssaj2008.0141

Brennan, J., Hackett, R., McCabe, T., Grant, J., Fortune, R., Forristal, P. D. (2014). The effect of tillage system and residue management on grain yield and nitrogen use efficiency in winter wheat in a cool Atlantic climate. *European Journal of Agronomy*, *54*, 61–69. doi:10.1016/j.eja.2013.11.009

Cameron, K.C., Buchan, G.D., 2006. Porosity and pore-size distribution. In: Lal, Ratan (Ed.), Encyclopedia of Soil Science, vol.2. Taylor and Francis, pp.1350–1353.

Cherubini,F., Ulgiati, S. (2010). Crop residues as raw materials for biorefinery systems—a LCA case study. *Applied Energy 87*, 47–57. doi: 10.1016/j.apenergy.2009.08.024.

Cnudde, V., Cwirzen, A., Masschaele, B., Jacobs, P. J. S. 2009. Porosity and microstructure characterization of building stones and concretes. Engineering Geology 103,76–83. doi: 10.1016/j.enggeo.2008.06.014.

Dal Ferro, N., Charrier, P., Morari, F. (2013). Dual-scale micro-CT assessment of soil structure in a long-term fertilization experiment. *Geoderma*, *204-205*, 84–93. doi:10.1016/j.geoderma.2013.04.012

Dal Ferro, N., Sartori, L., Simonetti, G., Berti, A., Morari, F. (2014). Soil macro- and microstructure as affected by different tillage systems and their effects on maize root growth. *Soil and Tillage Research 140*, 55–65. doi:http://dx.doi.org/10.1016/j.still.2014.02.003.

Dane , J. H., Topp, G. C. (2002). Methods of soil analysis. Part 4. Physical Methods. Soil Sci Soc Am Book Series 5. Soil Science Society of America, Madison,WI.

Deurer, M., Grinev, D., Young, I., Clothier, B. E., Müller, K. (2009). The impact of soil carbon management on soil macropore structure: a comparison of two apple orchard systems in New Zealand. *European Journal of Soil Science 60*,945–955. doi:http://dx.doi.org/10.1111/j.1365-2389.2009.01164.x.

Fageria, N. K. (2012). Management Strategies for Maximizing Root Systems. In *The Role of Plant Roots in Crop Production* (pp. 369–442). CRC Press. doi:doi:10.1201/b12365-10

FAO-UNESCO (2008). Soil Map of the World. Revised Legend. FAO, Rome.

Hammerbeck, A. L., Stetson, S. J., Osborne, S. L. (2012). Corn Residue Removal Impact on Soil Aggregates in a No-till Corn/Soybean rotation. *Soil Science Society of America Journal*, *76*, 1390–1398. doi:10.2136/sssaj2011.0421

Harrigan, T. P., Mann, R. W. (1984). Characterization of microstructural anisotropy in orthotropic materials using a second rank tensor. *Journal of Materials Science*, *19*(3), 761–767. doi:10.1007/BF00540446

Hildebrand, T., Rüegsegger, P. (1997). A new method for the model-independent assessment of thickness in three-dimensional images. *Journal of Microscopy*, *185*(1), 67–75. doi:10.1046/j.1365-2818.1997.1340694.x

Hillel, D. (1998). *Environmental soil physics: Fundamentals, applications, and environmental considerations*. Academic press.

Horvath, K , Kawazoe, G. (1983). Method for the calculation of effective pore size distribution in molecular sieve carbon. *Journal of Chemical Engineering of Japan*, (12). Retrieved from http://dns2.asia.edu.tw/~ysho/YSHO-English/1000 CE/PDF/J Che Eng Jap16, 470.pdf

Hsieh, J. (2009). Computed tomography: principles, design, artifacts, and recent advances. SPIE Bellingham, WA.

Kaiser, H. F. (1974). An index of factorial simplicity. *Psychometrika*, *39*(1), 31–36.

Kumar, K., Goh, K. M. (1999). Crop residues and management practices: effects on soil quality, soil nitrogen dynamics, crop and nitrogen recovery. *Advances in Agronomy*, *68*, 197–319.

Lal, R. (2004). Soil carbon sequestration to mitigate climate change. *Geoderma*, *123*(1-2), 1–22. doi:10.1016/j.geoderma.2004.01.032

Lal, R. (2005). World crop residues production and implications of its use as a biofuel. *Environment International*, *31*(4), 575–84. doi:10.1016/j.envint.2004.09.005

Lal, R. (2009). Soil quality impacts of residue removal for bioethanol production. *Soil and Tillage Research*, *102*(2), 233–241. doi:10.1016/j.still.2008.07.003

Lal, R., Shukla, M. K., 2004. Principles of Soil Physics. Marcel Dekker, New York p. 154.

Lemke, R. L., VandenBygaart, . J., Campbell, C. a., Lafond, G. P., Grant, B. (2010). Crop residue removal and fertilizer N: Effects on soil organic carbon in a long-term crop rotation experiment on a Udic Boroll. *Agriculture, Ecosystems & Environment*, *135*(1-2), 42–51. doi:10.1016/j.agee.2009.08.010

Lugato, E., Morari, F., Nardi, S., Berti, A., Giardini, L. (2009). Relationship between aggregate pore size distribution and organic–humic carbon in contrasting soils. *Soil and Tillage Research*, *103*(1), 153–157. doi:10.1016/j.still.2008.10.013

Lugato, E., Simonetti, G., Morari, F., Nardi, S., Berti, A., Giardini, L. (2010). Distribution of organic and humic carbon in wet-sieved aggregates of different soils under long-term fertilization experiment. *Geoderma*, *157*(3-4), 80–85. doi:10.1016/j.geoderma.2010.03.017

Lützow, M. V., Kogel-Knabner, I., Ekschmitt, K., Matzner, E., Guggenberger, G.,Marschner, B., Flessa, H., (2006). Stabilization of organic matter in temperate soils: mechanisms and their relevance under

different soil cnditions—a review. *European Journal of Soil Science. 57*, 426–445. doi: 10.1111/j.1365-2389.2006.00809.x.

Malhi, S. S., Nyborg, M., Solberg, E. D., Dyck, M. F., Puurveen, D. (2011). Improving crop yield and N uptake with long-term straw retention in two contrasting soil types. *Field Crops Research*, *124*(3), 378–391. doi:10.1016/j.fcr.2011.07.009

Mayer, L. M., Schick, L. L., Hardy, K. R., Wagai, R., McCarthy, J. (2004). Organic matter in small mesopores in sediments and soils. *Geochimica et Cosmochimica Acta*, *68*(19), 3863–3872. doi:10.1016/j.gca.2004.03.019

Mualem, Y. (1976). New model for predicting the hydraulic conductivity of unsaturated porous media. *Water Resources Research*, *12*(3), 513–522. doi: 10.1029/WR012i003p00513

Oades, J. M., Osmond, G., Fungalhyphae, E., Iron, G., Periodate, M., Rhizosphere, P., Slaking, R. (1984). Soil organic matter and structural stability : mechanisms and implications for management Microaggregates Swelling and dispersion, *337*, 319–337.

Pagliai, M., Vignozzi, N., Pellegrini, S. (2004). Soil structure and the effect of management practices. *Soil and Tillage Research*, *79*(2), 131–143. doi:10.1016/j.still.2004.07.002

Papadopoulos, A., Bird, N. R. A., Whitmore, A. P., Mooney, S. J. (2009). Investigating the effects of organic and conventional management on soil aggregate stability using X-ray computed tomography. *European Journal of Soil Science*, *60*(3), 360–368. doi:10.1111/j.1365-2389.2009.01126.x

Paul, B.K., Vanlauwe, B., Ayuke, F., Gassner, A., Hoogmoed, M., Hurisso, T. T.,Pulleman, M. M. (2013). Medium-term impact of tillage and residue management on soil aggregate stability, soil carbon and crop productivity. *Agriculture Ecosystems and Environments 164*, 14–22. doi:http://dx.doi.org/10.1016/j.agee.2012.10.003.

Petersen, S. O., Schjønning, P., Olesen, J. E., Christensen, S., Christensen, B. T. (2013). Sources of Nitrogen for Winter Wheat in Organic Cropping Systems. *Soil Science Society of America Journal*, *77*(1), 155. doi:10.2136/sssaj2012.0147

Powlson, D. S., Glendining, M. J., Coleman, K., Whitmore, A. P. (2011a). Implications for Soil Properties of Removing Cereal Straw: Results from Long-Term Studies. *Agronomy Journal*, *103*(1), 279. doi:10.2134/agronj2010.0146s

Powlson, D. S., Whitmore, A. P., Goulding, K. W. T. (2011b). Soil carbon sequestration to mitigate climate change: a critical re-examination to identify the true and the false. *European Journal of Soil Science*, *62*(1), 42–55. doi:10.1111/j.1365-2389.2010.01342.x

Reynolds, W. D., Elrick, D. E., Youngs, E. G., Amoozegar, A., Booltink, H. W. G., Bouma, J. 2002. 3.4 Saturated and field-saturated water flow parameters. Methods of Soil Analysis Part 4 — Physical Methods. Dane J.H.; Topp, G.C., Soil Science Society of America. Madison, WI, pp. 797–801

Richter, D. deB., Hofmockel, M., Callaham, M. A., Powlson, D. S., Smith, P. (2007). Long-Term Soil Experiments: Keys to Managing Earth's Rapidly Changing Ecosystems. *Soil Science Society of America Journal*, *71*(2), 266. doi:10.2136/sssaj2006.0181

Schindler, U., Durner, W., von Unold, G., Mueller, L., Wieland, R. (2010). The evaporation method: Extending the measurement range of soil hydraulic properties using the air-entry pressure of the ceramic cup. *Journal of Plant Nutrition and Soil Science*, *173*(4), 563–572. doi:10.1002/jpln.200900201

Šimůnek, J., Van Genuchten, M. T., Šejna, M. (2008). Development and applications of the HYDRUS and STANMOD software packages and related codes. *Vadose Zone Journal*, *7*(2), 587–600. doi:10.2136/vzj2007.0077

Sumner, M. E., 1999. Handbook of Soil Science. CRC Press; Taylor and Francis Group,London, UK.

Ulrich, D., van Rietbergen, B., Laib, A., Ŕuegsegger, P. (1999). The ability of three-dimensional structural indices to reflect mechanical aspects of trabecular bone. *Bone*, *25*(1), 55–60. doi:10.1016/S8756-3282(99)00098-8

van Genuchten, M. T. (1980). Closed – form equation for predicting the hydraulic conductivity of unsaturated soils. *Soil Science Society of America Journal*, *44*(5), 892–898. doi: 10.2136/sssaj1980.03615995004400050002x

Verhulst, N., Kienle, F., Sayre, K. D., Deckers, J., Raes, D., Limon-Ortega, A.,Tijerina-Chavez, L., Govaerts, B. (2011). Soil quality as affected by tillage-residue management in a wheat-maize irrigated bed planting system. *Plant and Soil*, *340*(1-2), 453–466.

Villamil, M. B., Little, J., Nafziger, E. D. (2015). Corn residue, tillage, and nitrogen rate effects on soil properties. *Soil and Tillage Research 151*, 61–66. doi: 10.1016/j.still.2015.03.005.

Vogel, H.-J., Weller, U., Schlüter, S. (2010). Quantification of soil structure based on Minkowski functions. *Computers & Geosciences*, *36*(10), 1236–1245. doi:10.1016/j.cageo.2010.03.007

Zaffar, M., Lu, S.-G. (2015). Pore Size Distribution of Clayey Soils and Its Correlation with Soil Organic Matter. *Pedosphere*, *25*(2), 240–249. doi:10.1016/S1002-0160(15)60009-1

Zeleke, T. B., Grevers, M. C. J., Si, B. C., Mermut, a. R., & Beyene, S. (2004). Effect of residue incorporation on physical properties of the surface soil in the South Central Rift Valley of Ethiopia. *Soil and Tillage Research*, *77*(1), 35–46. doi:10.1016/j.still.2003.10.005

Zhang, P., Wei, T., Jia, Z., Han, Q., Ren, X. (2014). Soil aggregate and crop yield changes with different rates of straw incorporation in semiarid areas of northwest China. *Geoderma 230-231*, 41–49. doi: 10.1016/j. geoderma.2014.04.007.

Chapter IV

Comparative effects of crop residues and biochar on maize (*Zea mais* L.) productivity, soil organic carbon and aggregate structure in three contrasting soils.

Background and objectives

Crop residues and biochar are two very different forms of organic inputs, whose utilisation and positive effects on soil ecosystem have been known from long time, however both have recently drawn the attention of scientific community for different reasons. Firstly, the debate on the effectiveness of crop residues has been revitalized by the fact that their availability is increasingly jeopardised by their widely spreading alternative use for bioenergy production. Regarding biochar, an increasing number of countries is developing a biochar legislation while its use is growing rapidly and is expected to further rise in the recent future. Despite the ample scientific literature available on both types of matrices, significant knowledge gaps still exist. For example, to date few studies investigated the potential of biochar to increase soil aggregate stability. From the available literature it emerges that generally low-temperature biochars have positive effects on clay and silty-clay soils (Sun and Lu, 2014; Soinne et al., 2014; Jien & Wang, 2013), with generally no verified benefits on sandy-loams (Hardie et al., 2013; Ojeda et al., 2015), the only exception being the study of Ouyang et al. (2013). Notably only one paper described biochar effects on aggregate stability in field conditions, while the others were all conducted in laboratory incubations. This represents a strong gap in our knowledge, since greenhouse and pot experiments, while giving a first overview of the phenomena, are surely not representative of the mechanisms taking place in natural environments. Additionally, both crop residues and biochar effects on crop yields and soil organic carbon are reported to be highly variable and strictly determined by the specific pedo-climatic conditions of the study area (Jeffery et al., 2011; Powlson et al., 2011). Due to this, the investigation on their comparative behaviour in field appears necessary in order to establish effective management guidelines for the soils of north-eastern Italy. According to the above described mechanisms, the objectives of the fourth chapter of this thesis are thus to evaluate the effects of crop residues and biochar on: i) crop yields, ii) soil organic carbon dynamics, and iii) soil aggregate stability and water repellence. An additional aim is to investigate if and how soil texture influences these responses.

Methodology

Experimental design

The field experiment is located on the Experimental Farm of the University of Padova (45°21' N; 11°50' E, 6 m a.s.l.). The climate is sub-humid with an annual mean rainfall of 825 mm. The temperature reaches minimum values in January (averaging 2.3 °C) and maximum between July and August (average 22.4 °C). Reference evapotranspiration (ET_0) is 945 mm, with maximum values in July (5 mm d^{-1}). ET_0 exceeds rainfall from April to September. The experiment is constituted by 108, 4 m^2 lysimeters, 80 cm deep, with three types of soil: sandy-loam (SNDL), sandy (SND) and clay (CL). In 2014 the total rainfall was 1311 mm, while 2015 was visibly a drier year, with cumulative precipitations of 522 mm. Average maximum and minimum temperatures were almost all months higher in 2015.

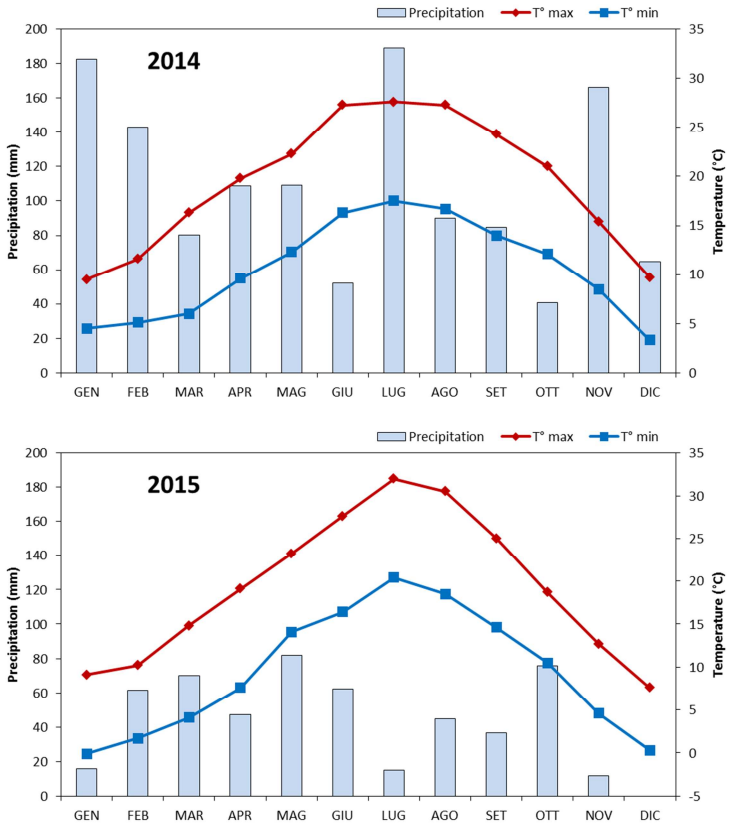

Figure 1. *Meteorological data of 2014 and 2015 in the experimental site. Source: ARPAV*

The main physical and chemical characteristics of the soils at the beginning of the experiment have been described in Chapter III. The experimental design is a randomized block with three replicates (Figure 2). The treatments are the result of the factorial combination of four carbon management methods: burial of crop residues (R), no burial of the residues (NR), biochar application at 20 t ha^{-1} (BC_{20}) and biochar application at 40 t ha^{-1} (BC_{40}); with three levels of nitrogen fertilisation: 0, 100 and 300 kg N ha^{-1}. Biochar was applied in December 2013 (during 2013 the plots were kept bare) and carefully incorporated to the first 20 cm of the soil. The two rates, 20 and 40 t ha^{-1}, correspond approximately to 13.7 t C ha^{-1}, and 27.4 t C ha^{-1}, i.e. 44% and 88% of the native soil organic carbon (SOC) for the clay soil and, to 67% and 133% for the loamy soil. For the sandy soil the amount of carbon applied with biochar was about 7 and 14 times the SOC contained in the soil.

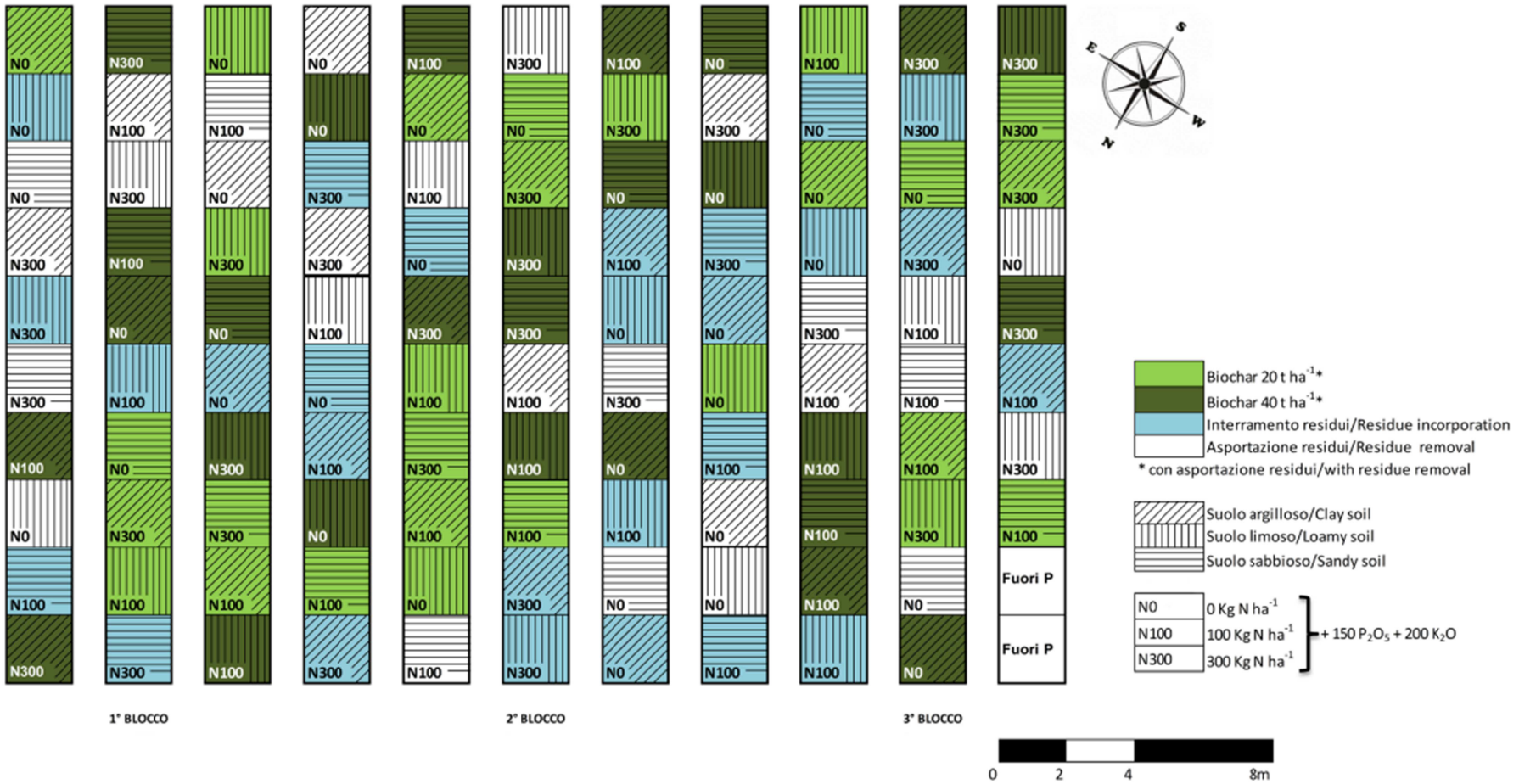

Figure 2. *Map of the field experiment.*

Biochar properties

The biochar was produced from waste wood by a gasification plant which operates at an average temperature of 800°C. It was characterized by a wide particle size with two distinct parts (Figure 3): a macroscopic one with particles ranging from 4 cm to several millimetres of diameter, and a powdery part which ranged from 1 µm to about 800 µm. The medium diameter of the particles in the powdery fraction resulted 8.79 µm. The specific surface area measured with N_2 adsorption was 13.78 m^2g^{-1} with a pore volume (0.025-5 nm) of 0.04 cm^3g^{-1}. The total C, N and S contents were 68.6%, 0.4% and 0.6%, respectively. The amount of available nitrogen resulted under detection limit. The biochar had an alkaline pH (8.43) and an electrical conductivity of 473 µS cm^{-1}, while the cation exchange capacity (CEC) resulted of 2.3 $Cmol_c$ Kg^{-1}. Nutrient contents were 10 g Kg^{-1} for K, and 1.2 g Kg^{-1} for P. The content of heavy metals is exposed in Table 1.

Table 1. *Heavy metal composition of the biochar.*

As	Cd	Cr	Cu	Ni	Zn
ppm					
7.1 ± 0.2	5.4 ± 0.0	277 ± 64	44.2 ± 0.4	129 ± 25	265 ± 7

Values are reported as means followed by standard errors.

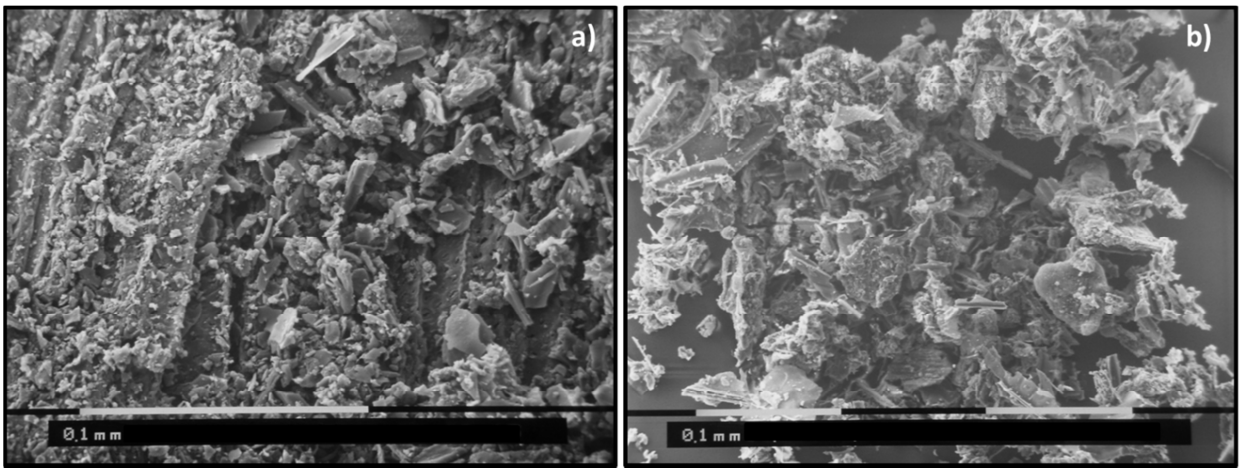

Figure 3. *SEM image of a) the macroscopic fraction of biochar and b) the powdery fraction.*

Average yields in 2014 and 2015

The yield and the total aboveground biomass (AGB) were recorded each year at the end of the growing season using all the plants of each plot.

Soil analyses

Sampling was carried out in June 2015. Disturbed samples from the 0-20 cm layer were taken from three points in each plot and then bulked together to form a sample of approximately 1 Kg. The soil was left to dry at ambient temperature and then gently broken along natural fissures. Finally it was sieved to obtain aggregates of the size 1-2 mm. The analysis on aggregates considered only four treatments, NR_0, R_{300}, $BC20_{300}$ and $BC40_{300}$ of clay and sandy-loam soil.

Soil organic carbon

Soil aggregates were analysed for their concentration of organic carbon (SOC) by dichromate oxidation (Walkley and Black, 1934). In order to evaluate if biochar carbon contributed to the total SOC measured, the same method was applied to samples of pure biochar. The carbon stock of soils was calculated for the upper soil layer (0-20 cm) that was the area in which biochar was incorporated.

Soil pore size distribution

Accessible porosity and pore size distribution within the diameter range of 0.0074-100 µm were measured using mercury intrusion porosimetry, by means of a Thermo Finnigan (Waltman, USA) Pascal 140 (3.8-100 µm) and a Pascal 240 (0.0074-15 µm). The pore radius was calculated using the Young-Laplace equation:

$$R = \frac{2\gamma cos\theta}{P} \quad (1)$$

where γ is the surface tension of pure mercury, θ is the contact angle (140°) between mercury and the sample and P is the pressure. Pores were then classified according to Cameron and Buchan (2006)

in: cryptopores (0.01-0.1 µm), ultramicropores (0.1-5 µm), micropores (5-30 µm), mesopores (30-75 µm) and macropores (75-100 µm)

Aggregate morphology

Mean diameter and shape parameters

The mean diameter of aggregates D_m, along with their shape parameters (Circularity, Solidity, Convexity and Elongation) were measured with an automated particle characterization system (Morphologi G3, Malvern Instruments, UK). Samples were manually dispersed over a glass plate and carefully separated between each other with a small brush. Dispersions and analysis parameters were adapted in order to analyse a minimum of 50 aggregates per each sample. Samples were illuminated with an episcopic light, lamp power was set at 55% and exposure at 100 ms. The focus was manually adjusted before each measurement. The instrument software was enabled to use the 'particle stitching' feature in order to consider particle parts included in different frames as a unique particle. After the analysis the images were manually filtered in order to eliminate particles attached between each other (which are considered by the software as a unique particle) that otherwise would create a bias in the calculation of particle shape parameters.

Scanning electron microscope images

SEM images of NR and BC_{40} treatments of the two soils were obtained with a Philips SEM 515 scanning electron microscope (Philips, Eindhoven, The Netherlands). Dry samples were mounted on aluminium stubs with silver glue and coated with gold-palladium film using an ion sputtering unit Balzer MED 010 (Balzers Union, Ltd, Balzers, Liechtenstein) and observed at 7 Kv. The pictures taken with a Nikon 5400 Coolpix digital camera (Nikon, Chiyoda-ku, Tokyo,Japan).

Aggregate stability

Two aggregate stability analysis methods were applied on aggregate samples which were previously subjected to a fast wetting (FW) for 30 min with 450 ml of deionized water. The fast wetting was applied also with other two pre-treatments which consisted in immersing the samples for 5 minutes in (i) 5 ml ethanol and (ii) 5 ml benzene before the dilution in water. When soil aggregates are immersed in ethanol, the air they contain is substituted by this liquid, causing a reduction of the slaking during the subsequent fast wetting procedure (Hénin et al., 1973). This pre-treatment is thus useful to emphasize the resistance of soil aggregates to dissolution and dispersive action of water (Dal Ferro et al., 2012). On the contrary, benzene coating accentuates the hydrophobic effects of soil organic matter (Hénin et al., 1973), and is expected to emphasize differences in stability of soil aggregates due to their organic carbon content.

Wet sieving

The analysis was carried out using a Tiulin apparatus and following the procedure described by Bocchi, et al., 2007. Briefly, 10g of aggregates were carefully transferred in a 200 µm mesh sieve previously submerged in deionised water and then subjected to a mechanical vertical oscillation applied for 30 min (30 oscillations min^{-1}). The aggregates remaining on the sieve at the end of the experiment were oven dried at 105°C overnight and weighted. Finally they were immersed for 24h in a dispersing solution in order to determine the coarse sand fraction. Wet stability index (WASI) was calculated as follows:

$$\text{WASI} = \frac{a_{as} - cs}{a_{bs} - cs} \times 100 \quad (2)$$

Where a_{as} , a_{bs} are the weights of the aggregates prior and after the sieving; and cs is the weight of the coarse sand fraction. The indexes calculated with the three pre-treatments were indicated as $WASI_w$, $WASI_e$ and $WASI_b$.

Laser diffraction

The kinetics of aggregate disintegration were measured by means of laser diffraction (Rawlins et al., 2013; Mason et al., 2011; Amézketa et al., 2003) using a Mastersizer 2000 (Malvern Instruments, UK). The amount of soil material used varied between 0.5 and 1g and was chosen in order to maintain a laser obscuration in the range between 10 and 18%. Aggregates were subjected to the pre-treatments previously described (water, ethanol and benzene), and after this procedure the suspensions were carefully transferred into the instrument dispersion unit. The pump speed was set at 1750 rpm and the stirrer speed at 700 rpm (Jozefaciuk and Czachor, 2014). A complete cycle of analysis was set to last 30 min, with 180 analysis in total. At the end of the analysis the sample was sonicated for at least 1 minute in order to calculate the coarse sand content. Soil refraction index was set at 1.53. Disaggregation curves were expressed as function of analysis time and interpolated using a power model:

$$D = a * t^b \tag{3}$$

Where D is the median aggregate diameter, a and b are the model parameters, and t is the measurement time. To further describe the disaggregation kinetics, several peculiar time steps in the disaggregation curve (Figure 4) were individuated.

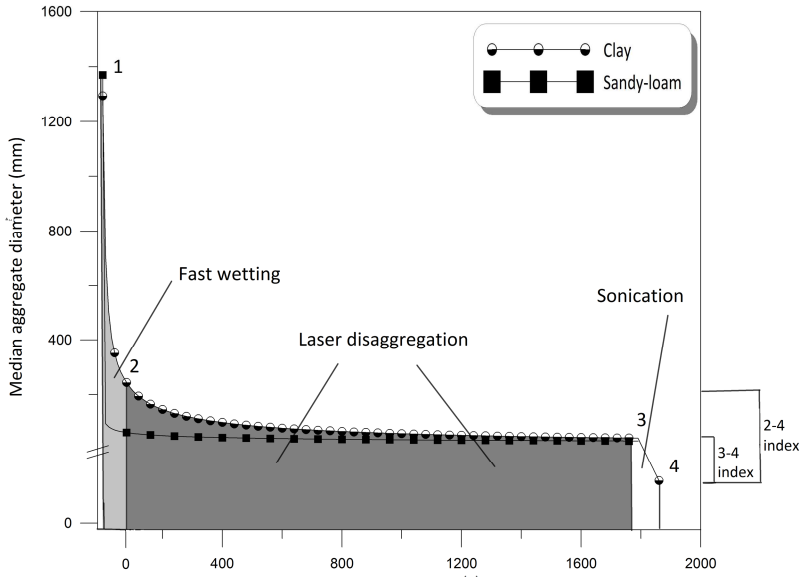

Figure 4. *Schematic representation of disaggregation curve, including a pre-fast wetting point (1) and the other peculiar time steps in the laser diffraction procedure (2, 3 and 4) with the two indexes individuated for the description of different soils and treatments' behaviours.*

The point 1 represents the median aggregate diameter measured with Morphologi and thus it is considered as a starting condition for the other measurements. The point 2 is the first measurement registered with laser diffraction and thus it is an index of the susceptibility of aggregates to the fast wetting procedure. Accordingly, point 3 represents the median aggregate diameter obtained after 30 mins of laser measurements, while point 4 is the recorded diameter after sonication, and thus after the complete disaggregation of material. On the basis of the key points above described, two indexes were calculated: index $\Delta_{2\text{-}4}$ and $\Delta_{3\text{-}4}$. These indicators express the difference in the median diameters between time step 4 and either time step 2 or time step 3 (Figure 4). The first index ($\Delta_{2\text{-}4}$) can be seen as an estimate of aggregate susceptibility to the fast wetting procedure and thus it expresses the stability index of the bigger aggregates or alternatively of their external part. Since the diameter of sonicated (i.e sandy particles) is assumed to be equivalent for all samples, the higher the diameter difference expressed by $\Delta_{2\text{-}4}$, the higher the stability of aggregates. Accordingly, the index $\Delta_{3\text{-}4}$ represents the stability of the smallest or inner part of aggregates. In this case too, an high value of the index represents an high stability of aggregates.

Contact angle

Contact angle represents an index of the water repellence of soils and was measured with the capillary rise method. This procedure is based on the difference in the rising of two liquids (water and ethanol) inside columns of soil. Soil aggregates were carefully introduced into glass tubes of 52 cm height and 1 cm diameter ,with a filter at the bottom. The tubes were previously coated with a film of paraffin wax in order to make the glass hydrophobic. With the purpose of obtaining the same bulk density, the columns were filled with the same mass of soil and then tapped in order to achieve an identical filling height. Two columns were filled with the same sample, one was immersed in water and the other in ethanol for 2 hours and then the height of the liquids in the columns was measured. The equation used to determine the contact angle was the following (Siebold et al., 1997):

$$H^2+2hL = \frac{r\gamma_L \cos\theta}{2\eta}t \quad (4)$$

Ethanol contact angle is assumed to be zero, while the behaviour of water is dependent on the presence of hydrophobic substances on the surface of soil particles. Thus, Eq. 4 for ethanol and water can be combined in order to obtain the water-soil contact angle.

Zeta potential at natural soil pH (ζn)

Zeta potential was measured with a Zetasizer Nanoseries (Malvern, UK). Aggregates were grounded and sieved at 200 µm, then 0.5 g were dispersed in 50 ml of deionized water and shaken for 12h. The potentials were measured at natural solution pH, which was considered to be more representative of field conditions.

Statistics

Yield, above ground biomass, soil organic carbon, WASI and parameters of disaggregation curves were analysed using a two way analysis of variance considering soil type and carbon management as main factors (CoStat 6.4 - CoHort Software, Monterey, CA, USA). The differences between group means were evidenced with a Duncan's post-hoc test. Regarding the disaggregation indexes, a one-way ANOVA considering carbon management type as main factor was used, coupled with a Duncan's post-hoc test to detect differences between group means (CoStat 6.4 - CoHort Software, Monterey, CA, USA). Linear regression coefficients were used to describe the correlation between WASI and stability indexes derived from laser diffraction. Multiple stepwise regression analysis with backward selection was also applied in order to identify dependencies between stability indexes and hydro- repellence, SOC, porosity and texture parameters of the two soils using Statistica software (StatSoft Inc., Tulsa, USA).

Results

Average yields in 2014 and 2015

In 2014 yields and above ground biomass (AGB) were significantly influenced by soil type, fertilisation level and carbon management type. Soils presented highly different yields ranging from 13.3 t ha^{-1} of clay, to 6.11 t ha^{-1} of sandy soil. Sandy-loam exhibited intermediate values averaging 10.9 t ha^{-1}. The AGB showed the same trend with averages of 21.10, 18.48 and 9.80 t ha^{-1} for clay, sandy-loam and sandy soil. A clear tendency in an increase in yield induced by carbon management is evident in all the soils examined, however this effect was not significant in sandy-loam soil (Figure 5a).

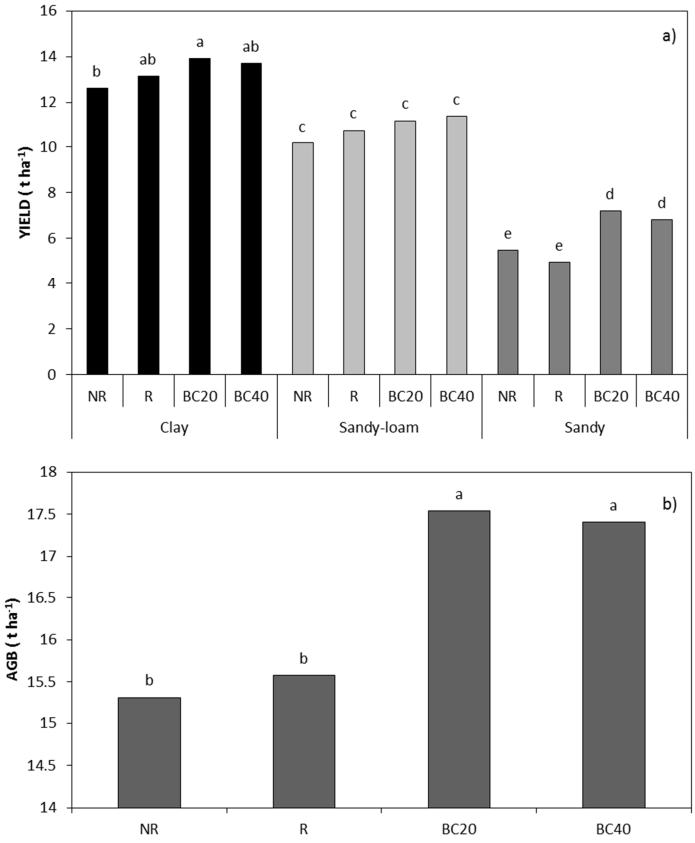

Figure 5. *Average yields(a) and AGB (b) in 2014*

Moreover, in sandy soil no significant effects of residues were found. On the contrary biochar increased yield of 28% on average, compared to the NR treatment ($p<0.01$), with no significant differences between the two application rates. In clay soil, BC_{20} increased yield of 10% ($p<0.01$) if compared with the NR treatment, and no effects of the other two treatments (R and BC40) were observed. AGB was found to be significantly higher in plots receiving biochar (Figure 5b), but no differences were found between the two application rates (17.54 and 17.40 t ha^{-1} for BC_{20} and BC_{40}, respectively). nor between the control (NR, 15.31 t ha^{-1}) and the R treatment (15.57 t ha^{-1}). Furthermore, the AGB response to carbon management did not differ between soils (interaction soil type x carbon management not significant).

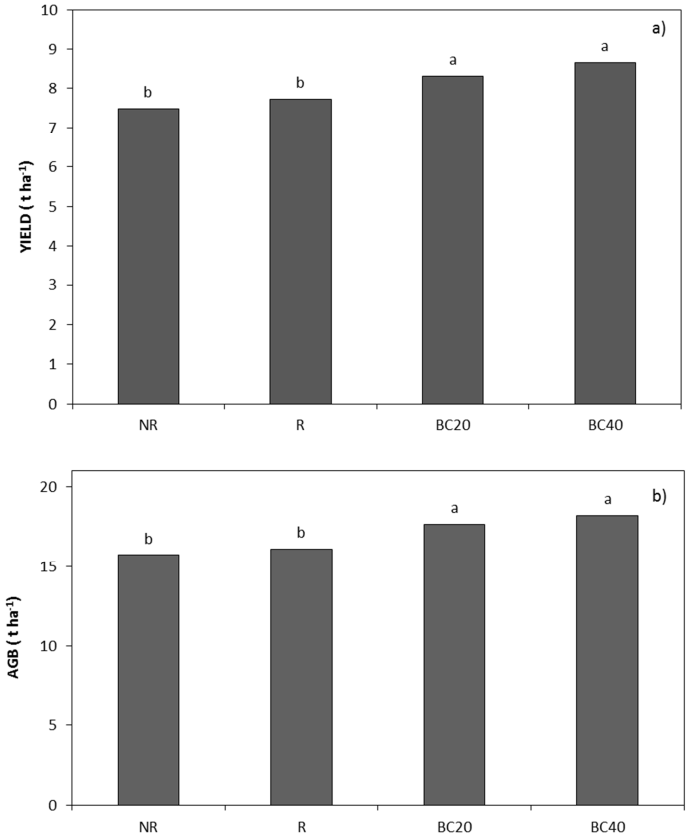

Figure 6. *Average yields(a) and AGB (b) in 2015*

Fertilisation clearly increased yield and aboveground biomass but its effect was not influenced by the carbon management type. As for 2014, in 2015 both yield and AGB were significantly influenced by soil

type, fertilisation level and carbon management. However the average yields were lower if compared to the preceding year, being 10.2 t ha^{-1} in clay, 8.3 t ha^{-1} in sandy-loam and 5.7 t ha^{-1} in sandy soil. The same can be appreciated if considering the AGB of clay soil (20.7 t ha^{-1}), while sandy-loam and sandy soil showed a rise in the AGB which was 18.6 and 11.4 t ha^{-1}, respectively. Notably, the carbon management effect persisted also in this growing season, with yields being significantly higher in plots with biochar (Fig. 6a) and no differences either between the two doses applied, neither between R and NR treatments. Specifically, in BC_{40} and BC_{20}, yields were 8.7 and 8.3 t ha^{-1}, followed by R (7.7 t ha^{-1}) and NR (7.5 t ha^{-1}). The same trend can be observed also for total biomass which was on average of 2 t ha^{-1} higher in plots receiving biochar if compared with the average of NR and R plots (Fig. 6b).

Aggregate pore size distribution and organic carbon content

Total pore volumes resulted highly different between soils, with sandy loam exhibiting the higher values of 0.25 cm^3g^{-1}, while clay soil showed an average pore volume of 0.11 cm^3g^{-1}. Carbon management significantly influenced total porosity of clay soil, with higher values detected for BC_{20} treatment (0.12 cm^3g^{-1}). Lower values were attributed to plots with residue incorporation (0.09 cm^3g^{-1}), while NR and BC_{40} exhibited intermediate values of 0.10 and 0.11 cm^3g^{-1}, respectively. No significant effects were found in sandy-loam, however the presence of higher pore volumes in plots receiving biochar (0.26 and 0.28 cm^3g^{-1} for BC_{20} and BC_{40}, respectively), than in plots not receiving it (0.23 cm^3g^{-1} for NR and 0.24 cm^3g^{-1} for R), could be observed. Pore size distributions revealed that the differences between treatments were concentrated in ultramicropores and micropores for clay soil (Fig. 7a), while in sandy-loam the variations were detected only in cryptopores (Fig. 7b). More specifically, ultramicropores resulted higher for clay soil with BC_{20} treatment, while only the highest biochar dose was effective in increasing micropores. In sandy loam, the BC_{40} treatment significantly increased the presence of cryptopores, with no differences detected between either BC_{20} or R if compared to the control (NR).

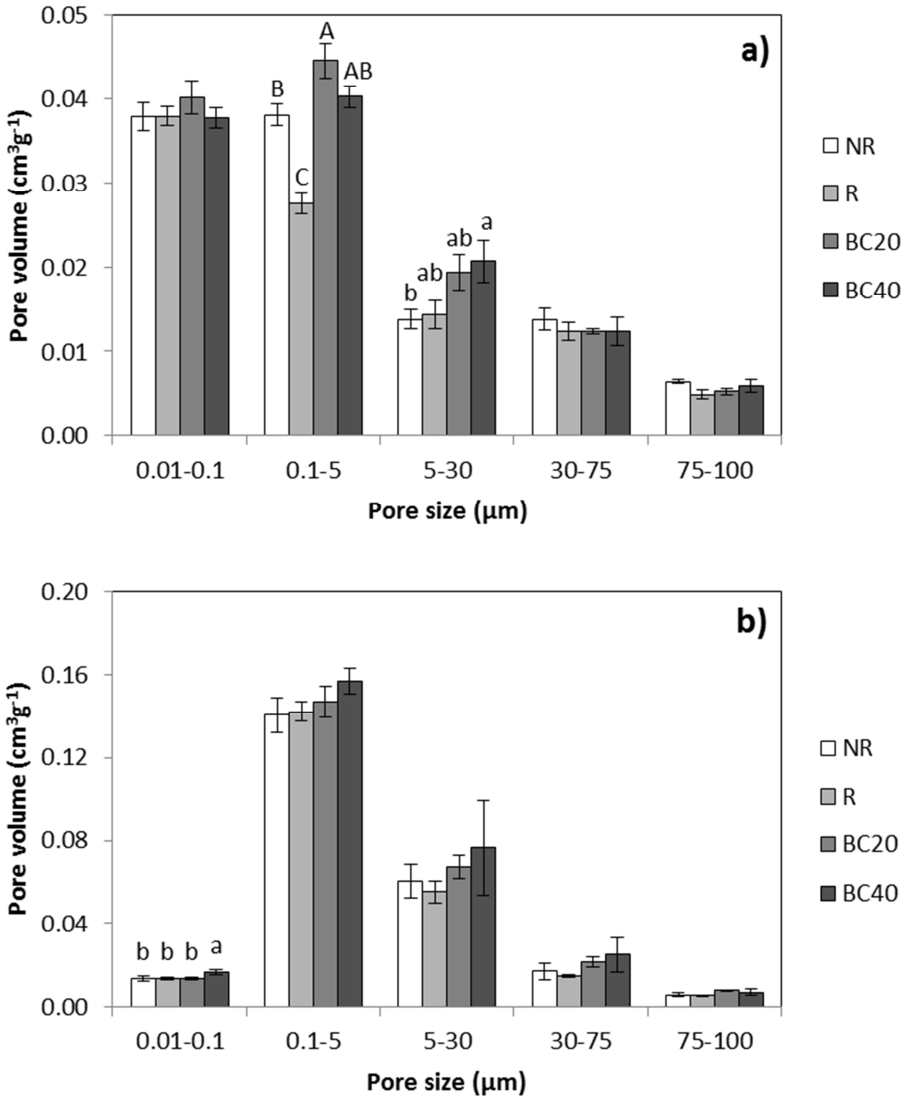

Figure 7. *Pore size distributions of a) clay and b) sandy-loam soil as a function of carbon management.*

The carbon concentration of the top soil layer (0-20 cm) was significantly different in the two soils, with an average SOC in clay of 1.02% (20.22 t ha^{-1}) and in sandy-loam of 0.80% (19.37 t ha^{-1}). The carbon amendment significantly increased SOC concentrations in both soils, on average +6%, +39% and +58% for R, BC_{20} and BC_{40}, respectively. In terms of carbon stock the changes corresponded to +0.29, +4.6 and +6.95 t ha^{-1}, respectively. However the two soils showed different behaviours in response to carbon management, indeed in clay soil R treatment decreased SOC by 2%, while the two biochar treatments increased soil carbon of 31% (BC_{20}) and 47% (BC_{40}). In sandy-loam soil residue effects were opposite, with a SOC increase of 18%. In this soil the magnitude of organic carbon increases in response to biochar

was more pronounced, in fact in BC_{20} and BC_{40} plots the SOC was respectively, 50% and 73% higher than in the control.

Soil morphology

Aggregate mean diameter and 2D shape parameters

Aggregate mean diameters (Table 2) did not differ significantly between treatments nor between soils, revealing the uniformity of initial conditions for subsequent analysis.

Table 2. *Sphere equivalent diameters of the samples analysed. Values are expressed as means (n=3), followed by standard errors (err.st).*

	CLAY				SANDY-LOAM			
	NR	R	BC20	BC40	NR	R	BC20	BC40
CE diameter (μm)	1413	1283	1360	1298	1197	1176	1168	1245
Err.st	83	75	123	74	28	41	37	16

The two soils exhibited small but significant differences in shape parameters, with clay aggregates showing the highest circularity and convexity indexes (0.64 and 0.88, respectively). Conversely, solidity and elongation indexes were higher in sandy-loam soil (0.92 and 0.23, respectively). Aggregates revealed asymmetrical shapes with irregular surfaces (Figure 8a and b).

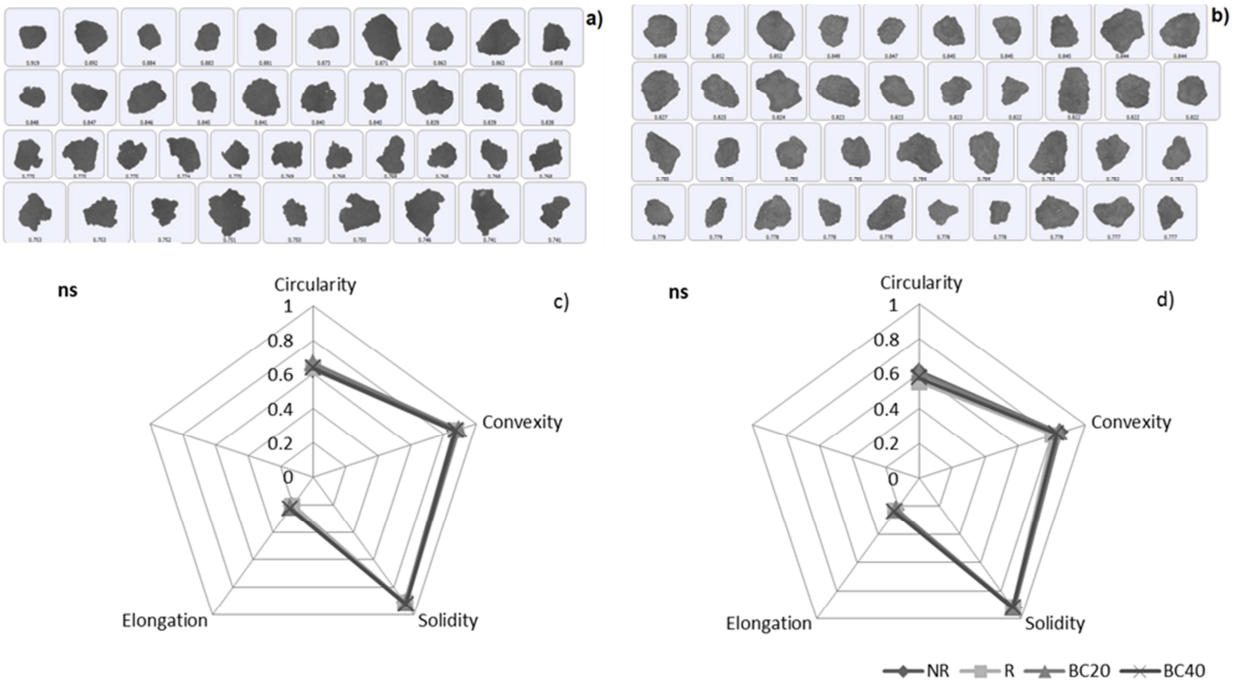

Figure 8. *Examples of soil aggregates of a) clay and b) sandy-loam soil classified according to their circularity parameters (from the more circular to the less circular). Shape parameters as a function of different carbon management types in c) clay soil and d) sandy-loam soil.*

Shape parameters, as can be seen in Figure 8c and d, were not significantly influenced by the carbon management type. Despite this, a tendency in a biochar-induced increase in solidity and elongation can be seen in clay soil. On the contrary no evident effects of residues or biochar are manifest in sandy-loam soil.

Scanning electron images

SEM images of soil aggregates with and without biochar are shown in fig. 9. Sandy-loam soil revealed prismatic particles intercalated by thinner, lamellar ones (Fig. 9a). On the opposite clay morphology was more irregular, and the particles were characterized by scabrous surfaces with a not well recognizable shapes (Fig. 9c).

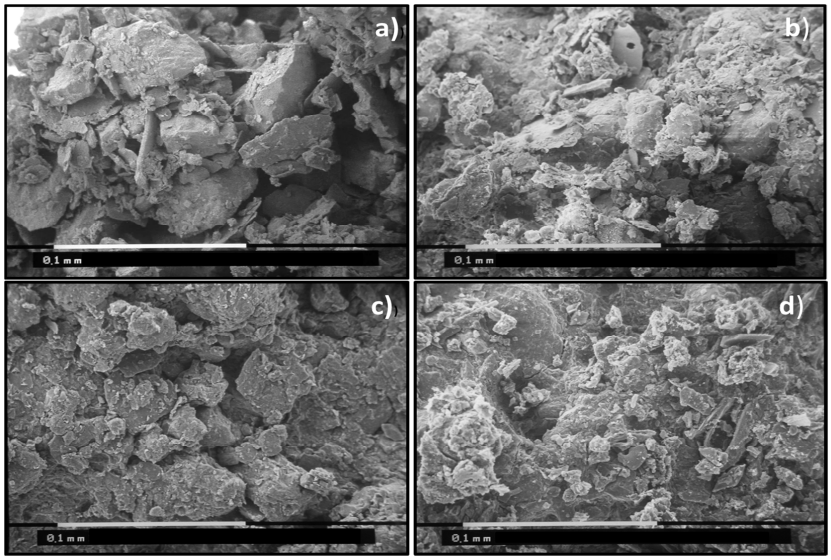

Figure 9. *SEM images of sandy-loam soil a) without biochar and b) with biochar; and of clay soil c) without biochar and d) with biochar.*

The presence of powdery biochar particles was evidently visible on the surface of the aggregates of both soils (Fig. 9b and d). In addition, it is clearly noticeable that the surface of the two soils interacted in a physical way with biochar particles and that they were included in the aggregation process, thus demonstrating that biochar remained uniformly mixed with soil particles during two years of field application. This is confirmed also by aggregate pictures in Figure 10, where it is evident that the interaction did not concern solely the surfaces of aggregates, but it was extended to the whole soil particle.

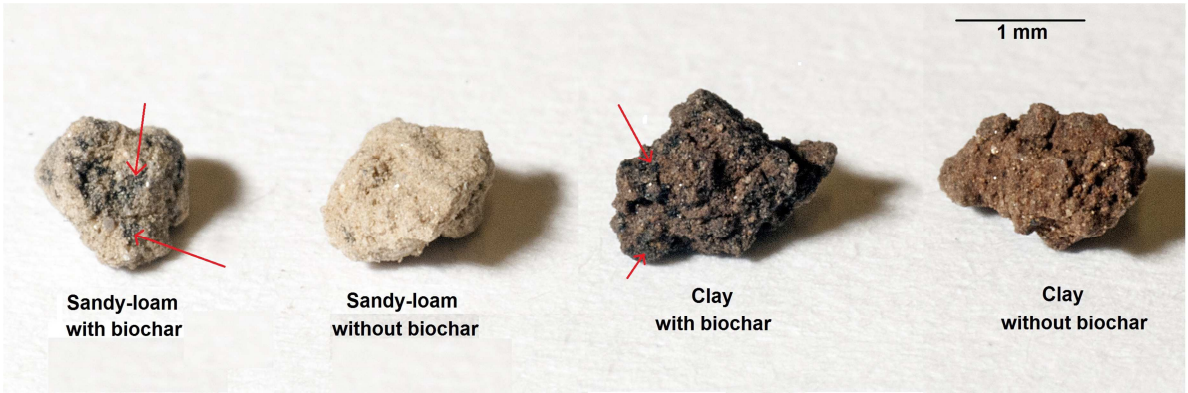

Figure 10. *Sandy-loam and clay aggregates with the application of biochar compared with aggregates without this treatment.*

Indeed the red arrows indicate points in which biochar was intercalated in between soil particles, and this was evident also at a naked eye observation.

Contact angle

Average contact angles were slightly different in the two soils (Figure 11), with clay soil showing a more pronounced water repellence (Θ=52.1°) if compared to sandy-loam (Θ=49.4°). No significant effects of carbon management type were detected in sandy-loam soil, even if a slight tendency in an increase in contact angles owing to biochar amendment can be detected. In clay soil the highest dose of biochar induced a significant increase in water repellence, with a contact angle varying from 48.9° in NR, to 56.0° in BC_{40} treatment. No effects of the other two treatments were detected.

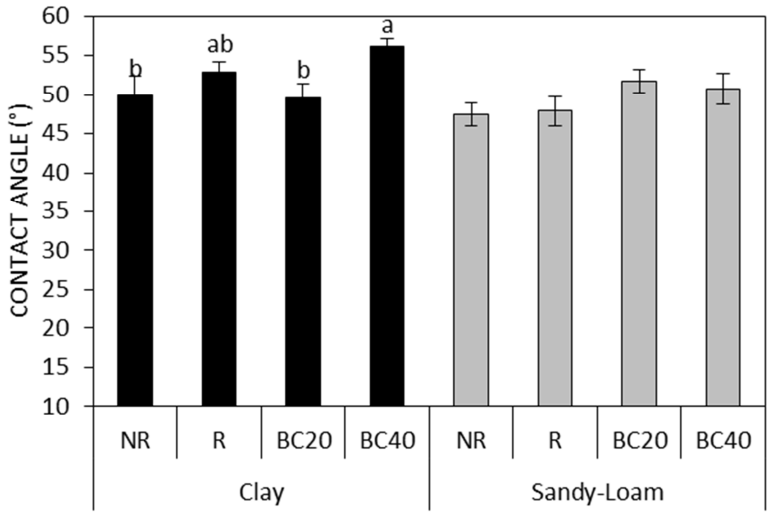

Figure 11. *Contact angles of the two soils with different carbon management methods.*

Aggregate stability

Wet sieving

As expected the two soils differed significantly in their aggregate stability, both in water and with the ethanol pre-treatment. The $WASI_w$ was on average 70.46% in clay soil and 9.72% in sandy-loam soil. The carbon management type caused a significant increase in the stability index (from 37.3% of the control to 40.2% of the BC_{40} treatment, Table 3). Ethanol pre-treatment increased the aggregate stability of both soils, with an effect particularly evident in sandy-loam. The carbon management type significantly influenced the aggregate stability index with ethanol pre-treatment, which varied from 58.49% in NR to 63.24%, 66.74% and 67.56% in R, BC_{20} and BC_{40}. The $WASI_b$ was on average 54.94% in clay soil, and 48.16% in sandy-loam. No significant effects of the carbon management type were detected with this pre-treatment.

Table 3. *WASI indexes of the samples with different carbon management types.*

		$WASI_w$	$WASI_e$	$WASI_b$
Soil				
	Clay	70.5a	80.2a	54.9
	Sandy-loam	9.7b	47.8b	48.2
Carbon manegement				
	NR	37.3b	58.5c	49.1
	R	41.9a	63.2b	56.3
	BC20	41.0a	66.7ab	51.7
	BC40	40.2a	67.6a	49.2
Interaction soil x carbon management				
Clay	NR	68.2	77.2	49.7
	R	75.9	80.4	63.7
	BC20	71.9	80.0	55.9
	BC40	65.8	83.2	50.5
Sandy-Loam	NR	6.4	39.8	48.5
	R	7.9	46.1	48.8
	BC20	10.0	53.5	47.4
	BC40	14.5	51.9	47.9

**Values are expressed as means (n=3); Different letters indicate significant differences between group means.*

Multiple regression analysis showed for clay soil (Table 5) a positive correlation of $WASI_w$ with cryptopores and contact angle, while the opposite was observed with mesopores and ultramicropores (R^2=0.91). Regarding $WASI_e$, mesopores and OC were positively correlated, with the opposite occurring for ultra-micropores (R^2=0.92). Lastly, WASI with benzene pre-treatment resulted positively influenced by OC and negatively by meospores, R^2=0.59. Considering sandy-loam, the stability indexes with water and ethanol pre-treatment resulted both positively linked with OC. For $WASI_e$ also a negative and a positive correlation was observed with mesopores and macropores, respectively (R^2=0.94). Regarding $WASI_b$, it resulted negatively correlated only with macropores (R^2=0.35).

Laser diffraction

The parameters (a and b) of the disaggregation curves are reported in Table 4 and Table 5. The two soils showed significant differences in their kinetics of disaggregation with all the pre-treatments (water, ethanol and benzene). Sandy-loam soil presented the highest values of parameters a and b (on average 13.37 and -0.22, respectively), than the clay soil (on average 4.90 and -0.56, respectively. Furthermore, this soil was also the less resistant to the FW procedure, since it showed a lower aggregate diameter in the starting point in the curve (Figure 12a), if compared to clay soil.

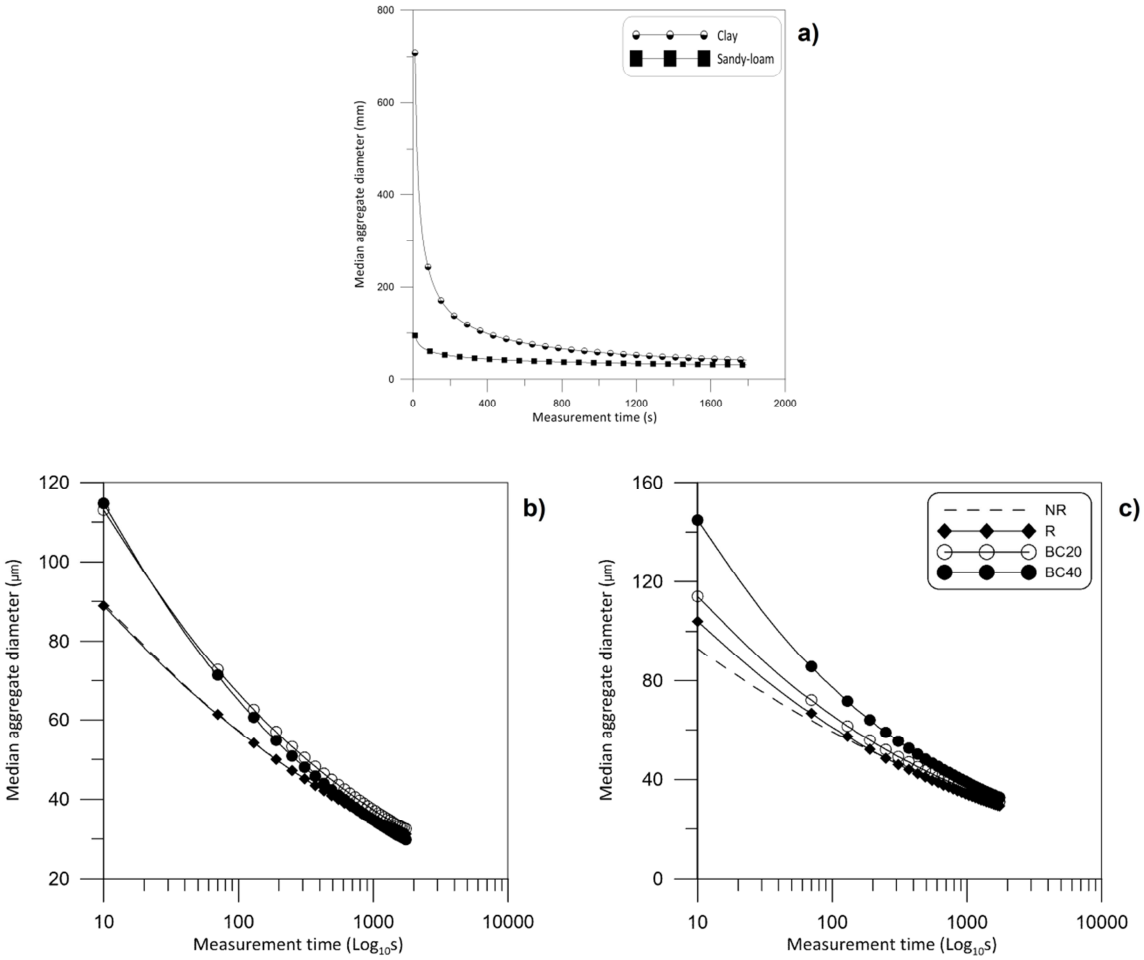

Figure 12. *Disaggregation curves of the two soils averaged between pre-treatments and carbon management types a); disaggregation curves of sandy-loam soil after water pre-treatment b) and ethanol pre-treatment c).*

Carbon management affected the shape of disaggregation curve only in sandy-loam soil. Indeed, in this soil water pre-treatment caused a significant decrease of 'a' parameter in plots receiving biochar (Figure 12b), while parameter 'b' was not affected in a significant way, even though a decreasing tendency can be noticed. In samples subjected to ethanol pre-treatment, the carbon management type induced a significant decrease in 'b' parameter and a tendency (even if not significant) in a decrement in 'a' parameter (Figure 12c). Benzene pre-treatment did not show significant effects owing to the carbon management type.

Table 4. *Disaggregation curve parameters as a function of soil, carbon management and their interaction.*

		Water		Ethanol		Benzene	
		a	b	a	b	a	b
Soil							
	Clay	3.1b	-0.62b	5.6b	-0.6b	6.0b	-0.5b
	Sandy-loam	12.8a	-0.23a	11.9a	-0.3a	15.4a	-0.2a
Carbon management							
	NR	8.5	-0.42	8.8	-0.4	11.1	-0.3
	R	8.5	-0.40	8.2	-0.4	10.3	-0.4
	BC20	7.6	-0.44	9.5	-0.4	11.0	-0.3
	BC40	7.2	-0.43	8.5	-0.4	10.4	-0.3
Interaction soil x carbon management							
Clay	NR	3.1c	-0.6	3.45	-0.62d	7.85	-0.42
	R	3.0c	-0.62	5.18	-0.58cd	4.77	-0.56
	BC20	2.6c	-0.64	7.4	-0.55c	5.73	-0.5
	BC40	3.7c	-0.6	6.37	-0.57cd	5.77	-0.48
Sandy-Loam	NR	13.89a	-0.21	14.16	-0.21a	14.39	-0.18
	R	14.06a	-0.21	11.3	-0.25ab	15.93	-0.17
	BC20	12.58ab	-0.25	11.56	-0.26ab	16.27	-0.18
	BC40	10.72b	-0.27	10.61	-0.29b	15.02	-0.2

**Values are expressed as means (n=3); Different letters indicate significant differences between group means.*

The stability index $\Delta_{2\text{-}4}$ resulted different in the two soils examined (Figure 13 and 14), indeed it averaged 532 µm in clay soil, and 67 µm in sandy loam. On the contrary, the index $\Delta_{3\text{-}4}$ was similar between the two soils, being 4.4 and 4.9 µm in clay and sandy-loam, respectively. Considering the clay soil, the carbon management variably influenced $\Delta_{2\text{-}4}$ with water pre-treatment (Fig. 13a), indeed the higher diameter reduction was detected in R and BC_{20} treatments, and both resulted significantly different from the control (NR). The maximum biochar dose did not cause significant reductions in diameter if compared with the control. The same tendency can be seen also for ethanol and benzene pre-treatments (Fig. 13c and e), even if the differences were not significant. Considering the second index ($\Delta_{3\text{-}4}$), a tendency in a biochar-mediated increase in diameter reduction can be observed, especially considering ethanol and benzene pre-treatments (Figure 13e and f). In this soil, the index $\Delta_{2\text{-}4}$

resulted positively influenced by cryptoporosity either considering water or benzene pre-treatment (Table 5). In the first case (water pre-treatment) it was found also a negative correlation with macropores (R^2=0.72). In addition, the Δ_{3-4} index was negatively influenced by cryptopores with ethanol pre-treatment, while an opposite behaviour was found for OC and benzene pre-treatment.

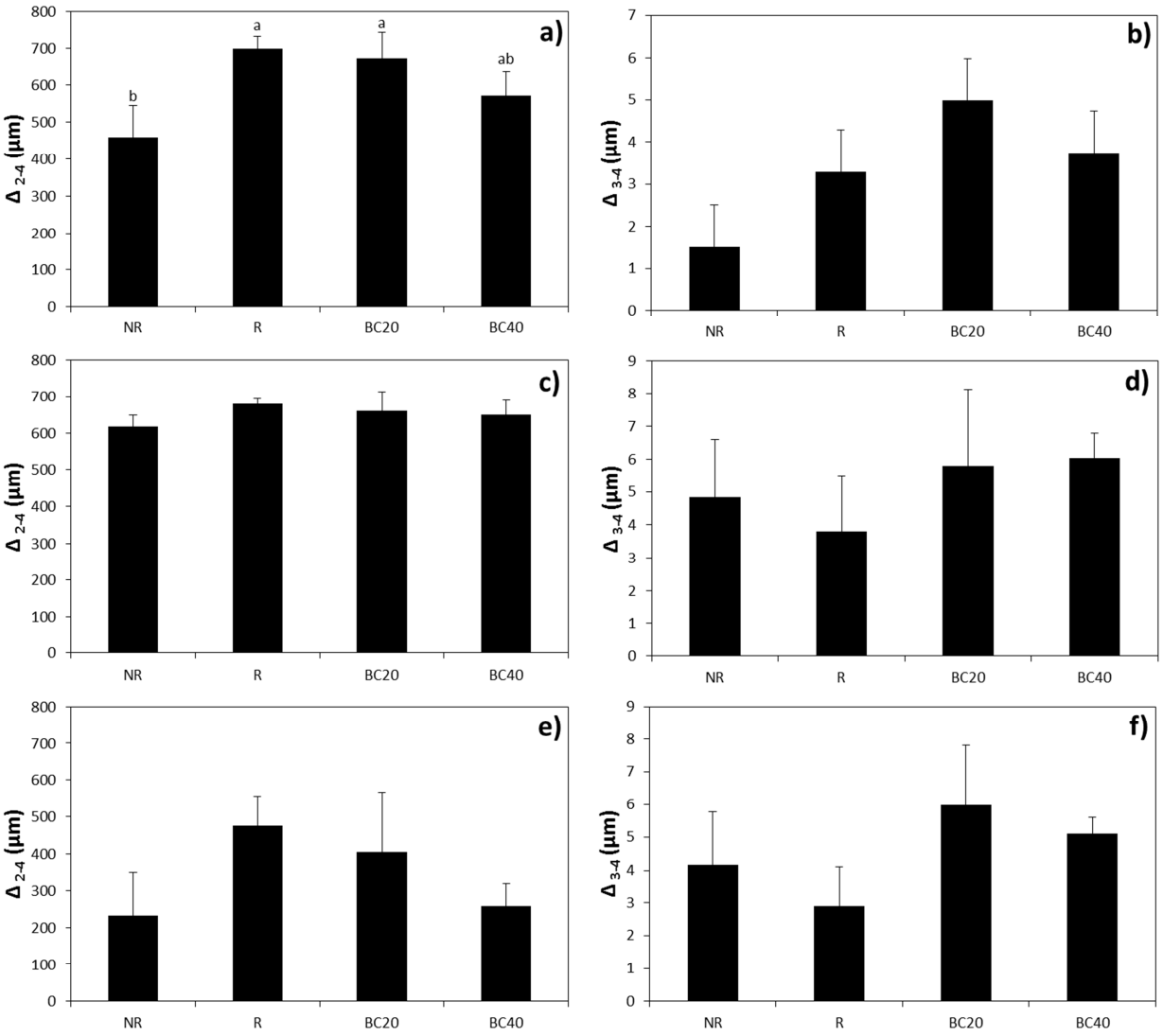

Figure 13. *Clay soil disaggregation indexes Δ_{2-4} and Δ_{3-4} with water pre-treatment (a and b); ethanol pre-treatment (c and d); and benzene pre-treatment (e and f).*

The Δ_{2-4} index of sandy-loam soil was affected by carbon management with the water and the benzene pre-treatments; indeed both biochar doses (BC_{20} and BC_{40}) significantly increased the index for the first case (Figure 14a), while only BC_{40} was effective in increasing the Δ_{2-4} with the benzene pre-

treatment (Figure 14e). The same trend could be seen also with ethanol pre-treatment, even if it did not result significant. Additionally, the $\Delta_{3\text{-}4}$ resulted lower with BC_{40} treatment (Figure 14b) if compared to the NR one with water pre-treatment ($p<0.05$). With the other two pre-treatments (ethanol and benzene) no significant effects of carbon management were detected, even if a tendency in the increase of index value for C treatments could be appreciated (Fig. 14d and f).

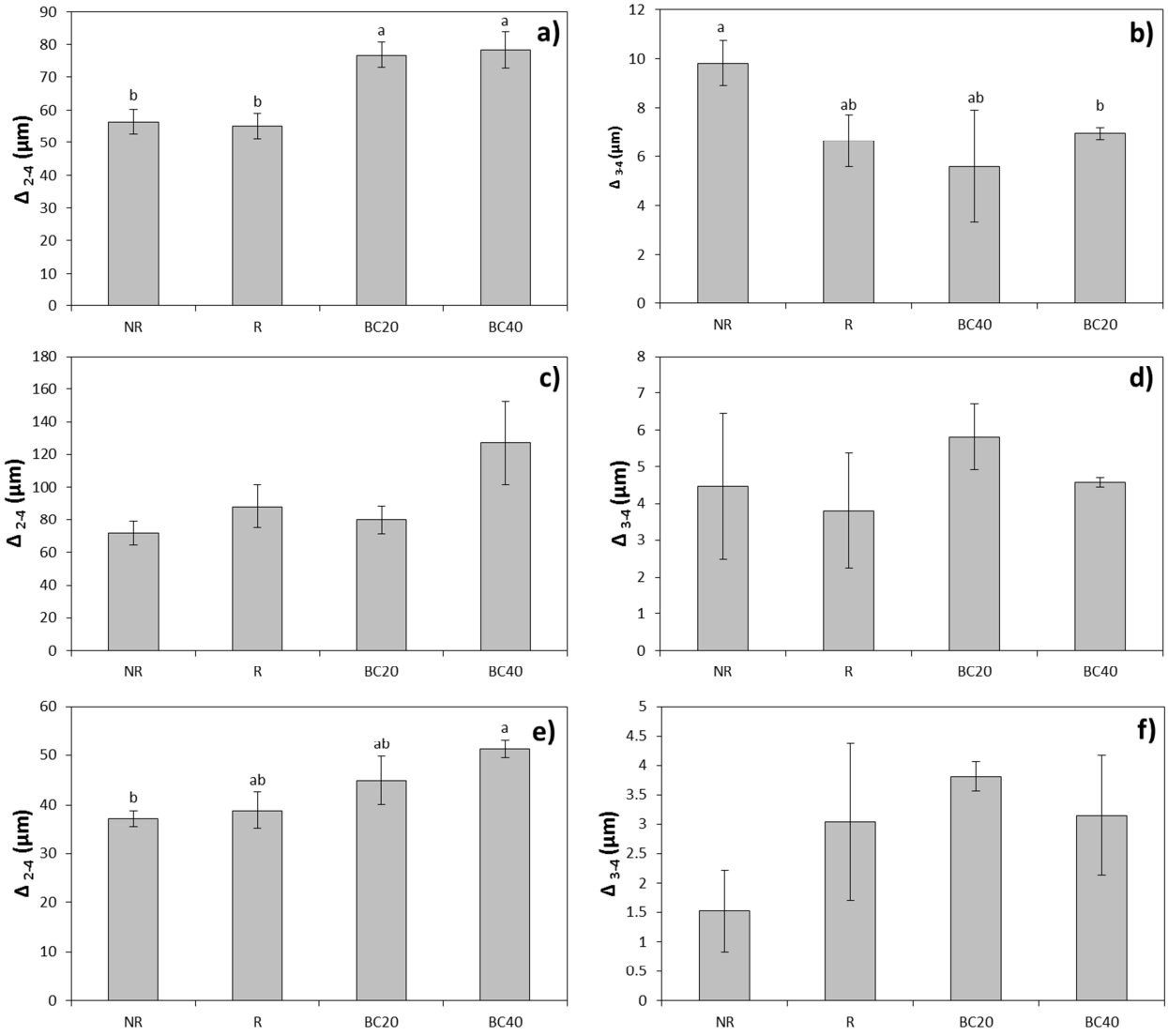

Figure 14. *Sandy-loam soil disaggregation indexes $\Delta_{2\text{-}4}$ and $\Delta_{3\text{-}4}$ with water pre-treatment (a and b); ethanol pre-treatment (c and d); and benzene pre-treatment (e and f).*

In sandy-loam soil the $\Delta_{2\text{-}4}$ indexes with all pre-treatments were positively correlated with OC (Table 6). In addition, the $\Delta_{2\text{-}4}$ index with benzene pre-treatment was also negatively correlated with

mesopores, and positively with micropores (R^2=0.80). The Δ_{3-4} index showed a negative correlation only with mesopores, considering ethanol pre-treament (R^2=0.46). Furthermore the Δ_{2-4} and WASI indexes resulted linearly correlated for both soils. More specifically, the Δ_{2-4} index was highly correlated with $WASI_w$ for both soils (R^2= 0.61 and 0.69 for clay and sandy-loam, respectively). Less strong correlations were observed considering the two other pre-treatments. Finally, Δ_{3-4} did not show correlations with WASI considering none of the pre-treatments applied.

Zeta potential at natural soil pH (ζn)

Average zeta potentials of the two soils with NR treatment were -15.25 mV and -10.8 mV for sandy-loam and clay soil, respectively. The application of biochar at the highest dose (40 t ha^{-1}) influenced this parameter only in sandy-loam soil (-13.18 mV). The increase in the absolute value of ζn indicates that the particles in solution ere less prone to flocculate. The ζn of clay soil with biochar was the same as the control. Pure biochar exhibited an average ζn of -27.7 mV, indicating the presence of negative charges on the surface.

Table 5. *Multiple regression analysis of the selected variables for clay soil.*

	Regression coefficients								
	Intercept α	Macro[a] β_1*	Meso β_2	Micro β_3	Ultra-micro β_4	Crypto β_5	OC% β_8	Contact angle β_9	Multiple R^2
Aggregate stability indexes									
Water pre-treatment									
WASI	38.8	-	-0.45	-	-0.54	0.64	-	0.33	0.91
Δ2-4	127.7	-0.64	-	-	-	0.46	-	-	0.72
Δ3-4		-	-	-	-	-	-	-	-
Ethanol pre-treatment									
WASI	69.5	-	0.28	-	-0.74	-	1.15	-	0.92
Δ2-4	-	-	-	-	-	-	-	-	-
Δ3-4	-	-	-	-	-	-0.60	-	-	0.36
Benzene pre-treatment									
WASI	34.9	-	-0.69	-	-	-	0.95	-	0.59
Δ2-4	-1900.0	-	-	-	-	0.75	-	-	0.56
Δ3-4	17.8	-	-	-	-	-	0.74	-0.69	0.80

**Standardised betas. aMacro: macropores; Meso: mesopores; Micro: micropores; Ultra-micro: ultra-micropores; Crypto: cryptopores. Correlations significant at p<0.05.*

Table 6. *Multiple regression analysis of the selected variables for sandy-loam soil.*

	Regression coefficients								
	Intercept α	Macro β_1*	Meso β_2	Micro β_3	Ultra-micro β_4	Crypto β_5	OC% β_8	Contact angle β_9	Multiple R^2
Aggregate stability indexes									
Water pre-treatment									
WASI	-3.5	-	-	-	-	-	0.77	-	0.60
Δ2-4	20.9	-	-	-	-	-	0.78	-	0.62
Δ3-4		-	-	-	-	-	-	-	-
Ethanol pre-treatment									
WASI	18.6	0.75	-1.18	-	-	-	1.03	-	0.94
Δ2-4	3.8	-	-	-	-	-	0.62	-	0.40
Δ3-4	0.1	-	0.68	-	-	-	-	-	0.46
Benzene pre-treatment									
WASI	50.4	-0.59	-	-	-	-	-	-	0.35
Δ2-4	-3.8	-	-2.22	2.38	-	-	0.88	-	0.80
Δ3-4	-	-	-	-	-	-	-	-	-

**Standardised betas. aMacro: macropores; Meso: mesopores; Micro: micropores; Ultra-micro: ultra-micropores; Crypto: cryptopores. Correlations significant at p<0.05.*

Discussion

Effects on maize yield

The incorporation of crop residues had no significant effects on maize yield in the two years of experiment. This, coupled with the results found in our long-term experiment (cfr. Chapter III Section *Crop yield and nitrogen use efficiency*) may indicate that longer periods are required for plant material to be effective. On the contrary biochar effects were readily visible after one year of incorporation. More specifically, the results of this study are partly in agreement with those reviewed by Jeffery et al. (2011), who found a more pronounced biochar effect on crop yield in soils with coarse texture. They also underlined that the effect was not proportional to biochar dose, and this is confirmed by our data which do not show differences between the two application rates. However their review did not indicate effects in soils with fine textures, on the contrary of those found in our clay soil. A more recent study reports no effects of biochar at 45 t ha^{-1} on a sandy and a silty soil (Borchard et al., 2014). On the contrary Haider et al. (2014) found an average increase of 7.9% maize productivity in German a loamy sand after addition of biochar at 34 and 69 t ha^{-1}, with no differences between doses. Biochar is reported to increase the mesoporosity of coarse-textured soils due to the clogging of macropores (Ajayi et al., 2016), increasing thus the plant available water and consequently crop productivity. This could be one of the mechanisms explaining the results of our study, and this conclusion is further strengthened considering that our sandy soil had mainly pores between 25 and 480 µm (cfr. Chapter III, Section *Pore architecture*), thus wider than the average particle dimension of the biochar applied (8.79 µm). On the contrary, in fine-textured soils biochar is reported to increase the surface area of pores smaller than 25 µm, and this is confirmed also by our experimental data (Cfr. Section *Soil pore size distribution* in the Results paragraph of this chapter). In this case, the water retention effect could be mainly due to biochar intrinsic porosity (Ajayi et al., 2016), in which water retained is not completely available for plants and thus not entirely effective in increasing yield. This could explain the slight effects found in our

fine-textured soils. Clearly, the effects on water retention may not be the only taking place in such a complex environment that soil represents, but in the first year of biochar application they are likely to play a major role, also considering that nitrogen in biochar is not bioavailable (data not shown). Indeed, during the second year of experiments, the differences between soils appear less evident while the effect of biochar continues. Evidently, other mechanisms become involved in the observed effects as long as a slight biochar mineralization takes place, including biochar carbon in the soil organic matter cycle.

Effects on aggregate organic carbon, structure and stability.

Residue effects on SOC were reviewed by Powlson et al. (2011), who found an average increase of 10% in organic carbon, which is in line with the responses found in our experiment for sandy-loam soil. It is notable that clay soil exhibited a decrease of SOC in response to residue incorporation. Notably, all the data reviewed by Powlson and collaborators was collected from experimental periods > 6 years, thus the slight effects found in our study may be mainly explained by its brevity (2 years). Regarding biochar, the effects found in our study are in line with those found by Liu and collaborators (2015) in a recent meta - analysis. They observed an average SOC increase of 23% at low biochar application rates (<20 t ha^{-1}), and of 59% for doses of 40-60 t ha^{-1} with no differences between soils with contrasting textures. They suggested that in soils with neutral to alkaline pH, the mineralization of soil C is inhibited by the further increase in soil reaction caused by biochar application, leading thus in a carbon accumulation. This could be one of the mechanisms explaining our results, however the analysis carried out on samples of pure biochar revealed that the method we used to analyse soil OC caused a partial oxidation of biochar carbon. Accordingly, it cannot be excluded that the increase in carbon content observed in plots subjected to its incorporation was partly due to the biochar intrinsic carbon and not only to a biochar-mediated stimuli to the accumulation of organic carbon in soils. Furthermore, even if soil analysis took place after two years, a residual effect of the preceding experimental design cannot be

excluded. In the soils examined the biochar effects on pore volumes were concentrated on the porosity < 25 µm, and this is consistent with the results found by Ajayi and collaborators (2016). However, the contribution of biochar also in the meso- and macroporosity has been detected by other authors (Andrenelli et al., 2016; Herath et al., 2013) At present no scientific literature on the analysis of aggregate shape in soils with organic amendments is available. Nevertheless our results highlight that particle aggregation is not affected in a macroscopic way, since the shape indicators did not show any effects due to the carbon management. On the contrary the visualisation of aggregates (SEM and photographs) allowed to conclude that biochar actively interacted with soil particles during aggregate turnover, and was occluded therein. The physical protection offered by the inclusion inside aggregates is considered one of the mechanisms supporting the evidence of biochar long-lasting stability in soil (Brodowski et al., 2006). The two techniques used to measure the stability of aggregates (wet sieving and laser diffraction) gave complementary (laser diffraction allowed to specifically evidence the behaviour of the outer and the inner part of the single aggregate particle, while wet sieving gave an overall index of stability) and coherent information (high correlation between WASIw and Δ2-4w). In addition, the use of three pre-treatments allows to have a first overview on the different mechanisms driving aggregate stability. Regarding the influence of biochar on aggregates, from recently published literature (Gul et al., 2015) it emerges that the major influence on soil stability is operated by low temperature biochars (400-600°C) while our results suggest that even high temperature biochars (800°C) can have positive effects and these appear texture dependent, due to the very different responses found in the two soils analysed. More specifically, the effects on sandy-loam soil were registered both with water and with ethanol pre-treatment, indicating that biochar action in this soil is mainly driven by the increase of mechanical resistance to the disruptive action of water. This could be caused by the increase in surfaces prone to form complexes with either mineral or organic molecules, thus increasing the number of electrostatic interactions between soil particles and finally, their stability. This is also confirmed by the zeta potential which shows an increase in the tendency to flocculate of the amended sandy-loam soil. Another factor which supports the above mentioned mechanisms, is the

biochar-mediated increase un cryptopores. Indeed, preceding studies have demonstrated that carbon inputs can affect aggregate stability by changing the pore size distribution of soils. More specifically by a shift from mesopores and micropores towards smaller ones (Dal Ferro et al. 2012). The contribution of other mechanisms like hydrophobicity seems to be excluded by the measurement of water repellence, which showed no differences between treatments in this soil. However, the laser diffraction with benzene pre-treatment indicates that at the highest dose of biochar, an organic matter-mediated increase in aggregate stability may not be completely excluded, and this is also confirmed by the positive correlations found for stability indexes with the organic carbon content of this soil. On the contrary of what found by Soinne and collaborators (2014), our clay soil was slightly affected by biochar incorporation, as its effects appear only at the highest dose with ethanol pre-treatment. This can be due to the fact that this soil exhibited an already high level of aggregate stability and thus the action of biochar was limited. Furthermore it is recognized that the biochar - mediated increase in structure stability is caused by an increase in surface area of the particles, which widens the surfaces available for the formation of complexes with inorganic and organic substances along with the accessible area for water menisci formation (Ajayi et al., 2016). These mechanisms could be less pronounced in our clay soil since its surface area is already high (42 m^2g^{-1}) and is not likely to be substantially increased by the applied amounts of biochar. This is apparently in contrast with the observed effect of biochar on clay porosity and water repellence which were both increased. It can be hypothesized that the increases observed were not enough to increase the stability in a soil already exhibiting a high level of it. In addition, the generally negative correlations found with the larger porosity classes (i.e. > 0.1 µm) may suggest that the action of bigger pores in increasing water penetration velocity and thus disaggregation as a consequence of slacking is more evident in this soil. This could produce a contrasting effect of biochar amendment, with an increase in slacking caused by the rise in porosity coupled with an intensification of aggregation forces caused by organic matter input.

The residue incorporation treatment showed the highest $WASI_b$, even if this effect was not found to be significant. This confirms the fact that the pre-treatment with benzene emphasizes the organic

matter protection of particles from the disruptive action of water. The slighter effects of residues on aggregate stability compared to those of biochar could be explained by the fact that in non-stabilized environments (i.e. short-term experiments) the maximum effects on aggregate stability are registered 1 to 3 months after residue incorporation, as reviewed by Abiven et al. (2009). Accordingly, in our experiment at the moment of sampling (more than 7 months after residue incorporation), the detectable effects were likely to be minimal. Nevertheless, a tendency in an increase in stability as a result of residue incorporation could be noticed in clay soil. This could be due to the physical protection operated by clay minerals, which is expected to be higher in clay soil if compared to sandy-loam, owing to its higher content of clay. In this soil the decomposition is likely to be slower, thus the accumulation of organic matter could be enhanced if compared to sandy-loam.

Conclusions

Crop residues and biochar evidenced different influences on the soil indicators examined, as it would be expected by the greatly different nature of these two types of carbon input. The incorporation of crop residues was not found effective in increasing crop yields while the effects on soil organic carbon were minor and took place only in sandy-loam soil. In addition, the effects on aggregate stability were in general lower if compared with those of biochar. These results were explained by the fact that the experimental period was too short to allow the residue carbon to produce measurable effects. Our results further suggest that the action of biochar in increasing soil stability is primarily due to the increase in soil surfaces prone to inter-particle bonding and to a lesser extent to the increase in the hydrophobic action of organic matter, and it is more pronounced in soils with a native low stability. It cannot be excluded however, that mineralization processes in the field which will include biochar carbon in the soil organic matter will further influence soil stability via mechanisms diverse from those found in our studies. The analytical approach was useful to disentangle the different mechanisms affecting aggregate stability, specifically the use of laser diffraction confirmed to be a solid technique and gave results coherent and complementary to the traditional wet sieving method. In conclusion, biochar confirmed its positive effects on crop yields and aggregate porosity and stability indexes. These effects were clearly visible after one year of application and on all the soils considered, even if with different intensities. This practice thus is recommendable in order to increase soil fertility in the climatic conditions of North-Eastern Italy. Its long-term effects however remain a knowledge gap that needs to be investigated to prevent possible side-effects and elaborate effective application and management guidelines. On the contrary, residue effects in the time interval of the present work appear slighter, and this practice appears advisable only with a long-term perspective.

References

Abiven, S., Menasseri, S., Chenu, C. (2009). The effects of organic inputs over time on soil aggregate stability – A literature analysis. *Soil Biology and Biochemistry*, *41*(1), 1–12. doi:10.1016/j.soilbio.2008.09.015

Ajayi, A. E., Holthusen, D., Horn, R. (2016). Changes in microstructural behaviour and hydraulic functions of biochar amended soils. *Soil and Tillage Research*, *155*, 166–175. doi:10.1016/j.still.2015.08.007

Amézketa, E., Aragüés, R., Carranza, R., Urgel, B. (2003). Macro- and micro-aggregate stability of soils determined by a combination of wet-sieving and laser-ray diffraction. *Spanish Journal of Agricultural Research, 1(4)*, 83-34. doi: 10.5424/sjar/2003014-50

Andrenelli, M. C., Maienza, A., Genesio, L., Miglietta, F., Pellegrini, S., Vaccari, F. P., Vignozzi, N. (2016). Field application of pelletized biochar: short term effect on the hydrological properties of a silty clay loam soil. *Agricultural Water Management, 163*, 190-196. doi:10.1016/j.agwat.2015.09.017

Bocchi, S., Confalonieri, R., Frigeni, S., Morari, F., Patruno, A. (2007). Wet Aggregate Stability Index: precision assessment of Tiulin method trough an inter-laboratory test, *LI*, 1–12.

Borchard, N., Siemens, J., Ladd, B., Möller, A., Amelung, W. (2014). Application of biochars to sandy and silty soil failed to increase maize yield under common agricultural practice. *Soil and Tillage Research*, *144*, 184–194. doi:10.1016/j.still.2014.07.016

Brodowski, S., John, B., Flessa, H., Amelung, W. (2006). Aggregate-occluded black carbon in soil. *European Journal of Soil Science, 57*, 539-546. doi: 10.1111/j.1365-2389.2006.00807.x

Cameron, K.C., Buchan, G.D., 2006. Porosity and pore-size distribution. In: Lal, Ratan (Ed.), Encyclopedia of Soil Science, vol.2. Taylor and Francis, pp.1350–1353.

Dal Ferro, N., Berti, a., Francioso, O., Ferrari, E., Matthews, G. P., & Morari, F. (2012). Investigating the effects of wettability and pore size distribution on aggregate stability: the role of soil organic matter and the humic fraction. *European Journal of Soil Science*, *63*(2), 152–164. doi:10.1111/j.1365-2389.2012.01427.x

Gul, S., Whalen, J. K., Thomas, B. W., Sachdeva, V., Deng, H. (2015). Physico-chemical properties and microbial responses in biochar-amended soils: Mechanisms and future directions. *Agriculture, Ecosystems & Environment*, *206*, 46–59. doi:10.1016/j.agee.2015.03.015

Haider, G., Koyro, H.-W., Azam, F., Steffens, D., Müller, C., Kammann, C. (2014). Biochar but not humic acid product amendment affected maize yields via improving plant-soil moisture relations. *Plant and Soil*, *395*(1-2), 141–157. doi:10.1007/s11104-014-2294-3

Hardie, M., Clothier, B., Bound, S., Oliver, G., Close, D. (2013). Does biochar influence soil physical properties and soil water availability? *Plant and Soil*, *376*(1-2), 347–361. doi:10.1007/s11104-013-1980-x

Hénin, S., Monnier, G., Gras, R., & Zanini, E. (1973). *Il profilo colturale*. Edagricole.

Herath, H. M. S. K., Camps-Arbestain, M., Hedley, M. (2013). Effect of biochar on soil physical properties in two contrasting soils: An Alfisol and an Andisol. *Geoderma*, *209-210*, 188–197.

doi:10.1016/j.geoderma.2013.06.016

Jeffery, S., Verheijen, F. G. A., van der Velde, M., Bastos, A. C. (2011). A quantitative review of the effects of biochar application to soils on crop productivity using meta-analysis. *Agriculture, Ecosystems & Environment*, *144*(1), 175–187. doi:10.1016/j.agee.2011.08.015

Jien, S.-H., Wang, C.-S. (2013). Effects of biochar on soil properties and erosion potential in a highly weathered soil. *Catena*, *110*, 225–233. doi:10.1016/j.catena.2013.06.021

Jozefaciuk, G., Czachor, H. (2014). Impact of organic matter, iron oxides, alumina, silica and drying on mechanical and water stability of artificial soil aggregates. Assessment of new method to study water stability. *Geoderma*, *221-222*, 1–10. doi:10.1016/j.geoderma.2014.01.020

Liu, S., Zhang, Y., Zong, Y., Hu, Z., Wu, S., Zhou, J., Jin, Y., Zou, J. (2015). Response of soil carbon dioxide fluxes, soil organic carbon and microbial biomass carbon to biochar amendment: a meta-analysis. *GCB Bioenergy*, n/a–n/a. doi:10.1111/gcbb.12265

Mason J.A., Greene R. S. B., Joeckel, R. M. (2011) Laser diffraction analysis of the disintegration of aeolian sedimentary aggregates in water. Catena, 87, 107-118. Doi: 10.1016/j.catena.2011.05.015

Ojeda, G., Mattana, S., Àvila, A., Alcañiz, J. M., Volkmann, M., Bachmann, J. (2015). Are soil–water functions affected by biochar application? *Geoderma*, *249-250*, 1–11. doi:10.1016/j.geoderma.2015.02.014

Ouyang, L., Wang, F., Tang, J., Yu, L., Zhang, R. (2013). Effects of biochar amendment on soil aggregates and hydraulic properties. *Journal of Soil Science and Plant Nutrition*, *13*(4), 991–1002. doi:10.4067/S0718-95162013005000078

Powlson, D. S., Glendining, M. J., Coleman, K., Whitmore, A. P. (2011). Implications for Soil Properties of Removing Cereal Straw: Results from Long-Term Studies. *Agronomy Journal*, *103*(1), 279. doi:10.2134/agronj2010.0146s

Rawlins, B. G., Wragg, J., Lark, R. M. (2013). Application of a novel method for soil aggregate stability measurement by laser granulometry with sonication. European Journal of Soil Science, 64, 92-103. doi:10.1111/ejss.12017

Siebold, A., Walliser, A., Nardin, M., Oppliger, M., Schultz, J. (1997). Capillary Rise for Thermodynamic Characterization of Solid Particle Surface. *Journal of Colloid and Interface Science*, *186*(1), 60–70. doi:http://dx.doi.org/10.1006/jcis.1996.4640

Soinne, H., Hovi, J., Tammeorg, P., Turtola, E. (2014). Effect of biochar on phosphorus sorption and clay soil aggregate stability. *Geoderma*, *219-220*, 162–167. doi:10.1016/j.geoderma.2013.12.022

Sun, F., Lu, S. (2014). Biochars improve aggregate stability, water retention, and pore-space properties of clayey soil. *Journal of Plant Nutrition and Soil Science*, *177*(1), 26–33. doi:10.1002/jpln.201200639

Walkley, A., Black, I. A. (1934). An examination of the Degtjareff method for determining soil organic matter, and a proposed modification of the chromic acid titration method. *Soil Science*, *37*(1).

Chapter V

General conclusions

The results of the present thesis regarding biochar confirmed the wide variability of this matrix as a function of feedstock and production temperatures, suggesting therefore that it is not possible to identify an "ideal" biochar able to improve crop yields and soil properties while increasing the stabile carbon content at the same extent. Moreover, the production of biochar from specific types of waste biomasses represents a still not feasible technique especially owing to the high content of heavy metals of these biomasses which would create serious environmental risks once they are used as amendants. Nonetheless, the production of biochar from waste biomasses with low or negligible contents of heavy metals (i.e. waste wood) and its subsequent application to soil showed positive effects on crop yields and aggregate porosity and stability indexes. Furthermore, biochar resulted useful in increasing the carbon content of the soils. All the effects were clearly visible after one year of application and on all the soils considered, even if with different intensities. Indeed, soil properties were affected in a more pronounced way in sandy-loam, while crop yield was especially boosted in sandy soil. The use of biochar is thus a recommendable practice to increase soil fertility in the climatic conditions of North-Eastern Italy, its long-term effects however remain a knowledge gap that needs to be investigated to prevent possible side-effects and elaborate effective application and management guidelines. On the contrary, residue effects in the short-term are slighter, and this practice appears advisable only with a long-term perspective. Indeed our results showed that soil organic carbon was significantly affected by the long-term (43 years) incorporation of crop residues with effects quantitatively more evident in clay soil and high relative increments in sandy soil. The effects were not limited to the upper soil layer, but extended to lower depths especially for sandy and sandy-loam soil. The residue-induced effects on soil organic carbon were not accompanied by a relevant change in soil pore size distribution from nano to macro scale, even if they induced an increase in total porosity. In addition, even if only slightly influenced in quantitative terms, the pore network showed a rearrangement towards a more elongated and irregular structure. On the contrary, residue influence on crop yields was relatively low, with modest increments of biomass in the most fertile soils, and their effect could be compensated by N fertilization.

Appendix

Scientific papers published

J Soils Sediments (2015) 15:792–804
DOI 10.1007/s11368-014-0964-7

Characterization of chemical–physical, structural and morphological properties of biochars from biowastes produced at different temperatures

Chiara Pituello · Ornella Francioso · Gianluca Simonetti · Annamaria Pisi · Armida Torreggiani · Antonio Berti · Francesco Morari

Received: 1 April 2014 / Accepted: 5 August 2014 / Published online: 16 August 2014

Abstract
Purpose Biochar production from biowastes (e.g. digestate) is currently one of the more innovative and unexplored fields of research. A complete characterization of these materials, also according to the production temperature, would be a key tool to assess their potential use as soil amendments.
Material and methods For this purpose, five feedstocks (sewage sludge, municipal organic waste, cattle manure and silage digestates, poultry litter and vineyard pruning residues) were pyrolyzed at different temperatures. Structural and morphological transformations of biomasses during heating were followed by using FT-IR, scanning electron microscopy (SEM) and hyperspectral enhanced dark-field microscopy, a novel technique that provides both spectral and spatial information in one measurement. In addition, biochar microstructure (i.e. surface area and pore size distribution) using CO_2 and N_2 adsorption isotherms was investigated. Specific density was also analysed by a helium pycnometer.
Results and discussion Biochars exhibited considerable chemical, structural and morphological differences depending on temperature and feedstock type. Moreover, specific density and surface area increased with the temperature. In particular, heating was able to produce a sharp increase of mesopore and micropore volume especially at 450 and 550 °C, but with different intensities for each feedstock. Thanks to the hyperspectral analysis, distinctive spectral patterns depending on the biochar chemical composition as well as the spatial distribution of the components were found.
Conclusions The results demonstrated that, from a physical–chemical point of view, it is not possible to identify an "ideal" biochar able to improve both soil nutrient content and structure. On the contrary, depending on feedstocks and temperature, each biochar exhibits specific features that would make it suitable for a specific purpose.

Keywords Biochar · Chemical–physical properties · Feedstocks · Temperature pyrolysis

Responsible editor: Chengrong Chen

Electronic supplementary material The online version of this article (doi:10.1007/s11368-014-0964-7) contains supplementary material, which is available to authorized users.

C. Pituello · G. Simonetti · A. Berti · F. Morari
Dipartimento di Agronomia Animali Alimenti Risorse Naturali e Ambiente, Università di Padova, Viale dell'Università 16, 35020 Padova, Italy

O. Francioso (✉) · A. Pisi
Dipartimento di Scienze Agrarie, Università di Bologna, V.le Fanin 40, 40127 Bologna, Italy
e-mail: ornella.francioso@unibo.it

A. Torreggiani
ISOF, Consiglio Nazionale delle Ricerche, Via Gobetti 101, 40129 Bologna, Italy

1 Introduction

In recent years, biochar has gained interest as a tool to improve soil quality and promote soil carbon sequestration (Biederman and Harpole 2013; Jeffery et al. 2013; Schmidt et al. 2011). The highly aromatic structure of biochar and its specific surface characteristics, along with its high porosity, have been considered as the main reason for its long-lasting stability in soils and its ability to increase nutrient bioavailability, thus increasing crop productivity under specific pedo-climatic conditions (Jeffery et al. 2011; Shackley and Sohi 2010). However, the biochar application to soil, in many instances, has been reported to cause priming of soil organic carbon (both negative and positive), specifically over short term trials

(Cross and Sohi 2011), or to alter the soil structure (density, pore size distribution, aggregate stability) and also influence the water dynamics, affecting soil pore size distribution and water holding capacity (Verheijen et al. 2010).

Biochar characteristics change widely according to pyrolysis conditions and feedstock type (e.g. bioenergy crops, crop residues and by-products, industrial organic by-products) (Spokas et al. 2011); therefore, a wide diversity of its composition and property is expected (Gaskin et al. 2008; Ro et al. 2010). Chars produced by wood with high lignin contents have higher carbon (C) amount than those obtained from herbaceous feedstocks (Zabaniotou et al. 2008; Jeffery et al. 2013), but they are depleted in N (Cao and Harris 2010). Nevertheless, these chars can still have positive effects on soils, favouring their microbial colonisation. Conversely, livestock manures are more enriched in nitrogen, phosphorus and micronutrients, and as a consequence, their pyrolysis produces biochars with higher nutrient content (Cantrell et al. 2012).

Biochar made from biowaste, such as digestate from biogas production plants and sewage sludge from anaerobic wastewater treatment, maximizes the waste disposal with benefits at different levels (Jeffery et al. 2011). Thus, processing biowastes through pyrolysis plants and the subsequent use of biochar as a soil amendment can give an additional value to those biomasses whose disposal routes (such as farmland application) may be subject to strict legislative constraints.

Robust information is still lacking on the potentialities of biochar production from biomasses of difficult disposal, also given that the heterogeneous nature of the feedstocks adds uncertainties to the results. For an agronomic benefit from biochar, it is important to understand how the physical and chemical properties are influenced by feedstock type and the pyrolysis conditions used in its production (Lehmann and Joseph 2009; Spokas et al. 2011). Moreover, hazardous materials may behave differently during pyrolysis, resulting in their elimination, enrichment or transformation in the final product.

There is currently no consensus in the scientific community regarding standardized analytical procedures for biochar characterization. Extensive analyses contribute to a better understanding of thermochemical transformations that take place during pyrolysis, providing support to the consumers on the use of a specific biochar for each particular agro-ecosystem. For this reason, there is an urgent need for simple analytical methods to obtain a "fingerprint" of each biochar.

Fourier transform infrared (FT-IR) spectroscopy is a commonly applied technique to distinguish the main functional groups of organic matter such as carbohydrates, lignin, cellulose, lipids and proteins. In recent years, FT-IR spectroscopy has become a powerful technique for the characterization of biochar (Cantrell et al. 2012). However, this technique may not provide structural information on char produced at high pyrolysis temperature because the carbon formation produces weak signals in the FT-IR spectral range.

Hyperspectral imagery is an emerging technique that combines conventional imaging and spectroscopy to obtain both spatial and spectral information from each pixel (Badireddy et al. 2012; Elmasry et al. 2012). It measures reflectance in a spectral range from the visible to the short-wave infrared region, and it has been recently found to be suitable and powerful for inspecting the quality and safety of food and agricultural products (Zhang et al. 2012). Currently, there are no applications of this technique to biochars.

The aims of this paper were to characterize the chemical–physical, structural and morphological properties of biochars produced from biowastes, to investigate the effect of pyrolysis temperature on these properties, and to evaluate the potential contribution of hyperspectral imaging in improving biochar characterization.

2 Materials and methods

2.1 Feedstocks

Five feedstocks were collected from plants and experimental farms located in Veneto Region, Northeast Italy: (i) sewage sludge digestate (SS) from an anaerobic digestion plant treating urban wastewater; (ii) municipal organic waste digestate (MW) from a biogas plant that treats the organic fraction of municipal waste; (iii) cattle manure and silage digestate (CD) from a biogas plant that uses cattle manure mixed with silage maize (30 % c.a.); (iv) dry poultry litter (PL) from Italpollina® Italpollina SpA, Verona; and (v) vineyard pruning residues (PR) from the University farm. Their reuse for agronomic purposes is regulated by EU Directives (e.g. Nitrate Directive 91/EEC No. 676 1991) and Italian laws (Dlgs. 27/03/2000 2000; DM 7/4/2006 C 2006; Dlgs. 152/2006 2006) that set limitations for their disposal.

Feedstocks were dried overnight at 65 °C until the initial moisture (ranging from 40 to 90 %) dropped to less than 7 % (except for dry poultry litter, moisture content 12 %) and then ground to a particle size of less than 2 mm.

2.2 Biochar production

The samples were pyrolyzed in lid-covered porcelain crucibles (Haldenwanger 79MF) in a muffle furnace, preheated at 100 °C, to a highest heating temperature of 250, 350, 450 and 550 °C with a heating rate between 16 and 19 °C/min and a residence time of 1 h. The crucibles were then moved with the lids on and left to cool at room temperature to prevent any loss in homogeneity due to accidental combustion.

The biochar produced was weighted and stored in air-tight Falcon vials prior to further analysis. Ground and

sieved biochar samples (500 μm) were used for chemical analysis.

2.3 Chemical analysis

Elemental analyses were carried out on raw feedstocks and biochars sieved at 500 μm. The total C, N and S contents were determined by combustion with an Elementar varioMACRO apparatus (Elementar Americas Inc., Mt. Laurel, NJ) and the metal concentration by using inductively coupled plasma–optical emission spectroscopy (ICP–OES) (Spectro Arcos, Ametek, Kleve, Germany). All samples were digested with 5 ml concentrated HNO_3 (67 % *w*/*w*, Suprapur Merck) and 3 ml $HClO_4$ (65 % *w*/*w*, Suprapur Merck).

The pH and electrical conductivity (EC) of raw feedstocks and biochars of samples sieved at 2 mm were measured in a suspension (1:20 *w*/*v*) in deionized water by shaking at 70 rpm for 1 h.

Ash was measured as the weight loss after heating for 8 h at 550 °C (Wiedner et al. 2013). All measurements were performed in triplicate.

2.4 Spectral and morphological analyses

2.4.1 Fourier transform infrared spectroscopy

Infrared spectral acquisition was performed on all feedstock and biochar samples by using a Nicolet 5700 FT-IR equipped with a diamond attenuated total reflectance (ATR) accessory and a DTGS detector (Nicolet, Madison, USA). The total number of scans averaged for each spectrum was 100 with a 4-cm^{-1} resolution. The background spectrum was acquired in air. Baseline correction and smoothing of spectra were obtained with Grams/386 spectral software (Galactic Industries, Salem, NH).

2.4.2 Hyperspectral imagery with enhanced dark-field microscopy

Ground biochar samples (500 μm) were visualized, in air and at room temperature, via their light scattering using an enhanced dark-field illumination system (CytoViva, Auburn, AL) attached to an Olympus microscope. The system consisted of a CytoViva 150 dark-field condenser in place of the microscope's original condenser, attached via a fibre optic light guide to a Solarc 24-W metal halide light source (Welch Allyn, Skaneateles Falls, NY). Improved optical performances are obtained by pre-aligned Koehler and the main feature of Critical illumination. A ×100 oil objective with an iris (Olympus UPlanAPO fluorite, N.A. 1.35–0.55) was integral to the system. Spectral data within each pixel of the scanned field of view were captured with a CytoViva spectrophotometer and integrated CCD camera. The visible near-infrared spectrophotometer operates in the range 400–1,000 nm. Spectral data were analysed by using the CytoViva Hyperspectral analysis software program (ENVI 4.4 and ITT Visual Information Solutions). Image processing and analysis involved the building of spectral libraries (spectral endmembers). The spectral endmembers were obtained by the selection of a region of interest on the scanned sample. Finally, Spectral Angle Mapper (SAM) was used to measure the similarity between the image pixels and endmember pixels.

2.4.3 Scanning electron microscopy

Dry samples of feedstocks and their pyrolysis products at 350 and 550 °C were mounted on aluminium stubs with silver glue and coated with gold-palladium film using an ion sputtering unit Balzer MED 010 (Balzers Union, Ltd, Balzers, Liechtenstein). The samples were observed under a Philips SEM 515 scanning electron microscope (Philips, Eindhoven, The Netherlands) at 7 Kv, and the pictures taken with a Nikon 5400 Coolpix digital camera (Nikon, Chiyoda-ku, Tokyo, Japan).

2.5 Physical analysis

Physical characterization was done on the 2-mm fraction. Specific density was determined using a helium pycnometer (Micro Ultrapyc 1200e, Quantachrome) (Lowell et al. 2004).

Specific surface area was determined using N_2 and CO_2 sorption data obtained with a Sorptomatic 1990 after degassing of the sample at 105 °C overnight. External surface area (pores>1.5 nm) was obtained from the linear part of the N_2 isotherm (at 77 K) using the Brunauer–Emmett–Teller theory (between pressure p/p_0 0.05 and 0.25). Internal surface area (including pores<1.5 nm) was obtained using the Dubinin–Raduskevich method from the CO_2 adsorption isotherm. Mesopores (diameter between 2.6 and 50 nm) from N_2 isotherms were obtained using Horwath and Kawazoe's method (Horvath and Kawazoe 1983); micropores from N_2 (0.8–2.6 nm) and CO_2 (0.5–0.8 nm) sorption data were obtained using the B.J.H. method (Barrett et al. 1951).

2.6 Statistical analysis

CoStat 6.4 (CoHort Software, Monterey, CA, USA) was used to perform a two-way ANOVA using production temperature and feedstock type as a main factors. The normal distribution of data was verified using the Brown–Forsythe test. The Tukey's honestly significant difference test was applied to compare the differences between group means.

3 Results and discussion

3.1 Feedstock properties

All the feedstocks had a neutral reaction, apart from CD that was alkaline (pH>8.3). EC ranged from 412 μs cm^{-1} in PL to 1,642 μs cm^{-1} in SD, while ash content was extremely variable with low values (2.9 and 5.6 %) in biomass-based feedstocks (CD and PR) and high values in SS (44 %). Feedstock materials differed consistently in their elemental composition and heavy metal content (Table 1 and Table S1, Electronic Supplementary Material). Total carbon was c.a. 30 % in SS and MW and >40 % in the others. Total nitrogen content ranged from 0.8 to 4.2 % for MW, SS and PL, whereas it was very low for PR. As a consequence, C/N was >30 in biomass-based feedstocks and around 10 in the others. Total S, P and K also showed a wide variability, ranging from 0.2 to 1.2 %, from 1 to 15 g kg^{-1} and from 3.8 to 20 g kg^{-1}, respectively (Table 1). As expected, the heavy metal content was higher in SS and MW with respect to other feedstocks (Table S1, Electronic Supplementary Material). In particular, Cu and Zn in SS exceeded the Italian guidelines for agronomic use of amendants (Dlgs. 27/03/2000 2000).

3.2 Biochar production and chemical properties

Biochar yield (% biochar weight/feedstock weight) decreased with rising temperature as observed by many other studies (e.g. Antal and Grønli 2003; Keiluweit et al. 2010). For example, the yield varied from 95 % (250 °C) to 63 % (550 °C) for SS and from 91 % (250 °C) to 31 % (550 °C) for PR (Fig. S3, Electronic Supplementary Material). In general, yield was higher for SS and MW than the biomass-based CD, PL and PR. These latter feedstocks appeared be more prone to thermal decomposition, which occurred between 250 and 350 °C. PR gave the lowest yield (31 %), likely due to cellulose and hemicellulose decomposition (Shinogi and Kanri 2003).

All chemical properties showed a significant interaction between feedstock type and temperature (Table 2). The temperature effect on pH value of PL was particularly relevant, as it varied from 6.9 (250 °C) up to 10.2 (550 °C). On the contrary, temperature did not influence the urban waste (SS and MW) pH, which remained neutral in the range of tested temperatures. Our results are not comparable with those described by Hossain et al. (2011) and Mendez et al. (2013) who found a substantial alkalization of biochar yielded from sewage sludge at temperatures over 500 °C.

In general, EC showed a U-shaped response with higher values at low and high temperatures, with the exception of PR whose EC decreased with rising temperature. As observed by many authors (Shinogi and Kanri 2003; Cantrell et al. 2012; Hossain et al. 2011), ash content increased with temperature and was higher in the feedstocks with low C content. Char with a high ash percentage might be less suitable for soil amendment with respect to char from low-ash feedstocks because high levels of heavy metals can cause soil pollution (Brewer et al. 2009).

Pyrolysis temperature significantly ($p<0.05$) influenced the nutrient content (Table 2). Total N content in the biochars increased with pyrolysis at 350 °C (Table 2). This may be related to the formation of recalcitrant N occurring in heterocyclic structures (Knicker 2007). In general, N concentrations decreased as the temperature increased to 550 °C to values lower than those of the initial feedstocks (Table 1). Nitrogen losses at 550° might be due to cracking of nitrile-N and heterocyclic-N compounds from the dehydrogenation and polymerization of amine-N during pyrolysis (Tian et al. 2013). On the contrary, CD and PR exhibited an increase in N concentration.

Sulphur content decreased in MW (from 1 to 0.6 %) while an opposite trend was observed in PR. No significant variation for the other biochars was detected. Generally, phosphorus and K contents increased with pyrolysis temperature in all biochars. The increase in P content at 550 °C in CD, PL and PR biochars (over 100 %) was particularly relevant if compared to the P values of the initial feedstocks. The use of

Table 1 Chemical composition of raw feedstocks

Feedstock	$pH_{1:20}$	EC μs cm^{-1}	Ash %	C $\%_{db}$[a]	N	S	P g kg^{-1}[a]	K
CD	8.3±0.08	1,642±52	5.6±0.4	44±1.0	1.7±0.02	0.40±0.05	4.5±0.01	8.8±0.1
MW	7.3±0.05	157±19	35±0.3	31±0.9	4.0±0.1	1.2±0.1	15±0.2	5.01±0.05
PL	7.5±0.03	412±2.9	12±0.03	40±1.7	4.2±0.1	0.80±0.02	7.90±0.03	20±0.9
PR	7.0±0.19	860±8.1	2.9±0.2	45±1.2	0.50±0.04	0.20±0.03	1.01±0.08	4.20±0.03
SS	7.2±0.03	721±7.1	44±0.07	27±0.6	3.60±0.08	0.80±0.04	14±0.1	3.80±0.04

Values reported as means ($n=3$) followed by standard error

CD cattle manure and silage digestate, *MW* municipal organic waste digestate, *PL* poultry litter, *PR* pruning residues, *SS* sewage sludge

[a] Values calculated on a dry basis

Table 2 Biochar chemical properties produced at different temperatures

Biochar (°C)		$pH_{1:20}$	EC µs cm^{-1}	Ash %	C $\%_{db}$[a]	N	S	K g kg^{-1}[a]	P
CD	250	7.9 d	1,156 bc	8.6 op	52.2 e	1.9 i	0.3 fghi	10.3 fgh	4.5 k
	350	8.6 c	691 f	14.5 n	60.7 d	2.6 fg	0.3 fghi	17.1 de	7.3 j
	450	10.3 a	1,070 cd	16.6 m	63.2 cd	2.2 hi	0.3 fghi	20.4 cd	7.7 ij
	550	10.3 a	1,695 a	18.6 l	65.9 bc	2.2 hi	0.5 efghi	23.2 c	11.3 h
MW	250	7.2 efg	1,207 b	37.6 h	33.7 gh	4.1 c	1.0 a	5.6 hij	17.8 e
	350	7.6 de	275 kl	44.2 g	34.8 g	4.0 c	0.9 ab	6.5 hij	20.5 d
	450	7.4 ef	362 jk	55.1 e	29.4 hi	3.0 e	0.8 abc	8.0 ghij	24.7 b
	550	7.1 efg	814 e	61.1 c	26.2 ij	2.7 ef	0.6 bcde	8.7 ghij	26.1 a
PL	250	6.9 fg	402 j	14.0 n	43.7 f	4.1 c	0.4 efghi	22.3 c	8.7 i
	350	8.0 d	353 jk	25.1 k	51.2 e	5.6 a	0.5 efghi	37.7 b	14.4 g
	450	9.9 ab	432 hIj	28.8 j	51.2 e	4.5 b	0.4 efghi	43.2 a	16.4 f
	550	10.2 a	419 Ij	32.6 i	51.1 e	3.7 d	0.5 defgh	48.0 a	19.4 d
PR	250	6.0 h	961 d	3.5 q	48.7 e	0.9 k	0.2 i	4.6 j	1.0 m
	350	6.8 g	590 fg	7.4 p	65.9 bc	1.3 j	0.2 hi	9.7 fghi	2.0 lm
	450	9.0 c	517 ghi	7.9 p	69.3 b	1.3 j	0.3 efghi	11.7 fg	2.4 l
	550	9.7 b	540 gh	9.8 o	75.1 a	1.3 j	0.4 efghi	14.2 ef	3.0 l
SS	250	6.9 fg	691 f	48.6 f	28.3 i	3.8 cd	0.8 abcd	4.2 j	17.3 ef
	350	7.3 efg	92 n	58.1 d	27.5 i	3.6 d	0.6 bcdef	4.4 j	19.6 d
	450	7.2 efg	130 mn	67.0 b	22.5 jk	2.8 ef	0.6 cdefg	4.9 ij	21.9 c
	550	7.1 fg	210 lm	73.2 a	20.1 k	2.3 gh	0.6 bcdef	4.2 j	23.6 b

Values reported as means (n=3). Different letters within columns indicate significant differences (p<0.05)

[a] Values calculated on a dry basis

biochars may be an alternative to mineral fertilization, P being an important element for plant growth. At this phase, it is not possible to determine whether these nutrients are bioavailable. The pyrolysis is a complex process that may influence in diverse ways the availability of elements of soil fertility (Yin Chan and Xu 2009).

Heavy metals were retained in the biochars during pyrolysis (Table 3); this is consistent with the fact that some heavy metals volatilize only at high temperatures (>600 °C) (Kristler et al. 1987). As a result, some heavy metals such as Cu, Pb and Zn in SS, Cu and Zn in MW and Zn in PL exceeded the Italian guidelines for amendants (Dlgs. 27/03/2000 2000) (Table 3). Some authors reported that these elements are stabilized in biochar (Kristler et al. 1987; Cao and Pawloski 2012). Then long-term soil applications of biochar should be carefully monitored in order to avoid the potential accumulation of heavy metals.

3.3 Spectral and morphological properties of biochar

3.3.1 FT-IR characterization

Attention was focused on the region between 1,800 and 1,200 cm^{-1}, as it is more sensitive to structural changes produced by temperature. Feedstocks from sludge (SS) and municipal solid wastes (MW) are mainly composed of protein, cellulose, lignin and fatty acids (Ábrego et al. 2009). Thus, their spectra showed (Fig. 1a, b) the typical amide I (1,642–1,638 cm^{-1}) and amide II (1,515–1,536 cm^{-1}) bands. However, other contributions cannot be excluded, such as C=O stretching in ketone and carboxylate groups (1,642 cm^{-1}) and C=C aromatic skeletal vibrations due to lignin structures (1,515 cm^{-1}). Vibration of CH_2 scissoring (1,434 cm^{-1}) of cellulose and saturated fatty acids and O–H bending vibrations of alcohols and symmetric stretching of carboxylate groups appeared in both samples in the interval between 1,500 and 1,240 cm^{-1}.

In poultry litter (PL) and silage digestate (CD) spectra the amide I and II bands at 1,640 and 1,534 cm^{-1} (Das et al. 2009; Cantrell et al. 2012) were predominant (Fig. 1c, d). A shoulder at 1,580 cm^{-1} may be due to C=C stretching of pyridine rings (Das et al. 2009). Only CD spectrum exhibited the bands at 1,509 cm^{-1} (lignin aromatic skeletal vibration) and 1,239 cm^{-1} (C–O stretching of aryl esters) arising from lignin decomposition products (Mante and Agblevor 2010). The presence of lignin residues could be from bedding material or partially digested feed (Keiluweit et al. 2010). Other bands between 1,417 and 1,457 cm^{-1} arose from the O–H in-plane bend of carboxylic acids, C=O stretch of carboxylates and aliphatic CH_2 group of alkanes.

Table 3 Heavy metal concentration in biochars

	As mg kg^{-1}_{ds}[a]	Cd	Cr	Cu	Ni	Pb	Zn
CD (°C)							
250	dl[b]	dl	6.55±0.1	18.85±1.07	3.72±0.13	15.23±2.86	70.77±1.54
350	dl	dl	7.72±0.3	32.42±2.95	4.36±0.12	6.50±2.25	115.28±3.32
450	dl	dl	7.70±0.03	40.81±6.54	4.75±0.25	3.69±0.27	129.44±3.80
550	dl	0.16±0.08[c]	10.21±1.10	38.89±11.3	5.45±0.21	8.78±1.18	171.49±0.34
MW (°C)							
250	4.14±0.56	0.46±0.01	45.01±0.55	170.37±3.23	53.76±0.82	21.51±0.28	407.72±8.29
350	3.71±036	0.68±0.02	48.81±0.35	203.35±2.01	61.71±0.79	23.91±0.51	480.10±5.60
450	4.56±0.21	0.96±0.11	59.44±0.66	253.61±2.59	76.30±0.73	28.31±0.75	601.61±10.05
550	6.77±0.21	1.13±0.04	64.17±0.19	268.93±0.66	83.42±0.89	30.71±0.45	690.48±4.73
PL (°C)							
250	dl	dl	7.67±0.16	62.02±0.39	4.96±0.07	1.28±0.09	315.41±1.55
350	dl	0.16±0.08	11.28±0.13	106.14±0.36	7.86±0.16	1.75±0.18	546.06±3.21
450	dl	0.16±0.08	12.23±0.16	123.24±1.18	8.53±0.11	1.52±0.10	627.13±1.80
550	dl	0.23±0.01	16.19±0.20	137.56±1.18	10.66±0.16	dl[b]	772.01±7.41
PR (°C)							
250	dl	dl	5.04±0.28	29.82±4.66	2.07±0.04	3.31±0.15	54.10±1.17
350	dl	dl	5.43±0.38	49.32±1.29	2.83±0.15	5.12±0.46	94.74±0.55
450	dl	dl	5.46±0.28	68.53±2.81	2.72±0.25	8.13±1.34	123.67±2.57
550	dl	dl	6.55±0.01	63.63±0.44	2.96±0.08	8.89±1.24	137.48±2.20
SS (°C)							
250	13.82±0.28	0.78±0.07	379.71±3.02	337.55±2.48	38.21±0.31	98.78±0.71	819.91±5.01
350	13.39±0.25	1.02±0.03	461.08±2.34	404.61±2.53	47.33±0.42	118.27±0.94	966.52±1.97
450	12.94±0.50	0.98±0.01	516.72±7.08	470.55±4.24	51.45±0.79	141.28±4.92	1,090.81±8.18
550	24.28±0.16	1.72±0.01	579.29±2.63	513.86±1.77	56.46±0.35	148.61±0.72	1,276.55±3.37

[a] Values calculated on a dry basis

[b] Values below detection limit

[c] Values reported as means (n=3) followed by standard error

FT-IR spectrum of PR showed the typical bands of functional groups associated to the lignin structure (Fig. 1e). The bands at 1,735 cm^{-1} (H-bonded acid/ketone carbonyl group), 1,600, 1,511 and 1,424 cm^{-1} were attributed to aromatic skeleton vibrations. As is common for the spectra of lignin samples, there was a weak band at 1,370 cm^{-1} originating from C–H bending in methyl groups. The presence of syringyl-type structures can be appreciated by the peak at 1,323 cm^{-1} (syringyl ring breathing with CO stretching) (Keiluweit et al. 2010). A strong vibration at 1,237 cm^{-1} can be associated with C–C plus C–O plus C=O stretching also COOH.

Pyrolysis temperature had an unequivocal effect on chemical properties as supported by other researches (Antal and Grønli 2003). In particular in this experiment, SS and MW showed structural modifications as the pyrolysis temperature increased from 350 to 550 °C. No considerable structural modification was observed for biochars pyrolyzed at 250 °C. Comparing the biochars heated at 350 °C with initial feedstocks (SS and MW), the formation of a new broad peak could be observed at around 1,596 cm^{-1}, while the peaks around 1,520 and 1,250 cm^{-1} disappeared. This phenomenon may be due to a deamination and decarboxylation process and the formation of amorphous C in both biochars (SS and MW) (Zhai et al. 2012). The biochars produced at 450 and 550 °C did not differ from one another in the investigated spectral region, being characterized by two broad bands (1,596 and 1,430 cm^{-1}) assigned to amorphous C formation. It can be inferred that the pyrolysis temperature of 350 °C represents a first step of interest in biochar yield because most decomposition reactions of macromolecules (proteins, carbohydrates) are involved and there is only a slight transformation at higher temperatures.

FT-IR spectra of PL and CD biochars heated at 250 °C resulted as being strongly influenced by the temperature (Fig. 1c, d). In fact, both biochars showed a structural modification ascribable to the deamination reaction, identified by a decrease of the amide I (1,640 cm^{-1}) and amide II

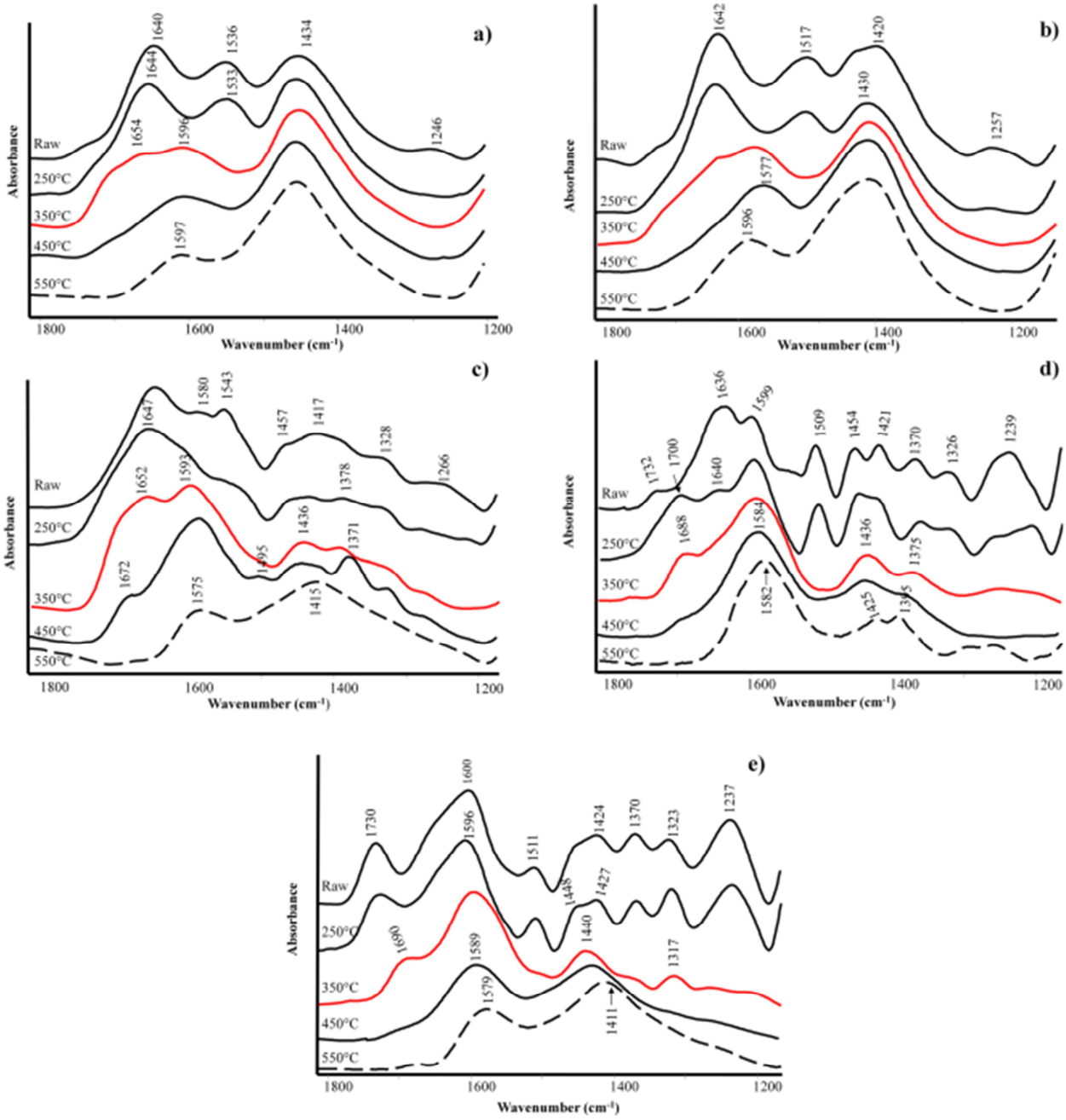

Fig. 1 FT-IR spectra of **a** sewage sludge (SS) and biochar produced at 250, 350, 450 and 550 °C; **b** municipal organic waste digestate (MW) and biochar produced at 250, 350, 450 and 550 °C; **c** poultry litter (PL) and biochar produced at 250, 350, 450 and 550 °C; **d** cattle manure mixed with silage digestate (CD) and biochar produced at 250, 350, 450 and 550 °C; and **e** pruning residues (PR) and biochar produced at 250, 350, 450 and 550 °C

(1,540 cm^{-1}) and secondary aromatic amines/pyridine rings (1,580 cm^{-1}) band intensity. The presence of amides associated with PL and CD biochars was supported by the high N content (Table 2). Particularly for CD, the peak intensity attributable to OH deformation of COOH and C–O stretching of aryl esters (1,239 cm^{-1}) decreased. The pyrolysis of PL and CD at 350 °C produced a strong structural transformation. They both exhibited a similar FT-IR spectral pattern characterized by an increase in the relative intensity of the bands due to the aromatic C=C stretching (1,590 and 1,436 cm^{-1}), C=O stretching of conjugated ketone (1,680 cm^{-1}), and O–H bending of phenols (1,375 cm^{-1}). By 450 °C, most of the CD

spectral features had been lost and the spectrum had begun to resemble graphite-like carbon or with a low degree of disorder. This is based on the relative intensity of band at 1,437 cm^{-1}, as it increases with the number of amorphous carbon structures, and at 1,582 cm^{-1}, as it is sharpened as the degree of graphitization increases (Kaufman et al. 1989).

For PL, the peaks attributable to C=C (centred at 1,577 cm^{-1}) and C=N functional groups (1,495, 1,371 and 1,320 cm^{-1}) (Xiu et al. 2010) were very intense. These changes might be due to the formation of pyridines which has been commonly observed during manure pyrolysis (Das et al. 2009). At 550 °C, the functional groups present in unpyrolyzed PL were not recognizable in char.

The PR biochar exhibited a considerable spectral profile change as the pyrolysis temperature increased from 350 to 550 °C (Fig. 1e). In particular, at 350 °C, the biochar lost C=O (1,730 and 1,237 cm^{-1}) and CH (1,370 cm^{-1}) groups, and the lack of the band at 1,511 cm^{-1}, assigned to aromatic skeletal vibration of lignin, was probably ascribable to condensation reactions. However, the observed changes would mainly involve hemicellulose and cellulose thermal decomposition that terminates at 400 °C, while lignin decomposes slowly over a much wider temperature range of 180–900 °C (Yang et al. 2007). At higher temperatures (450 and 550 °C), the biochar completely lost all the PR features and the spectra were dominated by typical bands of amorphous C (1,579 and 1,411 cm^{-1}). On the other hand, the carbon content was 45 %, and as a consequence of pyrolysis at higher temperatures, it increased up to 75 % (Table 2). In general, all biochar pyrolyzed from 450 to 550 °C became amorphous C. This material became IR active when N or O substitutes the C into the rings (Kaufman et al. 1989) during heating. This is in accordance with the N content found in biochars produced at high temperatures (Table 2).

3.3.2 Hyperspectral analysis

Hyperspectral analysis showed that the most affected samples were those yielded at 550 °C. The biochars imaged via their light scattering by EDFM showed seven distinctive spectra (endmembers) that were saved into a spectral library and used for mapping the samples. By mapping the library onto images of interest, the SAM classification showed the distribution of all the seven spectral profiles in the images as well as the quantification of their relative abundance (Fig. 2). The EDFM images of biochars from CD, PR and MW are shown in Fig. 2a–c, whereas the other two are shown in the Electronic Supplementary Material (Fig. S1). The biochars showed a different physical structure depending on the initial composition of the feedstocks. The bright spots in the EDFM image of CD (Fig. 2a), reflecting light more efficiently, indicated the formation of semicrystalline aggregates in this char, whereas amorphous structures prevailed in the other biochars as also supported by FT-IR analysis. Among the seven spectra originated from light scattering of the five samples and identified as characteristic, two (endmembers 1 and 3) give rise to the main contribution to the total scattering of CD (~80 %) (Fig. 2g), as shown from their spatial distribution on the sample (Fig. 2d). These two spectra (Fig. S2, Electronic Supplementary Material) may be due to the presence of anaerobic digestion products and can be considered the most representative for this char. On the contrary, other two spectral profiles (endmembers 2 and 7) are characteristic of both PR and MW (~70 and 90 %, respectively) (Fig. 2h, i). This similarity of spectral patterns between the two samples might be attributed to the abundance of hemicelluloses and lignin in the raw feedstocks. The contribution of all seven endmembers was also found for SS and PL, as shown by the maps displaying the relative distribution of the main spectra by colours (Fig. S1, Electronic Supplementary Material).

3.3.3 Scanning electron microscopy

Scanning electron microscopy (SEM) images of biochars produced at 350 and 550 °C are shown in Fig. 3. CD biochar at 350 °C (Fig. 3a) displayed longitudinal fibrous structures probably arising from the cellulosic structure of maize that can be grouped into fibrous, prismatic and spherical. At 550 °C (Fig. 3b), most of the morphology had changed, as revealed by the irregular surface. Similarly, the image of PR biochar at 350 °C (Fig. 3c) retained the fibrous structures of woody plants mainly composed of individual particles of lignin with polygonal shape and multiple conchoidal fracture surfaces. At 550 °C (Fig. 3d), the fibrous structures were destroyed. The surface texture had become coarse, and the cross-section image (Fig. 3d) showed that the internal texture of the fibre bundles had become sparse. Other regions showed signs of plastic deformation. MW biochar at 350 °C exhibited a partially smooth surface with irregular porosity (Fig. 3e). Residues of individual particles of lignin with polygonal shape and multiple conchoidal fracture surfaces were displayed. The biochar morphology had become more complex at 550 °C, reflecting the heterogeneity of the parent biomass and the depolymerization reaction that takes place during pyrolysis (Fig. 3f). The images of biochars yielded from CD, PR and MW showed clearly visible plant structure residues; this shows that lignin degradation takes place at the highest pyrolysis temperatures (>550 °C). In addition, the morphological modifications were not supported by functional group changes observed in the FT-IR spectra that were instead dominated by typical bands of amorphous C (1,579 and 1,411 cm^{-1}). PL biochar at 350 °C (Fig. 3g) exhibited a complex morphology due to the presence of particle aggregations of mineral compounds from chicken manure, such as K and P (Table 2). PL at 550 °C clearly revealed a more compact surface enriched with mineral components (Fig. 3h). The interactions among

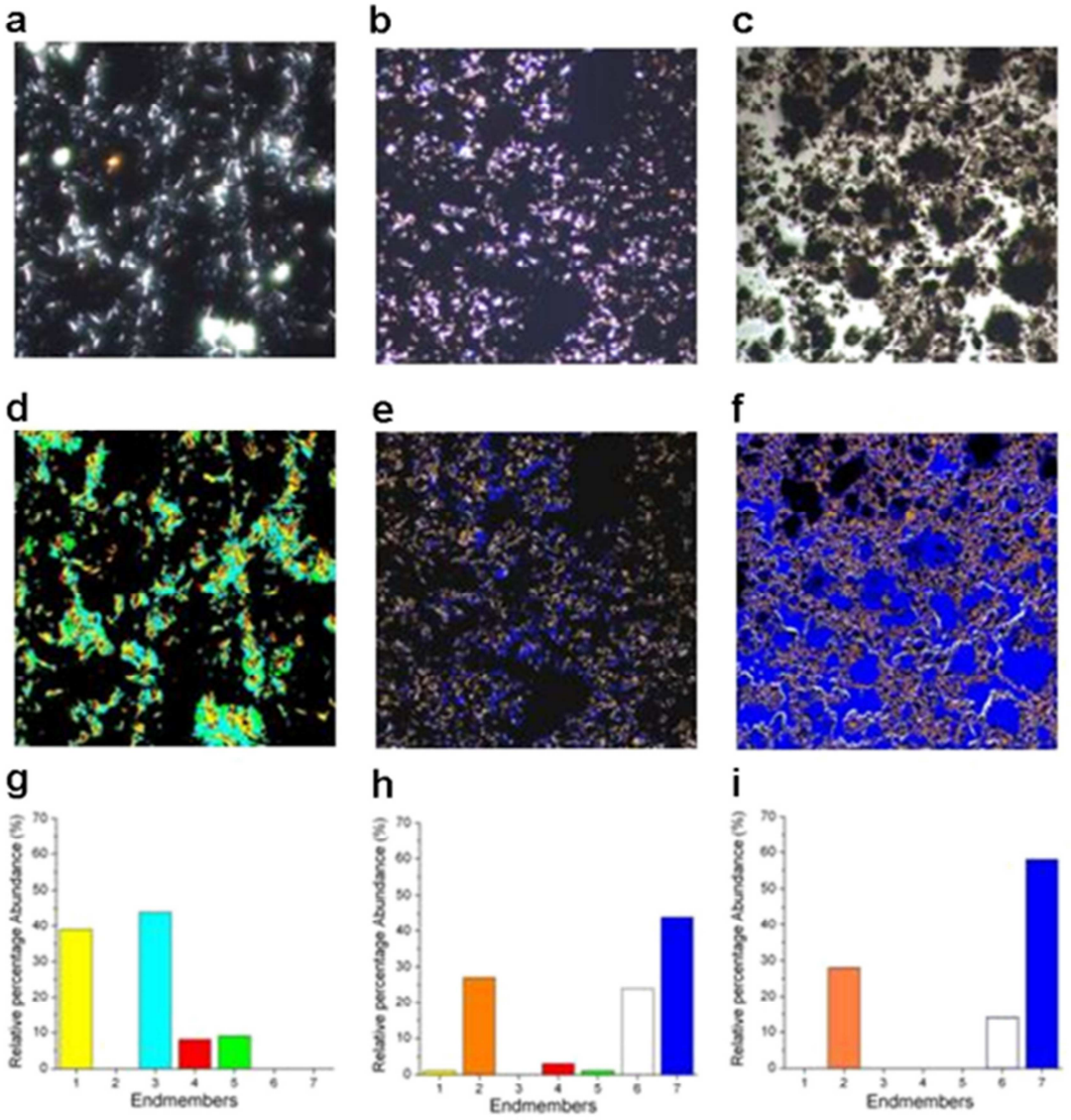

Fig. 2 Spectral mapping of biochars produced at 550 °C placed on glass slides. **a–c** EDFM images; **d–f** spectral mapping (*coloured areas* indicate the matching with the spectral profiles). **a**, **d** Cattle manure mixed with silage digestate (CD); **b, e** pruning residues (PR); and **c**, **f** municipal organic waste digestate (MW). Seven main spectra (endmembers) were found and marked with a *number from 1* to *7*. **g–i** Relative percentage abundance of the seven spectral profiles, revealed by the SAM analysis of the hyperspectral images

components of the mixture might affect pyrolysis behaviour of the various constituents and increase the heterogeneity of biochar. SS biochar at 350 °C (Fig. 3i) showed structures resembling nanotube bundles with different particle dispersal of inorganic components as also supported by high metal content (Table 3). At 550 °C, the surface had become rougher and visible pores were limited to some particles (Fig. 3j).

3.4 Physical properties

The relationship between SA (SA_{CO2} and SA_{N2}) and temperature was positive (Table 4) as already observed by other authors (Downie et al. 2009; Keiluweit et al. 2010). However, SA_{N2} showed a nonlinear response with sharp increases at 550 °C, while SA_{CO2} increased almost linearly with a higher ratio in C-rich feedstocks.

At 550 °C, SA_{N2} was highest in MW (77.72 $m^2\ g^{-1}$) and CD (58.60 $m^2\ g^{-1}$) and lowest in PL (3.61 $m^2\ g^{-1}$). At 250 °C, SA_{N2} showed a narrow range, from 0.5 $m^2\ g^{-1}$ (PL and PR) to 1.4 $m^2\ g^{-1}$ (CD). At 550 °C, SA_{CO2} was >230 $m^2\ g^{-1}$ for CD and PR (254.3 and 234.1 $m^2\ g^{-1}$) and <84 $m^2\ g^{-1}$ for chars from urban wastes (SS and MW).

Regarding SA_{CO2}, differences between feedstocks at 250 °C were more remarkable than for SA_{N2}, indicating a more

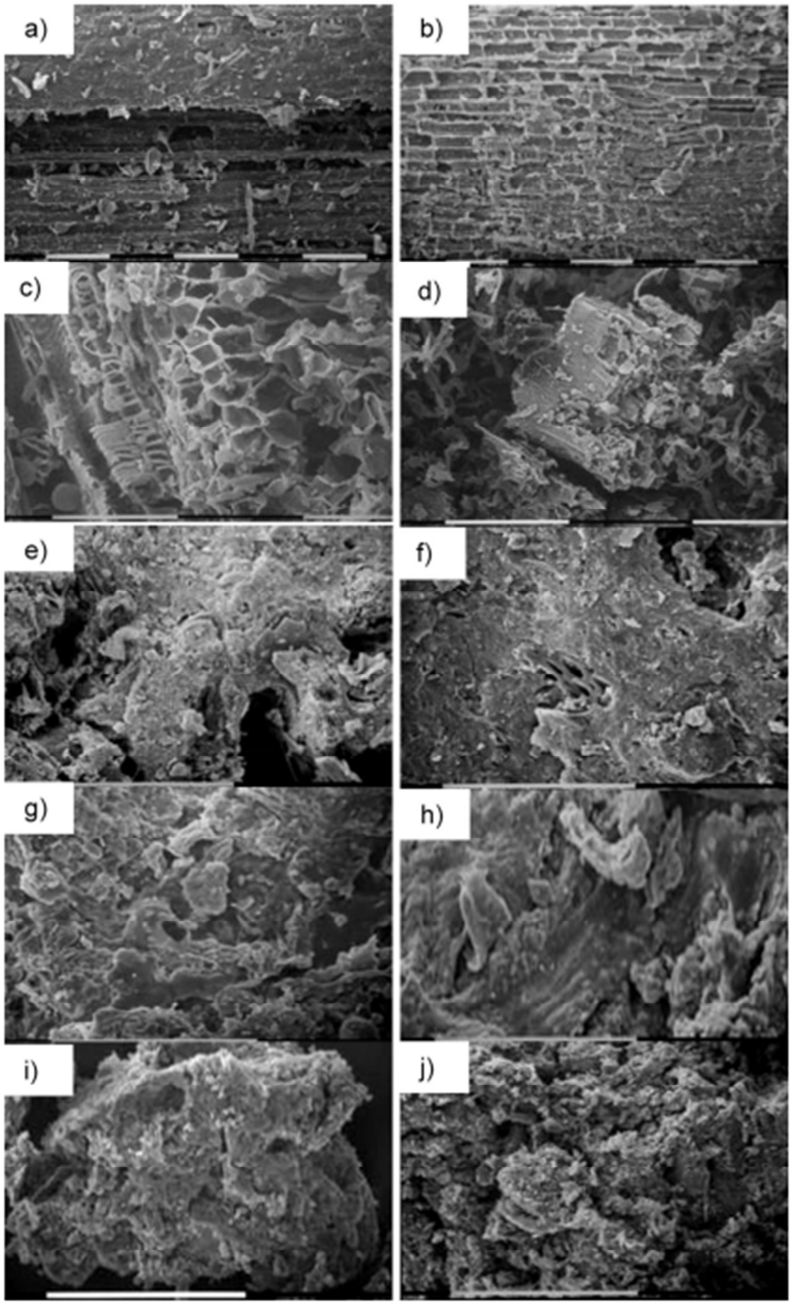

Fig. 3 Scanning electron micrographs (SEM) of biochars from: cattle manure and silage digestate (CD) at 350 °C (**a**) and 550 °C (**b**); vineyard pruning residues (PR) at 350 °C (**c**) and 550 °C (**d**); municipal organic waste digestate (MW) at 350 °C (**e**) and 550 °C (**f**); poultry litter (PL) at 350 °C (**g**) and 550 °C (**h**); and sewage sludge (SS) at 350 °C (**i**) and 550 °C (**j**). *Bars* 0.1 mm

complex variability in the pore matrix architecture at nanoscale (<2.7 nm).

The largest CO_2 surface area was found in samples that exhibited the highest C content, as the strong correlation between the two variables (r=0.84, p<0.05) suggests. This was maybe due to the conversion from amorphous C to graphene-like forms (Keiluweit et al. 2010), which create voids in the structure, increasing the microporosity (Amonette and Joseph 2009). The presence of semicrystalline aggregates was supported by previous FT-IR and hyperspectral analyses for CD, while it was less evident for PR.

Pore volumes calculated from N_2 isotherms increased for all feedstocks according to the rising temperature. The effect was particularly apparent in the transition from 450 to 550 °C in biomass-based chars, with 4-fold increments for CD and 9-fold for PR.

It is worth noting that both micro- and mesopores contributed to the increase of porosity, as highlighted by pore size

Table 4 Biochar surface area (N_2 and CO_2), total pore volume, average mesopore radius and specific density

Biochar (°C)		SA_{N2} $m^2\ g^{-1}$	Meso+microPV[a] 0.8–50 nm $cm^3\ g^{-1}$	SA_{CO2} $m^2\ g^{-1}$	MicroPV[b] 0.5–0.8 nm $cm^3\ g^{-1}$	Specific density g cm^{-3}
CD	250	1.4	0.003	70.2	0.011	1.3
	350	2.2	0.008	128.3	0.025	1.3
	450	2.9	0.014	185.9	0.038	1.4
	550	58.6	0.065	254.1	0.055	1.5
MW	250	0.7	0.006	47.9	0.007	1.5
	350	5.6	0.045	40.5	0.007	1.7
	450	27.3	0.123	62.8	0.011	1.9
	550	77.7	0.144	83.6	0.017	2.0
PL	250	0.5	0.002	36.9	0.004	1.4
	350	0.9	0.006	88.9	0.015	1.5
	450	2.4	0.020	110.0	0.021	1.5
	550	3.6	0.006	151.7	0.032	1.6
PR	250	0.5	0.002	73.1	0.009	1.1
	350	1.3	0.004	118.4	0.022	1.2
	450	1.1	0.004	235.5	0.046	1.3
	550	19.2	0.043	254.3	0.052	1.4
SS	250	0.8	0.005	25.7	0.004	1.7
	350	2.0	0.012	23.1	0.004	1.9
	450	7.2	0.023	36.4	0.007	2.1
	550	12.7	0.038	60.0	0.011	2.3

[a] Sum of micropore volume ?(0.8–2.7 nm) and mesopore ?volume (2.7–50 nm) calculated from N_2 adsorption data

[b] Micropore volume (0.5–0.8 nm) calculated from CO_2 adsorption data

distributions (Fig. S4a, d, Electronic Supplementary Material). At 550 °C, CD and PR showed a sharp increase in the range 0.5–2 and 17.3–19.3 nm, with the highest peaks in PR corresponding to pore diameter of 4.8–5.40, 14.0–15.6 and 32.7–36.4 nm. This suggests an ex novo formation of pores due to the voids left by physical–chemical degradation of biomass components, as confirmed by both FT-IR analysis and SEM images (Fig. 3b, d). The other feedstocks showed a similar behaviour, but the structural changes were more gradually distributed over all production temperatures (Fig. S4b, c, e, Electronic Supplementary Material).

Pore size distributions obtained from CO_2 isotherms showed a gradual increase in pore volumes (0.5–0.8 nm) caused by production temperature for CD, PL and PR (Fig. S5a, c, d, Electronic Supplementary Material). This is confirmed by micropore volume, which was linearly correlated with temperature for all these feedstocks (r=0.99, 0.98, 0.95; p<0.05). Urban waste-based biochars were shown to be less prone to thermal degradation below 450 °C, with the highest increases in pore volumes at 450 and 550 °C (Fig. S5b, e, Electronic Supplementary Material). Micropores in the range of 0.5–0.8 nm resulted as the more relevant component of total porosity in biomass-based chars, being up to five times the 0.8–50-nm porosity. On the contrary, the latter was predominant in chars from urban waste (SS and MW) with a shift towards large-pore diameters (mesopores) at 550 °C.

Production temperature positively influenced specific density, with the higher values found for MW and SS (2.0 and 2.3 g cm^{-3}, respectively). These values are relatively high if compared to the density of solid graphite (2.25 g cm^{-3}), but they could be explained by a high ash content of chars, as indicated by the high correlation coefficient (r=0.99 for MW and r=0.99 for SS, p<0.01) between this variable and specific density. SEM images (Fig. 3i, j) confirmed the presence of inorganic compounds on SS surface. Anyway, even in the other feedstocks, specific density increased according to the increase of temperature, most likely because of the conversion of low-density disordered carbon to high-density turbostratic carbon (Byrne 1996; Kercher and Nagle 2002).

4 Conclusions

Biochars derived from different feedstocks (SS, MW, CD, PL and PR) have contrasting physical and chemical properties depending on temperature. Pyrolysis of these feedstocks generates biochars with predominately aromatic carbon structures rich in inorganic minerals, as shown by FT-IR and SEM. These techniques have provided the structural and morphological information needed to reliably track changes in char structure. Some partially pyrolyzed biomass (in poultry litter and cattle manure digestate) may still be recognizable at low

temperature (350 °C), while most char morphology changes as the pyrolysis intensifies (550 °C). The presence of N-containing compound like pyridine is only found in poultry litter biochar. Biochars showed a wide variability in surface area and pore size distribution that increased by the temperature. Each one has displayed a distinctive hyperspectral image related to its chemical composition and inherent physical structure, scattering electromagnetic energy in distinctive patterns at specific wavelengths. This technique can thus be used to make a direct assessment of different components simultaneously, but also to locate their spatial distribution.

Thus, the results demonstrate that biochars exhibited specific physical–chemical properties according to feedstock and temperature, and therefore it is not possible to identify an "ideal" biochar able to improve both soil nutrient content and structure. Moreover, the long-term soil applications of biochar should be carefully monitored in order to avoid the potential accumulation of heavy metals. Finally, the application of different spectroscopic, morphological and physical techniques presented in this paper can be used in studies for rapid screening of feedstocks and their pyrolysis products.

Acknowledgments The authors are extremely grateful to Dr. Carla Marzetti (Antigenia srl Unipersonale), the Italian contact person of Cytoviva company (University of Auburn, AL, USA) for Hyperspectral System Imaging, and to Dr. Carla Ferreri (ISOF-CNR) for providing the CytoViva® hyperspectral microscope.

References

Ábrego J, Arauzo J, Sánchez JL, Ponzalo A, Cordero T, Rodríguez-Mirasol J (2009) Structural changes of sewage sludge char during fixed bed pyrolysis. Ind Eng Chem Res 48:3211–3221

Amonette J, Joseph S (2009) Characteristics of biochar: micro chemical properties. In: Lehmann J, Joseph S (eds) Biochar for environmental management: science and technology. Earthscan, London, pp 33–52

Antal MJ, Grønli M (2003) The art, science and technology of charcoal production. Ind Eng Chem Res 42:1619–1640

Badireddy AR, Wiesner MR, Liu J (2012) Detection, characterization, and abundance of engineered nanoparticles in complex waters by hyperspectral imagery with enhanced dark field microscopy. Environ Sci Technol 46:10081–10088

Barrett EP, Joyner LG, Halenda PP (1951) The determination of pore volume and area distributions in porous substances. I. Computations from nitrogen isotherms. J Am Chem Soc 73:373–380

Biederman LA, Harpole WS (2013) Biochar and its effects on plant productivity and nutrient cycling: a meta-analysis. GCB Bioenergy 5:202–214

Brewer CE, Schmidt-Rohr K, Satrio JA, Brown RC (2009) Characterization of biochar from fast pyrolysis and gasification systems. Environ Prog Sustain Energy 28:386–396

Byrne C (1996) Polymer, ceramic, and carbon composites derived from wood. PhD thesis. The Johns Hopkins University, USA

Cantrell KB, Hunt PG, Uchimiya M, Novak JM, Ro KS (2012) Impact of pyrolysis temperature and manure source on physicochemical characteristics of biochar. Bioresour Technol 107:419–428

Cao X, Harris W (2010) Properties of dairy-manure-derived biochar pertinent to its potential use in remediation. Bioresour Technol 101:5222–5228

Cao Y, Pawloski A (2012) Sewage sludge-to-energy approaches based on anaerobic digestion and pyrolysis: Brief overview and energy efficiency assessment. Renew Sust Energ Rev 16:1657–1665

Cross A, Sohi SP (2011) The priming potential of biochar products in relation to labile carbon contents and soil organic matter status. Soil Biol Biochem 43:2127–2134

Das DD, Schnitzer MI, Monreal CM, Mayer P (2009) Chemical composition of acid–base fractions separated from bio-oil derived by fast pyrolysis of chicken manure. Bioresour Technol 100:6524–6532

Dlgs. 152/2006 (2006) Norme in materia ambientale. Gazzetta Ufficiale n.88, 11 Aprile 2006

Dlgs. 27/03/2000 (2000) Disposizioni tecniche per l'aggiornamento degli allegati alla legge n. 748 del 1984, in materia di fertilizzanti. Gazzetta Ufficiale n. 149, 28 Giugno 2000

DM 7/4/2006 C (2006) Riteri e norme tecniche generali per la disciplina regionale dell'utlizzazione agronomica degli effluenti di allevamento, di cui all'articolo 38 del decreto legislativo 11 Maggio 1999, n.152. Gazzetta Ufficiale n.109. 12 Maggio 2006

Downie A, Crosky A, Munroe P (2009) Physical properties of biochar. In: Lehmann J, Joseph S (eds) Biochar for environmental management: science and technology. Earthscan, London, pp 13–29

EEC No. 676 (1991) Council directive 91/676/EEC of 12 December 1991 concerning the protection of waters against pollution caused by nitrates from agricultural sources

Elmasry G, Kamruzzaman M, Sun DW, Allen P (2012) Principles and applications of hyperspectral imaging in quality evaluation of agro-food products: a review. Crit Rev Food Sci Nutr 52:999–1023

Gaskin JW, Steiner C, Harris K, Das KC, Bibens B (2008) Effect of low-temperature pyrolysis conditions on biochar for agricultural use. Trans ASABE 51:2061–2069

Horvath G, Kawazoe K (1983) Method for the calculation of effective pore size distribution of molecular sieve carbon. J Chem Eng Jpn 16: 470–475

Hossain MK, Strezov V, Yin Chan K, Ziolkowski A, Nelson PF (2011) Influence of pyrolysis temperature on production and nutrient properties of wastewater sludge biochar. J Environ Manag 92:223–228

Jeffery S, Verheijen FGA, van der Velde M, Bastos AC (2011) A quantitative review of the effects of biochar application to soils on crop productivity using meta-analysis. Agric Ecosyst Environ 144: 175–187

Jeffery S, Bezemer TM, Cornelissen G, Kuypert TW, Lehmann J, Mommer L, Sohi SP, Van De Voordet F, Wardle DA, Van Groenigen JW (2013) The way forward in biochar research: targeting trade-offs between the potential wins. GCB Bioenergy 11–13, doi: 10.1111/gcbb.12132

Kaufman JH, Metin S, Saperstein DD (1989) Symmetry breaking in nitrogen-doped amorphous carbon: Infrared observation of the Raman-active G and D bands. Phys Rev B 39:13053–13060

Keiluweit M, Nico PS, Johnson MG, Kleber M (2010) Dynamic molecular structure of plant biomass-derived black carbon (biochar). Environ Sci Technol 44:1247–1253

Kercher AK, Nagle DC (2002) Evaluation of carbonized medium-density fiberboard for electrical applications. Carbon 40:1321–1330

Knicker H (2007) How does fire affect the nature and stability of soil organic nitrogen and carbon? A review. Biogeochemistry 85:91–118

Kristler RC, Widmer F, Brunner PH (1987) Behavior of chromium, nickel, copper, zinc, cadmium, mercury, and lead during the pyrolysis of sewage sludge. Environ Sci Technol 21:704–708

Lehmann J, Joseph S (2009) Biochar for environmental management: science and technology. Earthscan, London

Lowell S, Shields JE, Thomas MA, Thommes M (2004) Characterization of porous solids and powders: surface area, pore size and density. Springer-Kluwer Academic, Dordrecht, pp 152–156

Mante OD, Agblevor FA (2010) Influence of pine wood shavings on the pyrolysis of poultry litter. Waste Manag 30:2537–2547

Mendez A, Gómez A, Paz-Ferreiro J, Gascó G (2013) Effects of sewage sludge biochar on plant metal availability after application to a Mediterranean soil. Chemosphere 89:1354–1359

Ro KS, Cantrell KB, Hunt PG (2010) High-temperature pyrolysis of blended animal manures for producing renewable energy and value-added biochar. Ind Eng Chem Res 49:10125–10131

Schmidt MWI, Torn S, Abiven S, Dittmar T, Guggenberger G, Janssens AI, Kleber M, Kogel-Knabner I, Lehmann JDA, Manning C, Nannipieri P, Rasse DP, Weiner S, Trumbore SE (2011) Persistence of soil organic matter as an ecosystem property. Nature 478:49–56

Shackley S, Sohi S (2010) An assessment of the benefits and issues associated with the application of biochar to soil. UK Biochar Research Centre, Edinburgh

Shinogi Y, Kanri Y (2003) Pyrolysis of plant, animal and human waste: physical and chemical characterization of the pyrolytic products. Bioresour Technol 90:241–247

Spokas KA, Cantrell KB, Novak JM, Archer DA, Ippolito JA, Collins HP, Boateng AA, Lima IM, Lamb MC, McAloon AJ, Lentz RD, Nichols KA (2011) Biochar: a synthesis of its agronomic impact beyond carbon sequestration. J Environ Qual 41: 973–989

Tian Y, Zhang J, Zuo W, Chen L, Cui Y, Tan T (2013) Nitrogen conversion in relation to NH3 and HCN during microwave pyrolysis of sewage sludge. Environ Sci Technol 47:3498–3505

Verheijen F, Jeffery S, Bastos A.C, van der Velde M, Diafas I (2010) Biochar application to soils. A critical scientific review of effects on soil properties, processes and functions. Luxemburg: European Commission Joint Research Centre. Institute for Environment and Sustainability

Wiedner K, Rumpel C, Steiner C, Pozzi A, Maas R, Glaser B (2013) Chemical evaluation of chars produced by thermochemical conversion (gasification, pyrolysis and hydrothermal carbonization) of agro-industrial biomass on a commercial scale. Biomass Bioenergy 59:264–278

Xiu S, Shahbazi A, Wang L, Wallace CW (2010) Supercritical ethanol liquefaction of swine manure for bio-oils production. Am J Eng Appl Sci 3:494–500

Yang HP, Yan R, Chen HP, Lee DH, Zheng CG (2007) Characteristics of hemicellulose, cellulose and lignin pyrolysis. Fuel 86:1781–1788

Yin Chan K, Xu Z (2009) Biochar: nutrient properties and their enhancement. In: Lehmann J, Joseph S (eds) Biochar for environmental management: science and technology. Earthscan, London, pp 67–81

Zabaniotou A, Stavropoulos G, Skoulou V (2008) Activated carbon from olive kernels in a two stage process: industrial improvement. Bioresour Technol 99:320–326

Zhai Y, Peng W, Zeng G, Fu Z, Lan Y, Chen H, Wang C, Fan X (2012) Pyrolysis characteristics and kinetics of sewage sludge for different sizes and heating rates. J Therm Anal Calorim 107:1015–1022

Zhang R, Ying Y, Rao X, Li J (2012) Quality and safety assessment of food and agricultural products by hyperspectral fluorescence imaging. J Sci Food Agric 92:2397–2409

Agriculture, Ecosystems and Environment 217 (2016) 49–58

Contents lists available at ScienceDirect

Agriculture, Ecosystems and Environment

journal homepage: www.elsevier.com/locate/agee

Nano to macro pore structure changes induced by long-term residue management in three different soils

Chiara Pituello, Nicola Dal Ferro, Gianluca Simonetti, Antonio Berti, Francesco Morari*

Dipartimento di Agronomia Animali Alimenti Risorse Naturali e Ambiente, Viale dell'Università 16, 35020 Padova, Italy

ARTICLE INFO

Article history:
Received 1 July 2015
Received in revised form 30 October 2015
Accepted 31 October 2015
Available online xxx

Keywords:
Soil organic carbon
Soil pore architecture
X-ray microtomography
Long-term experiment

ABSTRACT

The use of crop residues for bioenergy production has gathered much attention in recent years. For this reason, the potential detrimental effects on soil quality caused by their removal need to be carefully evaluated before this practice becomes widely used.

Data from a long-term field experiment on residue management in three contrasting soils (clay, sandy-loam and sandy) were analysed in order to understand crop residue effects on soil organic carbon stocks. In addition, since soil structure is known to be a sensitive descriptor of soil quality, different techniques were combined to investigate a wide range of pore sizes (from 0.25 nm to 2.5 mm) and pore morphology.

Forty-three years of crop residue incorporation led to a significant increase in the organic carbon content of the three soils. The clay and sandy-loam soils were the most effective in retaining organic carbon as they exhibited the highest absolute increases. The sandy soil showed a residue-induced increase in organic carbon content, indicating that some protection mechanisms may act in the long term even in soils with a scarce ability to protect organic carbon from degradation.

Residues modified the soil structure, inducing an increase in total pore volume as measured by the core method, although their effect was not found in all pore size classes. Residues decreased mesoporosity (30–75 μm), while their effect on macropores (>75 μm) was in terms of shape, increasing the irregular and elongated pores rather than their size frequency. The results thus showed a limited overall effect of residues on soil structure. However, even minor pore network changes could affect other important soil properties such as water movement, solute transport and gas exchanges.

1. Introduction

The use of crop residues for bioenergy production has gathered a lot of interest in recent years (Monforti et al., 2015). It has been estimated that this practice, by substituting the use of fossil fuels, is more effective in mitigating climate change than residues use for carbon sequestration in soil (Powlson et al., 2011; Cherubini and Ulgiati, 2010). However, residue removal could produce detrimental effects on soil quality that need to be carefully considered (Lal, 2005).

Indeed, long-term effects of crop residues on soil organic carbon (SOC) stocks have been investigated by many authors with contrasting findings. Some studies confirmed crop residue incorporation as a way to increase SOC in agro-ecosystems, with effects averaging 0.10 t C ha^{-1} (Morari et al., 2006; Monteleone et al., 2015) On the contrary, other studies found small or non-significant effects (e.g. Powlson et al., 2011; Buysse et al., 2013) on SOC stocks. Powlson et al. (2011) reviewed 25 long-term experiments and found slight residue-induced effects on SOC concentration, while notable impacts were observed on soil physical properties such as aggregate stability, water infiltration and plough draft. These were due to a small fraction of SOC usually called "active C" (the fraction that can be oxidised by very dilute potassium dichromate, about 10% of total C) which increases – or decreases – faster than total soil OC when residues are incorporated—or removed. The residue effect on soil physical properties was also observed by other authors (e.g. Fuentes et al., 2009). For instance, maize residue incorporation or removal induced changes in soil bulk density and total porosity (Lal, 2009), as well as in soil water content and resistance to penetration (Fuentes et al., 2009). Thus, given the well-recognized importance of structure for soil functions and ecosystem services (Dominati et al., 2010), investigating the effects of residues on soil porosity is a key step towards the understanding of soil processes and the establishing of a rational bioenergy production policy.

* Corresponding author. Fax: +39 0498272784.
E-mail address: francesco.morari@unipd.it (F. Morari).

http://dx.doi.org/10.1016/j.agee.2015.10.029
0167-8809/

Most research regarding the long-term effects of organic input on the soil pore network focused on intra-aggregate structure (e.g. Wuest, 2007; Paul et al., 2013; Zhang et al., 2014; Villamil et al., 2015), without considering inter-aggregate porosity (i.e. macropores). Macropores play a pivotal role in several soil processes, e.g. water and biogeochemical cycles (Jarvis, 2007) and gas exchange with the atmosphere (Deurer et al., 2009). Moreover they are an efficient indicator of soil structure dynamics, as they are extremely sensitive to different types of stresses (Sumner, 1999).

As already highlighted by previous papers (e.g., Dal Ferro et al., 2014; Cnudde et al., 2009), the combined use of mercury intrusion porosimetry (MIP) and X-ray computed microtomography (μCT) is a promising way to analyse the complexity of the soil pore network at a scale ranging from 0.01 μm up to several mm. MIP can detect pores <100 μm, which are important for water retention mechanisms as well as for the physical protection of organic matter (Lützow et al., 2006). μCT is particularly useful for identifying the 2D and 3D macropores and cracks morphology (e.g. pore orientation, fractal dimension, shape and connectivity) that are mainly involved in water infiltration and gas exchanges. However, these two methods do not cover the nanoporosity below 0.01 μm which plays a major role in the physical–chemical interaction between soil matrix and solutes (Lal and Shukla, 2004). In this context, gas adsorption methods are valuable analytical tools to fully characterise crop-residue induced changes in soil porosity at the nanometre scale.

The Venetian plain (NE Italy) is a region subjected to the intensive removal of crop residues for biogas production. Thus the aim of this paper is to evaluate the potential negative effects of this practice on the SOC and pore network in representative agricultural soils of this region. For this reason, a long-term experiment (43 yrs) comparing different residue managements in three contrasting soils of the low-plain were analysed in order to obtain a complex and broad representation of soil organic carbon, soil structure from the nano (<2 nm) to the macropore scale (2500 μm), and their interactions between one another and with soil texture.

2. Materials and methods

2.1. Long-term experiment

The long-term experiment is located on the Experimental Farm of the University of Padova (45°21′ N; 11°50′ E, 6 m a.s.l.). The climate is sub-humid with mean annual rainfall of 825 mm. The rainfall shows inter-annual variability, with peaks in June and October (100 and 90 mm). The lowest values are recorded in winter (50–60 mm). The temperature reaches minimum values in January (averaging 2.3 °C) and maximum between July and August (average 22.4 °C). Reference evapotranspiration (ET_0) is 945 mm, with maximum values in July (5 mm d^{-1}). ET_0 exceeds rainfall from April to September. During the experimental period (1970–2013) mean annual rainfall followed an oscillatory pattern, without a clear long-time trend. The years 1972 and 1996 were the rainiest, with 1019 and 1014 mm, respectively, while the driest year (617 mm) was 1983. There has been a clear increase (+2.1 °C) in average maximum temperatures in the last 10 years, with peaks in 1997, 2000 and 2001. The coldest year was 1980 with an average maximum temperature of 15.1 °C.

The long-term experiment started in 1970 and is constituted by 108 4 m^2 lysimeters, 80 cm deep, with three types of soil: sandy-loam (SNDL), sandy (SND) and clay (CL). The main physical and chemical characteristics of the soils at the beginning of the experiment are listed in Table 1. The sandy-loam soil is classified according to FAO-UNESCO as a Fluvi-Calcaric Cambisol and contains prevalently dolomite (35%) and quartz (28%), with considerable amounts of feldspar (15%) and mica (13%). The other two were soil typological units of two locations in the Veneto region: the clay soil of the south-western plain, and the sandy soil of the central coastal area. The clay soil, classified as a Gleyi-Vertic Chernozem (FAO-UNESCO, 2008), has higher montmorillonite (16%) than the other soils, and a considerable presence of mica (19%) and dolomite (15%). The sandy soil (Calcaric Arenosol, FAO-UNESCO, 2008) contains predominantly quartz and feldspar and a significant amount of dolomite (16%). These soils were collected from their original sites and transported to the experimental site prior to the beginning of the experiment, where their original profiles were reconstructed in the lysimeters. The experimental design is a randomized block with three replicates and the treatments derive from the factorial combination of two residue management strategies (residue removal—NR, and residue incorporation—R) with six levels of nitrogen fertilisation (0, 50, 100, 200, 300, 400 kg N ha^{-1}) with three soils. Until 1987, the trial involved a biennial maize-wheat rotation, while from 1987 to 2013 a less rigid crop succession was adopted based on the quadrennial rotation of wheat, maize, tomato, and sugar beet. In this paper we consider only two fertilisation rates (NO FERT: 0 kg ha^{-1} and FERT: 400 kg ha^{-1}) in combination with the two crop residue management methods. Crop residues were incorporated by manually digging in the upper 20 cm. On average, the yearly amount of incorporated residues in NO FERT and FERT treatments was 4.69 and 9.09 t dry matter ha^{-1} in clay soil, 4.00 and 7.86 t dry matter ha^{-1} in sandy-loam and 1.73 and 5.73 t dry matter ha^{-1} in sandy soil.

Table 1
Main physical and chemical properties of the soils at the beginning of the experiment (1970).

	Clay	Sandy-loam	Sandy
Sand (2–0.05 mm)%	40.6	57.1	98.8
Silt (0.05–0.002 mm)%	18	23.7	0
Clay (<0.002 mm)%	41.4	19.2	1.2
pH (H_2O)	7.7	7.8	8.4
SOC%[a]	1.06	0.62	0.05
Total $CaCO_3$%	6.2	30.8	22.9
P_2O_5 labile (g kg^{-1})	5.29	1.24	1.19
P_2O_5 ass. (mg kg^{-1})[b]	59	23	19
K_2O exc. (mg kg^{-1})[c]	1.1	4.6	1.9
N tot (g kg^{-1})	1.7	0.9	0.1

[a] Rotini method.
[b] Ferrari method.
[c] Exchangeable K_2O with 25% $NaNO_3$ pre-treatment.

2.2. Soil sampling

Disturbed samples (upper 20 cm layer) were taken in July 2013 from three different points in the plot and bulked to obtain a sample of about 1 kg, which was then air-dried. Once dried, a fraction of the sample was ground and sieved at 0.5 mm for organic carbon analyses. The rest was sieved at 2 mm for texture and physical analyses. In order to measure bulk density and perform X-ray microtomography analysis, one undisturbed soil core per plot (6.1 cm height and 7.2 cm diameter) was taken from 7 to 14 cm layer using a manual hydraulic core sampler (Eijkelkamp, The Netherlands). Samples were then stored at 5 °C. Due to technical constraints of X-ray microtomography analysis, each core was reduced in size by carefully pulling a plastic cylinder of 2.5 cm height by 2 cm diameter through the moist soil sample. This was done taking care to avoid compaction of the soil.

2.3. Particle size distribution and chemical analysis

Soil texture was determined by laser diffractometry using a Malvern Mastersizer 2000 (Malvern Instruments, Malvern, England). Before analysis, samples were soaked for 24 h in a 5% (v/v)

sodium hexametaphosphate solution to enhance the dispersion of clay particles (Dane and Topp, 2002). Total organic carbon (OC) was determined using an elemental analyser (Elementar vario MACRO) after treatment with 10% HCl (ISO 10694).

2.4. Total porosity

Total porosity (TPV_{core}) was obtained according to the following equation:

$$TPV_{core} = \left(1 - \frac{\rho_b}{\rho_p}\right)100 \quad (1)$$

where ρ_b is the bulk density, and ρ_p is the particle density. Soil bulk density was determined using the core method (ISO/DIS 11272), a sample of air-dried and ground soil was then used to determine particle density using a helium pycnometer (Micro Ultrapyc 1200e, Quantachrome, England).

2.5. Soil pore distribution and morphology

Soil pore size distribution was analysed from nanometre to millimetre scale by applying different techniques: gas adsorption (N_2) in the range 0.25–50 nm; mercury intrusion porosimetry (MIP) from 0.01 μm to 100 μm; X-ray microtomography (μCT) in the range 25–2500 μm (Fig. 1). Total porosities obtained from both MIP (TPV_{MIP}) and μCT ($TPV_{\mu CT}$) were calculated as the sum of the volumetric pore size classes that were measured by the respective methods. By contrast, total porosity from gas adsorption was not calculated because the methods used to obtain the porosities in the two ranges tested were based on different models, and thus not comparable. In order to facilitate statistical comparison between treatments pores were classified according to different size classes. Pores measured by MIP encompassed cryptopores (0.01–0.1 μm), ultramicropores (0.1–5 μm), micropores (5–30 μm), mesopores (30–75 μm) and macropores (75–100 μm) (Cameron and Buchan, 2006). Pore classes analysed by μCT mainly included mesopores and macropores that were classified as follows: (1) 25–76 μm; (2) 76–126 μm; (3) 126–480 μm; and (4) 480–2500 μm. Ultramicropores analysed by BET were split according to the methods used for their calculation (B.J.H and Horvath and Kawazoe), with pores between 2 and 50 nm divided in four size classes: (1) 2–10 nm; (2) 10–18 nm; (3)18–26 nm; and (4) 26–50 nm.

2.5.1. Gas adsorption

The Brunauer–Emmett–Teller (BET) surface area was determined using the linear part of the N_2 isotherm (between pressure p/p_0 0.05 and 0.35) obtained with a Sorptomatic 1990 at a temperature of −195.15 °C, after degassing the sample at 105 °C overnight. Pore size distribution (PSD_{N2}), including pores between 0.25 and 50 nm, was calculated with B.J.H. method (Barrett et al., 1951) in the range 2–50 nm and Horvath and Kawazoe method (Horvath and Kawazoe, 1983) in the range 0.25–2 nm.

2.5.2. Mercury intrusion porosimetry (MIP)

Accessible porosity and pore size distribution within the diameter range of 0.0074–100 μm were measured with a Thermo Finnigan (Waltman, USA) Pascal 140 (3.8–100 μm) and a Pascal 240 (0.0074–15 μm). The pore radius (R) was calculated using the Young–Laplace equation:

$$R = \frac{2\gamma\cos\theta}{P} \quad (2)$$

where γ is the surface tension of pure mercury, θ is the contact angle (140°) between mercury and the sample and P is the pressure.

2.5.3. X-ray microtomography analyses (μCT)

All samples were equilibrated to a matric potential of −3 kPa and then scanned using a Skyscan 1172 X-ray microtomography system (Skyscan, Belgium). Source was set at 100 kV and 100 μA. The distance between the source, sample and camera was adjusted to obtain a final image resolution of 13.62 μm, then 2D projections were resized to obtain a final pixel size of 27.25 μm. Lastly, projections were elaborated using NRecon® to obtain a stack of at least 600 slices in 8-bit depth.

Single slices were filtered to reduce noise and the thresholding was done using Otsu's method (Otsu, 1979). After binarisation, black and white objects <5 pixels were removed due to difficulties in their attribution to either porosity or soil matrix (Vogel et al.,

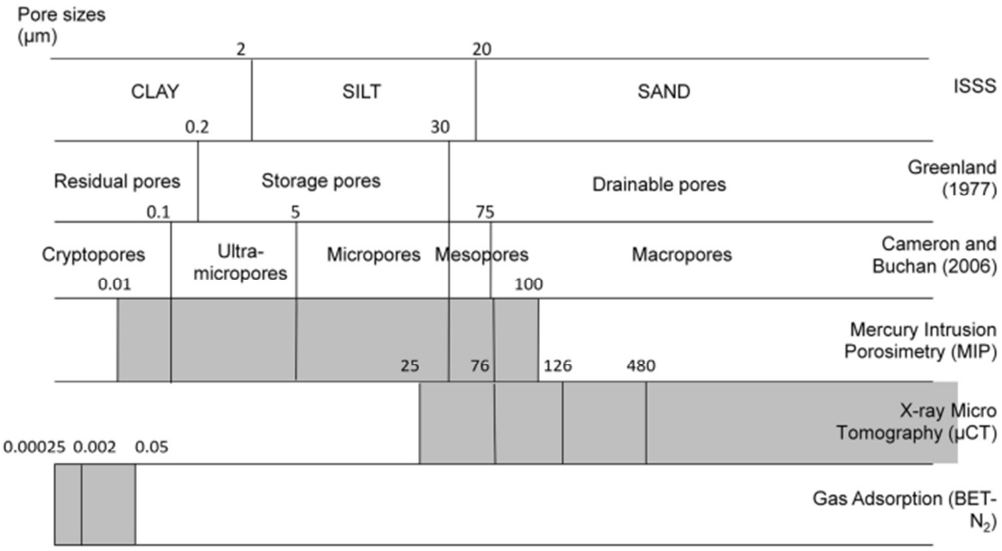

Fig. 1. Pore size ranges and different techniques adopted in this paper, compared with texture particle size, functional pore classification (Greenland, 1977) and size classification of pores (Cameron and Buchan, 2006).

2010). Pore size distribution was obtained as an average of the local thickness for each voxel representing pores (Ulrich et al., 1999). Local thickness for a point in a solid is defined by Hildebrand and Rüegsegger (1997) as the diameter of a sphere that encloses the point and is entirely bounded within the solid surfaces. Degree of anisotropy (DA), i.e. an indicator of the 3D global symmetry of the structure that varies between 0 (totally isotropic) and 1 (totally anisotropic), was calculated according to the mean intercept length (MIL) method (Harrigan and Mann, 1984). Fractal dimension (FD) was inferred using the Kolmogorov or "box counting" method, and connectivity was obtained following the Euler–Poincaré equation divided by the volume analysed to provide a more comparable measure of "connectivity density" (CD):

$$CD = \frac{(\beta_0 - \beta_1 + \beta_2)}{VOI} \quad (3)$$

where $\beta_0$is the number of pores, $\beta_1$is the connectivity (number of redundtant connections or loops), β_2 is the number of enclosed cavities and VOI is the volume analysed (pixel^3). 2D pore shape (S) was analysed for each slice using the freeware ImageJ (vs. 1.47 v, National Institute of Health, http://rsb.info.nih.gov/ij) and calculated according to Pagliai et al. (2004):

$$S = \frac{P^2}{4\pi A} \quad (4)$$

where A is the pore area and P is the pore diameter. Pores were classified as regular ($S < 2$), irregular ($2 < S < 5$), and elongated ($S > 5$).

2.6. Statistical analysis

A three-way ANOVA considering soil type, residue management and fertilisation level as main factors was used, applying Duncan's post-hoc test to compare the differences between group means. Multiple stepwise regression coefficients with backward selection were also applied in order to identify dependences between pore classes, OC and texture. A principal component analysis (PCA) on 19 selected variables was adopted to highlight the general interdependences between pore size distributions, pore morphological parameters and texture indices of the samples. The variables were selected according to Kaiser's measure of sampling adequacy (MSA), which resulted as 0.74 indicating that the group of variables were appropriate for the analysis (Kaiser, 1974). Only rotated orthogonal components with eigenvalues >1 were extracted. Statistical analyses were performed using Statistica (StatSoft Inc., Tulsa, USA).

3. Results

3.1. Soil organic carbon

Soil organic carbon (SOC) concentration (Table 2) was significantly influenced by soil type, residue management and nitrogen fertilisation, with only two significant interactions between soil type x residue management (Fig. 2) and soil type x nitrogen fertilisation.

Residues affected SOC concentration causing higher values with incorporation (R) (1.01%) than with removal (NR) (0.80%). Moreover, SOC increased from 1.4% to 1.7% (+26%) in CL, from 0.8% to 0.9% (+21%) in SNDL and from 0.3% to 0.4% (+29%) in SND for non-residue and residue incorporation, respectively. SOC was 0.8% in NO FERT (0 kg N ha^{-1}) and 1% in FERT (400 kg N ha^{-1}), on average. N effect was more marked in CL as SOC increased from 1.5% (NO FERT) to 1.7% (FERT), while a less noticeable effect was found in SNDL (from 0.8 to 0.9%) and SND (from 0.3 to 0.4%). Furthermore, even in plots without residue incorporation the carbon concentration increased from 1970 of 0.34%, 0.18% and 0.25% in CL, SNDL and SND. Residue incorporation increased the C stock in the top layer (20 cm) with respect to NR by 3.6, 3.5 and 2.3 t C ha^{-1} in SNDL, CL and SND, with annual rates of 0.08 t C ha^{-1} year^{-1}, 0.08 t C ha^{-1} year^{-1} and 0.05 t C ha^{-1} year^{-1}, respectively ($p < 0.001$). The increase in carbon stock of plots non receiving residues from 1970 was higher in CL and SND (7.9 and 6.4 t C ha^{-1}, respectively) and averaged 3.8 t C ha^{-1} in SNDL. These correspond to yearly increases of 0.18 t C ha^{-1} year^{-1} and 0.15 t C ha^{-1} year^{-1}and 0.09 t C ha^{-1} year^{-1}, for CL SND and SNDL, respectively. When managed with residue incorporation and high N fertilisation rate, the maximum amount of C was stored in CL (34.0 t ha^{-1}), while the lowest values were found in SND, where C accumulation was always <10 t ha^{-1}.

3.2. Surface area

Specific surface area, as determined by N_2 gas adsorption, was significantly higher in CL (42.3 m^2 g^{-1}) than in SNDL (6.0 m^2 g^{-1}) and SND (1.7 m^2 g^{-1}), being affected by the particle size distribution. Residue incorporation caused a reduction in surface area especially in SND (−9.8%), while a less pronounced effect was found in the other soils (−4.6% and −4.7% in CL and SNDL, respectively).

Table 2
Average organic carbon contents, total pore volumes and selected pore morphological parameters of the soils.

	SOC (%)	SOC (t ha^{-1}[a])	TPV_{core} (cm^3 cm^{-3})	TPV_{MIP} (cm^3 cm^{-3})	$TPV_{\mu CT}$ (cm^3 cm^{-3})	DA (μm^{-3})	CD × 10^{-8}	FD
Clay	1.6[b]a	30.8a	0.63a	0.16	0.07b	0.60	0.79b	1.98b
Sandy-loam	0.8b	20.8b	0.47c	0.42	0.07b	0.56	0.45b	2.05b
Sandy	0.3c	9.0c	0.55b	0.33	0.16a	0.57	3.41a	2.30a
NR	0.8[c]b	18.7b	0.54b	0.31	0.09	0.57	1.38	2.10
R	1.0a	21.8a	0.56a	0.29	0.10	0.58	1.68	2.11
NO FERT	0.8[c]b	19.0b	0.54b	0.33	0.09	0.58	1.38	2.08
FERT	1.0a	21.4a	0.56a	0.27	0.11	0.57	1.68	2.13

NR, Residue removal; R, residue burial; NO FERT, no N fertilisation; FERT, fertilization 400 kg N ha^{-1}; TPV_{MIP}, total pore volume measured with mercury intrusion porosimetry; $TPV_{\mu CT}$, total pore volume measured with X-ray μCT; TPV_{core}, total pore volume measured with helium pycnometer; DA, degree of anisotropy; CD, connectivity; FD, fractal dimension. Different letters indicate significant differences between treatments.

[a] SOC stock in the first 20 cm of soil.

[b] Values are reported as means ($n = 12$).

[c] Values reported as means ($n = 24$).

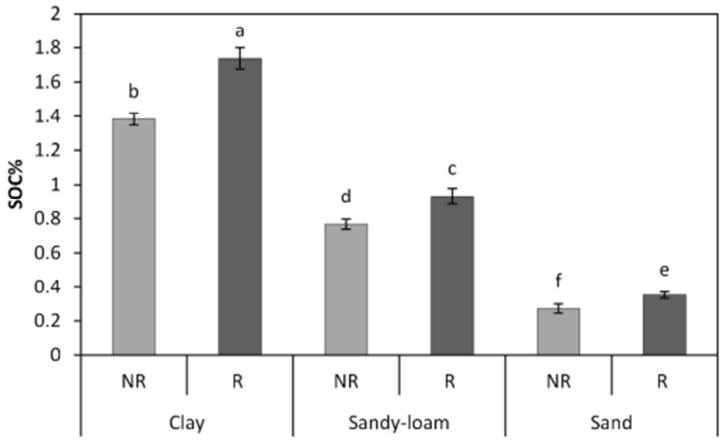

Fig. 2. Soil organic carbon concentration (SOC%) of the three soils with (R) and without (NR) residue incorporation.

3.3. Soil pore architecture

3.3.1. Total pore volume (TPV_{core})

Total pore volume (TPV_{core}) varied between treatments, ranging from a minimum of 0.46 $cm^3\,cm^{-3}$, observed in SNDL without residue incorporation and fertilisation, to a maximum of 0.66 $cm^3\,cm^{-3}$ in CL managed with residue incorporation and N fertilisation. In fact, both nitrogen and residue inputs significantly increased TPV_{core} by 3.6% and 3.2% if compared to the NR and NO FERT treatments (Table 2). Moreover, multiple regression analysis showed a positive correlation between TPV_{core} and both sand ($\beta_2 = 1.86$) and clay ($\beta_3 = 2.32$) content (Table 3).

3.3.2. Pore size distribution

Pore size distribution, investigated with gas adsorption (PSD_{N2}) in the range 0.25–50 nm, was not affected by either residue management or fertilisation. However, a clear difference was observed between soils since almost all the pore classes were predominant in CL with respect to the others (Table 4). The smallest PSD_{N2} class (0.25–2 nm), estimated by the Horvath and Kawazoe method, occupied 0.019 $cm^3\,cm^{-3}$ in CL, 0.002 $cm^3\,cm^{-3}$ in SNDL and only 0.001 $cm^3\,cm^{-3}$ in SND. Similarly, the pores of 2–50 nm (B.J.H. method) increased from 0.006 $cm^3\,cm^{-3}$ in SND to 0.016 $cm^3\,cm^{-3}$ in SNDL and to 0.070 $cm^3\,cm^{-3}$ in CL. Pore frequency, expressed in relative terms (Table 4), highlighted that pores of 2–10 nm were very numerous in all soils, being 54.6%, 38.0% and 46.6% in CL, SNDL and SND, respectively. SOC affected PSD_{N2} over the whole range, apart from the pore size class 2–10 nm (Table 3). Indeed, SOC was negatively correlated with pores in the range 0.25–2 nm ($\beta_1 = -0.24$, $p < 0.05$) and positively correlated with those >10 nm ($p < 0.05$). An opposite effect was observed for the clay content, with positive dependences with the smallest pores <10 nm and negative with the largest (26–50 nm).

Total porosity, estimated by mercury intrusion porosimetry (TPV_{MIP}), was significantly different between soils as it averaged 0.42 $cm^3\,cm^{-3}$ in SNDL, decreasing to 0.33 $cm^3\,cm^{-3}$ and 0.16 $cm^3\,cm^{-3}$ in SND and CL, respectively. FERT was also a significant factor influencing TPV_{MIP} in all soil types, with a reduction of total pore volume in fertilised plots of 28% in CL, 19% in SNDL and 6% in SND.

Pore size distribution, as revealed by MIP in the range 0.01–100 μm (PSD_{MIP}), differed significantly between soils (Table 4). Indeed, SNDL showed the highest pore volume between 0.1 and 30 μm (totally 0.35 $cm^3\,cm^{-3}$, i.e. 84% of TPV_{MIP}) while SND in pore classes >30 μm (0.26 $cm^3\,cm^{-3}$, i.e. 79% of TPV_{MIP}). In contrast, CL mainly had pores of a few micrometres, especially in the range 0.1–5 μm (0.04 $cm^3\,cm^{-3}$, i.e. 27% of TPV_{MIP}). Residue incorporation affected PSD_{MIP} only in the pore class 30-75 μm ($p < 0.01$), being reduced by 0.027 $cm^3\,cm^{-3}$ in SNDL, followed by CL (0.016 $cm^3\,cm^{-3}$) and SND (0.002 $cm^3\,cm^{-3}$). Similar findings

Table 3
Correlation factors of selected variables following the multiple regression equation $y = \alpha + \beta_1$ OC(%) $+ \beta_2$ sand(%) $+ \beta_3$ clay(%). Correlation factors are significant at $p < 0.05$.

Regression coefficients					
	Intercept α	OC β_1	Sand β_2	Clay β_3	Multiple R^2
TPV_{core}[a]	14.85	–	1.86	2.32	0.80
TPV_{MIP}[b]	0.8422	–	−1.34	−1.95	0.73
$TPV_{\mu CT}$[c]	−4.23	–	1.32	0.60	0.62
PSD_{N2}[d] (nm)					
0.25–2*	−0.0169	−0.24	0.61	1.77	0.92
2–10	−0.0422	–	0.62	1.54	0.96
10–18	−0.0022	0.96	–	–	0.93
18–26	−0.0006	0.96	–	–	0.92
26–50	−0.0004	2.13	–	−1.40	0.84
PSD_{MIP}[e] (μm)					
0.01–0.1**	0.0014	–	–	0.97	0.95
0.1–5	0.60	–	−2.61	−2.52	0.90
5–30	0.4973	–	−2.13	−2.17	0.63
30–75	−0.0352	−0.56	1.27	1.0	0.90
75–100	−0.1335	–	1.83	0.99	0.95
$PSD_{\mu CT}$[f](μm)					
25–76**	−36.54	–	1.81	1.54	0.45
76–126	3.28	–	1.35	0.68	0.57
126–480	76.90	–	−1.48	−1.12	0.35
480–2500	56.37	–	−1.58	1.23	0.39
Pore shape					
Regular	82.67	–	−1.17	-1.32	0.23
Irregular	11.77	–	1.48	1.53	0.31
Elongated	4.40	0.38	–	–	0.15
DA[g]	0.5553	–	–	0.33	0.11
CD[h]	−0.0009	–	1.77	1.08	0.77
FD[i]	1.93	–	0.67	–	0.45

* Pore size range (nm).
** Pore size range (μm).
[a] Total pore volume analysed with helium pycnometer.
[b] Total pore volume calculated with MIP.
[c] Total pore volume calculated with μCT.
[d] Pore size distribution obtained with gas adsorption.
[e] Pore size distribution obtained with MIP.
[f] Pore size distribution obtained with μCT.
[g] Degree of anisotropy.
[h] Connectivity density.
[i] Fractal dimension.

Table 4
Pore size distributions of the three soils examined with the three different techniques.

Pore size classes		Clay		Sandy-loam		Sandy	
		($cm^3\,cm^{-3}$)	(%)	($cm^3\,cm^{-3}$)	(%)	($cm^3\,cm^{-3}$)	(%)
0.25–2	nm	0.019 ± 1E − 03[a]	20.8 ± 2.0	0.002 ± 4E − 04	11.5 ± 2.1	0.001 ± 1E-04	12.7 ± 1.0
2–10		0.048 ± 1E − 03	54.6 ± 1.7	0.007 ± 6E − 04	38.0 ± 2.2	0.003 ± 2E − 04	46.6 ± 1.1
10–18		0.012 ± 2E − 03	13.9 ± 1.4	0.004 ± 3E − 04	20.8 ± 1.0	0.001 ± 4E − 05	18.8 ± 1.1
18–26		0.006 ± 7E − 04	6.4 ± 0.7	0.002 ± 4E − 04	12.3 ± 2.3	0.001 ± 1E − 04	12.1 ± 1.5
26–50		0.004 ± 1E − 03	4.4 ± 1.3	0.003 ± 7E − 04	17.4 ± 2.9	0.001 ± 1E − 04	9.7 ± 2.4
0.01–0.1	μm	0.038 ± 2E − 03	23.2 ± 5.3	0.018 ± 2E − 03	4.3 ± 0.7	0.006 ± 1E − 03	1.8 ± 0.3
0.1–5		0.043 ± 4E − 03	26.6 ± 3.3	0.188 ± 7E − 03	46.3 ± 5.1	0.025 ± 2E − 03	7.7 ± 0.7
5–30		0.034 ± 1E − 02	20.7 ± 3.5	0.165 ± 4E − 02	37.9 ± 6.0	0.036 ± 5E − 03	10.9 ± 0.9
30–75		0.032 ± 1E − 02	19.3 ± 4.4	0.038 ± 5E − 03	9.1 ± 1.1	0.154 ± 2E − 02	46.2 ± 3.5
75–100		0.011 ± 4E − 03	6.5 ± 2.0	0.009 ± 1E − 03	2.6 ± 0.8	0.106 ± 9E − 03	32.8 ± 3.9
25–76	μm	0.019 ± 3E − 03	36.2 ± 3.9	0.013 ± 1E − 03	21.4 ± 3.4	0.075 ± 7E − 03	47.2 ± 3.0
76–126		0.010 ± 2E − 03	17.7 ± 0.8	0.012 ± 2E − 03	18.1 ± 1.2	0.047 ± 8E − 03	28.6 ± 1.2
126–480		0.026 ± 1E − 02	34.9 ± 5.0	0.030 ± 9E − 03	41.9 ± 2.8	0.040 ± 9E − 03	24.0 ± 2.4
480–2500		0.009 ± 6E − 03	11.1 ± 1.6	0.017 ± 1E − 02	18.6 ± 3.4	0.001 ± 3E − 04	0.2 ± 0.1

[a]Values are reported as means ($n = 12$) followed by standard errors.

were observed as a result of N fertilisation input, which caused a reduction of the pore size class 30–75 μm in all three soils.

Multiple regression analysis showed that both TPV_{MIP} and PSD_{MIP} were significantly affected by sand and clay. Negative correlations were observed with MIP total porosity as well as with PSD classes 0.1–5 μm and 5–30 μm, while there were positive correlations with the largest pores (>30 μm). Lastly, SOC and the pore size class 30-75 μm showed a negative relationship ($\beta_1 = -0.56$).

Total pore volume in the size range revealed by μCT ($TPV_{\mu CT}$) was significantly higher in SND (0.16 $cm^3\,cm^{-3}$) than in CL and SNDL (0.07 $cm^3\,cm^{-3}$ in both soils) (Table 2 and Fig. 3). Furthermore, residue incorporation caused a reduction of 0.016 $cm^3\,cm^{-3}$ in $TPV_{\mu CT}$ managed without mineral fertilisation, while an opposite effect (+0.035 $cm^3\,cm^{-3}$) was found when R was associated with FERT treatment (interaction FERT × R significant at $p < 0.05$). The analysis of μCT pore size distribution (25–2500 μm diameter) revealed that sandy soils were mainly composed of pores in the range 25–480 μm (Table 4), with the largest pore class (480–2500 μm) being only 0.2% of μCT total porosity, while in clay and sandy-loam the largest pore class was more numerous (11% and 18%, respectively).

3.3.3. Pore morphology

There were significantly more regular pores ($S < 2$) in SNDL (41.37%) than in the other two soils (29.24% in SND and 23.88% in CL). However, irregular porosity ($2 < S < 5$) was the most numerous class in all soils (averaging 59.94%), although more predominant in clay and sandy (65.16 and 63.80%) than in sandy-loam (50.82%) ($p < 0.001$). Residues decreased the regular pores ($S > 5$) by 11.25% ($p < 0.05$), while significantly increasing the irregular and elongated ones (+6.78 % and +4.50%, respectively), as shown in Fig. 4.

Structural differences between soil types were also observed in terms of 3D pore morphology. The pore connectivity (CD), estimated by means of the Euler number algorithm, had the highest value (3.41 μm^{-3}) in the sandy soils, emphasizing a low number of redundant connections between pore branches (Table 2). This effect was especially pronounced when residue incorporation was coupled with N fertilisation (4.94 μm^{-3}), underlining their negative effect on the soil macropore connections (interaction FERT × R significant at $p < 0.05$). By contrast, degree of anisotropy (0.58, on average) and fractal dimension (2.11, on average) were not able to identify any morphological difference in pore architecture, either between soils or between treatments.

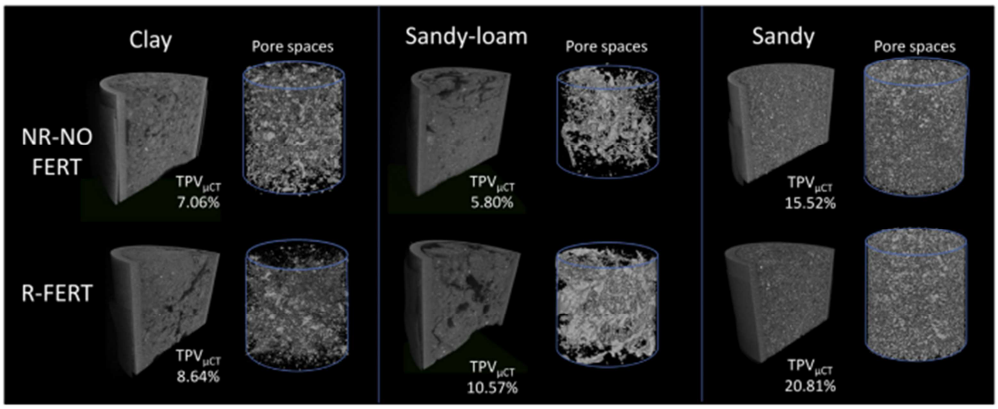

Fig. 3. 3D reconstruction of selected soil cores and pore spaces of residue removal and no fertilisation (NR-NOFERT) treatment and residue incorporation and 400 kg N ha^{-1} fertilisation (R-FERT) treatment with respective total pore volumes measured with microtomography ($TPV_{\mu CT}$).

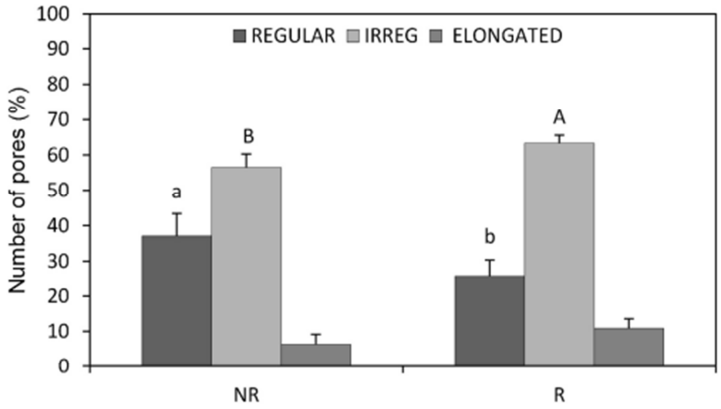

Fig. 4. Pore shape differences between plots with residue removal (NR) and residue incorporation (*R*).

Table 5
Correlation between principal components and variables (Bolded factors >0.7).

Variables	Principal component 1	Principal component 2
TPV_{core}[a]	0.39	**0.77**
$TPV_{\mu CT}$[b]	**−0.80**	0.17
PSD_{MIP}[c] (μm)		
0.01–0.1	**0.94**	0.13
0.1–5	0.17	**−0.88**
5–30	0.05	**−0.78**
30–75	**−0.84**	0.37
75–100	**−0.87**	0.46
$PSD_{\mu CT}$[d] (μm)		
25–76	−0.23	**0.85**
76–126	−0.68	0.49
126–480	0.30	−0.70
480–2500	0.36	−0.67
Pore shape		
Irregular	0.05	0.62
Elongated	0.40	0.28
DA[e]	0.40	0.59
CD[f]	**−0.76**	0.51
FD[g]	**−0.74**	−0.07
Sand%	**−0.97**	0.14
Clay%	**0.94**	0.17
SOC%	**0.95**	0.09
Eigenvalue	8.69	4.77
Explained variance %	45.77	25.11

[a] Total pore volume analysed with helium picnometry.
[b] Total pore volume calculated with μCT.
[c] Pore size distribution obtained with MIP.
[d] Pore size distribution obtained with μCT.
[e] Degree of anisotropy.
[f] Connectivity density.
[g] Fractal dimension.

A general overview of the factors influencing the soil structure was provided by PCA (Table 5 and Fig. 5). Two principal components with eigenvalue >1 were extracted, which accounted for 70.9% of the total variance. The first principal component explained 45.8% of the variance and was positively correlated with PSD_{MIP} class 0.01–0.1, clay and SOC content, while negatively with the largest PSD_{MIP} classes (30–100 μm), $TPV_{\mu CT}$, the pore morphological parameters (CD and FD) and sand content. The second accounted for 25.1% of explained variance and was only correlated with TPV_{core} from helium pycnometry and pore size classes from MIP (0.1–30 μm) and μCT (25–76 μm).

The distribution of variables on the *xy*-plane identified three clusters corresponding to the three soils (Fig. 5). SND was associated to sand content and highly unconnected (high CD) pores in the range 30–126 μm, CL was identified by clay content and cryptopores as detected by MIP (0.01–0.1 μm), while SNDL was associated to both micro- and macropores. PCs were not able to separate the single soil treatments on the planes (residues and/or fertilisation management).

4. Discussion

4.1. Crop residue effects on soil organic carbon

Adopting residue incorporation management in the long term (43 years) led to a significant accumulation of organic carbon, in terms of both concentration (+25%) and stock (+20%), in all soil types irrespective of their very different textures. By contrast, Powlson et al. (2011), reviewing 25 experiments on residue incorporation or removal, found that the C increase was relatively low (<10%) in the majority of cases and significant only in six, although they observed a high variability in C content (0–37.5%) as a result of soil type, straw input and experiment duration. Our results show that the highest increase in SOC content (R vs. NR) was found in the clay soil (+3 g kg^{-1}) as a result of the major role of fine particles (both clay and silt) on the physical protection of soil organic carbon (Six et al., 2002).

It is of particular interest that sandy soil exhibited the lowest C increase (+1.0 g kg^{-1}) in absolute terms, although the highest in relative terms (+29%) between NR and R treatments, indicating that some stabilisation mechanisms may act in the long term independently of the scarce ability of coarse-textured soils to physically protect SOC from degradation. Lugato et al. (2009), in a similar long-term experiment, observed that when larger porosity dominates (e.g. sandy soils), physical protection mechanisms are less relevant and the protection of SOC is mainly due to the selective preservation of more recalcitrant or less decomposable materials. A general C accumulation was also observed as a result of high N input. According to Lemke et al. (2010), the application of fertilisers induced an increase in the amount of residues (on average, the fertilised plots of our study produced 4 t ha^{-1} $year^{-1}$ more residues than unfertilised ones) and most likely of root debris and exudates as a result of nutrient stimuli to plant growth. In all the soils, the increase in organic carbon from the beginning of the experiment in plots non receiving residues is more pronounced if compared to that induced by crop residues, indicating the importance of root-derived carbon on soil C dynamics. Nevertheless, our data thus suggest that residue incorporation may have a significant role on carbon stock, under the pedo-climatic and management conditions of this study.

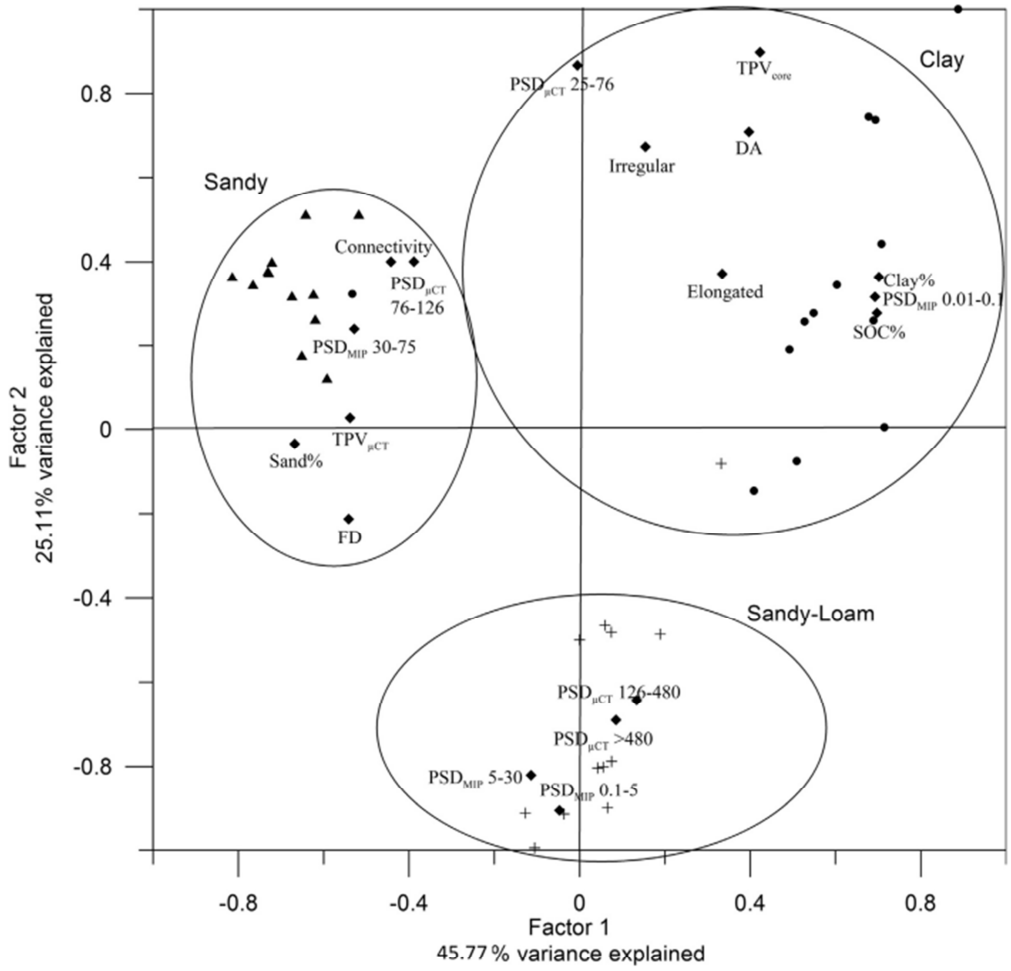

Fig. 5. Principal component analysis of selected variables. TPV_{core}, total pore volume analysed with helium pycnometer; DA, degree of anisotropy; Irregular, percentage of irregular pores; Elongated, percentage of elongated pores; SOC%, concentration of soil organic carbon; FD, fractal dimension; PSD_{MIP}, pore size distributions obtained with mercury intrusion porosimetry and $PSD_{\mu CT}$ pore size distributions obtained with microtomography (each followed by pore size range). Symbols without labels represent the cases analysed (triangles: sandy soil samples; points: clay soil samples; crosses: sandy-loam soil samples).

4.2. Crop residue effects on pore architecture

Multiple methods allowed a full evaluation of the pore network from 0.25 nm to *ca.* 2.5 mm (i.e. seven orders of magnitude). The comparison of clay, sandy-loam and sandy soils showed substantial differences in terms of soil structure, while the effect of residue incorporation was only partially detectable. In fact, the highly contrasting soil texture was crucial to distinguish the pore network characteristics, as also emphasized by the clusters in the PCA analysis, probably masking the subtle structure changes induced by residues. In particular, the pore size classes <0.1 μm dominated in the clay soil as their volume, detected with N_2 adsorption and partly with MIP, was always higher than in sandy-loam and sandy soils. Conversely pores >30 μm, although negligible when >480 μm, were particularly numerous in the sandy soils. Indeed, the sandy soil was unable to form stable aggregates due to the absence of clay–OC complexes (Lugato et al., 2010), while the soils dominated by fine particles (both clay and sandy-loam soils) showed pores greater than 480 μm, a symptom of existing cracks and inter-aggregate pores (Hillel, 1998).

Nevertheless, total pore volume measured with the core method gave higher values as affected by both residue incorporation (+3.6%) and high fertilisation rate (+3.2%), while total pore volumes measured with MIP and microtomography did not show differences between treatments. In fact, both MIP (0.01–100 μm) and μCT (25–2500 μm) porosities were only partial measures of the total pore volume within the samples, while the core method included all the pores. The decrease in soil porosity caused by residue removal could be particularly harmful in soils with a tendency towards compaction. Similar results were observed by Blanco-Canqui and Lal (2008), who showed that an increase in maize straw removal produced a decrease in soil water content at saturation and consequently in soil porosity. In addition, the full evaluation of pore size distribution from nanometres to millimetres highlighted the effect of crop residue incorporation, and consequently of organic carbon accumulation, on the soil structure. Indeed nanopores, estimated by means of N_2 adsorption, were significantly correlated with SOC as they interacted with it in two ways. Firstly, the pores in the range 0.25–2 nm were negatively correlated with OC content, emphasising its effect on pore filling or blockage. This was also reported by Zaffar and Lu (2015), who

found a SOC pore occlusion effect for pores <2 nm. Secondly, the positive correlation between 10 and 50 nm pore size class and C content was likely due to an OC-mediated stimulus to clay particle aggregation (Mayer et al., 2004). The effect of OC content on the soil structure also extended to the micrometre scale. Indeed a reduction of mesopores (30–75 μm) was estimated by means of MIP in correspondence to the increase in OC values, as reported by other authors (Lugato et al., 2009). Lugato et al. (2009) also found a positive correlation between MIP pore size class 0.01–0.1 μm and SOC which, on the contrary, was not observed in our MIP results.

Although μCT analysis did not reveal significant differences between treatments in terms of pore size distribution, it still allowed the effect of crop residues on the pore structure to be identified. Indeed, their incorporation led to morphological changes in the pore structure, decreasing regular pores and increasing irregular and elongated ones, as already observed by other authors. Pagliai et al. (2004), studying the effects of different organic carbon inputs on pore morphology, found a significantly high percentage of elongated pores in amended treatments. Furthermore, Papadopoulos et al. (2009) suggested that the pores of aggregates fertilised with organic input were mainly cracked and elongated. Although their findings were obtained as a consequence of manure instead of crop residue inputs, a similar effect between treatments can be hypothesised as both had high straw content.

5. Conclusions

The long-term incorporation of crop residues produced a significant increase in the amount of soil organic carbon, suggesting that if their removal for bioenergy production would become widely used, this will surely deprive soils from a valuable source of organic carbon. The residue-induced effects on soil organic carbon were not accompanied by a relevant change in soil pore size distribution from nano to macro scale. On the contrary, they induced an increase in total porosity. This indicates that, especially in soils with a tendency towards compaction, the removal of residues could bereave farmers from a cost-effective practice able to at least alleviate the problem. Furthermore, residues caused a rearrangement of the pore network towards a more elongated and irregular structure, confirming these parameters as sensitive indicators of management effects on soil quality. Since these changes of pore structure could affect other important soil properties such as water movement, solute transport and gas exchanges, additional research on these topics is recommended to achieve a sound knowledge on the usefulness of incorporating crop residues.

Acknowledgments

The research leading to these results has received funding from the European Union Seventh Framework Programme (FP7/2007-2013) under grant agreement no.603498 (RECARE project)

Bibliography

Barrett, E., Joyner, L., Halenda, P., 1951. The determination of pore volume and area distributions in porous substances. I. Computations from nitrogen isotherms. J. Am. Chem. Soc. 73, 373–380. doi:http://dx.doi.org/10.1021/ja01145a126.
Blanco-Canqui, H., Lal, R., 2008. Corn stover removal impacts on micro-scale soil physical properties. Geoderma 145, 335–346. doi:http://dx.doi.org/10.1016/j.geoderma.2008.03.016.
Buysse, P., Roisin, C., Aubinet, M., 2013. Fifty years of contrasted residue management of an agricultural crop: Impacts on the soil carbon budget and on soil heterotrophic respiration. Agric. Ecosyst. Environ. 167, 52–59. doi:http://dx.doi.org/10.1016/j.agee.2013.01.006.
Cameron, K.C., Buchan, G.D., 2006. Porosity and pore-size distribution. In: Lal, Ratan (Ed.), Encyclopedia of Soil Science, vol. 2. Taylor and Francis, pp. 1350–1353.
Cherubini, F., Ulgiati, S., 2010. Crop residues as raw materials for biorefinery systems—a LCA case study. Appl. Energy 87, 47–57. doi:http://dx.doi.org/10.1016/j.apenergy.2009.08.024.
Cnudde, V., Cwirzen, A., Masschaele, B., Jacobs, P.J.S., 2009. Porosity and microstructure characterization of building stones and concretes. Eng. Geol. 103, 76–83. doi:http://dx.doi.org/10.1016/j.enggeo.2008.06.014.
Dal Ferro, N., Sartori, L., Simonetti, G., Berti, A., Morari, F., 2014. Soil macro- and microstructure as affected by different tillage systems and their effects on maize root growth. Soil Till. Res. 140, 55–65. doi:http://dx.doi.org/10.1016/j.still.2014.02.003.
Methods of soil analysis. Part 4. Physical Methods. Soil Sci Soc Am Book Series 5. In: Dane, J.H., Topp, G.C. (Eds.), Soil Science Society of America, Madison, WI.
Deurer, M., Grinev, D., Young, I., Clothier, B.E., Müller, K., 2009. The impact of soil carbon management on soil macropore structure: a comparison of two apple orchard systems in New Zealand. Eur. J. Soil Sci. 60, 945–955. doi:http://dx.doi.org/10.1111/j.1365-2389.2009.01164.x.
Dominati, E., Patterson, M., Mackay, A., 2010. A framework for classifying and quantifying the natural capital and ecosystem services of soils. Ecol. Econ. 69, 1858–1868. doi:http://dx.doi.org/10.1016/j.ecolecon.2010.05.002.
FAO-UNESCO, 2008. Soil Map of the World. Revised Legend. FAO, Rome.
Fuentes, M., Govaerts, B., De León, F., Hidalgo, C., Dendooven, L., Sayre, K.D., Etchevers, J., 2009. Fourteen years of applying zero and conventional tillage, crop rotation and residue management systems and its effect on physical and chemical soil quality. Eur. J. Agron. 30, 228–237. doi:http://dx.doi.org/10.1016/j.eja.2008.10.005.
Greenland, D.J., 1977. Soil damage by intensive arable cultivation: temporary or permanent? Phil. Trans. R. Soc. London 281, 193–208. doi:http://dx.doi.org/10.1098/rstb.1977.0133.
Harrigan, T.P., Mann, R.W., 1984. Characterization of microstructural anisotropy in orthotropic materials using a second rank tensor. J. Mater. Sci. 19, 761–767. doi:http://dx.doi.org/10.1007/bf00540446.
Hildebrand, T., Rüegsegger, P., 1997. A new method for the model-independent assessment of thickness in three-dimensional images. J. Microsc. 185, 67–75. doi:http://dx.doi.org/10.1046/j.1365-2818.1997.1340694.x.
Hillel, D., 1998. Environmental Soil Physics. Academic Press, San Diego, CA. USA p. 106.
Horvath, K., Kawazoe, G., 1983. Method for the calculation of effective pore size distribution in molecular sieve carbon. J. Chem. Eng. Jpn. 16, 470–475. doi:http://dx.doi.org/10.1252/jcej.16.470.
Jarvis, N.J., 2007. A review of non-equilibrium water flow and solute transport in soil macropores: principles, controlling factors and consequences for water quality. Eur. J. Soil Sci. 58, 523–546. doi:http://dx.doi.org/10.1111/j.1365-2389.2007.00915.x.
Kaiser, H.F., 1974. An index of factorial simplicity. Psychometrika 39, 31–36. doi:http://dx.doi.org/10.1007/bf02291575.
Lal, R., 2005. World crop residues production and implications of its use as a biofuel. Environ. Int. 31, 575–584. doi:http://dx.doi.org/10.1016/j.envint.2004.09.005.
Lal, R., 2009. Soil quality impacts of residue removal for bioethanol production. Soil Till. Res. 102, 233–241. doi:http://dx.doi.org/10.1016/j.still.2008.07.003.
Lal, R., Shukla, M.K., 2004. Principles of Soil Physics. Marcel Dekker, New York p. 154.
Lemke, R.L., VandenBygaart, A.J., Campbell, C.A., Lafond, G.P., Grant, B., 2010. Crop residue removal and fertilizer N: effects on soil organic carbon in a long-term crop rotation experiment on a Udic Boroll. Agric. Ecosyst. Environ. 135, 42–51. doi:http://dx.doi.org/10.1016/j.agee.2009.08.010.
Lugato, E., Morari, F., Nardi, S., Berti, A., Giardini, L., 2009. Relationship between aggregate pore size distribution and organic-humic carbon in contrasting soils. Soil Till. Res. 103, 153–157. doi:http://dx.doi.org/10.1016/j.still.2008.10.013.
Lugato, E., Simonetti, G., Morari, F., Nardi, S., Berti, A., Giardini, L., 2010. Distribution of organic and humic carbon in wet-sieved aggregates of different soils under long-term fertilization experiment. Geoderma 157, 80–85. doi:http://dx.doi.org/10.1016/j.geoderma.2010.03.017.
Lützow, M.V., Kogel-Knabner, I., Ekschmitt, K., Matzner, E., Guggenberger, G., Marschner, B., Flessa, H., 2006. Stabilization of organic matter in temperate soils: mechanisms and their relevance under different soil conditions—a review. Eur. J. Soil Sci. 57, 426–445. doi:http://dx.doi.org/10.1111/j.1365-2389.2006.00809.x.
Mayer, L.M., Schick, L.L., Hardy, K.R., Wagai, R., McCarthy, J., 2004. Organic matter in small mesopores in sediments and soils. Geochim. Cosmochim. Acta 68, 3863–3872. doi:http://dx.doi.org/10.1016/j.gca.2004.03.019.
Monforti, F., Lugato, E., Motola, V., Bodis, K., Scarlat, N., Dallemand, J.-F., 2015. Optimal energy use of agricultural crop residues preserving soil organic carbon stocks in Europe. Renewable Sustainable Energy Rev. 44, 519–529. doi:http://dx.doi.org/10.1016/j.rser.2014.12.033.
Monteleone, M., Cammerino, A.R.B., Garofalo, P., Delivand, M.K., 2015. Straw-to-soil or straw-to-energy? An optimal trade off in a long term sustainability perspective. Appl. Energ. 154, 891–899. doi:http://dx.doi.org/10.1016/j.apenergy.2015.04.108.
Morari, F., Lugato, E., Berti, A., Giardini, L., 2006. Long-term effects of recommended management practices on soil carbon changes and sequestration in north-eastern Italy. Soil Use Manage. 22, 71–81. doi:http://dx.doi.org/10.1111/j.1475-2743.2005.00006.x.
Otsu, N., 1979. A threshold selection method from gray-level histograms. IEEE Trans. Syst. Man Cybern. Syst. 11, 23–27. doi:http://dx.doi.org/10.1109/TSMC.1979.4310076.

Pagliai, M., Vignozzi, N., Pellegrini, S., 2004. Soil structure and the effect of management practices. Soil Till. Res. 79, 131–143. doi:http://dx.doi.org/10.1016/j.still.2004.07.002.
Papadopoulos, A., Bird, N.R.A., Whitmore, A.P., Mooney, S.J., 2009. Investigating the effects of organic and conventional management on soil aggregate stability using X-ray computed tomography. Eur. J. Soil Sci. 60, 360–368. doi:http://dx.doi.org/10.1111/j.1365-2389.2009.01126.x.
Paul, B.K., Vanlauwe, B., Ayuke, F., Gassner, A., Hoogmoed, M., Hurisso, T.T., Pulleman, M.M., 2013. Medium-term impact of tillage and residue management on soil aggregate stability, soil carbon and crop productivity. Agric. Ecosyst. Environ. 164, 14–22. doi:http://dx.doi.org/10.1016/j.agee.2012.10.003.
Powlson, D.S., Glendining, M.J., Coleman, K., Whitmore, A.P., 2011. Implications for soil properties of removing cereal straw: results from long-term studies. Agron. J. 103, 279. doi:http://dx.doi.org/10.2134/agronj2010.0146s.
Six, J., Conant, R.T., Paul, E.A., Paustian, K., 2002. Stabilization mechanisms of soil organic matter: implications for C-saturation of soils. Plant Soil 241, 155–176. doi:http://dx.doi.org/10.1023/A:1016125726789.
Sumner, M.E., 1999. Handbook of Soil Science. CRC Press; Taylor and Francis Group, London, UK.
Ulrich, D., van Rietbergen, B., Laib, A., Ruegsegger, P., 1999. The ability of three-dimensional structural indices to reflect mechanical aspects of trabecular bone. Bone 25, 55–60. doi:http://dx.doi.org/10.1016/s8756-3282(99) 00098-8.
Villamil, M.B., Little, J., Nafziger, E.D., 2015. Corn residue, tillage, and nitrogen rate effects on soil properties. Soil Till. Res. 151, 61–66. doi:http://dx.doi.org/10.1016/j.still.2015.03.005.
Vogel, H.-J., Weller, U., Schlüter, S., 2010. Quantification of soil structure based on Minkowski functions. Comput. Geosci. 36, 1236–1245. doi:http://dx.doi.org/10.1016/j.cageo.2010.03.007.
Wuest, S.B., 2007. Surface versus incorporated residue effects on water-stable aggregates. Soil Till. Res. 96, 124–130. doi:http://dx.doi.org/10.1016/j.still.2007.05.001.
Zaffar, M., Lu, S.G., 2015. Pore size distribution of clayey soils and its correlation with soil organic matter. Pedosphere 25, 240–249. doi:http://dx.doi.org/10.1016/s1002-0160(15) 60009-1.
Zhang, P., Wei, T., Jia, Z., Han, Q., Ren, X., 2014. Soil aggregate and crop yield changes with different rates of straw incorporation in semiarid areas of northwest China. Geoderma 230-231, 41–49. doi:http://dx.doi.org/10.1016/j.geoderma.2014.04.007.

G Model
EURAGR-25453; No. of Pages 9
ARTICLE IN PRESS

Europ. J. Agronomy xxx (2015) xxx–xxx

Contents lists available at ScienceDirect

European Journal of Agronomy

journal homepage: www.elsevier.com/locate/eja

Outcomes from a long-term study on crop residue effects on plant yield and nitrogen use efficiency in contrasting soils

Chiara Pituello*, Riccardo Polese, Francesco Morari, Antonio Berti

Dipartimento di Agronomia Animali Alimenti Risorse Naturali e Ambiente, Viale dell'Università 16, 35020 Padova, Italy

ARTICLE INFO

Article history:
Received 1 September 2015
Received in revised form
13 November 2015
Accepted 30 November 2015
Available online xxx

Keywords:
Crop residues
Crop yield
Nitrogen use efficiency
Long-term
Field experiments

ABSTRACT

The use of crop residues to increase crop yield and NUE is still a matter of debate since studies in different climates and soil types have led to inconclusive results and this could be partly explained by the numerous and complex factors that affect the residue-derived N cycle in field conditions. Given this complexity, long-term field experiments appear to be the more suitable tools to investigate these dynamics and develop effective management practices. In this paper, we hypothesized that residue incorporation affects crop yield and NUE, both through a direct nutritional effect given by residue decomposition and an indirect influence on soil physical and biological properties related to the input of organic carbon. We used data from a long-term field experiment started in 1970 in North-eastern Italy to evaluate the effects of crop residue incorporation on the productivity and nitrogen use efficiency of different crops (i.e., maize, winter wheat, sugarbeet, tomato and potato) in three contrasting soil types: a Fluvi–Calcaric Cambisol, a Gleyi–Vertic Chernozem and a Calcaric Arenosol. The results showed that incorporation of residues seems to have different effects depending on crop and soil type. For potato and tomato and, to a lesser extent, for sugarbeet, residues can improve crop productivity, while the effects on cereals seem to be lower. Regarding soil type, residues are proportionally more effective in sandy and sandy-loam soils, both through a direct nutritional effect and, possibly, an improvement of soil characteristics. Anyway the residue effect is relatively low, with modest increments of biomass in the most fertile soils and their effect can be compensated by N fertilization. The use of residues as organic amendment or their re-use in other processes (e.g., as a source of bioenergy) therefore has to be carefully analysed considering both the energy and C balances and the positive effects on soil productivity.

1. Introduction

World demand for nitrogen (N) fertilizers increased by 2.3 million tons annually from 2002 to 2012 (Faostat, 2012) and is expected to reach 115.9 million tons in 2016 (Fao, 2012). Given the trends in world population growth and the consequent increase in food production, it is expected that N consumption will continue to increase accordingly. The misuse of fertilizers can create serious environmental problems (Galloway et al., 2008) (i.e., eutrophication, groundwater pollution and GHGs emissions) through mechanisms such as leaching, volatilisation, surface runoff and denitrification (Van Grinsven et al., 2015). The predominant role of agriculture in N-derived pollution is underlined by the fact that fertilizers account for 63% of all anthropogenic sources of reactive nitrogen (Dobermann, 2005). The term reactive nitrogen encompasses every biologically, photochemically or radiatively active form of N that can contribute to pollution in different compartments of the biosphere (i.e., every form of nitrogen other than N_2) (Sutton, 2011). An index commonly used to detect potential excess nitrogen is the nitrogen use efficiency (NUE), which is the proportion of applied fertilizer that is effectively converted into yield by the crop. Despite the recent improvements in N use efficiency obtained by farming systems in Europe, also as a consequence of application of the Nitrates Directive, N losses from agricultural fields are still 50 kg N ha^{-1} $year^{-1}$ on average (Lassaletta et al., 2014). Reducing the production and release in the environment of reactive nitrogen is thus a primary goal that can be achieved through appropriate soil management (i.e., reducing soil acidity, using conservation tillage practices and proper water management, growing cover crops or incorporating crop residues); an optimization of N input (using organic fertilizers such as manure, controlled release fertilizers and NH_4/NO_3 inhibitors with an accu-

* Corresponding author.
E-mail address: chiara.pituello@studenti.unipd.it (C. Pituello).

http://dx.doi.org/10.1016/j.eja.2015.11.027
1161-0301/

rate selection of the rates and timing of application); and through the adoption of crop rotations and nitrogen efficient genotypes.

The use of crop residues to increase NUE is still a matter of debate since studies in different climates and soil types have led to inconclusive results. Malhi et al. (2011) studying two long-term (26 years) rotations in a Black Chernozem and in a Orthic Gray Luvisol in Canada, found an increase (5.2 Kg N ha^{-1}) in N uptake by seed and straw almost ubiquitous in the first type of soil while only for a reduced period in the second. On the contrary, three years of straw incorporation in a Haplic Luvisol produced no significant improvements in NUE of winter wheat (Brennan et al., 2014). In a recent meta-analysis summarizing studies on rice cultivations in China, Huang et al. (2013) found that the incorporation of rice residues allowed a 29.4% reduction of inorganic N inputs without significant decreases in yield. These apparently contrasting results could be partly explained by the numerous and complicated factors that affect the residue-derived N cycle in field conditions, such as soil pH, salinity and texture, temperature and moisture conditions, freezing and thawing cycles, wetting and drying cycles, along with macro and microorganisms (Kumar and Goh, 1999). Given this complexity, long-term field experiments appear to be the more suitable tools to investigate these dynamics and develop effective management practices (Richter et al., 2007), especially in light of increasing future demands from agricultural ecosystems (Janzen, 2009). Long-term field experiments are fundamental not only to draw up local management guidelines, but can indubitably contribute to assessing global patterns and trends (Rasmussen, 1998) by building common databases and posing multi-site questions (Janzen, 2009).

In this paper we hypothesized that residue incorporation affects NUE, both through a direct nutritional effect given by residue decomposition and an indirect influence on soil physical and biological properties related to the input of organic carbon. We used data from a long-term field experiment started in 1970 in Northeastern Italy to evaluate the effects of crop residue incorporation on the productivity and nitrogen use efficiency of different crops in three contrasting soil types. The large crop database allowed empirical models to be built that could disentangle the multiple effects of residue incorporation on crop performances.

2. Materials and methods

2.1. The experiment

The long-term experiment is located at the experimental farm of the University of Padova (Veneto region, NE Italy 45° 21′N; 11° 58′E; 6 m a.s.l.). The local climate is sub-humid, with annual rainfall of about 850 mm. In the median year, rainfall is highest in June (100 mm) and October (90 mm) and lowest in winter (50–60 mm). Temperatures increase from January (minimum average: −1.5 °C) to July (maximum average: 27.2 °C). Reference evapotranspiration (ETo) is 945 mm with a peak in July (5 mm d^{-1}). ETo exceeds rainfall from April to September. The site has a shallow water table ranging from about 0.5–1.5 m in late winter–early spring to 1–2 m in summer.

Since 1970, the experimental design has been constituted by 108 open lysimeters of 4 m^2, filled with three types of soil: sandy, sandy-loam and clay. The main physical and chemical characteristics of the soils at the beginning of the experiment are listed in Table 1. The sandy-loam soil is classified according to FAO-UNESCO as a Fluvi–Calcaric Cambisol and is native to the experimental farm. The other two soils were brought from locations in the Veneto region: the clay soil from the south-western plain, and the sandy soil from the central coastal area. The clay soil is classified as a Gleyi–Vertic Chernozem, the sandy one as Calcaric Arenosol (Fao-Unesco, 2008).

Table 1
Main physical and chemical properties of the soils at the beginning of the experiment (1970).

	Clay	Sandy-loam	Sandy
Sand (2–0.05 mm)%	40.6	57.1	98.8
Silt (0.05–0.002 mm)%	18	23.7	0
Clay (<0.002 mm)%	41.4	19.2	1.2
pH (H_2O)	7.7	7.8	8.4
SOC% [a]	1.06	0.62	0.05
Total $CaCO_3$%	6.2	30.8	22.9
P_2O_5 labile (g Kg^{-1})	5.29	1.24	1.19
P_2O_5 ass. (mg Kg^{-1}) [b]	59	23	19
K_2O exc. (mg Kg^{-1}) [c]	1.1	4.6	1.9
N tot (g Kg^{-1})	1.7	0.9	0.1

[a] Rotini method.
[b] Ferrari method.
[c] Exchangeable K_2O with 25% $NaNO_3$ pre-treatment.

Table 2
Average N contents of product and residue biomass.

	$N_{product}$	$N_{residues}$
	g kg^{-1} dm	
Maize	15	9
Potato	16	14
Sugarbeet	10	19
Tomato	26	14
Wheat	21	5

The original soil profiles were reconstructed in the lysimeters. The experimental design is a randomized block with three replicates. Until 1986/87 the trial was conducted with a maize–wheat rotation, comparing 12 treatments deriving from the factorial combination of three nitrogen doses with four methods of crop residue management (removal of all residues, burial of just wheat straw, burial of just maize stalks, and burial of both straw and stalks).

The annual doses of nitrogen were 0, 100 and 200 kg ha^{-1} for maize and 0, 80 and 160 kg ha^{-1} for wheat, splitting the distributions into 1/3 when incorporating the crop residues into the soil, 1/3 at sowing and the rest at canopy closure. The doses of P_2O_5 and K_2O were 150 and 200 kg ha^{-1} in all treatments, respectively.

The trial was modified in 1987/88, abandoning the biannual rotation and adopting a less rigid crop sequence, based on a four-year rotation of wheat, maize, tomato and sugarbeet, with the possibility of altering the crops, in particular substituting tomato with potato. The management methods of the crop residues were consequently simplified, comparing only two situations (burial of the previous crop residues–RI or their removal-RR), and the range of nitrogen doses was increased to 6 constant levels over the years (0, 50, 100, 200, 300, 400 kg ha^{-1}) in a factorial combination with the burial or removal of the crop residues. These experimental treatments were maintained until the end of the experiment in 2012.

At the end of the growing season, the fresh and dry weights of yield and aerial biomass were measured. Average N contents of product and residue biomass are given in Table 2.

2.2. Statistical analysis

The long-term trends of biomass production with and without residue incorporation were compared through a Sign test within each of the three soils considered.

The relationships between $N_{applied}$ and yield were studied with a hyperbolic model:

$$\text{Yield} = Y_0 + \frac{a \times N_{applied}}{1 + a \times N_{applied}/b} \quad (1)$$

Please cite this article in press as: Pituello, C., et al., Outcomes from a long-term study on crop residue effects on plant yield and nitrogen use efficiency in contrasting soils. Eur. J. Agron. (2015), http://dx.doi.org/10.1016/j.eja.2015.11.027

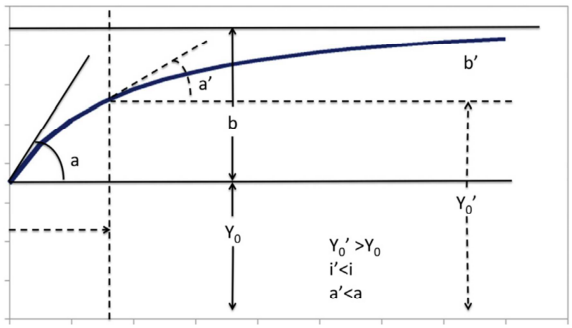

Fig. 1. Scheme of the hyperbolic model used to describe the relationship between Yield and $N_{applied}$. 'Y_0' is the yield without N distribution and '*a*' and '*b*' are the initial slope and asymptote of the hyperbola. The asymptotic maximum yield (Y_M) is equal to $Y_0 + b$. Y_0', *a*' and *b*' are the yield without N distribution, the initial slope and asymptote of the hyperbola in the case of a purely nutritional effect.

where Y_0 is the yield without N distribution, *a* is the initial slope and *b* is the asymptote of the hyperbola. The asymptotic maximum yield (Y_M) is then equal to $Y_0 + b$.

The effects of residue incorporation can be mainly due to nutritional effects (i.e., rapid mineralization of residues and interception of this amount of nutrients by crop roots) and/or to an improvement of soil characteristics (e.g., increased soil organic carbon – SOC – with possible effects on structure, porosity, and water retention). In the first case it is expected that the potential crop yield is unaffected passing from RR to RI. The effect of residues should then correspond to an increase of N availability, graphically equivalent to a shift toward right of the origin of the graph relating N applied to yield (Fig. 1). If the effect of residues is solely due to their nutrient content an increase of 'Y_0' is then expected and a decrease of both '*a*' and '*b*', with the maximum yield 'Y_M' remaining constant.

On the other hand, if the effect of residues is mediated by changes in overall soil fertility, not directly related to the nutrient effect, Y_M should increase, while the behavior of the other parameters is not directly predictable.

To directly express the maximum yield as a function parameter, Eq. (1) was rewritten as:

$$\text{Yield} = Y_M - b + \frac{a \times N_{applied}}{1 + a \times N_{applied}/b} \quad (2)$$

Curves were at first fitted for each 'crop × year' combination separately for each soil and with or without residue incorporation (complex model–modC). Two possible simplifications of this model were then considered:

(a) Y_M unaffected by residue incorporation, the other parameters being allowed to change from RR to RI (simplified model 1–modS1);
(b) Same Y_M, *a* and *b* parameters independently of residue management (simplified model 2–modS2).

The complex model (modC) considered corresponds to the independent fit of each data set (crop *x* year *x* soil *x* residue management combinations). The two simplified models are intended to test the constancy of Y_M (modS1) or the absence of effects of residue incorporation (modS2). Depending on the significance of the comparison between models, it is then possible to determine if residue incorporation affects crop yield and, in this case, if the effect is mainly due to the nutritional input or also depends on the modification of other soil parameters, leading to an increase in the potential yield (Fig. 2).

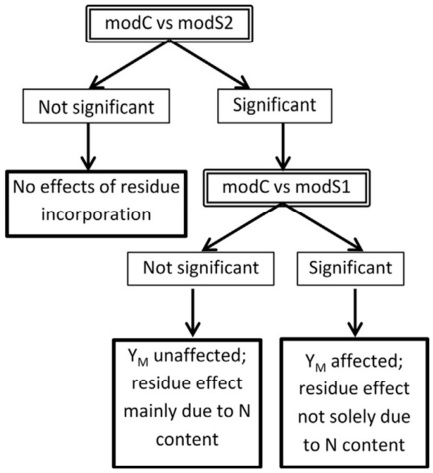

Fig. 2. Decision tree for the comparison of crop yield models.

The reduction of model complexity (i.e., presence of common parameters within a soil for RR and RI) was tested with a partial *F* test comparing the complex (all the parameter specific) and simplified (some parameter common) models.

To estimate the amounts of N recovered from mineral fertilisation and from residues, the observed N recoveries were fitted with the following equation:

$$N_{rec} = N_0 + \frac{N_{min} \times k_{min} \times a}{1 + (N_{min} \times k_{min} \times a)/b} + \frac{N_{res} \times k_{res} \times a}{1 + (N_{res} \times k_{res} \times a)/b} \quad (3)$$

where N_0 is the amount of N recovered from natural availability for a specific soil-crop combination, N_{min} and N_{res} are the amount of N of mineral fertilisation and of incorporated residues, k_{min} and k_{res} are constants related to nitrogen availability for mineral fertilisers and residues and a and b are regression parameters.

The Nitrogen use efficiency (NUE) for both mineral and organic forms can then be obtained dividing the amount recovered from a specific source by the amount distributed;

$$NUE_{min} = \frac{N_{min} \times k_{min} \times a}{1 + N_{min} \times k_{min} \times a/b} \times \frac{1}{N_{min}} = \frac{k_{min} \times a}{1 + N_{min} \times k_{min} \times a/b} \quad (4)$$

and:

$$NUE_{res} = \frac{N_{res} \times k_{res} \times a}{1 + N_{res} \times k_{res} \times a/b} \times \frac{1}{N_{res}} = \frac{k_{res} \times a}{1 + N_{res} \times k_{res} \times a/b} \quad (5)$$

The relative efficiency of N from residues can be obtained as the ratio of the constants related to nitrogen availability for mineral fertilisers and residues:

$$\text{Relative efficiency} = \frac{k_{res}}{k_{min}} \quad (6)$$

3. Results

3.1. Average yields

Biomass production trends present a discontinuity passing from the maize–wheat rotation (until 1986) to the more complex open rotation adopted since 1987. In the first period yields were almost constant on average, while modification of the crop sequence led to an higher variability and apparently to a slight increase in yields, particularly evident in the sandy soil (Fig. 3). In all soils, residue incorporation caused an increase in yields in comparison with

Please cite this article in press as: Pituello, C., et al., Outcomes from a long-term study on crop residue effects on plant yield and nitrogen use efficiency in contrasting soils. Eur. J. Agron. (2015), http://dx.doi.org/10.1016/j.eja.2015.11.027

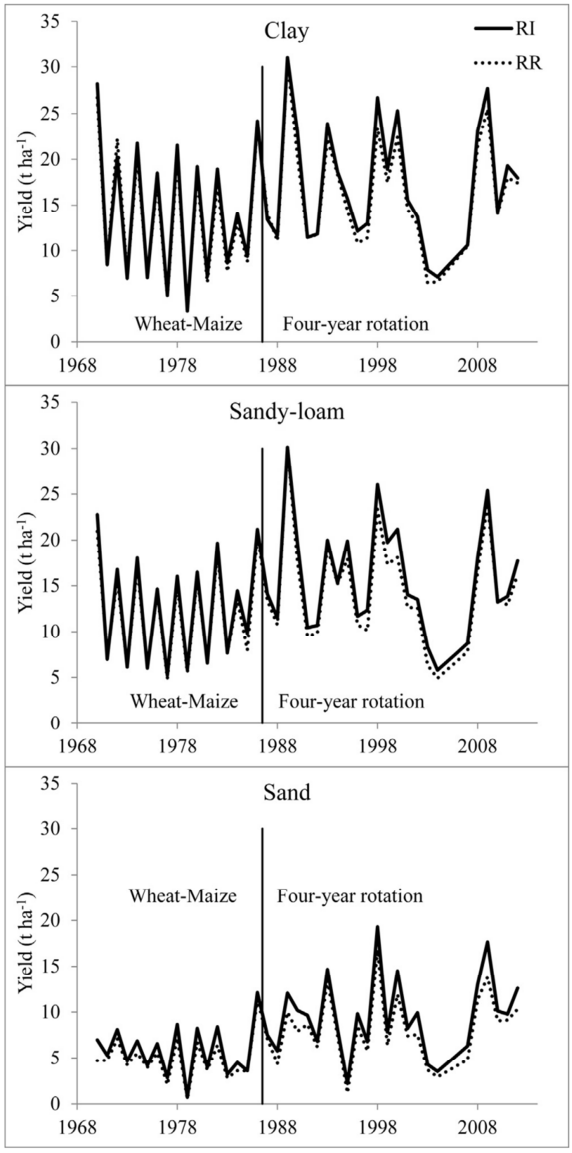

Fig. 3. Total aerial biomass trends over the 43 years (average of the N fertilizations).

residue removal (sign test with $p < 0.01$ for the three soils). The effect of residue incorporation is however inversely proportional to soil fertility, with an average increase of biomass equal to 5.5, 7.4 and 18.1% respectively for clay, sandy-loam and sandy soils. This is mainly visible in sugarbeet, winter wheat and maize, for which the increases in yield were very pronounced in sandy soil (+27.6%, +19.5% and +21.7%, respectively), if compared with clay (+4.8%, +2.1% and +7.3%) and sandy-loam (+7.7%, +2.8% and +7.5%). On the contrary, in potato and tomato, the residue-induced increase in yield was less pronounced in clay soil (+8.5% and +5.8%, respectively), than in the other two (+14.1% and +10.8% in sandy-loam; +14.5% and 13.5% in sandy). It has to be noticed that in the same period SOC content varied significantly owing to residue incorporation (Table 3) with an increase of 16%, 19% and 22% respectively for the clay, sandy-loam and sandy soil. Yields and SOC increases

Table 3
SOC variations between RI and RR treatments.

fsdfsdf	Clay	Sandy-loam	Sandy
	SOC (t ha^{-1})		
RR	30.3[a] ± 0.6	19.8 ± 0.7	8.1 ± 0.4
RI	35.2 ± 1.0	23.6 ± 0.8	9.9 ± 0.3

[a] Values are reported as means followed by standard errors ($n = 18$).

present then a rough proportionality, which can be due either to nutritional effects or to an improvement of soil physical traits.

3.2. Yield response to N application with or without residue incorporation

The comparison of the complex model with modS2 (Table 4) indicates highly significant differences for maize ($p < 0.001$) in all soil types, thus highlighting a residue-mediated effect on yield. The comparison of modS1 with the complex one was never significant. With modS1 (Y_M constant with or without residue incorporation), '*a*' parameter with RI shows a reduced variability (Fig. 4) and a tendency to be lower than RR (mean value 0.0544 with RI against 0.0588 with RR). Along with the absence of significant differences between modC and modS1, this indicates that the increase in productivity for all soils could be caused mainly by a nutritional effect.

Wheat seems to undergo a mainly nutritional effect only in clay and sandy-loam soil, while in sandy soil other indirect mechanisms (i.e., variation of soil physical traits) could be involved in the observed increase in yield, as the significant difference between the complex model and modS1 points out.

In sugarbeet, significant differences are detected between the complex model and the modS2 in sandy-loam ($p = 0.005$) and sandy soil ($p = 0.018$), with the opposite in clay soil. Considering modS1, when Y_M is constant, the parameter '*a*' increases with residue incorporation, while parameter '*b*' remains constant (data not shown), thus suggesting that the mechanisms involved in the observed effect may be different from the purely nutritional one.

In potato, residues caused significant increases in yield only in clay and sandy-loam soil (comparison between complex model and modS2 significant at $p = 0.017$ and $p = 0.006$, respectively). The absence of effect in sandy soil could be ascribable to the low yields observed. For clay and sandy-loam soils, the absence of significant differences between the complex model and modS1, along with the increase in parameter '*a*' suggests that residue effect on yield is caused by a mixture of direct nutritional effects and changes in soil physical properties.

Residue effects on tomato yield were observed only in sandy-loam soil (complex model vs modS2 significant at $p = 0.004$). Considering the comparison of the complex model with modS1 ($p > 0.05$), an increase in parameter '*a*' is observed, thus suggesting mechanisms other than the purely nutritional effect also being present in this crop.

The relationships between crop yield and N distribution, calculated on the average yields for each N level (Fig. 5), show the general positive effect of residue incorporation on crop yield. While the differences between soil types are reduced for maize and wheat, the differences between the sandy and the two other soils are substantial in sugarbeet, potato and tomato. As observed above, the effects of residue incorporation in wheat seems to be negligible in the most fertile soils.

3.3. Nitrogen recovery with and without residue incorporation

The model used for the estimation of the amounts of N recovered from mineral fertilisers and residues relies on some assumptions. First of all, the natural availability parameter N_0 is unique for all

Please cite this article in press as: Pituello, C., et al., Outcomes from a long-term study on crop residue effects on plant yield and nitrogen use efficiency in contrasting soils. Eur. J. Agron. (2015), http://dx.doi.org/10.1016/j.eja.2015.11.027

Table 4
Comparison between complex and simplified models for the relationship between crop yield and N supply.

Crop	Model	Soil type	Residual SS	Total SS	d.f.	*F*	*p*
Sugarbeet	ModC	Clay	278.3	3243.9	90		
		Sandy-loam	262.3	2540.2	90		
		Sand	135.0	1156.1	90		
	ModS1	Clay	282.2	3243.9	93	0.430	0.732
		Sandy-loam	281.4	2540.2	93	2.190	0.095
		Sand	141.5	1156.1	93	1.452	0.233
	ModS2	Clay	296.2	3243.9	99	0.645	0.755
		Sandy-loam	337.9	2540.2	99	2.886	0.005
		Sand	167.3	1156.1	99	2.393	0.018
Wheat	ModC	Clay	29.3	931.2	246		
		Sandy-loam	32.7	879.0	246		
		Sand	37.1	920.6	246		
	ModS1	Clay	30.6	931.2	259	0.865	0.590
		Sandy-loam	34.3	879.0	259	0.882	0.572
		Sand	42.4	920.6	259	2.713	0.001
	ModS2	Clay	36.1	931.2	99	1.461	0.046
		Sandy-loam	41.9	879.0	99	1.762	0.006
		Sand	58.8	920.6	99	3.695	0.000
Maize	ModC	Clay	287.9	5151.9	306		
		Sandy-loam	273.5	5707.9	306		
		Sand	430.5	5623.1	306		
	ModS1	Clay	305.0	5151.9	321	1.213	0.260
		Sandy-loam	288.7	5707.9	321	1.137	0.322
		Sand	451.7	5623.1	321	1.003	0.451
	ModS2	Clay	415.2	5151.9	351	3.007	0.000
		Sandy-loam	366.3	5707.9	351	2.309	0.000
		Sand	645.3	5623.1	351	3.391	0.000
Potato	ModC	Clay	270.6	2803.0	90		
		Sandy-loam	385.3	1468.8	90		
		Sand	193.4	985.2	90		
	ModS1	Clay	280.1	2803.0	93	1.051	0.374
		Sandy-loam	389.5	1468.8	93	0.321	0.810
		Sand	207.2	985.2	93	2.130	0.102
	ModS2	Clay	336.1	2803.0	99	2.419	0.017
		Sandy-loam	492.3	1468.8	99	2.777	0.006
		Sand	223.5	985.2	99	1.555	0.141
Tomato	ModC	Clay	105.7	1172.2	60		
		Sandy-loam	74.0	852.9	60		
		Sand	87.1	537.3	60		
	ModS1	Clay	111.9	1172.2	62	1.784	0.177
		Sandy-loam	78.7	852.9	62	1.906	0.158
		Sand	88.8	537.3	62	0.598	0.553
	ModS2	Clay	117.1	1172.2	66	1.086	0.381
		Sandy-loam	100.9	852.9	66	3.630	0.004
		Sand	95.2	537.3	66	0.933	0.478

Table 5
Parameters of the model describing N recovery with and without residue incorporation.

Crop	Soil	N_0	k_{min}	k_{res}	*a*	*b*	Residual SS	Total SS	*n*
Sugarbeet	Clay	155.2	1.354	0.192	1.244	384.0	1431.60	74337.76	12
	Sandy loam	174.1	1.666	0.267	0.992	315.9	637.04	58131.73	12
	Sandy	16.0	1.037	0.445	0.721	297.4	1247.96	28304.92	12
Wheat	Clay	67.4	2.605	0.017	0.941	124.6	1763.75	22216.94	20
	Sandy loam	57.4	2.271	0.041	0.941	125.6	1653.40	22255.97	20
	Sandy	19.0	1.782	0.168	0.816	126.5	480.66	21409.61	20
Maize	Clay	182.7	0.927	0.247	0.968	295.6	725.98	44636.24	12
	Sandy loam	140.1	0.917	0.207	0.950	358.6	335.56	51148.85	12
	Sandy	51.1	0.763	0.450	0.921	402.8	983.89	51864.32	12
Potato	Clay	127.4	1.658	0.438	0.935	283.2	926.98	61606.01	12
	Sandy loam	109.7	2.084	0.618	0.841	188.8	1361.51	38835.75	12
	Sandy	48.3	2.059	0.400	0.764	131.9	958.38	20254.94	12
Tomato	Clay	160.3	2.222	0.300	1.021	284.3	1781.68	73400.61	12
	Sandy loam	143.8	1.422	0.446	0.988	282.0	1682.85	58954.31	12
	Sandy	46.1	1.732	0.317	0.887	172.9	978.15	29662.03	12

the treatments and is strongly related to the N adsorption in the unfertilised check with residue removal. The natural availability should be higher for high fertilisation treatments and with residue incorporation but the experimental layout did not allow to consider a unfertilised strip within each treatment. Assuming a constant N_0 would lead to an overestimation of NUE for fertilised treatment and this effect should be more evident at low fertilisation levels. Furthermore, the model does not consider explicitly the interaction between mineral and organic forms of N. The values obtained have then to be considered as a first approximation of the real values. Nevertheless, we assume that these values can be used to estimate

Please cite this article in press as: Pituello, C., et al., Outcomes from a long-term study on crop residue effects on plant yield and nitrogen use efficiency in contrasting soils. Eur. J. Agron. (2015), http://dx.doi.org/10.1016/j.eja.2015.11.027

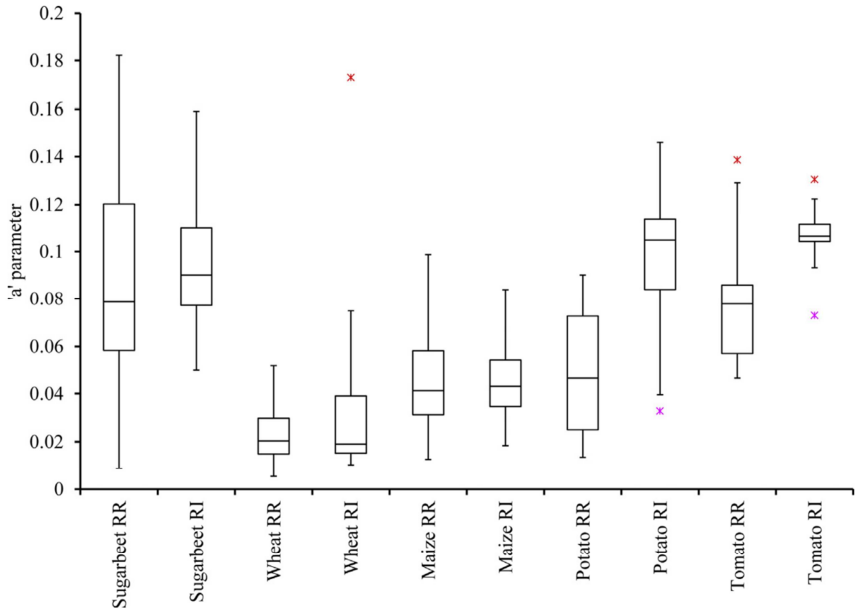

Fig. 4. Initial slope of the yield response curve ('*a*' parameter) with or without residue incorporation.

Table 6
Relative efficiency (%) of residue nitrogen compared to mineral nitrogen.

	Clay	Sandy-loam	Sandy
Sugarbeet	14.19	16.01	42.95
Wheat	0.66	1.80	9.42
Maize	26.69	22.57	58.98
Potato	26.43	29.65	19.44
Tomato	13.51	31.34	18.30

the relative contribution of mineral and organic forms of N to plant uptake.

The equation gave an excellent fit to observed data in all the combinations 'crop × soil' (Table 5), with natural N availability (N_0) and maximum N uptake (b) decreasing from clay to sandy soil and constants related to nitrogen availability of N inputs (k_{min} and k_{res}) always higher for the mineral inputs.

For both the N forms, the model allows to estimate a specific NUE, as the ratio of N uptake and the N input for this form of N (mineral fertilisers or residues).

The NUE for mineral sources (Fig. 6) is highly variable, depending on soil type and crop. For the more fertile soils the amount of N recovered from soil is high and, for the lower mineral N inputs, uptake is higher than input, leading to NUE greater than 1. For all the crops, NUE for mineral sources is lower and less variable across fertilisations in the sandy soil. In this soil the strong limitation of crop potential yield reduces N adsorption and, in turn NUE.

The efficiency of residue N follows an opposite trend (Fig. 6), with lower values in clay and sandy-loam soils and higher in the sandy soil. Furthermore, crops show a very different behavior: while in wheat the effect of residues seems always low, in sugarbeet and maize NUE for residues varies from ca. 0.2 for clay and sandy-loam soils, to quite high values (0.6–0.8) in the sandy soil. In the two solanaceous crops, recovery of residue N is still high in the sandy soil, as in the other summer crops, but is also appreciable in the clay and sandy loam soils.

The relative efficiency of N input for residues (ratio between k_{res} and k_{min}) is very low in wheat, confirming that this crop is only marginally affected by residue incorporation (Table 6).

In the spring–summer crops, residues have a higher relative efficiency, ranging from 15 to 30% of that of mineral inputs in clay and sandy-loam and higher (from 18 to 60%) in the sandy soil.

4. Discussion

The long-term incorporation of crop residues caused a slight but almost ubiquitous increase in yield, however the mechanisms behind this increase differ for the different crops and types of soil, as the coupled analysis of yield response curves and nitrogen use efficiency highlights. The crop- and soil-specific response to residue use is confirmed by the apparently contrasting results found in the literature (e.g., Brennan et al., 2014; Malhi et al., 2011). In sugarbeet and cereals, the efficiency of residue incorporation appears more pronounced in soils with the lowest fertility, thus this practice is surely advisable in these soils in order to increase their fertility.

The absence of evident effects on sugarbeet yield in clay may be due to the fact that in these soils the crop finds an intrinsic high nutrient content that is sufficient to reach maximum production levels and so nutrient input by residue decomposition is not very effective in increasing crop yield. Indeed, it is well recognised that sugarbeet gives its best growth performances in rich loamy soils (Fageria, 2012). In the sandy soil, the productivity enhancement attained seems to be caused by other mechanisms along with the purely nutritional effect, especially at low fertilization levels, where the increase in yield is coupled with an increase in nitrogen use efficiency. Consequently, residue use for this crop appears more useful in medium to low fertility soils and at low fertilization levels.

In accordance with the results found by Petersen et al. (2013) and Brennan et al. (2014), winter wheat appears to be slightly influenced by residue incorporation. In our study this may be attributed to the fact that the period of maximum N uptake is earlier than in other crops and takes place when the mineralization of residues is still slow due to low soil temperature. Accordingly residue effect is likely to be marginal both on crop yield and on nitrogen use efficiency especially in highly fertile soils. On the other hand, in sandy soil their use is likely to favor crop yield, even if the effect is lower than that observed in summer crops

Please cite this article in press as: Pituello, C., et al., Outcomes from a long-term study on crop residue effects on plant yield and nitrogen use efficiency in contrasting soils. Eur. J. Agron. (2015), http://dx.doi.org/10.1016/j.eja.2015.11.027

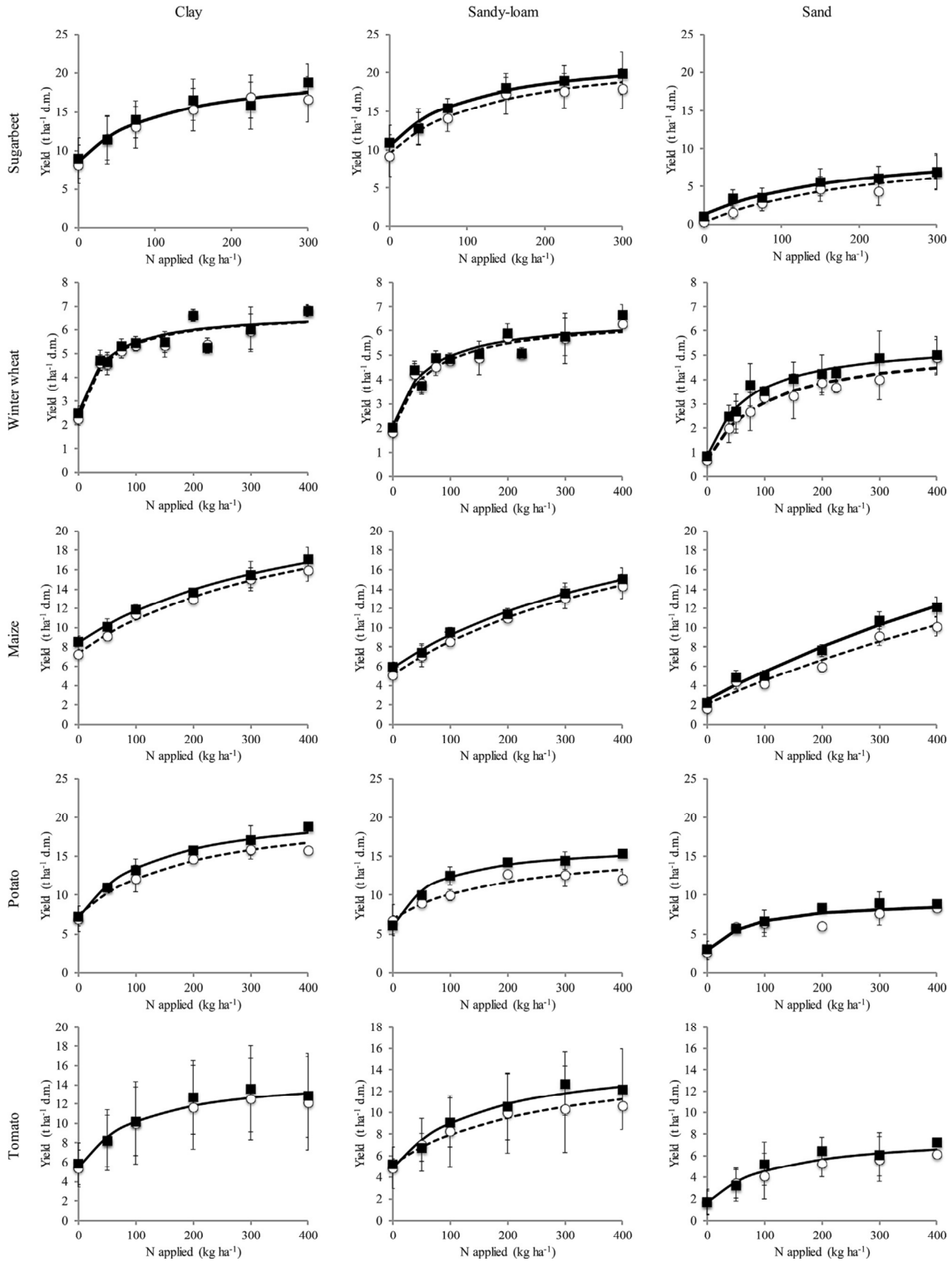

Fig. 5. Yield response curves to N with and without residue incorporation. Continuous lines represent RI treatment, dashed lines represent RR treatment.

Please cite this article in press as: Pituello, C., et al., Outcomes from a long-term study on crop residue effects on plant yield and nitrogen use efficiency in contrasting soils. Eur. J. Agron. (2015), http://dx.doi.org/10.1016/j.eja.2015.11.027

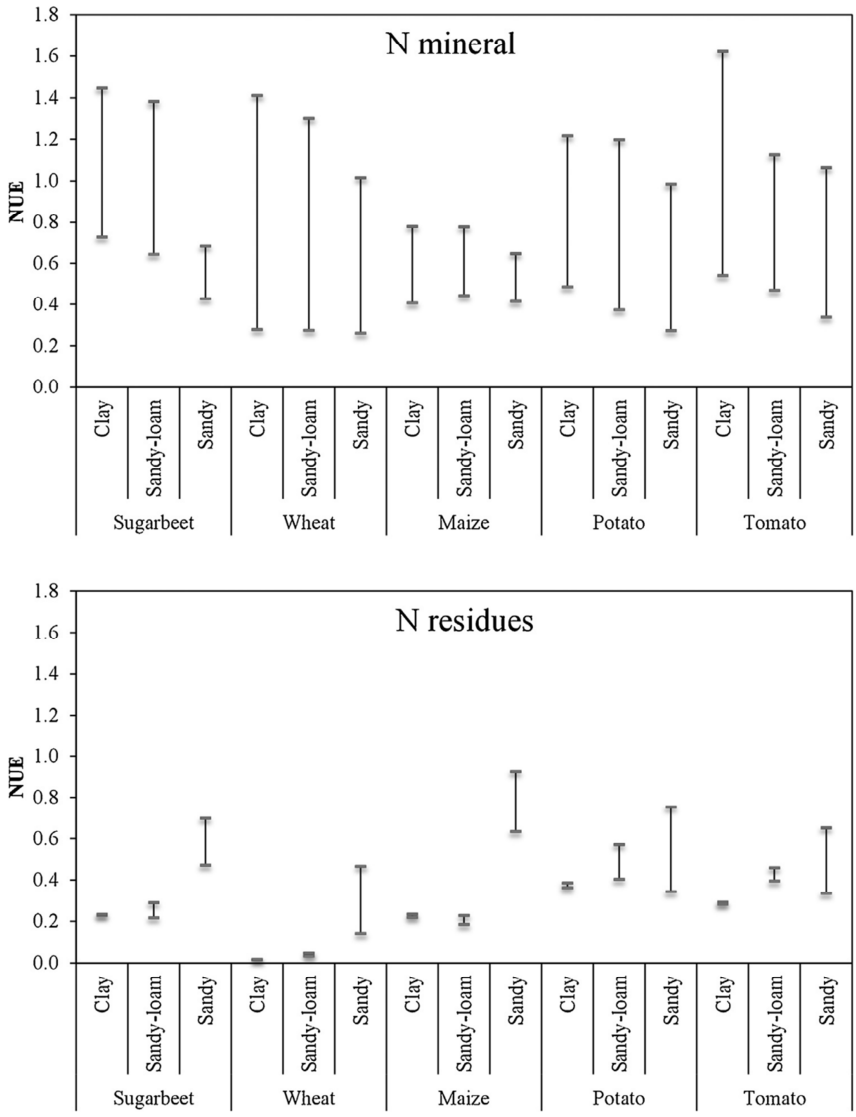

Fig. 6. Nitrogen use efficiencies from a) mineral and b) crop residues N sources.

In maize the effects of residues on yields are modest in clay and sandy-loam soils. Instead, the more pronounced increase in yields in sandy soil can be related to a relatively high uptake of N from residues.

Potato and tomato are not affected by residue incorporation in sandy soil while strong effects are evident in the sandy-loam. The sandy-loam soil has a relatively high silt and carbonates content, leading to a tendency to form a surface crust. Residue incorporation can lead to an improvement of soil characteristics and particularly to surface permeability, with positive effects for both solanaceous crops.

5. Conclusions

Incorporation of residues seems to have different effects depending on crop and soil type. For potato and tomato and, to a lesser extent, for sugarbeet, residues can improve crop productivity, while the effects on cereals seem to be lower. Regarding soil type, residues are proportionally more effective in sandy and sandy-loam soils, both through a direct nutritional effect and, possibly, an improvement of soil characteristics and soil water retention in particular. Anyway the residue effect is relatively low, with modest increments of biomass in the most fertile soils and their effect can be compensated by N fertilization, as the constancy of Y_M indicates. The use of residues as organic amendment or their re-use in other processes (e.g., as a source of bioenergy) therefore has to be carefully analysed considering both the energy and C balances and the positive effects on soil productivity.

Acknowledgments

This research was financially supported by the Italian Ministry of Education, University and research (MIUR); Grant no. 2010FRE7J4.

Please cite this article in press as: Pituello, C., et al., Outcomes from a long-term study on crop residue effects on plant yield and nitrogen use efficiency in contrasting soils. Eur. J. Agron. (2015), http://dx.doi.org/10.1016/j.eja.2015.11.027

References

Brennan, J., Hackett, R., McCabe, T., Grant, J., Fortune, R.A., Forristal, P.D., 2014. The effect of tillage system and residue management on grain yield and nitrogen use efficiency in winter wheat in a cool Atlantic climate. Eur. J. Agron. 54, 61–69, http://dx.doi.org/10.1016/j.eja.2013.11.009.

Dobermann, A.R., 2005. Nitrogen Use Efficiency-State of the Art. Agronomy & Horticulture - Faculty Publications, pp. 316.

Fageria, N.K., 2012. Management strategies for maximizing root systems. In: The Role of Plant Roots in Crop Production. CRC Press, pp. 369–442, http://dx.doi.org/10.1201/b 12365-10.

Fao (2012). Current world fertilizer trends and outlook to 2016. Food and Drug Organisation of the United Nations, Rome.

Faostat (2012). Food and Drug Organisation of the United Nations. Statistics Division, Rome. http://faostat3.fao.org.

Fao-Unesco, 2008. Soil Map of the World. Revised Legend. FAO, Rome.

Galloway, J.N., Townsend, A.R., Erisman, J.W., Bekunda, M., Cai, Z., Freney, J.R., Sutton, M.A., 2008. Transformation of the nitrogen cycle: recent trends, questions, and potential solutions. Science 320 (5878), 889–892, http://dx.doi.org/10.1126/science.1136674.

Huang, S., Zeng, Y., Wu, J., Shi, Q., Pan, X., 2013. Effect of crop residue retention on rice yield in China: a meta-analysis. Field Crop Res. 154, 188–194, http://dx.doi.org/10.1016/j.fcr.2013.08.013.

Janzen, H.H., 2009. Long-term ecological sites: musings on the future, as seen (dimly) from the past. Glob. Change Biol. 15 (11), 2770–2778, http://dx.doi.org/10.1111/j.1365-2486.2009.01971.x.

Kumar, K., Goh, K.M., 1999. Crop residues and management practices: effects on soilquality, soil nitrogen dynamics, crop and nitrogen recovery. Adv. Agron. 68, 197–319, http://dx.doi.org/10.1016/S0065-2113(08) 60846-9.

Lassaletta, L., Billen, G., Grizzetti, B., Anglade, J., Garnier, J., 2014. 50 year trends in nitrogen use efficiency of world cropping systems: the relationship between yield and nitrogen input to cropland. Environ. Res. Lett. 9 (10), 105011, http://dx.doi.org/10.1088/1748-9326/9/10/105011.

Malhi, S.S., Nyborg, M., Solberg, E.D., Dyck, M.F., Puurveen, D., 2011. Improving crop yield and N uptake with long-term straw retention in two contrasting soil types. Field Crop Res. 124 (3), 378–391, http://dx.doi.org/10.1016/j.fcr.2011.07.009.

Petersen, S.O., Schjønning, P., Olesen, J.E., Christensen, S., Christensen, B.T., 2013. Sources of nitrogen for winter wheat in organic cropping systems. Soil Sci. Soc. Am. J. 77 (1), 155, http://dx.doi.org/10.2136/sssaj2012.0147.

Rasmussen, P.E., 1998. Long-term agroecosystem experiments: assessing agricultural sustainability and global change. Science 282 (5390), 893–896, http://dx.doi.org/10.1126/science.282.5390.893.

Richter, D. deB, Hofmockel, M., Callaham, M.A., Powlson, D.S., Smith, P., 2007. Long-term soil experiments: keys to managing earth's rapidly changing ecosystems. Soil Sci. Soc. Am. J. 71 (2), 266, http://dx.doi.org/10.2136/sssaj2006.0181.

Sutton, M., 2011. Too much of a good thing. Nature 472, 159–161, http://dx.doi.org/10.1038/472159a.

Van Grinsven, H.J.M., Bouwman, L., Cassman, K.G., van Es, H.M., McCrackin, M.L., Beusen, A.H.W., 2015. Losses of ammonia and nitrate from agriculture and their effect on nitrogen recovery in the European Union and the United States between 1900 and 2050. J. Environ. Qual. 44 (2), 356–367, http://dx.doi.org/10.2134/jeq2014.03.0102.

Please cite this article in press as: Pituello, C., et al., Outcomes from a long-term study on crop residue effects on plant yield and nitrogen use efficiency in contrasting soils. Eur. J. Agron. (2015), http://dx.doi.org/10.1016/j.eja.2015.11.027

Acknowledgments

Non è semplice condensare tre anni di vita e lavoro in poche righe. Il contenuto di questa tesi è il frutto di un impegno mentale profondo e costante che non è sempre facile da sostenere e portare avanti. E non sempre si riesce a trovare gli alleati giusti con cui farlo. Se mi guardo indietro però posso dire che il bilancio di crescita professionale e personale di questa esperienza è sicuramente positivo, a prescindere dalla direzione verso cui mi porterà.

Vorrei ringraziare il Prof. Morari per la sua supervisione e i suoi preziosi e fondamentali suggerimenti, ed il Prof. Berti per la guida e le utili delucidazioni in materie statistiche e agronomiche. Ringrazio anche tutto il mio gruppo di ricerca, c'è un pezzettino di ognuno di loro dentro questa tesi. In special modo il mio ringraziamento va a Gianluca che ha contribuito in maniera sostanziale alla buona riuscita degli esperimenti in laboratorio, fornendo sia un supporto tecnico che uno (non meno importante) di amicizia e confronto. Ringrazio anche Nicola per le innumerevoli volte in cui l'ho disturbato con le mie domande e per l'aiuto con gli esperimenti idraulici e l'elaborazione dei dati. Infine ringrazio la Prof. Ornella Francioso e tutti coloro con cui ho collaborato in questi tre anni.

Un ringraziamento speciale va a mio padre e mia sorella per il supporto che mi hanno dato durante tutto il mio lungo percorso di studi e per essere una "base sicura" a cui è bello tornare. Ringrazio anche Alberto che fa da reminder a tutti, la zia Nives e Christian per i carciofi ripieni, le lavagne magiche e tutto il resto. Poi vorrei ringraziare gli amici e colleghi con cui ho condiviso l'esperienza del dottorato, senza di voi non sarebbe stato lo stesso. Infine, un ringraziamento speciale va ad Alessandro "per l'ultimissimo pezzettino di strada fatto insieme", e per milioni di altri motivi.